A NON-LINEAR DIGITAL SIMULATION OF THE DYNAMIC BEHAVIOUR OF A STEAM GENERATOR

by

Davar Abi-Zadeh, B.Sc., D.I.C., M.Sc.

Thesis submitted for the degree of

Doctor of Philosophy

in the

University of London

Department of Mechanical Engineering,
Imperial College of Science and Technology,
London SW7 2BX.

September 1976

ABSTRACT

A theoretical study is presented for the prediction of the steady-state and dynamic behaviour of a helically-coiled tube once-through steam generator. A primary fluid is utilised, in counter-flow, to heat the secondary flow which is water, and to produce wet or superheated vapour at outlet.

In the dynamic modelling, attention is paid to the different regions along the secondary boiling flow and the boiling boundaries. A criterion is developed for predicting subcooled flow boiling in a helically-coiled tube. The heat removal of the subcooled liquid core is calculated by taking into account the effective conductivity and the mean liquid temperature. The onset of subcooled boiling is established on the basis of equality of the heat removal of the subcooled core and the imposed heat flux. Predictions are compared to experimental results.

The dynamic analysis is based on the solution of the non-linear differential equations of continuity, energy, and momentum of the secondary flow, energy equations of the tube wall and the primary flow, together with the appropriate equations of slip factor, heat transfer coefficients and frictional pressure drop. Axial vapour quality, enthalpy, mass flow velocity and pressure drop of the secondary side, the primary flow and the tube wall temperatures are obtained at each time interval from the numerical solution of the conservation equations. The boundary conditions comprise the inlet conditions of the primary flow, and the inlet subcooling, enthalpy and inlet mass velocity or the pressure drop of the secondary flow.

The program has been developed with the objective of studying boiler behaviour under various operational conditions, particularly the stability

of the boiler. The static and the dynamic stabilities are investigated and discussed, predictions being made for the threshold of instabilities.

Effects of heat flux-flow coupling and certain parametric variations of operating conditions are investigated on various modes of instabilities. It is concluded that the simulation can be useful as a research and development tool, particularly in studying the feasibility of design options and performance of once-through systems aimed at safe operation.

ACKNOWLEDGEMENTS

The author wishes to thank his supervisor, Professor W. Murgatroyd, for his kind encouragement, guidance and interest in the work, and also Dr A.A. El-Shirbini, who gave such sincere advice at all stages of the work.

Thanks are also due to Miss D. Day, Miss E.M. Archer and Mrs S.D. Boote of the Mechanical Engineering Department for their efforts in obtaining necessary manuscripts and papers, etc.

The author acknowledges the help given to him by Mr W.T. Anglesea and Dr R.C. Jeffrey of Babcock and Wilcox (Operations) Limited, Renfrew, during his stay in their research station.

Financial support of the British Council is gratefully acknowledged.

Thanks are extended to Miss E.A. Quin for her conscientious typing of the manuscript.

I wish to express my gratitude and my respect to my parents, who supported me financially and encouraged me in all aspects during the thirty years of my life. I am very much indebted to my wife, whose patience helped me in devoting all of my time to my work. Thanks are also extended to my colleagues, Dr M. Marzouk, Dr L. Beynon and Mr M. Megerdichian for stimulating discussions, help and advice.

CONTENTS

		Page
Abstract		2
Acknowledgements		4
Contents		5
Nomenclature		11
CHAPTER 1:	INTRODUCTION	16
1.1	Introduction	16
1.2	Objectives of the Study	19
CHAPTER 2:	A REVIEW OF FLOW OSCILLATION	20
2.1	Introduction	20
2.2	Flow Excursion or Ledinegg Instabilities	21
2.2.1	Pressure drop/mass flow characteristics	21
2.2.1.1	Internal characteristics	22
2.2.1.2	External characteristics	25
2.2.2	The mechanism of flow excursion	26
2.2.3	Stability criteria	28
2.2.4	Effect of different parameters and preventing the instability	29
2.3	Density Wave Oscillations	31
2.3.1	Introduction	31
2.3.2	The mechanism	31
2.3.3	Stability of complete circuits	33
2.3.4	Effects of different parameters on the stability	37

Page

2.3.4.1 Effects of inlet and exit restriction 37
2.3.4.2 Effect of system pressure 38
2.3.4.3 Effect of inlet subcooling 38
2.3.4.4 Effect of mass velocity and power input 42
2.3.5 Methods of analysis 44
2.3.5.1 General equations 44
2.3.5.2 Assumptions and simplifications 45
2.3.5.3 Linear analyses 48
2.3.5.4 Non-linear analyses 52
2.4 Discussion and Conclusion 61

CHAPTER 3: BASIC EQUATIONS AND BOUNDARY CONDITIONS 64
3.1 Introduction 64
3.2 Energy Equation of the Primary Flow 66
3.3 The Tube Wall Model 69
3.4 Thermo-Hydrodynamic Equations of the Secondary Flow 70
3.4.1 A simplified model 70
3.4.2 Assumptions 70
3.4.3 Conservation equations 73
3.4.4 Constitutive equations 74
3.5 Boundary Conditions 76
3.6 Wall Shear Stresses and Voidage in Helically-Coiled Tubes 77
3.6.1 Frictional pressure drop 77

Page

3.6.2 Single-phase friction factor 77
3.6.3 Two-phase frictional multiplier and voidage 79
3.6.4 Conclusion 81
3.7 Transition Boundaries 84
3.7.1 Introduction 84
3.7.2 Subcooled boiling 84
3.7.2.1 Introduction 84
3.7.2.2 Onset of subcooled boiling 84
3.7.2.3 Assumptions and formulations 86
3.7.2.4 Vapour generation function 97
3.7.3 Bulk boiling boundary 100
3.7.4 Annular flow and dryout boundary 100
3.7.5 Onset of superheating 105
3.8 Heat Transfer Coefficients in Different Regimes in Helically-Coiled Tubes 106
3.8.1 Liquid phase 106
3.8.2 Two-phase heat transfer coefficient 106
3.8.3 Post dryout heat transfer 109
3.8.4 Convective heat transfer to vapour phase 112
3.9 Summary and Remarks 114

CHAPTER 4: NUMERICAL TECHNIQUES AND SIMULATION PROGRAM 117
4.1 Introduction 117
4.2 Review of Governing Equations 118
4.3 Numerical Methods 120
4.4 General Calculation Procedure 126

Page

4.5 Iteration Procedure for the Inlet Mass Velocity 131

4.6 Transition Boundaries 133

4.6.1 Method of approximation of the time derivatives 135

4.6.2 Position of the transition boundary 138

4.6.3 Remarks 138

4.7 Computer Program 141

4.7.1 Input data and disturbances 141

4.7.2 Outputs 143

4.7.3 General description of subroutines 144

CHAPTER 5: EVALUATION OF SIMULATION RESULTS (STEADY-STATE) 152

5.1 Evaluation of the Onset of Subcooled Boiling 153

5.1.1 Experimental location of the onset of subcooled boiling 153

5.1.2 Comparison and discussion 156

5.2 Steady-State Results 165

5.2.1 Axial distribution of temperatures 165

5.2.2 Heat flux distribution 165

5.2.3 Subcooled boiling region 168

5.2.4 Pressure drop distribution 170

5.3 Static Stability Results 185

5.3.1 Pressure drop/mass velocity characteristic 185

5.3.2 Stable operating regions 188

5.3.3 Effects of the primary side parameters on the static characteristics 189

Page

5.3.3.1 Effect of mass flow rate 189
5.3.3.2 Effect of the primary side heat transfer coefficient and inlet temperature 190
5.3.4 Effects of the secondary side parameters on the static characteristics 191
5.3.4.1 Effect of system pressure 191
5.3.4.2 Effect of secondary side heat transfer coefficient 192
5.3.4.3 Effect of the coil geometry 192
5.3.5 Conclusions 193

CHAPTER 6: DYNAMIC SIMULATION RESULTS 211
6.1 Introduction 211
6.2 Transient Response Analysis 213
6.2.1 Response of exit mass flow and boiling boundaries 213
6.2.2 Heat flux variations at boiling boundaries 215
6.2.3 Response of outlet temperature 217
6.2.4 Response of pressure drop 218
6.3 Frequency Response Analysis 230
6.3.1 Operating conditions 230
6.3.2 Characteristics of the input and the output variables 230
6.3.3 Response of exit mass velocity 232
6.3.4 Effect of flux-flow coupling 235

Page

6.3.5 Pressure drop oscillations 239

6.3.6 Stability implication 241

6.3.7 Frequency response of pressure drop 244

6.3.8 Onset of instability 246

6.3.9 Responses of temperatures 249

6.4 Flow Oscillations in Fixed Pressure Drop Systems 278

6.4.1 Character of prediction 278

6.4.2 Self-sustained oscillations 279

6.4.3 Effect of operating parameters on stability 282

6.5 Concluding Remarks 300

CHAPTER 7: CONCLUSIONS AND RECOMMENDATIONS 303

APPENDIX A: STABILITY TESTS - TRANSIENT RESULTS AND ANALYSIS 308

APPENDIX B: NUMERICAL STABILITY OF CSDT METHOD AS APPLIED TO THE LINEAR HEAT EXCHANGER 349

References 354

Note: All computer programs are available at the Imperial College of Science and Technology (Thermal Power Section), London University.

NOMENCLATURE

a	:	$d/2$ radius of tube (m)
A	:	cross-section area (m^2) and constant given by equation (3.41)
B	:	constant given by equation (3.60)
c_p	:	specific heat (kJ/kg^oC)
C	:	constant given by equations (3.28) and (3.42)
d	:	tube diameter (m)
D	:	helix diameter (m) and constant given by equation (3.43)
D_h	:	$a/2$ equivalent heated diameter (m)
E	:	$H - pv$, specific internal energy (kJ/kg)
f	:	friction factor
F	:	constant given by equation (3.27)
g	:	gravitational acceleration (m/sec^2)
G	:	mass velocity (kg/m^2sec)
h	:	heat transfer coefficient ($kW/m^2{}^oC$)
H	:	enthalpy (kJ/kg)
H_{fv}	:	heat of evaporation (kJ/kg)
i	:	refers to number of iterations
I	:	refers to number of time steps
k	:	thermal conductivity (kW/m^oC) and constant of inlet or outlet restrictions
L	:	tube or boiler length (m)
$\dot{m}''$	:	mass flux (kg/m^2sec)
M	:	mass of unit length (kg/m) and constant given by equation (3.57)
n	:	refers to number of length steps
N	:	constant given by equation (3.46)

N_{sub} : subcooled number (equation (2.18))

N_{pch} : phase change number (equation (2.19))

Nu : Nusselt number ($h\ d/k$)

p : pressure (N/m^2)

P : perimeter (m)

Pr : Prandtl number ($c_p\ \mu/k$)

$\dot{q}''$: heat flux (kW/m^2)

Q'' : dimensionless heat flux defined by equation (3.35)

Q'' : circumferential averaged heat flux (dimensionless)

r : radial co-ordinate

R : radius of coil (m)

Re : Reynolds number ($G\ d/\mu$)

S : slip factor

t : time (sec)

T : temperature (^oC)

T' : temperature at the core (^oC)

u : axial velocity (m/sec)

u' : velocity of the core (m/sec)

U : dimensionless velocity defined by equation (3.33)

U^{*2} : shear velocity defined by equation (3.34)

v : specific volume (m^3/kg)

v_1 and v_2 : defined by equations (3.15) and (3.17) (m^3/kg)

x : vapour flow quality

X : Lockhart-Martinelli parameter given by equation (3.100)

z : axial co-ordinate

Z_1 : $\alpha\ G\ \Delta\ H_i/2\dot{q}''$

Z_o : Z_1/d

Z_D : distance of bubble detachment position from inlet

Z_D^* : Z_D/Z_1

α : void fraction

α_o : constant given by equation (3.45)

β : helix angle (Rad)

γ : vapour generation rate (kg/m^{2}sec)

δ : dimensionless film thickness given by equation (3.44) and small increments

ΔH : $H_{sat} - H$

Δp : pressure drop (N/m^2)

Δp_s : imposed or system pressure drop (N/m^2)

Δt : time increment

ΔT_{in} : $T_{sat} - T_{in}$, inlet subcooling (^{o}C)

Δz : length increment

ε : very small quantity

η : r/a dimensionless radial co-ordinate

θ : dimensionless temperature (equation (3.37))

θ_{sub} : $\Delta T_{sub}/\Delta T_{in}$

μ : viscosity (N sec/m^2)

ρ : density (kg/m^3)

ρ_1 and ρ_2 : quantities defined by equations (3.9) and (3.12), respectively (kg/m^3)

τ : shear stress (N/m^2)

ϕ^2 : two-phase frictional multiplier

χ : heat division parameter

ψ : angular co-ordinate (Rad)

ω : frequency (Rad/sec)

Ω : characteristic frequency (equation (2.20))

Subscripts

c	:	core or coil
cr	:	critical condition
D	:	detachment point
e	:	outlet of the tube
ext	:	external
f	:	film edge of the bubble layer, or saturated liquid
g	:	gas
i	:	inside of the tube wall
in	:	channel inlet condition
int	:	internal
l	:	liquid phase
m	:	mean value
o	:	outside of the water tube
p	:	primary flow
th	:	thermodynamic equilibrium
tp	:	two-phase
s	:	secondary side and straight tube
sat	:	saturation
sh	:	superheater
sp	:	single-phase
sub	:	subcooled or economiser region
v	:	vapour phase
w	:	wall

Abbreviations

exp	:	experimental value
f( )	:	function of
HCL	:	centre line of helix
ln	:	natural logarithm
pred	:	predicted value
sat	:	saturation
sub	:	subcooled

CHAPTER 1

INTRODUCTION

1.1 INTRODUCTION

A steam generator is one of the major components of both nuclear and non-nuclear power stations and strongly influences their overall performance.

Once-through boilers are employed in advance gas cooled reactors (AGR) due to their features (C.E.G.B. (1971) and Taylor et al (1973)). In a once-through system, the working fluid is pumped continuously through the boiler by the feed pump, there being no circulation as with other boilers. The chief advantages of once-through boilers are that they require no drum and have controlled flow in the evaporator stage (C.E.G.B. (1971)). The flow rate is a direct function of load, and therefore a high mass velocity, with a consequential high pressure drop, has to be provided at the full load conditions so that there is still sufficient flow velocity even at low loads to keep the tube walls cool.

The tubes in once-through boilers used in AGR-type stations are often of a helical type and are presently arranged in removable boiler units inside cylindrical holes of pressure vessels (Beckmann and Gilli (1973)). The concept of helically-coiled boilers was applied earlier in the US space project with liquid mercury as the cooling liquid (Bell (1976)). The strong self-induced radial acceleration and secondary recirculation inside the helical tube ensured the contact of the liquid with the heating surface and a high rate of heat transfer coefficient (Bell (1976) and Owhadi (1966)). The interesting features of helically-coiled tubes have even led to the construction of mobile and compact once-through boiler units which are already in operation (M.E. Boilers).

From the point of view of dynamics and control, once-through systems are the most difficult but also the most interesting ones. Absence of a reserve of feed water in these units means that output variations require immediate input action.

When designing a boiler for a power complex, it is essential to know the dynamic conditions imposed during its operation, e.g. fault operation, start up and shut down. The boiling boundaries along the tube and the outlet temperatures of vapour and gas are of prime interest in a once-through unit. A knowledge of these variables is necessary for control and protection of the boilers.

One of the important problems in the design of once-through steam generators for AGR concerns the stability of the liquid-vapour flow under various operational conditions. Adequate provisions in the design to prevent flow oscillations are necessary for the safe and satisfactory operation of the boilers and turbines (Potter (1973)). Apart from the considerable forced mechanical vibrations of components, the flow oscillation can cause liquid carry-over to the austenitic sections of the boiler tubing. This may result in a stress corrosion failure. Thermal cycling of the tube wall, failure to achieve design operating conditions, and problems in the control system design are of special concern to designers. These are possible consequences of instabilities in a boiler operation.

These requirements have led to extensive experimental studies of the dynamics of helically-coiled tube once-through boilers. A typical example is the work conducted at the research laboratory of Babcock and Wilcox (Operations) Limited (e.g. Anglesea et al (1974), Ruffell et al (1973) and Taylor et al (1973)).

At the same time, research programmes were initiated at the

Mechanical Engineering Department of Imperial College under the supervision of Professor Murgatroyd to investigate the dynamic stability of flow-boiling in helically-coiled tubes. The research was divided into two lines: an experimental investigation using Freon as the simulating liquid (Rakopoulos (1976)), and a theoretical investigation. The latter investigation was started by the author by spending five months at the research station of Babcock and Wilcox (B & W) to become acquainted with the dynamics of boilers in a large scale test rig. Some preliminary analysis of this work which was carried out by the B & W staff in collaboration with the author is given in Appendix A.

In conjunction with B & W's experimental programme, the present study was therefore directed towards studying the dynamic behaviour of a helically-coiled tube once-through boiler, and in particular, the dynamic stability of the boiler.

1.2 OBJECTIVES OF THE STUDY

An account of the published information of two-phase flow instabilities and different mathematical approaches, which are covered in chapter 2, reveals that in the analysis of once-through systems one or more of the following assumptions are made:

i) axially uniform heat flux;
ii) single-phase variable density models;
iii) linearised conservation equations;
iv) negligible inertia of the primary flow or the tube wall;
v) absence of a valid criterion of the onset of subcooled boiling in coils; and
vi) thermal equilibrium between the vapour and liquid phases.

These assumptions are controversial in the sense that they replace the physical phenomena which are essential to the description of a flow-boiling in helically-coiled tubes particularly when the heat source is a primary flow.

The dynamic model presented in this work includes none of the above assumptions. The model is directed primarily towards achieving the following objectives:

1. Developing a criterion for the onset of subcooled boiling in helically-coiled tubes.
2. Developing a non-linear mathematical simulation of a helically-coiled tube once-through boiler heated by a counter-flowing primary fluid, capable of predicting the dynamic behaviour of the system.
3. Investigating the flow instabilities of the boiler.

CHAPTER 2

A REVIEW OF FLOW OSCILLATION

2.1 INTRODUCTION

In any natural or forced boiling flow system, consisting of one or a number of parallel channels running between a common inlet and a common outlet header, gross variations in the flow in tubes can occur under certain circumstances. This chapter presents a review of two main types of flow oscillations which are of practical interest in the design of once-through steam generators.

Part one opens with a study of the flow excursion which occurs under apparently steady conditions. Part two introduces the dynamic oscillation due to the density wave instability. The mechanism and characteristics of instability phenomena are discussed and reviewed. There are very few reported experimental and theoretical programmes in open literature which cover the subject in helically-coiled tubes. Therefore, in order to be familiar with different aspects of the instability, the survey is not restricted to the case of helically-coiled tube once-through systems. However, in the review of the effect of various parameters on the stability of a boiling system, experimental evidence of straight tube boiling systems has been used to assist in understanding the situation. Finally, different theoretical approaches are reviewed and discussed.

2.2 FLOW EXCURSION OR LEDINEGG INSTABILITIES

The term "flow excursion" is used to denote a sudden change of flow rate. It may occur in a heated tube into which subcooled liquid is fed during small fluctuations or gradual changes of one of the system parameters. If the new operating conditions are unstable, undesirable secondary effects can occur such as burn out, chugging, pressure drop or flow oscillation which make the original flow excursion difficult to detect (Boure et al (1973)).

One of the early investigators to study such behaviour of two-phase flow systems was Ledinegg (1938) and instabilities of this type are often named after him. A thorough investigation of this phenomenon has been carried out by Maulbetsch et al (1966,1967) and Deleas et al (1965).

2.2.1 Pressure Drop/Mass Flow Characteristics

The pressure drop between the inlet and outlet boundaries of a boiling channel can be defined as the sum of the hydrostatic pressure drop, ΔP_h, the acceleration pressure drop, ΔP_a, and the friction pressure drop, ΔP_f:

$$\Delta P_{int} = \Delta P_h + \Delta P_a + \Delta P_f \qquad (2.1)$$

In order to maintain a steady mass flow rate (G) in the channel, an external pressure head (ΔP_{ext}) is required to balance the demand pressure drop of the channel (ΔP_{int}), i.e.

$$\Delta P_{int} \begin{Bmatrix}\text{due to internal}\\ \text{characteristics}\end{Bmatrix} = \Delta P_{ext} \begin{Bmatrix}\text{due to external}\\ \text{characteristics}\end{Bmatrix} \qquad (2.2)$$

Generally, both sides of equation (2.1) are dependent on the mass velocity (G) of the fluid. Within the range of practical conditions

of boiling channels, there is at least a single value of G which satisfies the relationship of equation (2.2). The Ledinegg stability arises in certain conditions when equation (2.2) has more than one solution for mass velocity G. This arises mainly as a result of the shape of the internal and external characteristics which are discussed in the following sections.

2.2.1.1 Internal characteristics

Consider a system having a constant heat input, inlet subcooling and inlet pressure. At very high mass velocities where no boiling takes place, the pressure drop will follow the single phase law, and the variation of pressure drop with different mass velocities is nearly a parabolic curve (Figure 2.1). At low mass velocity, supposing that vapour only flows in the tube, the characteristic will follow another similar curve as shown in Figure 2.1. The pressure drop for the vapour is, of course, much higher than that for the liquid at the same mass flow rate because of its higher velocity. Now, consider the case when boiling takes place, at an intermediate mass velocity, it is expected that the corresponding pressure drop will fall between the all-liquid and the all-vapour curves. Therefore, if the mass velocity is increased from a low to a high value, the practical shape of the pressure drop-mass velocity characteristics either follows curve 1, Figure 2.1, i.e. the flow rate is a monotonic function of pressure drop, or curve 2 which possesses a maximum and minimum. The reason for the shape of curve 2 can be explained qualitatively as follows: starting from a position A, where the outlet vapour quality is very high, as mass velocity increases, the overall pressure drop increases while the position at which boiling takes place moves towards the outlet. Thus, the length

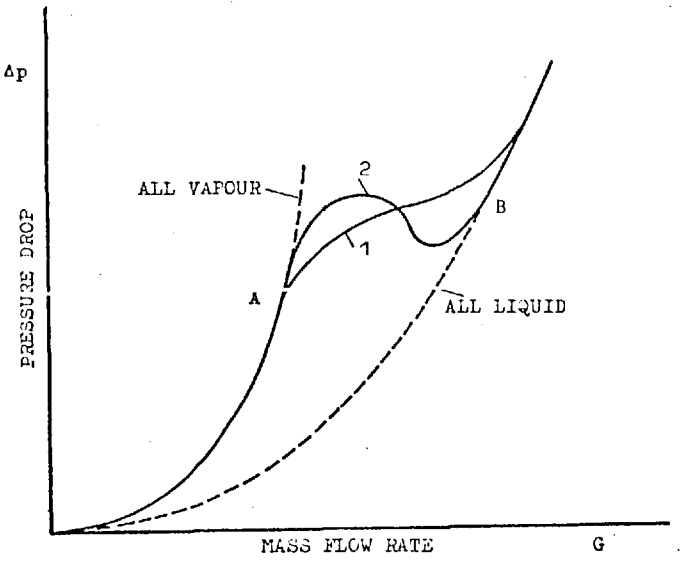


Figure 2.1: Internal characteristics of ΔP as a function of G

of the two-phase zone reduces which in turn reduces the two-phase pressure drop. In certain conditions, the increase of pressure drop due to the increase of mass velocity becomes less or identical to the reduction of ΔP which is caused by the reduced length of the boiling zone. Hence, further increase of mass velocity causes the pressure drop to reduce, and finally it becomes identical to that of the single-phase liquid when the input heat flux is no longer enough for the generation of vapour.

In the cases when the frictional and accelerational pressure drops are relatively low, e.g. high operating pressure systems, mass velocity can be a single valued function of pressure drop (curve 1), and also when the system is working at low heat flux, the maximum and minimum of the characteristic curve may disappear. Figure 2.2 is given by Stenning et al (1967) and shows the characteristic curves for Freon 11 at different heat fluxes as obtained experimentally.

Figure 2.3, due to Fraas and Ozisik (1965), shows the effect of density ratio $((\rho_f - \rho_v)/\rho_v)$ and hence system pressure on the

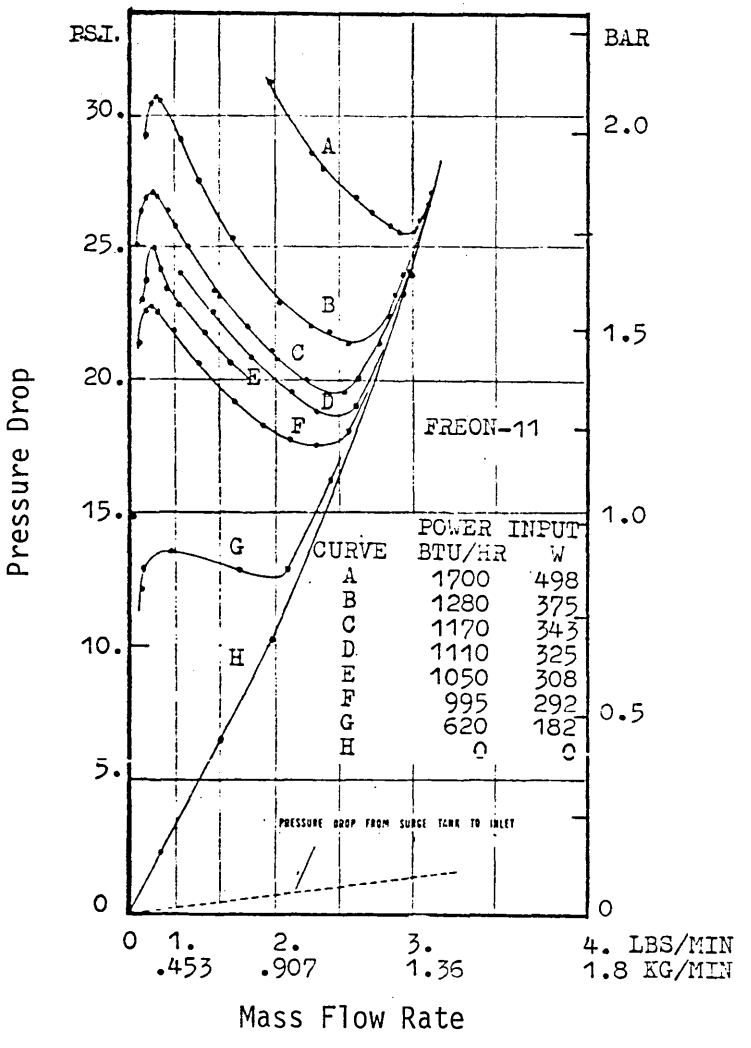


Figure 2.2: Pressure drop versus mass flow rate; experimental values of Stenning et al (1967)

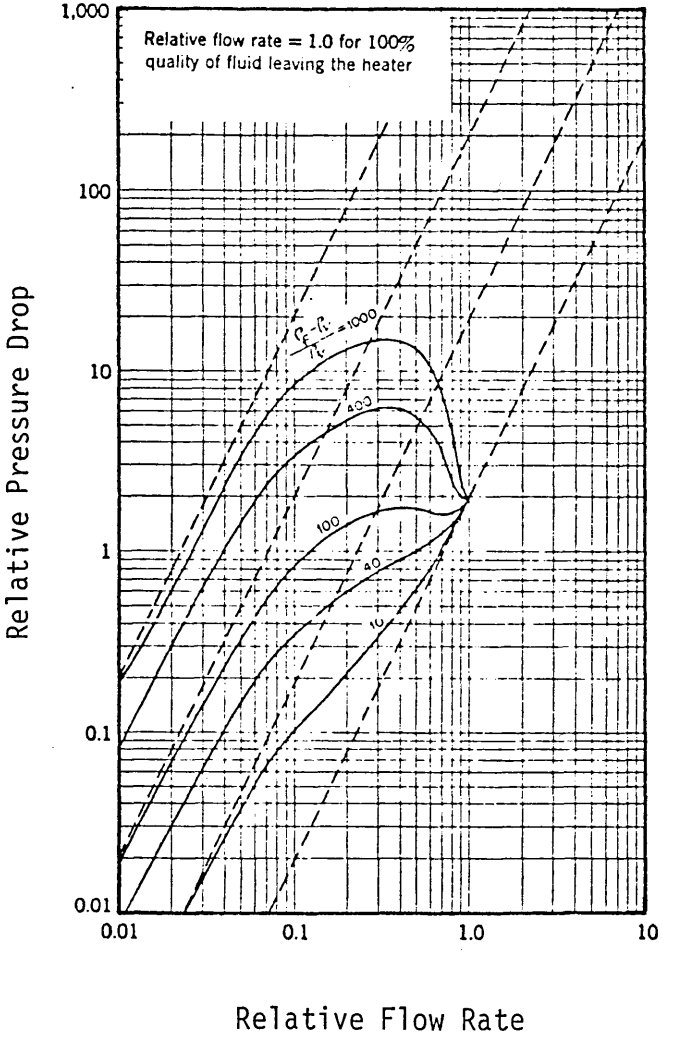


Figure 2.3: Relation between the pressure drop and the flow rate in a once-through boiler tube for five specific volumes of water steam (Fraas et al (1965))

characteristic curve. Examination of the curves in Figure 2.3 shows that, at a constant heat input, if the mass velocity is reduced to a value less than that required for onset of subcooled boiling, the pressure drop increases instead of decreases. This is due to the increasing importance of the subcooled boiling and usually occurs in low pressure systems (Deleas and Bergles (1965)).

2.2.1.2 External characteristics

Figure 2.4 shows the practical external relationship between the pressure head and mass velocity. Curve 1 resembles the pressure drop of a channel in parallel with a large number of channels between the two headers (nuclear reactors, steam generators) or with a large by-pass channel (experimental rigs). Variations of mass in one channel do not have a large effect on the others, nor on the overall pressure drop.

In some practical cases, where channels are operating under forced circulation, the pressure head decreases as the flow rate increases (curve 2); this represents a typical centrifugal pump performance curve.

When a positive displacement pump is used, the external characteristic is similar to curve 3 and the mass velocity is almost independent of the pressure head.

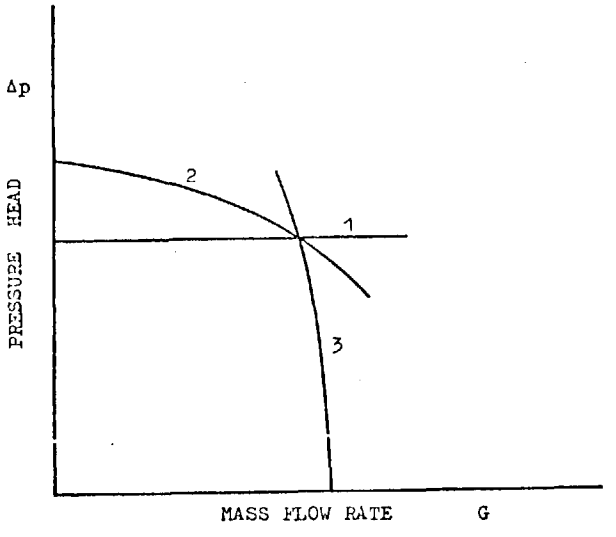


Figure 2.4: External characteristics

2.2.2 The Mechanism of Flow Excursion

Consider a boiling channel under constant operational conditions. The internal characteristic of pressure drop-mass velocity may be described by curve C in Figure 2.5. Suppose the external pressure head curves are of the form of curves C_1 to C_5 which, for example, can be regarded as the pump characteristic at different velocities of the pump. At imposed pressure head of C_1 or C_5, the mass velocity in the channel has only one possible value, G_1 or G_9, respectively. The flow condition in the channel is stable for both points S_1 (liquid flow only) and S_9 (high outlet quality). For a pressure drop curve C_3 there are three possible solutions, G_3 (liquid only), G_5 (low outlet quality), and G_7 (high outlet quality). When the system is operating at point S_5 with the pressure head at curve C_3, a slight decrease of mass velocity from G_5 causes the demand pressure drop to be greater than the supplied pressure head which gives a further reduction in pressure drop; hence, the operating point will shift to S_7. Similarly, a slight increase in mass

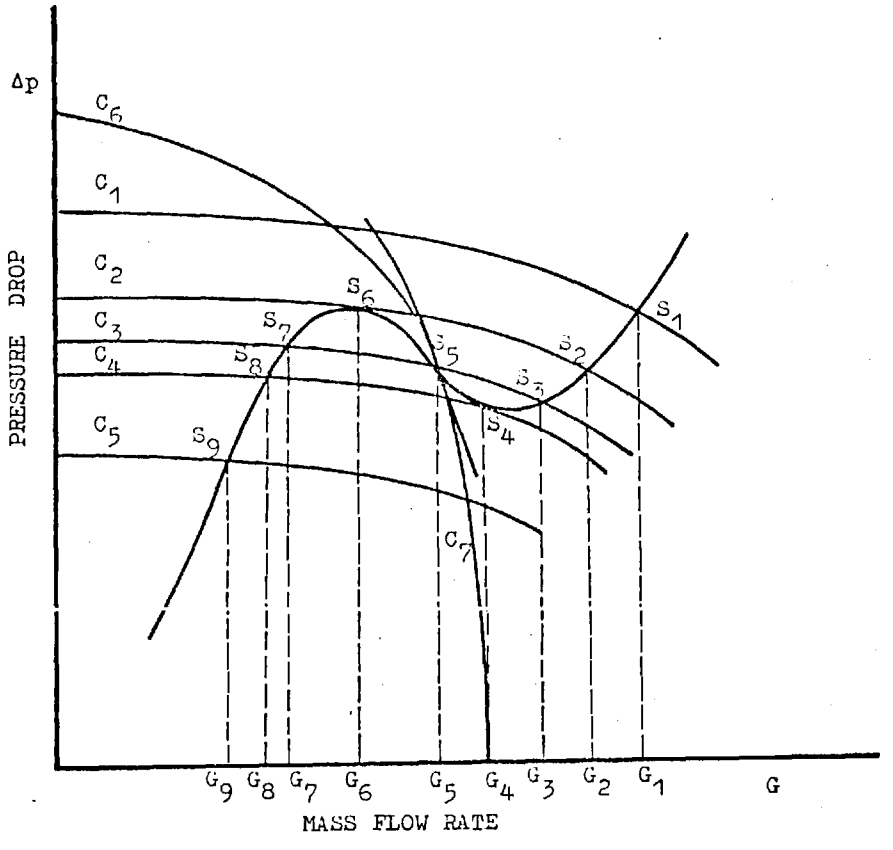


Figure 2.5: Pressure drop-mass flow characteristics

velocity from G_5 causes the operating point S_5 to move to S_3. Operation at point S_5 is, therefore, unstable while the other two points, S_3 and S_7, give stable flow conditions. The operation of point S_7 is established by increasing the mass velocity up to G_7 at constant heat input. On the other hand, if the mass velocity and pressure drop are increased up to G_3 without heat input, point S_3 is reached (Bailey et al (1973)).

Now, suppose the pressure head characteristic, C_3, reduces slowly from stable point S_3 due to, for example, the gradual reduction of the pump velocity to C_4. Further decrease of pressure head beyond C_4 causes the mass velocity G_4 to jump to a lower value of G_8. Similar

mechanisms can occur with slow increasing mass velocity when the operation point is at S_7 and the flow excursion happens from G_6 to G_2. Hence, for pressure head curves C_2 and C_4, there are two solutions for which one of them, S_4 or S_6, is an unstable condition.

In the preceding description, the channel conditions were kept constant. However, if the external characteristic curve is kept unchanged, any slow changes of system parameters may cause similar unstable conditions. Figures 2.2 and 2.3 show the different internal pressure drop characteristics of a boiling channel under different heat input and pressure which may lead to flow excursion under certain conditions of the external pressure head.

For a pressure head characteristic similar to C_6 or C_7, e.g. positive displacement pump, there is only one solution (S_5), and it is possible to operate the channel in the zone S_6-S_4 which is regarded as an unstable zone for those characteristics similar to C_1-C_5.

2.2.3 Stability Criteria

Examination of Figure 2.5 leads to the conclusion that the steady state condition is stable when and only when the slope of the pressure drop characteristic is greater than the slope of the pressure head characteristic:

$$\left(\frac{\partial \Delta P}{\partial G}\right)_{int} > \left(\frac{\partial \Delta P}{\partial G}\right)_{ext} \tag{2.3}$$

In practice, the slope of external pressure head characteristic is always negative (pump) or it is zero (parallel channels). Therefore:

$$\left(\frac{\partial \Delta P}{\partial G}\right)_{ext} \leq 0 \tag{2.4}$$

Thus, a sufficient condition of stability can be expressed as:

$$\left(\frac{\partial \Delta P}{\partial G}\right)_{ext} > 0 \qquad (2.5)$$

Therefore, the evaluation of the possibility of the occurrence of excursive instability requires the calculation of the pressure drop curve for the channel as a function of mass velocity. For constant heat flux systems, e.g. nuclear reactors and electrically heated rigs, where the heat input is independent of the flow conditions, this may be carried out fairly simply. Generally, in the systems where the heat input rate depends on the heat transfer coefficients of the channel and hence on the flow conditions, numerical integration of the channel conservation equations are required to investigate the relationship between the total pressure drop and mass velocity.

2.2.4 Effect of Different Parameters and Preventing the Instability

High voidage in the subcooled boiling region increases the negative slope zone of the internal characteristics curve as was demonstrated by Deleas and Bergles (1965), Stenning et al (1967), and Bergles and Dormer (1969). Therefore, at high heat flux and low pressure the possibility of flow excursions occurring is increased. For a high pressure system (Figure 2.3), subcooled boiling is almost suppressed and this has a stabilising effect. Maulbetsch and Griffith (1966,1967) have reported the operation near the minima of the pressure drop-mass velocity curve (point S_4, Figure 2.5), leading to a critical heat flux due to flow reduction. Similar phenomena have been observed by Margetts (1972) in the economiser of a large number of parallel helically-coiled tubes heated by primary hot gas at the condition of high heat load.

A much more likely mechanism to produce a static instability on a gas heated once-through steam generator is the interaction of heat flux and the secondary side. Moxon (1973) has postulated that the heat flux may be expected to change with the secondary side flow for two reasons: firstly, the change in the secondary side flow will result in a changed heat extraction from the primary side and hence a change in the level of the primary temperature, and secondly, the flow change will result in a changed heat transfer coefficient on the secondary side. The latter has a stabilising effect while the former will be destabilising. The margin against static stability, therefore, will depend on the balance between these two effects.

Beckmann et al (1973) have demonstrated the effects of tube tolerance, gravity and parallel units on the stability of the system. It is shown that incomplete mixing of gas can lead to static instability due to the increasing length of the superheater region.

Almost all the above investigators have improved the instability by the use of inlet throttling or gagging. Flow excursion can be avoided either by increasing the slope of the internal pressure drop characteristic or by decreasing the slope of the external pressure head curve.

Installing a throttle valve at the inlet of the channel increases the single phase friction pressure drop, and hence $(\partial \Delta P/\partial G)_{int}$ is increased. This is the most common method in nuclear reactors, e.g. Hinkley's point "B" and Dungeness's point "B" (Hope (1973)), but the required increase in the supply pressure head may be considerable. This method also prevents other kinds of instabilities. The use of a pump having steeper pressure head-mass velocity curve decreases $(\partial \Delta P/\partial G)_{ext}$, and has a stabilising effect.

2.3 DENSITY WAVE OSCILLATIONS

2.3.1 Introduction

Flow oscillations may occur whenever a flowing fluid is heated and produces a change of density along the heated channel. Oscillations or so called hydrodynamic instabilities can occur in different systems depending on the type of heating or features of configuration. The differences between the different systems are not fundamental in the sense that different instability mechanisms are involved. In all cases the destabilising phenomenon is the flow of a density wave along the channel and the feedback effects of imposed conditions (Boure (1966), Davies and Potter (1966), Bailey et al (1973)). The prediction of instability in all systems consists of the solution of the conservation and related equations. The real differences are embodied in boundary conditions.

2.3.2 The Mechanism

Consider the flow of a fluid within a channel under a constant heat flux. Suppose there is a temporary reduction of the inlet mass flow rate. The rate of vapour production will be increased; this will increase the average void fraction or decrease the average effective density along the channel. The heat transfer behaviour and the total pressure drop will be affected. These responses to a flow change do not occur instantaneously, and they depend upon the transit time of the fluid through the channel (delayed effects). The temporary reduction of the mass flow rate results in a decrease of the total pressure drop, and if the total pressure drop is imposed as a boundary condition, an increase of the inlet flow rate will follow (feedback effects). Therefore, the system behaves like a servomechanism and it may undergo self-sustained or diverging oscillations when the feedback effects are large in amplitude

and out of phase relative to the initial disturbance (Boure (1966), Davies and Potter (1967)).

When a flow is disturbed, the presence of vapour void and evaporation results in changes in the density and velocity distribution which in turn produces phase angle between the different components of the pressure drop and initiating disturbances. The components of pressure drop are shown in Figure 2.6 which illustrates the explanation of Davies and Potter (1967) for the oscillatory behaviour of a once-through boiler.

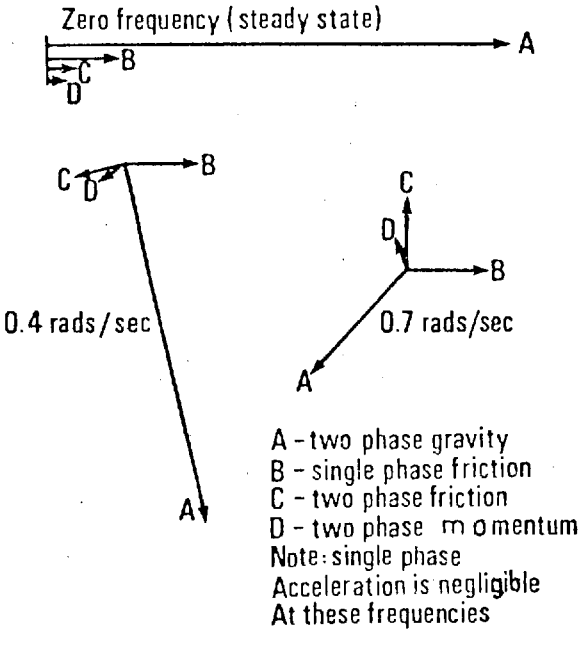


Figure 2.6: Components of pressure drop in steady-state and oscillatory state once-through boilers (Davies and Potter (1967))

In general terms, flow oscillation in boiling systems arises because the vapour production rate depends upon the mass flow rate as a consequence of energy conservation, while the mass flow rate depends upon

the residence of vapour in the system as a result of momentum conservation. An instability can occur in this process when a phase of 180^{o} exists between disturbance in the flow rate and its responses.

2.3.3 Stability of Complete Circuits

In the preceding section, a single channel was considered and it was argued that the dynamic interactions of flow conditions cause the flow oscillation. In the dynamic analysis of practical situations, however, the behaviour of the flow in the channel may be strongly affected by the other circuit features. The simple case of a single channel under constant pressure drop operation is of great theoretical importance and it can be used in the analysis of different circuit configurations by considering the other additional feedback effects.

For example, a closed loop natural circulation system can be investigated in a similar way by adding the dynamic characteristic of the return circuit (downcomer), or in forced convection systems operating with a centrifugal pump, the dynamic characteristic of the pump can be considered quadratic over the range of operating points in the dynamic modelling of the system.

Operation of a bank of parallel channels is of great practical importance in nuclear reactors and steam generators. Theoretically, changes of flow in a single channel can have a negligible effect on the bulk flow and hence on the pressure drop between the headers. Therefore, it is possible in these for flow in one of the channels to oscillate in a mode such that there is no change in the pressure drop across the channel. The simplest case in practice tends to be that of two parallel channels in which the oscillations can be out of phase in each channel so that the total circuit flow remains unchanged and hence no change in the pressure

drop occurs across the tubes (Vezirogla and Lee (1970)).

In practice, several other modes of oscillation may also occur in parallel channels. Crowley et al (1967) have reported that the experimental results of one, two, and three test sections in parallel are identical and that single channel experiments are a valid representation of multi-tube flow for the range of their experiments. The random nature of the flow modes has been reported by Fallows et al (1973) in a study of oscillatory behaviour of three parallel helically-coiled tubes of a high pressure once-through boiler with steam superheat at the outlet (Figure 2.7). These principal modes which have been experienced were:

i) three channels operating uniformly at 120^{o} out of phase;

ii) any two channels operating at 180^{o} out of phase with the third one stable.

Similar experimental results have also been observed by Koshelov (1970). Kakac and Vezirogla et al (1973) have investigated boiling flow instabilities in a four parallel channel system. It is interesting that four channels exhibit oscillations in phase.

Single heated channels with a single phase by-pass are often used experimentally to simulate several parallel channels (Collins and Gacesa (1970)). Any change in flow is therefore manifested immediately by a change in pressure drop across the by-pass and hence across the heated channel too. If the total flow is kept constant, any reduction in by-pass flow can only occur in conjunction with a corresponding increase in heated channel flow. Figure 2.8 illustrates the oscillation of the by-pass and the feed flow of the test section which contained two

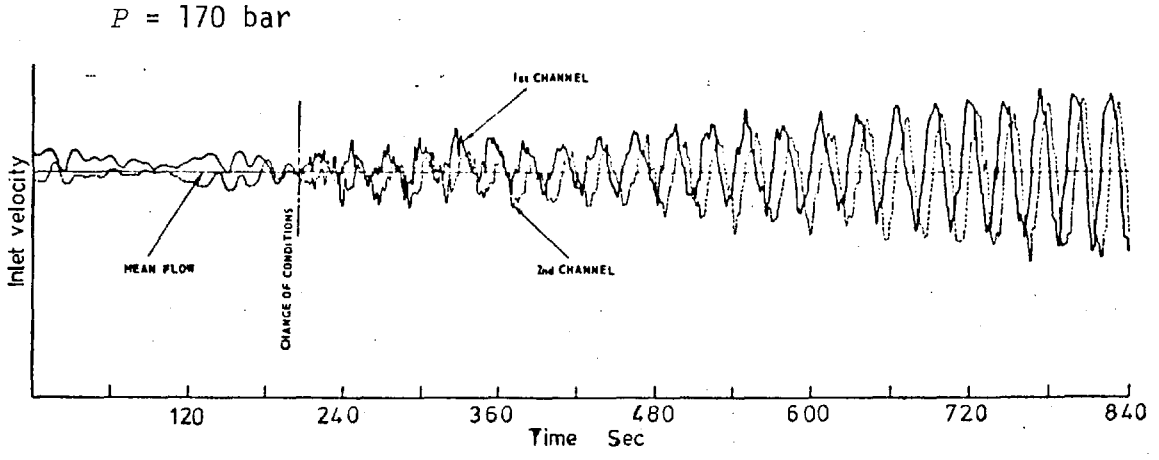


Figure 2.7: Onset of instability in once-through boiler rig for two parallel channels, from Fallows et al (1973)

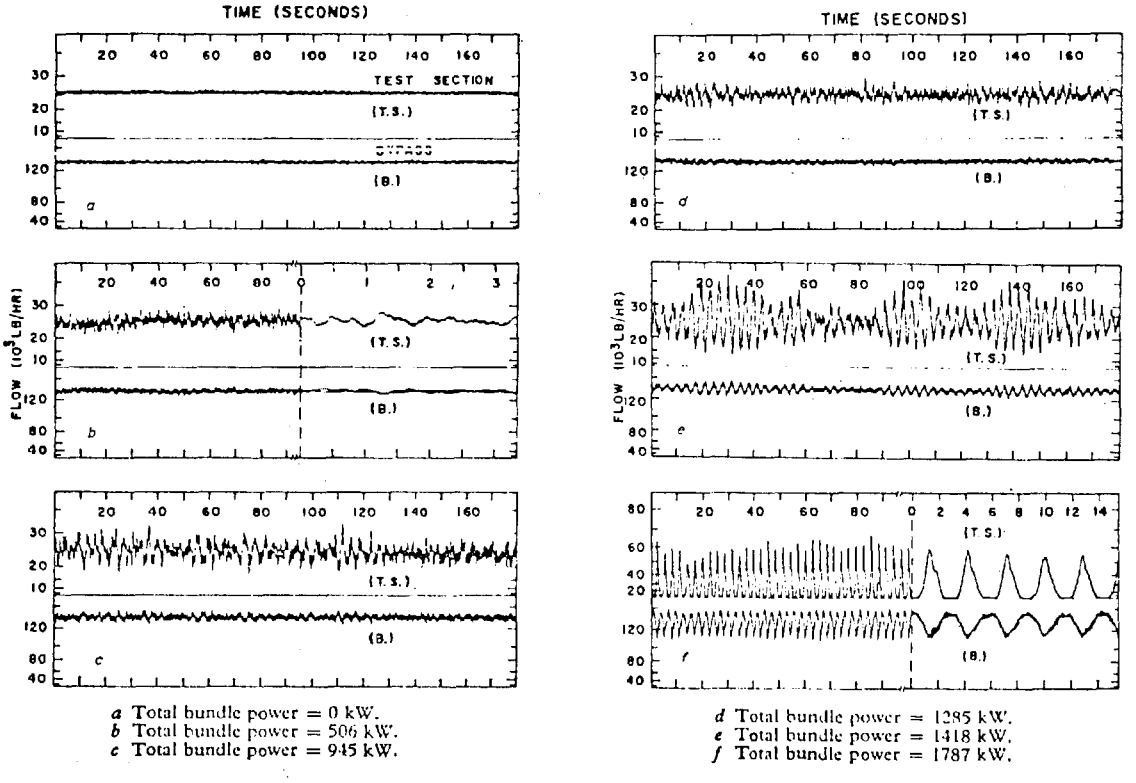
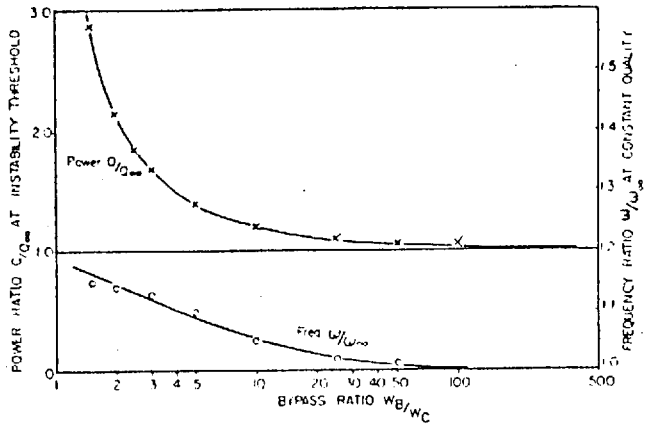


Figure 2.8: Oscillations of the by-pass and heated channel flow at different power levels (Carver (1970))

19-rod electrically heated bundles, as reported by Collins and Gacesa (1970). In Appendix A it has been shown that the effect of a by-pass in parallel to a heated channel corresponds to an inlet resistance in the channel with a constant pressure drop, and a very large by-pass flow is required to simulate a bank of parallel channels. Large by-pass flow is less affected by small changes of the heated channel flow and hence it will result in a small variation of pressure drop across the heated channel. Carver (1970) has thoroughly analysed the effect of the ratio of the by-pass flow to the heated channel (Figure 2.9). It has been shown that the oscillations of the heated channel are less likely to be affected by the feedback effects of the by-pass flow when the by-pass ratio is large enough.



Subscript ∞ refers to infinite by-pass ratio.

Figure 2.9: Effect of by-pass ratio on threshold of stability and frequency for a typical set of flow conditions (Carver (1970))

Generally speaking, in order to simulate several channels by means of one channel and a large by-pass, it is necessary for the by-pass to be able to act as the remainder of the channels in every respect.

Large by-pass ratios can satisfy the hydrodynamic boundary conditions of the heated parallel channels, but from the point of view of heat transfer characteristics, the simulation of parallel channels by a large by-pass is imperfect.

2.3.4 Effects of Different Parameters on the Stability

2.3.4.1 Effects of inlet and exit restriction

Any resistance to flow oscillation which occurs without phase lag with the inlet flow oscillation provides a stabilising effect. Single-phase flow friction fulfils this condition, while the two-phase or single-phase vapour friction have phase differences with change of the inlet liquid flow (Figure 2.6).

Therefore, additional pressure drop at the inlet is stabilising at a given system pressure but for the same reason any additional pressure drop in the two-phase or superheated region (e.g. due to bends, valves, change of cross-section of tube, etc.), is destabilising.

Inlet restrictions of flow by means of "gags" or valves are thus reasonable devices for increasing the stability of the system. This method is effective over a wide range of operating conditions but it is often not possible to cover all operating conditions with a fixed gag (Potter (1973)).

In the case of a bank of parallel channels, stability can be achieved by gagging each tube, e.g. Hinkley point "B" (Hope (1973)). This increases the difficulty and the cost of the maintenance of the system. Also, another disadvantage of this method is the requirement for higher pressure supply by, for example, a pump.

Inlet gagging has a damping effect. Lis (1973) has reported large amplitude oscillations of helically-coiled parallel

tubes in which the negative part of the oscillations are flat and less than the positive part due to the inlet gagging. Furthermore, Beckmann (1973) has pointed out the damping effect of the inlet gag which prevents the flow reversal at large oscillations.

2.3.4.2 Effect of system pressure

Increase of system pressure increases the density ratio ρ_v/ρ_f and thus reduces the void fraction and density effects. The two phase friction and momentum pressure drops are reduced and hence, at a fixed power input and subcooling, increase of pressure provides a stabilising effect.

During the investigation of parallel channels for a once-through boiler with steam superheat, Fallows et al (1973) have reported the effect of pressure on flow stability as is shown in Figures 2.10 and 2.11. The system pressure has been decreased beyond the threshold of the stability to examine the behaviour of the flow oscillations. It has been noted (Figure 2.11) that the amplitude of oscillations has increased at first rather slowly and then very rapidly as the system pressure has been reduced to below the threshold point.

Figures 2.12 and 2.13 exhibit the effect of pressure on flow instability of a natural circulation of single and parallel channels during the test of Mathisen (1967).

2.3.4.3 Effect of inlet subcooling

An increase in inlet subcooling increases the single phase region and decreases the outlet vapour void fraction. Therefore, the single-phase pressure drop is increased while the two-phase friction pressure drop is decreased. Thus, increasing the inlet subcooling

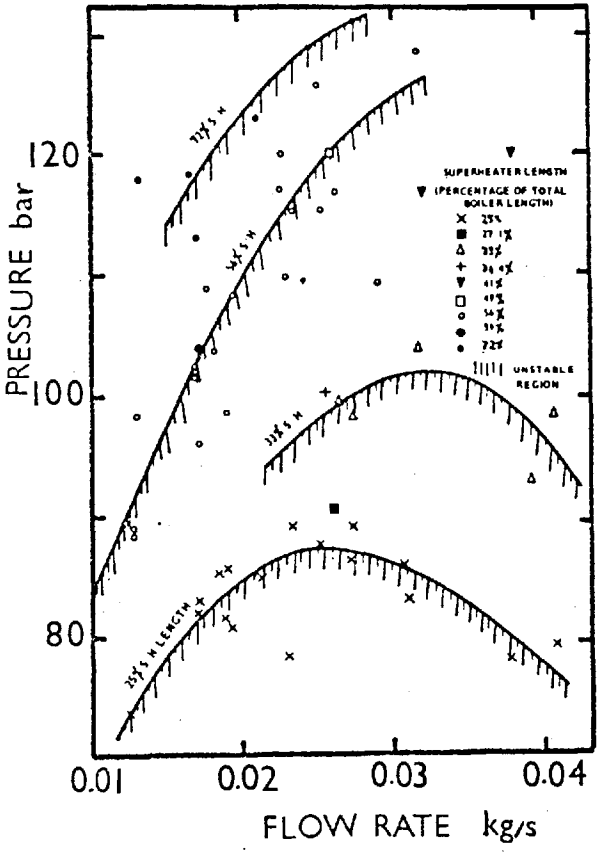
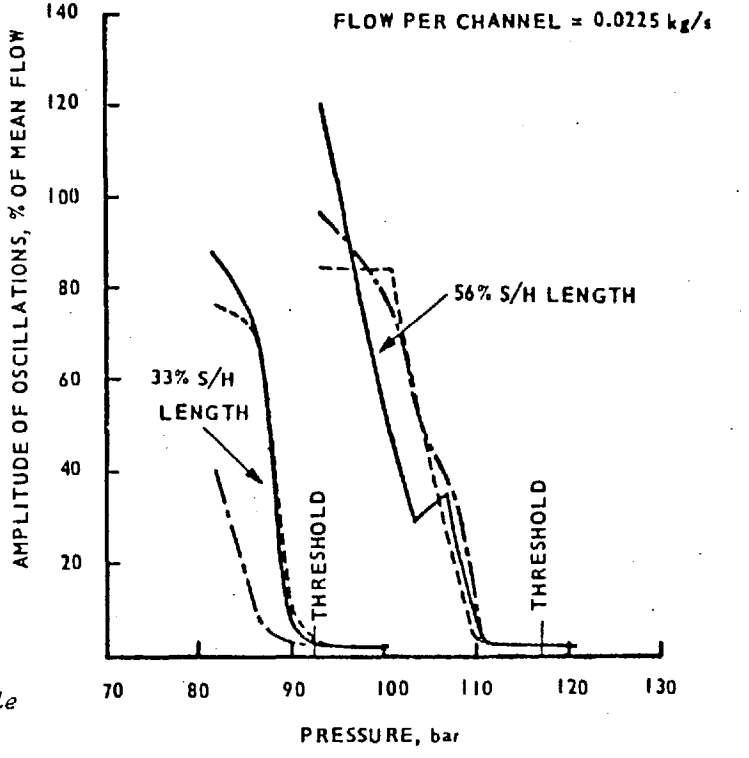


Figure 2.10: Thresholds of flow instability in once-through boiler rig



able

Figure 2.11: Development of oscillations in an unstable flow region

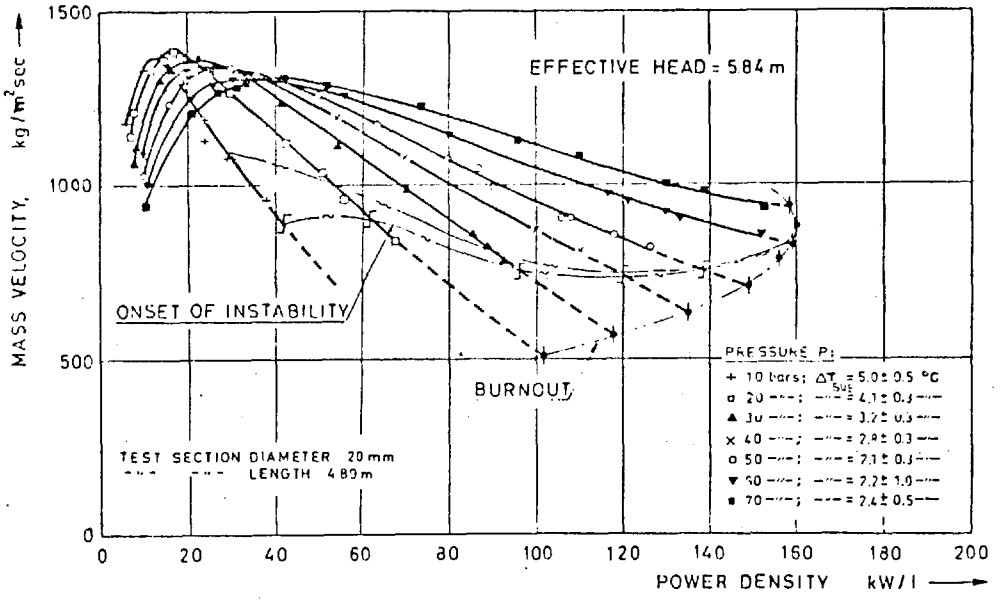


Figure 2.12: Effect of pressure on the flow in single boiling channel

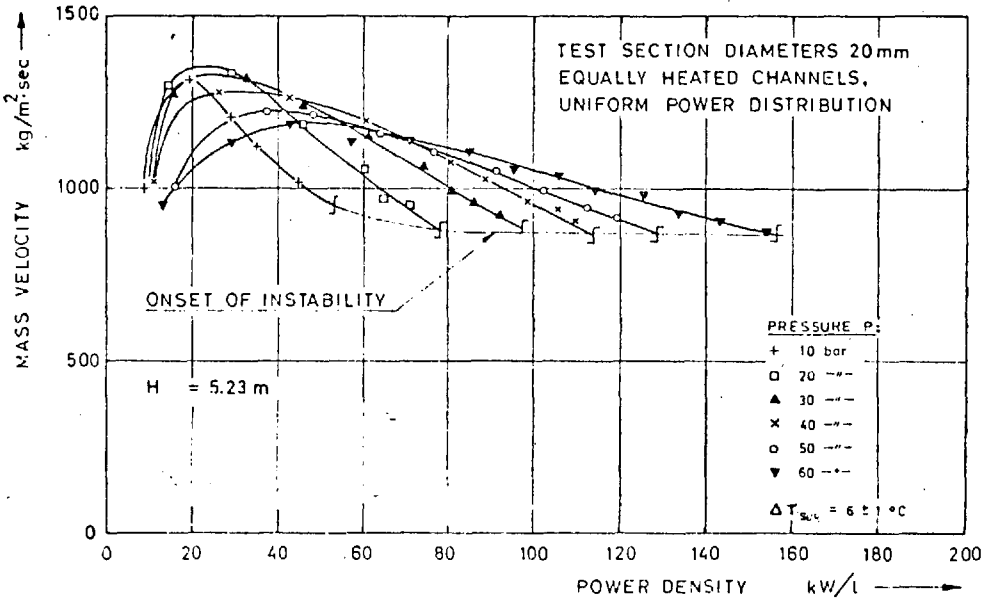


Figure 2.13: Effect of pressure on the flow in parallel boiling channels

stabilises the system at medium and high subcoolings. Figure 2.14 illustrates the effect of inlet subcooling for a natural circulation system (Mathisen (1967)) in which the reverse effect has been noticed at very low inlet subcoolings. Similar experiments by Becker et al (1964) and Spigt (1966) have confirmed such a destabilising effect. It has been postulated that two competing processes are involved when the inlet subcooling is varied, one process being stabilising as described above, and a second destabilising. The destabilising process with increasing subcooling is due to an increase in the subcooled boiling length which, firstly, increases the enthalpy transportation time in the non-boiling region (Neal et al (1967)) and secondly, introduces an inertia term in the two-phase region (Boure (1967)). Therefore, at low inlet subcoolings, the feedback effects are dominated by the destabilising process; nevertheless, as the inlet subcooling is increased, it exhibits a minimum as shown in Figure 2.14. Crowley et al (1967) observed similar effects of inlet subcooling in a forced circulation system. Moreover, they noticed that starting a system with high subcoolings can lead to a large amplitude oscillation.

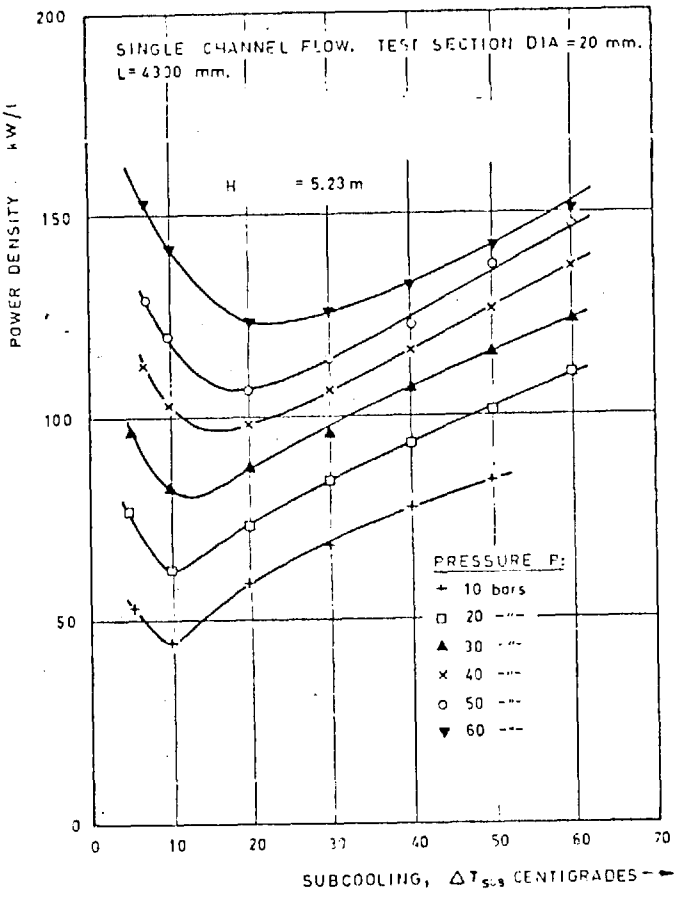


Figure 2.14: Effect of subcooling and pressure in single boiling channel flow

2.3.4.4 Effect of mass velocity and power input

At a fixed inlet subcooling and system pressure, a reduction of mass flow rate or an increase of power input reduces the single-phase liquid region and increases the vapour void fraction or the length of the superheater region; thus, the system is destabilised (Figures 2.12 and 2.13).

Collins et al (1970,1971) have tested the effects of mass velocity and power input on flow oscillations in a 19-rod bundle. They have found that the frequency of oscillation increases with mass

velocity as well as power input to the channel. A similar trend has been reported by Fallows et al (1973) for a system of counterflow gas fired steam generators. Figures 2.10 and 2.11 show the effect of heat flux in terms of the length of the superheater region. Figure 2.11 compares the amplitude of oscillation for two cases of 33% and 56% superheater length. The rate of the increase of amplitude is more rapid for the system operating at higher heat flux (56% superheater length).

The effect of the flow oscillation on dryout has been pointed out by Fallows et al (1973). They have found that for the maximum amplitude of oscillations encountered in their experiments, the movement of the dryout boundary did not exceed ± 4.5% of the total length from the steady-state position of this boundary. Moreover, they have proposed a correlation which defines the boundaries of oscillatory flow in terms of the threshold pressure as follows:

$$P = (113.4\ R + 56.1) - (0.074 - 0.061\ R)\ \left[(62.2\ R + 10.6) - \dot{q}''\right]^2 \quad (2.6)$$

where P is pressure in bars and q is the mean heat flux in kW/m^2 and:

$$R = \frac{\rho_{sh}}{\rho_{sub}} \frac{\Delta P_{sh}}{\Delta P_{sub}} \quad (2.7)$$

ρ_{sub} and ρ_{sh} are the average fluid densities in the subcooled and superheater regions, respectively. The pressure losses are calculated between the boiling boundaries and the headers.

The threshold pressures predicted by equation (2.6) have been compared with the measured to within ± 10% accuracy, based solely on the experimental data of the authors. Therefore, the general validity of the correlation for different once-through boilers is open to

question.

2.3.5 Methods of Analysis

2.3.5.1 General equations

Analysis of flow oscillation starts with the prediction of the transient behaviour of the system. The dynamic model of a boiling channel is described by a system of non-linear partial differential and algebraic equations which consist of the conservation and constitutive equations. These and their related relationships have been discussed by Boure (1972,1975) under the heading "Two Fluid Models". The one-dimensional conservation equations of each phase are as follows:

Mass conservation:

$$\frac{\partial(A_k \rho_k)}{\partial t} + \frac{\partial(A_k \rho_k u_k)}{\partial z} = \Gamma_k \qquad (2.8)$$

Momentum:

$$A_k \frac{\partial p}{\partial z} + \frac{\partial(A_k \rho_k u_k)}{\partial t} + \frac{\partial(A_k \rho_k u_k^2)}{\partial z} + A_k \rho_k g \cos\beta + F_{ki} + F_{kw} = 0 \qquad (2.9)$$

Energy:

$$\frac{\partial(A_k \rho_k H_k)}{\partial t} + \frac{\partial(A_k \rho_k u_k H_k)}{\partial z} = A_k \left[\frac{\partial p}{\partial t} + u_k \frac{\partial p}{\partial z}\right] + u_k F_{kw} + q_{ki} + q_{kw} \qquad (2.10)$$

With the interface relationships as:

Mass transfer:

$$\Sigma \Gamma_k = 0 \qquad (2.11)$$

Momentum:

$$\Sigma F_{ki} = 0 \tag{2.12}$$

$$\Sigma F_{kw} = F_{TP} \quad \text{(two-phase friction pressure gradient)} \tag{2.13}$$

Energy:

$$\Sigma q_{ki} = 0 \tag{2.14}$$

$$\Sigma q_{kw} = \dot{q}''' \quad \text{(heat input per unit volume)} \tag{2.15}$$

where the subscripts k (= l and v) refer to liquid and vapour phases, respectively. Also, $A_l = 1 - \alpha$ and $A_v = \alpha$.

2.3.5.2 Assumptions and simplifications

A rigorous analysis of the system in terms of six basic differential equations requires the information about the interface conditions or so-called constitutive equations which are not well established for the different two-phase flow patterns. Unfortunately, the more numerous the conservation equations are, the more detailed the constitutive laws have to be. As a consequence, most of the existing models employ further assumptions to reduce the number of conservation equations to three or four in some cases. The simplifications are based on the following main assumptions.

1. In all existing models, a pair of momentum equations (2.9) are replaced by one momentum conservation for the two-phase mixture and one empirical correlation for the "slip equation" which results from the elimination of $\partial p/\partial z$ between the two equations (2.9).

2. The densities of the liquid and vapour phases are assumed to be constant or a function of enthalpy, hence allowing the momentum equation to be uncoupled from the other conservation equations.
3. In the two-phase region, the enthalpy of the liquid and vapour phases are assumed equal to the saturation values. It therefore allows only one continuity and one energy equation to be written for the two-phase mixture.

The first assumption may be controversial in the sense that the partial differential equation for the dynamics of slip is replaced by a non-differential correlation. This requires clear examinations particularly when fast transient or large pressure drop flows are involved. However, no serious study has yet been made for the reason that almost nothing is known about the distribution of wall friction on the phases and about the interface momentum exchanges.

The second assumption is less valid for systems having high pressure drop. And also the assumption of constant densities may cause unrealistic results due to the existence of long single-phase regions particularly in once-through boilers in which the system pressure is relatively high.

Finally, the last assumption hardly applies to the case of subcooled boiling flow. The effect of thermal non-equilibrium is taken into consideration by some investigators. This has been achieved by writing either two continuity equations (Zuber and Dougherty (1967) and Hancox and Nicoll (1971)), or two energy equations (Bowring (1962), Verheugen et al (1967) and Dijkman (1969)) for two separate phases. In the former case, the information of the vapour generation rate is required while in the latter approach a heat distribution

parameter between the phases is introduced.

Generally, the number of differential equations required depends on the number of physical parameters which one wishes to take into consideration. In all published models, the starting point has been the formulation of three principal laws of conservation for two-phase mixtures.

By considering the above assumption and neglecting the frictional, potential and kinetic energies, the system of partial differential equations are reduced to the following:

Continuity:

$$\frac{\partial}{\partial t}\left[(1-\alpha)\,\rho_l + \alpha\,\rho_v\right] + \frac{\partial}{\partial z}\left[(1-\alpha)\,\rho_l\,u_l + \alpha\,\rho_v\,u_v\right] = 0 \qquad (2.16)$$

Momentum:

$$\frac{\partial}{\partial t}\left[(1-\alpha)\,\rho_l\,u_l + \alpha\,\rho_v\,u_v\right] + \frac{\partial}{\partial z}\left[(1-\alpha)\,\rho_l\,u_l^2 + \alpha\,\rho_v\,u_v^2\right] + \frac{\partial p}{\partial z} + \tau_w + \left[(1-\alpha)\,\rho_l + \alpha\,\rho_v\right] g\cos\beta = 0 \qquad (2.17)$$

Energy:

$$\frac{\partial}{\partial t}\left[(1-\alpha)\,\rho_l\,H_l + \alpha\,\rho_v\,H_v\right] + \frac{\partial}{\partial z}\left[(1-\alpha)\,\rho_l\,u_l\,H_l + \alpha\,\rho_v\,u_v\,H_v\right] = \dot{q}''' \qquad (2.18)$$

The above system of equations is to be solved for the main parameters α, u_v, u_l and p in which there are more unknown parameters

than the equations. A relation between the main parameters has to be provided by means of a correlation, for example, for slip ratio.

The various existing models differ in the degree of completeness retained in the conservation equations, the degree of sophistication applied in the representation of the flow characteristics and in the solution technique. In general, the models may be grouped into two classes. In the first, the non-linear equations have been directly solved numerically and the solutions are obtained as a function of time. In the second class, further simplifications are made, then the equations are linearised, and in most cases direct analytical solutions are obtained in, for example, the frequency domain. All models, whether linear or non-linear, have been used to find the flow conditions beyond which a single perturbation from the steady-state will result in unbounded oscillations (stability threshold).

In the following sections, typical analyses of linear approaches will be reviewed with respect to their structure and the nature of prediction. Then analyses of the non-linear methods will be reviewed; methods which form the foundation for the present work.

2.3.5.3 Linear analyses

The simplest models such as those presented by Quandt (1960) and Wallis and Heasley (1961) imply small perturbations about steady-state conditions. Then the linearised equations lead to a determination of the transfer function relating the mass flow rate and the heat flux perturbations. Quandt has argued that the flow is governed by second order equations similar to those describing the motion of a damped spring-mass system where the damping coefficient is an inverse function of the heat flux. The stability threshold is then

defined as the locus of conditions for which the damping coefficient has zero value. Wallis et al used a Lagrangian approach. They have used a perturbation of inlet velocity of the form of $v_o e^{st}$ to investigate the stability by Nyguist criterion. v_o is very much smaller than the steady-state velocity and s is a complex number.

Boure (1966) has expanded the analysis of Wallis and Heasley (1961), which provides more insight into the mechanisms contributing to flow instability. The analysis is based on the one-dimensional conservation laws and the assumption of variable density single-phase model which yields a fifth order exponential polynomial as the characteristic equation. Zuber (1967) has extended this analysis to include the effects of the drift velocity (i.e. relative velocity between the vapour and liquid phases). In the above techniques, the stability threshold is defined as the locus of conditions at which the real part of any of the roots of the characteristic equation changes sign from negative to positive. In the extension of their investigations, Boure (1966,1967) and Ishii and Zuber (1970) have proposed dimensionless parameters which are useful tools in reducing the number of independent parameters. The basic concepts of the principal dimensionless groups used by Boure and Ishii and Zuber are compared by Boure et al (1973) for the case of homogeneous and equilibrium flows. In a constant pressure and inlet velocity, Ishii and Zuber have presented the stability boundaries in a two-dimensional plane where the axes are defined as:

$$N_{sub} = \frac{\rho_l - \rho_v}{\rho_v} \frac{\Delta H_{sub}}{H_{fv}}$$ The subcooled number representing void and subcooled effects (2.18)

$$N_{pch} = \frac{\Omega L}{u_{in}}$$ The phase change number representing flow and heat input effects (2.19)

where the "characteristic frequency", Ω, is defined as:

$$\Omega = \frac{\rho_l - \rho_v}{\rho_l} \frac{\gamma}{\rho_v} \tag{2.20}$$

γ is the rate of the generation of vapour per unit volume which for the case of thermal equilibrium is given by:

$$\gamma = \frac{P}{A} \frac{\dot{q}''}{H_{fv}} \tag{2.21}$$

Figures 2.15 and 2.16 show typical stability planes compared to the data of Solberg (1966) and Chexal and Bergles (1973). Assuming homogeneous flow with negligible gravity effects, the stability criterion can be derived in the following form (Chexal (1973)):

$$N_{pch} - N_{sub} < \frac{2\left(k_i + \frac{L f_{sp} C_m}{2d} + k_e\right)}{1 + \frac{1}{2}\left(\frac{L f_{sp} C_m}{2d} + 2k_e\right)} \tag{2.22}$$

where k_i and k_e refer to inlet and outlet restrictions, respectively, and c_m is the two-phase friction factor coefficient. The above simplified stability criterion (equation (2.22)) predicts the boundary of stability to within about 15% (more stable system) for water and within 50% for Freon 113 (more unstable system) according to Chexal and Bergles.

Recently, Grass and See (1973) have shown sustained oscillations due to the interaction of the enthalpy, density and mass flow rate by analysing the energy, continuity and state equations. The stability maps of the theory and experimental data have been constructed on the basis of two-dimensionless groups. Complex shapes of the

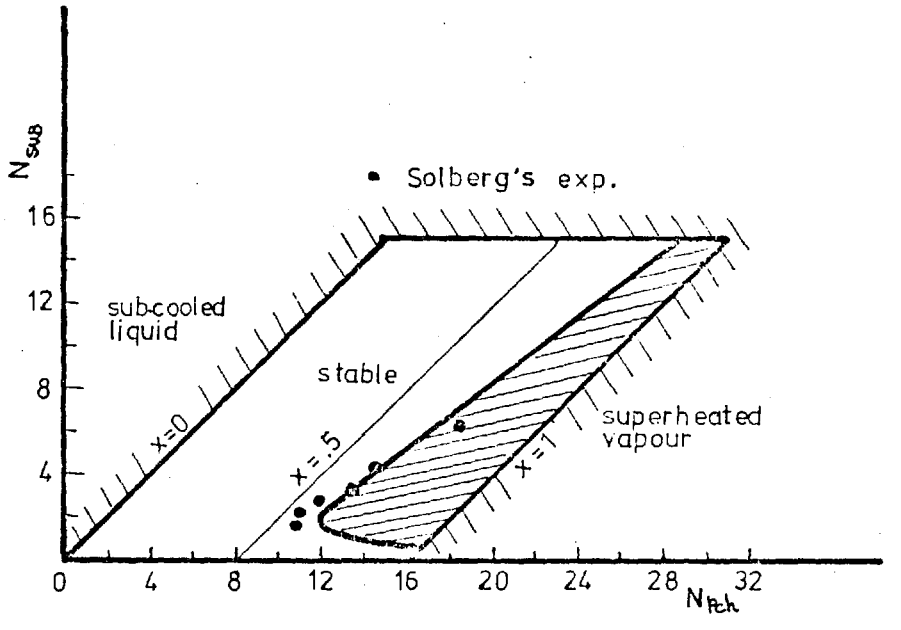


Figure 2.15: Stability plane of Ishii and Zuber (1970)

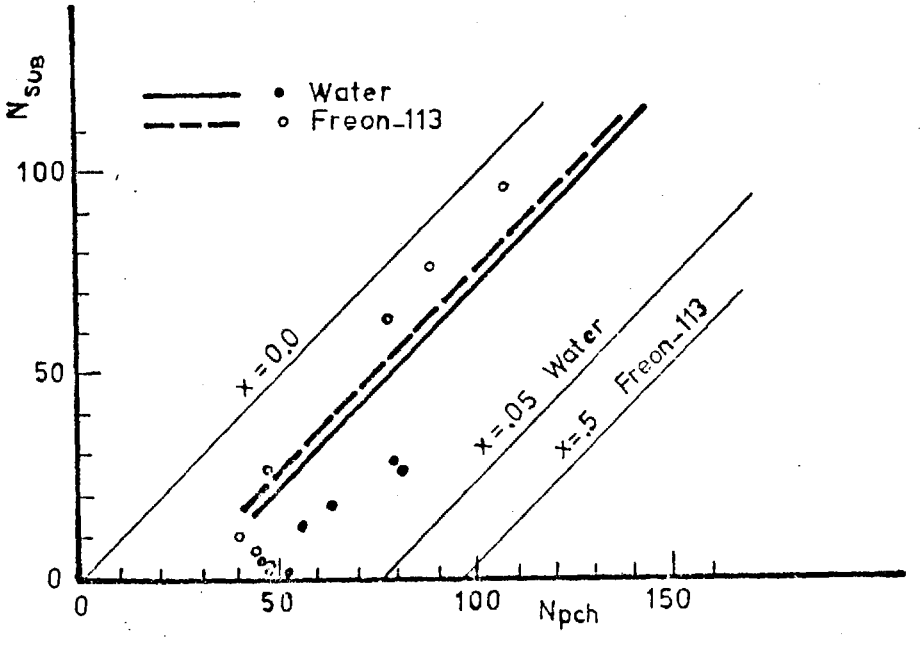


Figure 2.16: Comparison of simplified stability criterion of Ishii and Zuber with Chexal and Bergles's experiment (1973)

thoeretical and experimental stable regions have been reported with qualitative agreements. Conclusions have been made that the momentum equation, and the pressure drop boundary condition of the heater, may not take a part in sustaining the stability but play an important role in determining whether or not the instability actually exists.

Within the framework of linearised approaches, the computer codes STABLE by Jones (1961-1964) and LOOP by Davies and Potter (1966,1967) are the most attractive ones. Jones (1961) has taken into consideration the slip ratio of Bankoff (1960) modified to give better representation of the two-phase region. A characteristic equation for the system was obtained employing Laplace transformations and numerical integrations along the boiling channel. Efferding (1968) has developed a similar model for a superheater or a supercritical once-through boiler which can be incorporated with STABLE for the dynamic prediction of sub-critical once-through boilers. STABLE has been in operation for many years in the USA. These codes have been developed for straight tubes only.

Attempts to concentrate more on understanding the mechanisms of stability without the implication of numerical integration have been made by Davies and Potter (1966) in the development of the LOOP code. The assumptions of the LOOP program are similar to those made by Boure (1967). The main differences lie in the density and friction assumptions and in the boundary conditions on the system pressure drop. The superheated region is also included in the LOOP code which enables it to be used for the analysis of once-through boilers with steam superheat at outlet. In the LOOP code, Laplace transformations of linearised conservation equations are determined for each section of the boiler. The outputs of this code are the open loop response $\Delta\ (\Delta P_{tp} + \Delta P_{sh})/\Delta\ (\Delta P_{sub})$

and the closed loop response $(\Delta G/G)/\Delta\ (\Delta P_{sub} + \Delta P_{tp} + \Delta P_{sh})$. The open loop response is dimensionless and the closed loop response has dimensions equal to the reciprocal of the input pressure drop values in the program. A further useful response is the reciprocal closed loop response which shows the response of the channel pressure drop to a flow perturbation. Instability is investigated by the Nyguist criterion (i.e. the open loop response should not cross the negative real axis outside (-1,0) on a polar diagram). This code has been frequently used in the UK (Moxon (1973)).

2.3.5.4 Non-linear analyses

In the non-linear analyses, such as those presented by Currin et al (1961), Meyer and Rose (1963), Carver (1967) and Solberg and Bakstad (1967), the one-dimensional conservation equations are solved numerically in the time domain. The basic principle of these techniques is to divide space and time into discrete intervals and to solve the conservation equations (2.16), (2.17) and (2.18) over each mesh.

The method of assessing stability is to disturb one of the system parameters from its steady-state value, for example, by a step function, and to monitor the output parameters. If the amplitudes of the responses, for example, successive oscillation, decay and die out, the condition is deemed stable; and if they persist and grow, the condition is regarded as unstable. Another method to assess the stability threshold is to determine the frequency response of the total pressure drop for sinusoidal variations imposed on the inlet flow. This method is similar to the transfer function approach in the linear analyses.

One of the non-linear programs which is widely used in the UK is SLIP which was developed by Moxon (1968) for solving the

thermal-hydraulic equations of electrically heated test rigs with straight tubes. Some aspects of the SLIP are as follows:

SLIP can be used to calculate the temperature distribution in the walls of the heated tube and hence the inside wall temperature in contact with the fluid, or the power input can be assumed to go directly to the coolant with uniform distribution along the tube. It solves equations (2.16) to (2.18). The ratio of velocities or slip, $S = u_v/u_f$, is considered either constant, or depends on the local void fraction as in the correlation of Bankoff (1960) modified for steam-water flows by Jones (1962) as follows:

$$S = \frac{1 - \alpha}{k - \alpha} \quad , \quad \text{Bankoff (1960)} \tag{2.23}$$

where $k = 0.85$

$$S = \frac{1 - \alpha}{(k_1 - \alpha) + (1 - k_1)\ \alpha^{k_2}} \quad , \quad \text{Jones (1962)} \tag{2.24}$$

where $$k_1 = 0.71 + \frac{0.29\ p}{3206.2}$$

$$k_2 = 3.33 + 0.18\ \left(\frac{p}{1000}\right) + 0.46\ \left(\frac{p}{1000}\right)^2$$

and p is system pressure in psia.

In the subcooled region, equations (2.16) and (2.18) are solved for a fixed value of velocity by a central space and backward time differences technique up to the boiling boundary where $H = H_f$. In the two-phase region, the continuity equation (2.16) is rearranged as:

$$(\rho_f - \rho_v) \frac{\partial \alpha}{\partial t} = \frac{\partial G}{\partial t} \tag{2.25}$$

assuming $$U = [1 + (S - 1)\,\alpha]\, u_f \tag{2.26}$$

The mass flow rate is defined as:

$$G = \frac{1 + \left[\frac{S\,\rho_v}{\rho_f} - 1\right] \alpha}{1 + (S - 1)\,\alpha}\, \rho_f U \tag{2.27}$$

Eliminating $\partial\alpha/\partial t$ between equations (2.18) and (2.25) yields:

$$\frac{\partial U}{\partial z} = \left[\frac{1}{\rho_v} - \frac{1}{\rho_f}\right] \frac{\dot{q}'''}{H_{fv}} \tag{2.28}$$

which is integrated by the trapezoidal rule to find U at each mesh (z_1, t_1). This value is substituted in the finite difference form of equation (2.25) to obtain values of $\alpha(z_1, t_1)$ in terms of the slip ratio, which is either constant or can be calculated by an iteration procedure using equations (2.24). The whole process is repeated at each equal length interval along the tube for a fixed time t_1 until the integration from the inlet to the outlet of the two-phase region is completed. The momentum equation (2.17) is integrated by the trapezoidal rule to give the pressure drop. Then the sum of the total circuit pressure drop including the pump is set equal to zero to find the inlet mass flow rate by an iteration procedure. Figure 2.17 illustrates a typical output of the SLIP program at different heat inputs. Also, a comparison of the outputs of SLIP and LOOP are made in Figure 2.18.

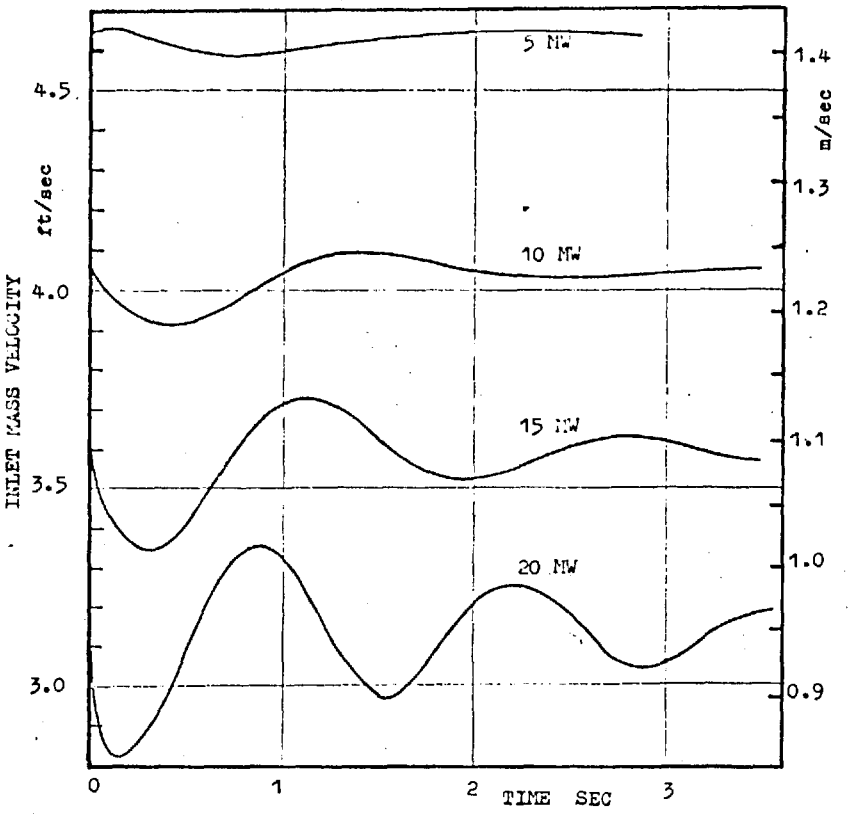


Figure 2.17: Response to flow perturbation calculated with SLIP (Bailey et al (1972))

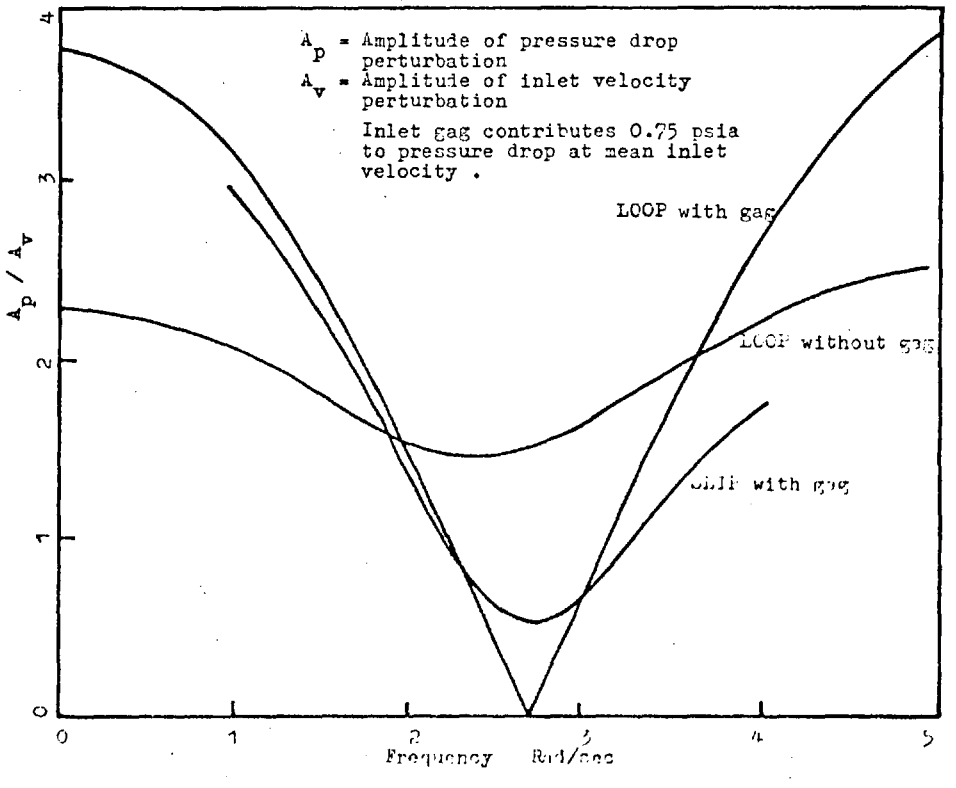


Figure 2.18: The variation of the magnitude of pressure drop perturbation with frequency predicted by SLIP and LOOP (Bailey et al (1972))

Some investigators, such as Hannson and Axelsson (1965), Spigt (1966), and Dijkman (1969), have considered thermal non-equilibrium in the subcooled boiling region which is treated according to the model of Bowring (1962). The two energy equations (equation (2.10)), are considered for the liquid and vapour phases. Then the total heat supply is split into two parts. A part χ of the total heat is applied to the vapour phase while the rest, $(1 - \chi)$, is supplied for warming up the liquid phase. Accordingly, the two energy equations are written as follows:

$$\frac{\partial}{\partial t}\left[(1-\alpha)\,\rho_l\,H_l\right] + \frac{\partial}{\partial z}\left[(1-\alpha)\,\rho_l\,u_l\,H_l\right] = (1-\chi)\,\dot{q}''' \qquad (2.29)$$

$$\frac{\partial}{\partial t}\left[\alpha\,\rho_v\,H_v\right] + \frac{\partial}{\partial z}\left[\alpha\,\rho_v\,u_v\,H_v\right] = \chi\,\dot{q}''' \qquad (2.30)$$

The ratio χ is given by a correlation based on experimental and theoretical studies. Bowring (1962) and Hannson et al (1965) have considered χ to be constant while Spigt (1966) and Dijkman (1969) have chosen χ as a function of local temperature of the liquid phase.

Zuber (1967) has shown that, in vapour-liquid systems, the net vaporisation term, γ_v, plays the dominant role in determining the degree of thermal non-equilibrium of the two-phase mixture. In addition to equations (2.16) to (2.18), he has introduced the vapour phase continuity equation in the form of equation (2.8), to formulate the two-phase non-equilibrium flow.

Most of the existing models are based on the assumption that there is complete mixing across the channel at any given section. Only Hancox and Nicoll (1971) have considered the effects of radially non-uniform voids and velocity profiles in the modelling of the

two-phase dynamics. Development of such a model in helically-coiled tubes requires void distribution at any cross-section along the boiler. Such information is almost non-existent in the open literature for helically-coiled tubes.

Most of the codes represent, or may be considered to represent, a nuclear or electrically heated boiling channel. The heat source is, therefore, considered either to be constant or at a given value along the channel at any time.

Brereton and Carling (1967) have developed the program NUBOIL which evaluates the transient and steady-state performance of a counter flow gas heated once-through boiler. The boiling region in this model is treated as homogeneous with variable density as a function of pressure and entropy. The heat flux is calculated from the heat transfer characteristics of the primary (gas) and the secondary (water) flows. Various assumptions and simplifications have been made in NUBOIL which do not adequately represent some aspects of a boiling flow. e.g. The code ignores the subcooled boiling and the post-dryout region along the steam generator. The heat transfer coefficients on both sides vary in proportion to mass flow rates raised to the 0.8 power which hardly fulfils the boiling heat transfer rate. The two-phase friction factor is assumed independent of the vapour void fraction or quality. The thermal inertia of the gas side is neglected.

Preston et al (1973) have compared the NUBOIL code with the results of transient experiments which were carried out on a helical tube once-through boiler rig simulating the cross-counter flow gas/water system of a nuclear heat exchanger. Some appreciable discrepancies have been reported between the model and the experimental results. A number of modifications have been introduced to improve the

response prediction of the model.

More attention has been recently focused on different aspects of once-through boilers. A number of investigators (Taylor (1973), Bickers and Carstairs (1973), Knowles and Robins (1973) and Beckmann et al (1973)) have attempted to predict the transient response of once-through steam generators. Most of the models are based on simplified assumptions which are not developed for predicting the stability behaviour of the boiler. Moxon (1973) has reported a program SUPERSLIP which is modified from SLIP. In SUPERSLIP, the heat source can be either electric or a counter flowing primary fluid. This model is preferable to the others in the sense that the basic assumption and approach is most appropriate for a boiling system. At the present time, the work has been classified confidential, and the information about it is limited only to the report of Moxon (1973).

Moxon has mentioned the stabilising effect of the flux-flow couplings in the experimental test of helically-coiled tube once-through boilers in which the heat source was a primary counter-flowing pressurised water. The frequency response of the outlet mass velocity (Figure 2.19) has been constructed by using the SUPERSLIP code (for steady-state results) and the modified LOOP code (LOOP 20). This has been compared with the corresponding plot with no flux-flow couplings (Figure 2.20). A greatly reduced exit velocity perturbation results particularly at higher frequencies for the case of flux-flow couplings (Figure 2.19).

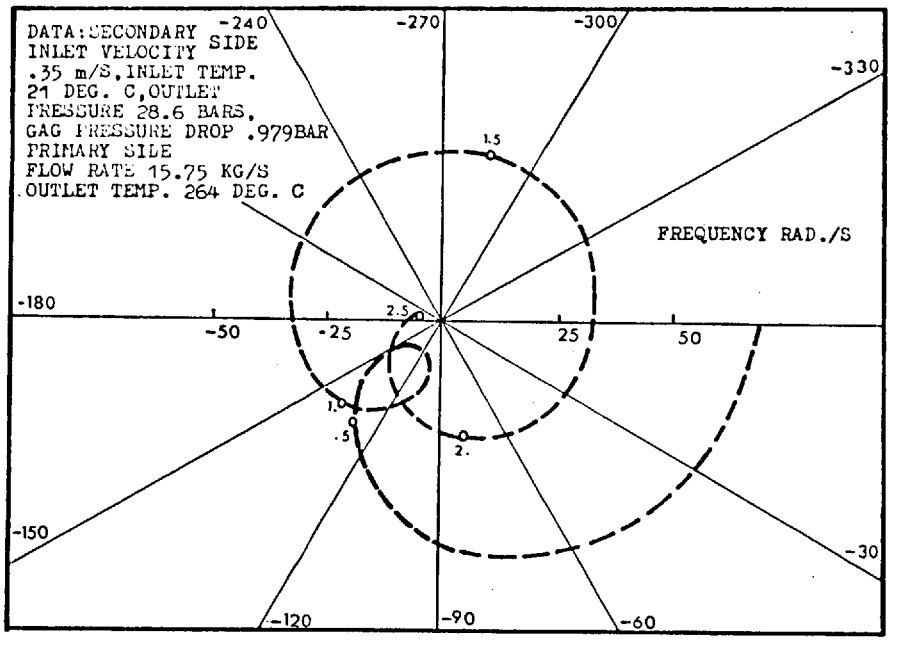


Figure 2.19: Frequency response of outlet mass to inlet velocity perturbations. With flux-flow coupling (Moxon (1973))

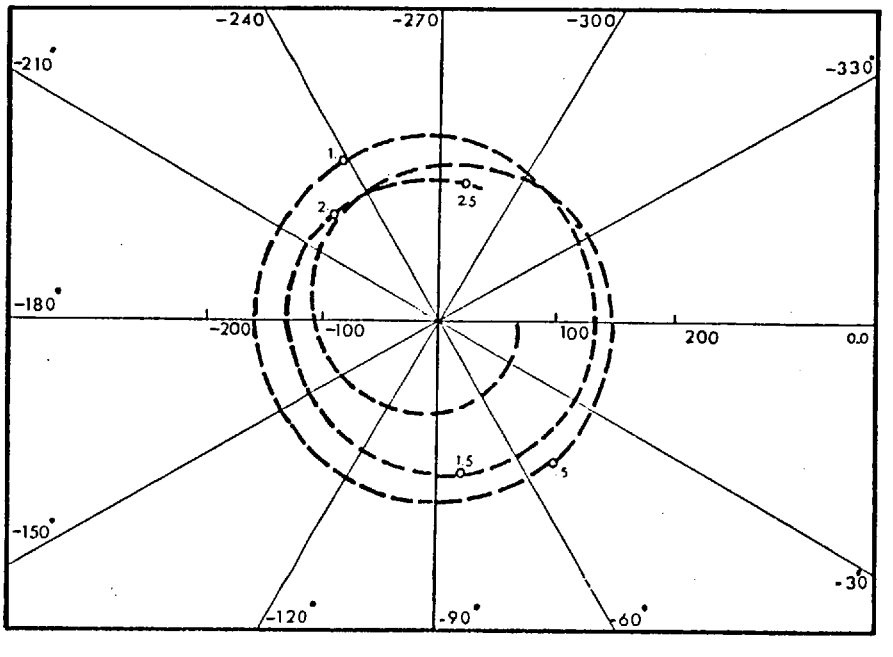


Figure 2.20: Frequency response of outlet velocity to inlet velocity perturbations. No flux-flow coupling (Moxon (1973))

2.4 DISCUSSION AND CONCLUSION

For flow along heated channels, the conservation equations are often written in one space dimension in terms of average values across the channel. In this form, it is necessary to use empirical correlations for the viscous forces and heat transfer coefficients. In the two-phase region, additional empirical correlations are required to take into consideration the different velocity distributions of the phases. This leads to a set of complete non-linear partial differential equations, the direct solution of which is not possible except in trivial cases.

The use of correlations is suppressed in some investigations by making simplifications and linear approaches. Such models are usually most economic in computer time. The use of empirical correlations and detailed treatments of the system usually favours the non-linear and numerical methods.

Although the linear approaches have the advantages that they completely avoid the problem of determining what is exciting the oscillations, but a system may be stable against an infinitesimal disturbance and unstable against a finite disturbance. This can be misleading since it results from the linearisation of the governing equations. It has not been shown that when the non-linearity of the equations is accounted for that disturbances will continue to grow; it may well reach a stable limit of tolerable amplitude. Moreover, it is possible for a system to be stable for infinitesimal disturbances but unstable for large ones.

The steady-state solutions have to be calculated in all non-linear models and this provides an initial means of testing the model against experimental data; hence, the validity and improvement of the model may be carried out to reduce the uncertainties in the dynamic modelling of

the system. In the linear analyses, the steady-state values must be provided by some other sources, e.g. a non-linear program or experiment, in order to start the stability investigation. For example, the stability can be produced by any component or a combination of components of pressure drop (gravity, acceleration, and friction). Thus, even when measurements of overall pressure drop are available from experiments, a steady-state calculation is required to break the total pressure drop down to its components.

Recirculating and once-through boilers differ markedly in the sense that there is no dryout region in the recirculating systems. The omission of the effects of the subcooled boiling and post-dryout regions in a once-through boiler, which certainly affects the dynamic response of the system, can also lead to unrealistically high or low tube wall temperatures in these regions.

The assumption of a certain rate of heat input into the channel, which is appropriate for electrical or nuclear heating, ceases to be valid for heating by primary fluids. For instance, variation of heat flux with flow rate and fluid temperatures in the single phase regions where the heat is transferred by forced convection is an important factor (Presten et al (1973)), and representation by a constant heat flux is not satisfactory (Fallows et al (1973)). Hence, a much more likely mechanism to influence the stability of such a boiler is the interaction between heat flux and the secondary flow.

The results of these investigations indicate that the flow stability in boiling systems is a complicated function of system configuration, the amount of subcooling, the heat flux, the system pressure, and the flow conditions. No general rules can be set forth to obtain quantitative criteria for the stability of the flow resulting from various feedback

effects. In analysing the stability of boiling flow in the more complicated systems, high speed digital or analogue computers provide the only means for solving the resulting set of equations and then, of course, only for a particular case.

CHAPTER 3

BASIC EQUATIONS AND BOUNDARY CONDITIONS

3.1 INTRODUCTION

This chapter is concerned with the dynamics and steady-state performance of a helically-coiled tube once-through steam generator as used, for example, in a nuclear power station. Primary hot gas is utilised, in counter flow, to heat the secondary flow which is water, and to produce superheated vapour at the outlet. The secondary fluid is operating at a given differential pressure between two headers, or it is subjected to known inlet conditions without the differential pressure restriction (Figure 3.1).

In the following sections, the thermo-hydrodynamic equations of the primary and the secondary fluids are presented and are applicable to different regions along the coiled tube. The frictional pressure drop and the heat transfer regions in helically-coiled tubes are reviewed and the most appropriate correlations have been employed in the calculations.

Four boundaries are considered, which are: the onset of subcooled boiling boundary, the bulk-boiling boundary, the dryout boundary, and the superheater boundary. The criteria for each boundary are discussed and relations for the subcooled boiling boundary are developed and examined by applying available experimental data for coiled tubes. Simple models are used for the dryout and the superheater boundaries.

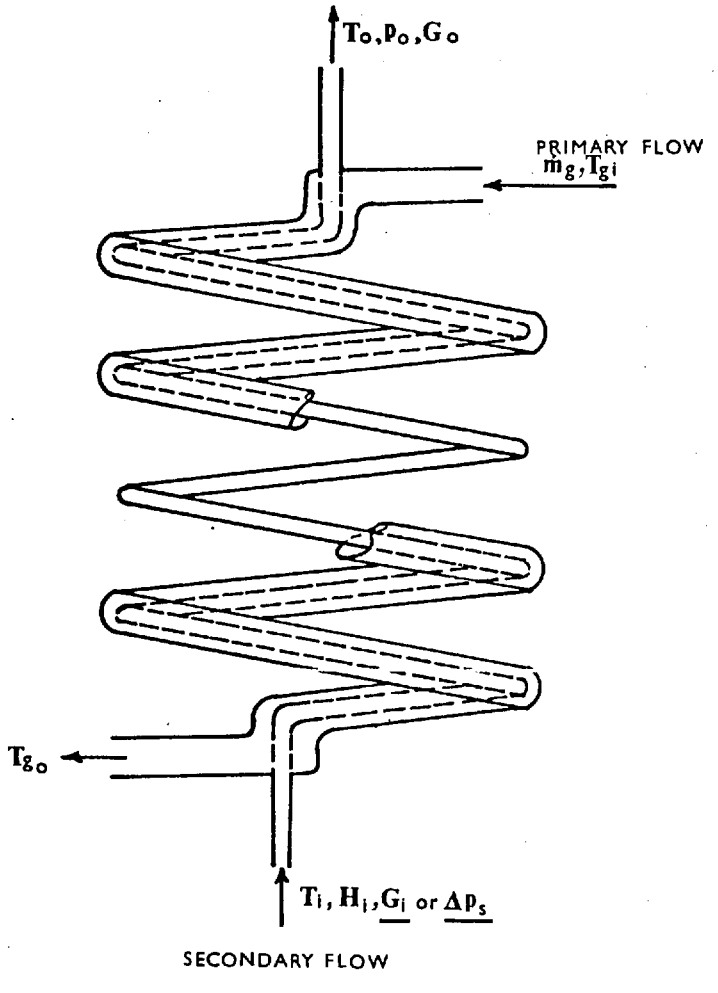


Figure 3.1: The Schematic Diagram of the Model

3.2 ENERGY EQUATION OF THE PRIMARY FLOW

The primary fluid (i.e. carbon dioxide) is considered to operate at constant pressure and it flows in a direction which is counter to the direction of the secondary fluid (Figure 3.2). The differential equation describing the energy balance of the primary fluid is:

$$\rho_g A_g c_{pg} u_g \frac{\partial T_g}{\partial z} = \rho_g A_g c_{pg} \frac{\partial T_g}{\partial t} + \pi d_o h_g (T_g - T_{wo}) + \dot{q}'_{loss} \qquad (3.1)$$

The direction of the secondary fluid is taken as positive. $\dot{q}'_{loss}$ is the heat lost to the surroundings per unit time and unit length. The value of $\dot{q}'_{loss}$ is assumed to be either a constant proportion of the local enthalpy of the primary fluid or small and negligible. h_g is the primary side heat transfer coefficient and it is a function of the Reynolds and Prandtl numbers of the primary fluid. Furthermore, the geometrical characteristic of the surface of the tube has been assumed to affect the heat transfer performance of the primary side. That is, for finned tubes, the heat transfer coefficient depends on the fin height (l) and the gap between the two adjacent fins (s). In general, the primary side heat transfer coefficient is calculated from:

$$Nu = K Re_g^m Pr_g^n (\frac{s}{l})^r \qquad (3.2)$$

where, for a tube without a fin, $r = 0$, and the appropriate constants are given by McAdams (1954).

For a plain radial fin, the constants are as follows (Sherwin (1972)

and Briggs et al (1965)):

$$K = 0.1378 \quad , \quad m = 0.718$$
$$n = 1/3 \quad , \quad r = 0.296$$

We assume that the mixing of the primary fluid is complete at any cross-section and that the same heat transfer equation is applicable for both steady and unsteady states. The primary fluid physical properties are calculated at the local temperature.

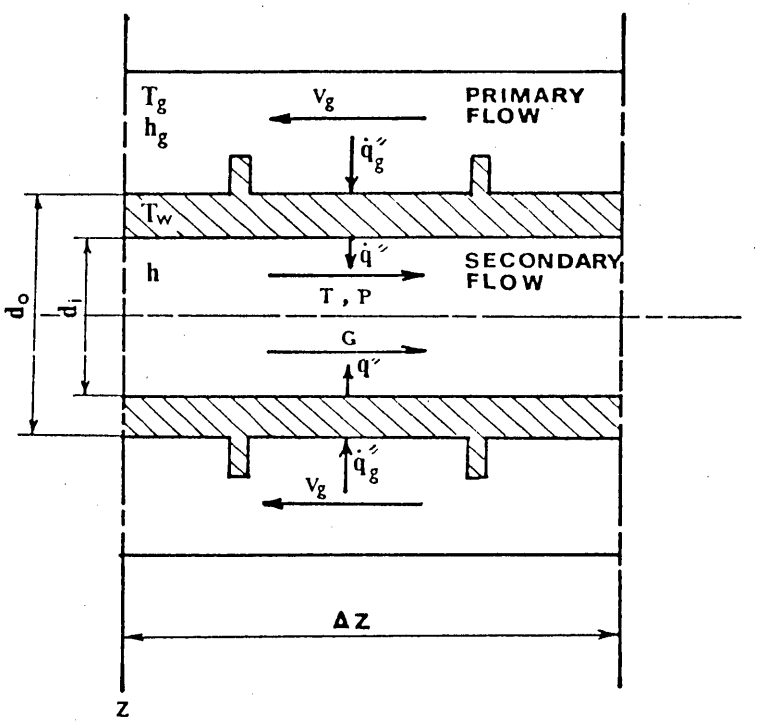


Figure 3.2: The Concentric Tube Model

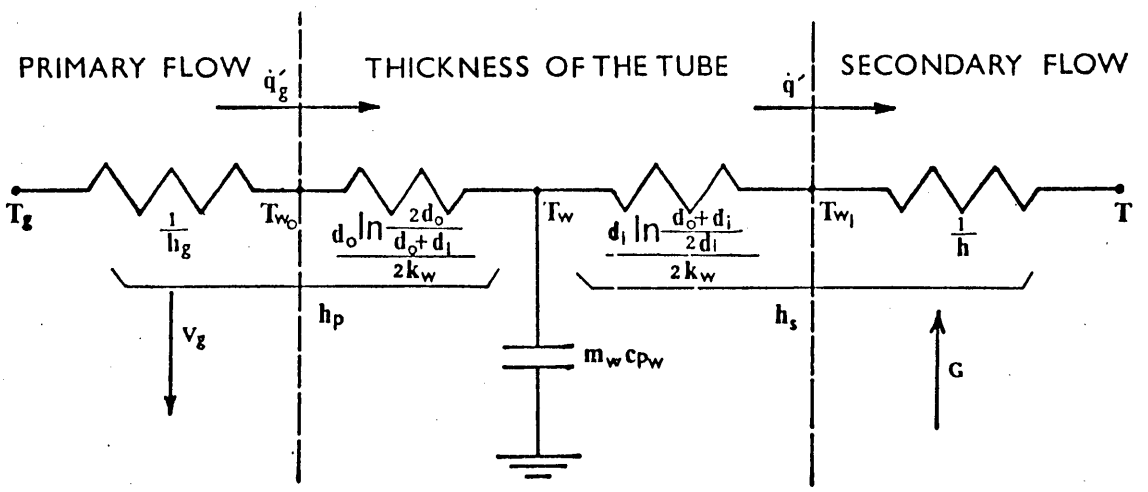


Figure 3.3: Nodal Thermal Model of the Tube Wall

3.3 THE TUBE WALL MODEL

The one point lumped capacity model (Figure 3.3) is used to describe the nodal thermal state of the tube wall. This model is adequate for a thin wall with high heat conductivity. The energy balance for the average wall temperature T_w may be written:

$$m_w c_w \frac{\partial T_w}{\partial t} = \pi d_o h_p (T_g - T_w) - \pi d_i h_s (T_w - T) \tag{3.3}$$

h_p and h_s are the overall coefficients of heat transfer between the wall and the primary and secondary fluids, respectively.

$$\frac{1}{h_p} = \frac{1}{h_g} + \frac{d_o \ln (2d_o/(d_i + d_o))}{2k_w} \tag{3.4}$$

$$\frac{1}{h_s} = \frac{1}{h} + \frac{d_i \ln ((d_i + d_o)/2d_i)}{2k_w} \tag{3.5}$$

k_w is the thermal conductivity of the tube wall and h is the secondary side heat transfer coefficient which will be discussed later.

The following equations evaluate the heat fluxes entering ($\dot{q}''_g$) and leaving ($\dot{q}''$) the wall:

$$\dot{q}''_g = h_p (T_g - T_w) = h_g (T_g - T_{wo}) \tag{3.6}$$

$$\dot{q}'' = h_s (T_w - T) = h (T_{wi} - T) \tag{3.7}$$

3.4 THERMO-HYDRODYNAMIC EQUATIONS OF THE SECONDARY FLOW

3.4.1 A Simplified Model

In a once-through steam generator, the incoming subcooled liquid is heated up to saturation temperature, then vaporised and superheated during its transit along the tube (Figure 3.4). Five regions are considered: the subcooled single-phase region, with increasing tube wall and liquid temperatures, extends to some point at which the subcooled boiling occurs. Onset of subcooled boiling is accompanied by augmentation of heat transfer which suppresses the rise of the tube wall temperature. When the liquid temperature reaches the saturation temperature, thermodynamic equilibrium is attained and bulk boiling starts during which the tube wall temperature remains constant and slightly higher than the local saturation temperature due to the high rate of nucleate boiling heat transfer. At some critical value of vapour quality the dryout occurs, and is accompanied by a rise in the wall temperature. Lastly, the transition to dry saturated vapour is initiated, and furthermore, the fluid is then superheated. Experimental evidence (Collier (1972), Appendix A) justifies this model for a coiled tube steam generator.

3.4.2 Assumptions

The basic formulation of the problem contains the following assumptions:

1. The separated flow model is employed in the two-phase region;
2. The thermal non-equilibrium between the liquid and vapour phases is assumed to be in the subcooled boiling region;
3. The vapour phase is always at the local saturation temperature.

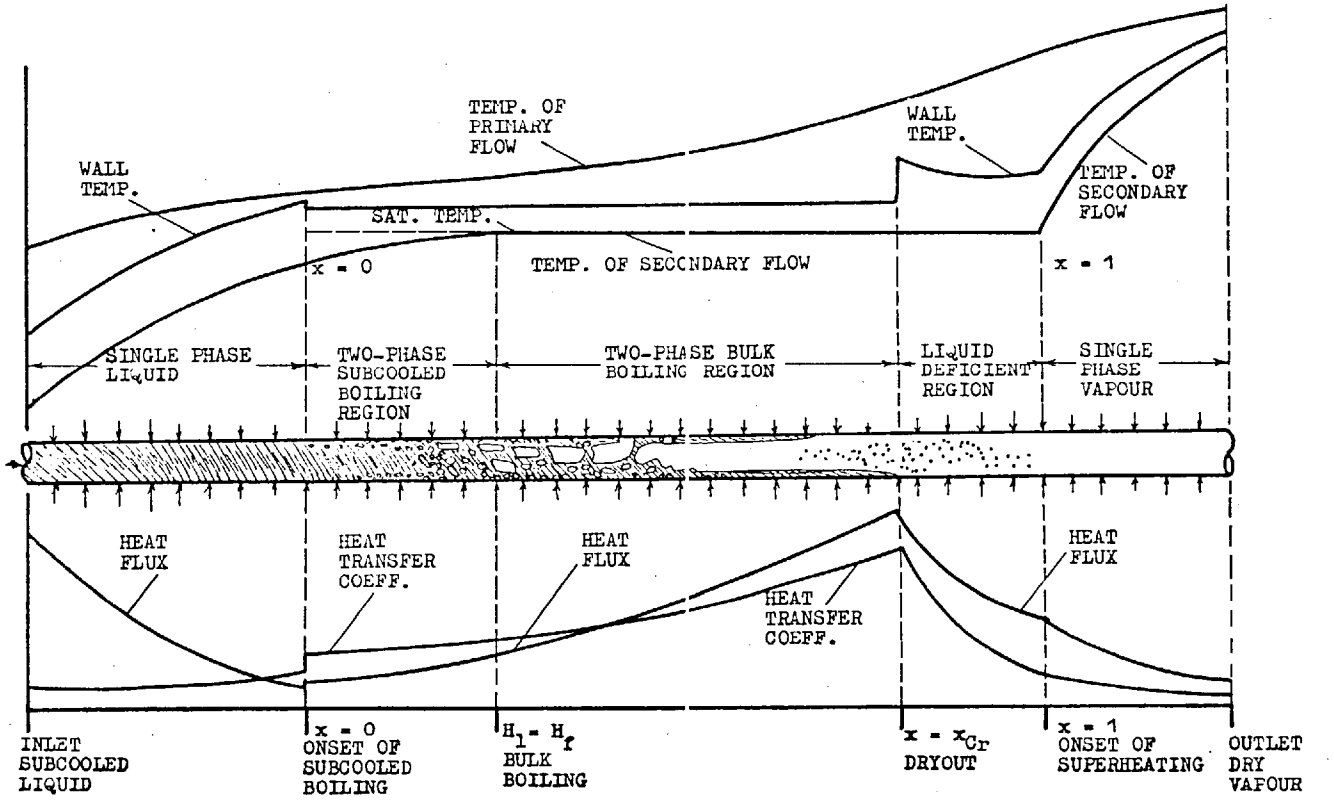


Figure 3.4: Regimes of Heat Transfer

(Collier (1972))

The first assumption is one of the usual approaches in the two-phase problems. This model includes different cross-section average velocities for phases, and it requires further information about the vapour slip along the heated length.

The second assumption is desirable in the subcooled boiling region and it necessitates the information of the vapour generation in the subcooled region.

The third assumption is valid in the subcooled and quality regions. However, it appears to become less valid, due to vapour superheating, beyond the dryout point. Fortunately, the secondary circulation in helically-coiled tubes not only affects the occurrence of the average dryout steam quality but also causes the rise in the tube wall temperature to be gradual and small. Such phenomena are reported by many investigators (Carver et al (1964); Owhadi (1967); Kozeki et al (1970); Naitoh et al (1974)) and it is concluded that the dryout takes place at very high quality regions. Therefore, it appears that the solutions are hardly affected by the third assumption. Although, if necessary, this assumption may be replaced by an extra relation which describes the heat transfer to the vapour phase and liquid droplets as the model of Bailey et al (1973).

The pressure variations are taken into account along the flow. It is a reasonable procedure for high pressure drop systems or systems in which the significant contribution to the driving head is hydrostatic. In fact, this is proved by experimental evidence on industrial helically-coiled tube once-through steam generators (M.E. Boilers Limited) in which the pressure drop exceeds 10 per cent of the inlet high pressure. Pressure wave propagation is neglected. However, the model may be modified to include the effect of wave propagation by manipulation of the

numerical technique.

3.4.3 Conservation Equations

The basic conservation equations have been presented in the previous chapter, equations (2.8) to (2.10), and can be re-arranged as follows:

Two-phase continuity equation:

$$\frac{\partial \rho_1}{\partial t} + \frac{\partial G}{\partial z} = 0 \tag{3.8}$$

where $$\rho_1 = \rho_l - (\rho_l - \rho_v)\,\alpha \tag{3.9}$$

and $$G = \rho_l\,(1 - \alpha)\,u_l + \rho_v\,\alpha\,u_v \tag{3.10}$$

Vapour phase continuity equation:

$$\frac{\partial \rho_2}{\partial t} + G\,\frac{\partial x}{\partial z} + x\,\frac{\partial G}{\partial z} = \gamma \tag{3.11}$$

where γ is the vapour generation rate and:

$$\rho_2 = \rho_v\,\alpha \tag{3.12}$$

$$x = \frac{\rho_v\,\alpha\,u_v}{G} \tag{3.13}$$

Momentum equation:

$$\frac{\partial G}{\partial t} + 2\,v_1\,G\,\frac{\partial G}{\partial z} + G^2\,\frac{\partial v_1}{\partial z} + \rho_1\,g\,\sin\beta + \frac{P}{A}\,\tau_w + \frac{\partial p}{\partial z} = 0 \tag{3.14}$$

where τ_w is the shear stress and:

$$v_1 = \frac{(1 - x)^2}{(1 - \alpha)\,\rho_l} + \frac{x^2}{\alpha\,\rho_v} \tag{3.15}$$

Energy equation:

$$\frac{\partial H_1}{\partial t} + G\,\frac{\partial H}{\partial z} + H\,\frac{\partial G}{\partial z} - v_2\,G\,\frac{\partial p}{\partial z} = \frac{P}{A}\,\dot{q}'' \tag{3.16}$$

where

$$v_2 = \frac{1 - x}{\rho_l} + \frac{x}{\rho_v} \tag{3.17}$$

$$H_1 = \rho_l\,E_l + (\rho_v\,E_v - \rho_l\,E_l)\,\alpha \tag{3.18}$$

$$H = \frac{\rho_l\,(1 - \alpha)\,u_l\,H_l + \rho_v\,\alpha\,u_v\,H_v}{\rho_l\,(1 - \alpha)\,u_l + \rho_v\,\alpha\,u_v} \tag{3.19}$$

and hence:

$$x = \frac{H - H_l}{H_v - H_l} \tag{3.20}$$

3.4.4 Constitutive Equations

The additional parameters used in formulations which correspond to constitutive equations are:

1. State equations:

$$\begin{aligned} T &= Fun.(p,H) \quad , \quad T_{sat} = Fun.(p) \\ \rho_i &= Fun.(p,T) \quad , \quad c_{pi} = Fun.(p,T) \\ \mu_i &= Fun.(p,T) \quad , \quad k_i = Fun.(p,T) \\ \sigma_l &= Fun.(T_{sat}) \quad , \quad i = l,v \end{aligned} \tag{3.21}$$

2. The mechanical constitutive equation which expresses the frictional pressure drop in terms of vapour quality and other system parameters.

3. The constitutive equation for void fraction which expresses void fraction, α, in terms of the vapour quality.

4. The energetic constitutive equation which relates the heat flux at the tube wall, $\dot{q}''(z,t)$, equation (3.7), to the temperatures of the tube wall, T_w, and the bulk coolant, T, is required to find the heat flux as a function of space and time.

The set of equations (3.8), (3.11), (3.14) and (3.16) describe the dynamic performance of once-through steam generators and are to be solved for unknown parameters G, x, p and H as a function of distance along the tube z and time t after considering the boundary conditions and other two-phase constitutive equations related to the flow in question.

3.5 BOUNDARY CONDITIONS

The primary flow equations and the tube wall energy equations together with the secondary flow conservation equations and appropriate correlations can be solved numerically subject to the following conditions:

1. Thermal boundary conditions
   (a) The primary flow:
   Inlet temperature, $T_g\ (L,t)$
   (b) The secondary flow:
   Inlet subcooling, $\Delta T_{in}\ (o,t) = T_{sat} - T\ (o,t)$

2. Hydrodynamic boundary conditions
   (a) The primary flow:
   Mass flow rate, $\dot{m}_g$
   (b) The secondary flow:
   i) Inlet pressure, $p\ (o,t)$
   ii) Either: Inlet mass flow rate, $G\ (o,t)$
   or : System pressure drop, $\Delta p_s\ (t)$

The steady-state conditions are sought by putting $\partial/\partial t = 0$, then the steady-state results are replaced as the initial conditions along the tube for dynamic calculations.

The delay and feedback effects can be obtained by imposing a specific perturbation, e.g. secondary mass flow, in the relationship to specified boundary conditions. On the other hand, if the system pressure drop is specified, the onset of sustained or divergent oscillations is sought for systems having such a pressure drop, e.g. a bank of parallel channels.

3.6 WALL SHEAR STRESSES AND VOIDAGE IN HELICALLY-COILED TUBES

3.6.1 Frictional Pressure Drop

The pressure drop contribution due to the wall shear force τ_w can be expressed in terms of friction factor f as:

$$-\left(\frac{dp}{dz}\right)_{fric} = \frac{P}{A}\tau_w = f\frac{2G^2}{d\rho} \tag{3.22}$$

f and ρ are appropriate values of friction factor and density of the fluid along the tube. After Lockhart-Martinelli and Nelson (1948,1949), the local values of two-phase frictional pressure drop are often expressed in terms of the single-phase pressure gradient for the total flow considered as liquid:

$$-\left(\frac{dp}{dz}\right)_{fric} = -\left(\frac{dp}{dz}\right)_{sp}\phi^2 = f_c\frac{2\,G^2}{d\,\rho_l}\phi^2 \tag{3.23}$$

where ϕ^2 is known as the two-phase frictional multiplier and f_c is the single-phase Fanning friction factor for coiled tubes.

3.6.2 Single-Phase Friction Factor

A number of theoretical and experimental equations have been proposed for use in calculating the pressure drop for laminar and turbulent flow in coils. Most of these equations predict either the Fanning friction factor f_c or the ratio of f_c to the Fanning friction factor for straight tubes, f_s. Other equations which predict the critical Reynolds number transformation from laminar to turbulent flow have also been published.

The various published correlations are critically examined and classified in the reviews by Srinivasan et al (1968,1970) and Lacey

(1970). Also, as was suggested by Lacey, the numerical simulation of Patankar (1974) has made a further contribution to the laminar fluid flow in coils without the restrictions and simplifications of earlier publications. For the purpose of the present work, the following studies are of significant interest.

Among the theoretical studies, Mori and Nakayama (1967) have made an analysis of fully turbulent flow in curved pipes under the condition of constant heat flux. They have developed expressions for the tube wall resistance coefficient using the boundary layer velocity profiles. The following equation has been recommended for normal practical use:

$$f_c \left(\frac{d}{D}\right)^{-0.5} = \frac{0.075}{Re\ (d/D)^2}^{0.2} \left\{1 + \frac{0.112}{Re\ (d/D)^2}^{0.2}\right\} \qquad (3.24)$$

From a practical point of view Ito's (1959) semi-empirical equation is recommended by many investigators, e.g. Srinivasan et al (1968) and Anglesea et al (1974), for fluids in turbulent flow in helically-coiled tubes:

$$f_c = 0.076\ Re^{-0.25} + 0.00725 \left(\frac{d}{D}\right)^{0.5} \qquad (3.25)$$

$$0.034 < Re \left(\frac{d}{D}\right)^2 < 300$$

Equations (3.24) and (3.25) agree very well and have been derived for coils of smooth tubing.

Recently, Anglesea et al (1974) have conducted experimental investigations of single-phase and two-phase friction pressure drops using coil geometry and test conditions similar to those used in the

Babcock and Willcox designs of steam generators for AGR nuclear power stations. They have found close agreement between equations (3.24) and (3.25) and their experimental results where $Re\ (d/D)^2$ ranges between 0.5 and 85. Furthermore, they have mentioned that their experimental evidence showed that the effect of surface roughness on frictional pressure drop was less in coiled tubes than straight tubes.

In the present study, Ito's correlation will be employed for calculating the Fanning friction factor and hence the frictional pressure gradient.

3.6.3 Two-Phase Frictional Multiplier and Voidage

Investigations of two-phase friction factor and void fraction in helically-coiled tubes fall into two groups: two component systems and one component systems with forced convection boiling.

Two component systems have been examined by many investigators, most of the experiments have been carried out at low pressures using an air-water system. The various two-phase flow regimes experienced in straight tubes (bubble, slug, annular, etc.), have all been observed in helical coils (Banarjee et al (1970,1969); Boyce et al (1968); Akagawa et al (1971)). Measurements of parameters such as liquid film velocity and thickness, droplet path length and secondary flow velocity, have been attempted by Maddock et al (1974), Banarjee et al (1969,1967) and Lacey (1970) using high speed cameras. The effect of liquid viscosity on the flow parameters has been investigated by Banarjee et al (1969) and Kasturi et al (1972).

Most authors concluded that the Lockhart-Martinelli (1949) correlation could be used to predict two-phase flow frictional pressure drop within the accuracy of the Lockhart-Martinelli correlation for

straight horizontal tubes.

Liquid hold-up has been obtained by Banarjee et al (1969,1967) and Boyce et al (1968) and satisfactory agreements have been confirmed with Lockhart-Martinelli correlation. Akagawa and Sakaguchi (1971) have stated that the values of void fraction in the coil were approximately equal to those in a straight tube for the same condition of water-air flow rate. They have suggested a relation similar to the Bankoff (1960) equation for vertical upward flow.

Kozeki et al (1970) carried out an investigation of one component flow in coiled tube once-through steam generators at pressures of 5 to 21 bars. The frictional pressure drop was found on the basis of an homogeneous model for two-phase flow which was hardly the case for the experimental ranges of pressure. At low mass velocity, the results were in agreement with Martinelli-Nelson (1948) correlation but at high mass velocities the data were greater than that estimated from the Martinelli-Nelson method.

Study of the two-phase pressure drop was carried out by Akagawa et al (1972,1971) in electrically heated coils at pressure ranges of 18-180 bars. The frictional pressure drop was deduced employing Thom's charts (1964). The results were compared to the Martinelli-Nelson and Thom's correlations. Satisfactory agreement of the data and Thom's correlation was reported.

A programme of experimental work has been recently mounted to obtain empirical correlations of pressure drop and heat transfer for coils at practical conditions, by Babcock and Wilcox (UK) (Anglesea et al (1974), Taylor et al (1973), Ruffel (1974)). Tests have been conducted at 180 bars and constant heat flux. Measurements of pressure drops and heat transfer parameters have been made for a range of enthalpies from subcooled water

to superheated steam.

Tests, and also different correlation curves, have been produced by Anglesea et al (1974). The two-phase friction multiplier has been deduced from the measurements of pressure drops and subtracting the values of gravitational and accelerational components of pressure drop which were calculated by employing the voidage correlation of Massena (1960). In the extension of Babcock and Wilcox's research programmes, Ruffel (1974) has derived the following empirical equations for a two-phase friction multiplier:

$$\phi^2 = \frac{\rho_l}{\rho_1} (1 + F) \tag{3.26}$$

$$F = C \left\{0.875 - \frac{3.14\ D}{1000\ d} - \frac{0.74\ G}{1000} \left(0.152 - \frac{0.7\ D}{1000\ d}\right) - x \left(0.7 + \frac{0.155\ G}{1000} - \frac{1.9\ D}{1000\ d}\right)\right\} \tag{3.27}$$

$$C = \left\{1 - 12\ (x - 0.3)(x - 0.4)(x - 0.5)(x - 0.6)\right\} \sin \left(\frac{1.16\ G}{1000}\right) \tag{3.28}$$

Equation (3.26) has been developed for the pressure drop data of Babcock and Wilcox and it has been compared with overall pressure drop data of gas-fired once-through model boilers of Babcock and Wilcox, described by Ruffel with satisfactory agreement within the range of the accuracies of single-phase and experimental data.

3.6.4 Conclusion

The results of two component systems have almost agreed with the Lockhart-Martinelli technique in most investigations. In most cases, Lockhart-Martinelli correlation is modified to take into account

the curvature of the tube for single-phase frictional pressure drop. Although the results of two-phase friction multipliers are comparable with those estimated by Lockhart-Martinelli correlation, scattering of the data exists in most of the investigations. It appears that the liquid hold-up does not disagree with the straight tube results over the range of accuracy of straight tube correlations. Void fraction data in one component systems are almost non-existent. Therefore, the processing and deduction of the pressure drop data are different in every investigation of one component systems; and they seem largely based on personal interpretation.

At present, it is difficult to draw a firm conclusion due to the uncertainty in the existing experimental data. The relevance of two component systems to the high pressure boiling situation is also open to question due to very large differences in density ratios of the two systems.

In the present study, therefore, the choice of void fraction and two-phase friction multiplier is based on the two requirements for pressure drop, namely, the ability of the correlations to provide reasonable agreement with experimental measurements of pressure drop and to produce systematic and logical two-phase pressure drop components.

Confidence is placed in work on the high pressure boiling systems which are more suitable for practical conditions of once-through boilers. Equations (3.26) to (3.28) are used in the present work to predict the two-phase frictional pressure drop. Also, on the basis of simplicity and good overall agreement with experimental data, the Smith correlation (1970) is chosen for local void fraction as follows:

$$\alpha = \left\{1 + 0.4 \frac{\rho_v}{\rho_l}\left(\frac{1}{x} - 1\right) + 0.6 \frac{\rho_v}{\rho_l}\left(\frac{1}{x} - 1\right)\left(\frac{\rho_l/\rho_v + 0.4\,(1/x - 1)}{1 + 0.4\,(1/x - 1)}\right)^{\frac{1}{2}}\right\}^{-1} \quad (3.29)$$

It is appropriate to mention that equation (3.26) is the best fit for the data of Babcock and Willcox which were produced by the use of Massena (1960) void correlation:

$$\alpha = \frac{(0.833 + 0.167\ x)\ x}{\rho_v/\rho_l + x\ (1 - \rho_v/\rho_l)} \tag{3.30}$$

However, it has been shown (Ruffel (1970)) that the discrepancies between equations (3.29) and (3.30) are very small.

3.7 TRANSITION BOUNDARIES

3.7.1 Introduction

In the following sections, the transition boundaries for helically-coiled tubes are discussed and appropriate relations have been developed in the subcooled boiling region.

Furthermore, the regimes of heat transfer, in different regions between the transition boundaries, are reviewed and proper relations chosen for the dynamics calculation.

3.7.2 Subcooled Boiling

3.7.2.1 Introduction

Subcooled boiling inside conduits under forced circulation has been studied by many investigators, e.g. Bowring (1962), Larson and Tong (1969). However, the validity of their use for helical tubes is questionable.

It is the purpose of the following section to carry out a preliminary investigation into the subcooled boiling regime in a helically coiled tube and to present equations for the prediction of the growth of bubbling and vapour generation rate in subcooled boiling along the coiled tubes.

3.7.2.2 Onset of subcooled boiling

Consider the flow of subcooled liquid in a heated conduit. The single-phase region will extend to the axial position z_s at which the wall temperature becomes slightly superheated (Figure 3.5). Downstream of z_s, bubble formation may start at the wall while attached to the wall. At some point z_D the conditions of the fluid layer adjacent to the wall are such that bubble detachment starts and bubble

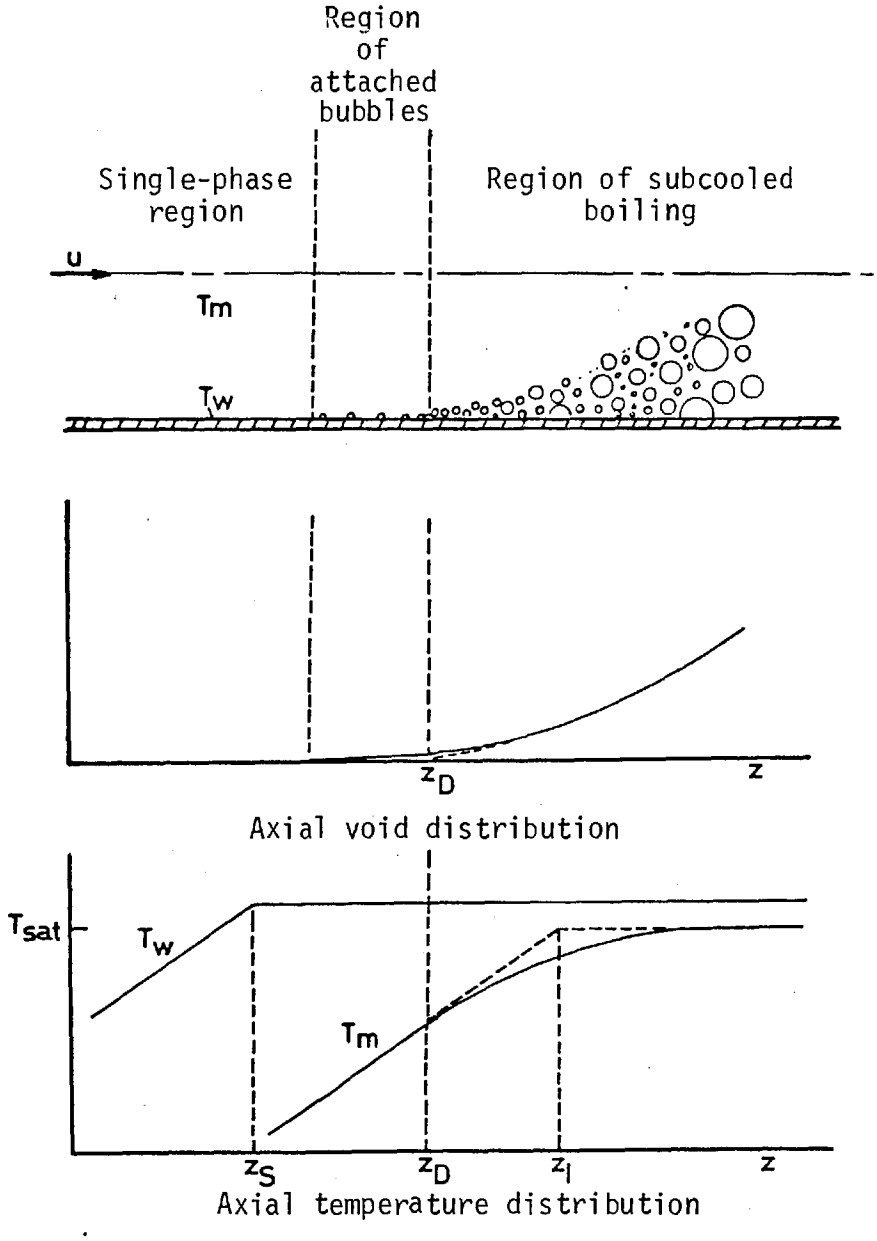


Figure 3.5: Axial Temperature and Void Distribution in the Subcooled Boiling Region

growth takes place in the presence of subcooled liquid.

In the subcooled boiling region, the wall temperature remains essentially constant a few degrees above the saturation temperature, while the mean bulk liquid temperature is increasing to the saturation temperature. As bubble detachment occurs, the inside wall temperature slightly drops and the heat transfer coefficient starts to increase.

Larson and Tong (1969) showed that vapour bubbles form on the heated wall and remain in the near wall region, and it is postulated that the presence of bubbles increases the effective conductivity in the near wall region, hence reduces the resistance to heat transfer through the bubble layer to the liquid core.

Hancox and Nicoll (1971), in the extension of the above model, stated that in the region of attached bubble, vapour formation is suppressed due to higher values of heat flux that could be transferred to the liquid core, based on the effective conductivity and mean liquid subcooling, and is greater than the specified wall heat flux.

The present work employs the above criteria to define the bubble detachment position. That is, vapour bubble growth must begin at a position along the tube where the heat flux to the subcooled liquid core based on the effective conductivity and mean subcooled liquid temperature becomes equal to the specified wall heat flux.

In the following section, an equation is derived for predicting the position of bubble detachment in a helically-coiled tube as a function of Reynolds number and channel geometry.

3.7.2.3 Assumptions and formulations

Starting with the velocity field of single-phase flow

in a curved tube, it is known that the pressure distribution at the tube cross-section is affected by the centrifugal force, and the pressure at the outer surface is higher than the pressure at the inner surface. As shown in Figure 3.6, the fluid in the central part of the tube cross-section is driven towards the outer surface and the fluid near the wall flows within a boundary along the wall surface to the inner part region of low pressure.

The theory of single-phase flow in a curved pipe has been developed by many investigators (e.g. Cummings (1955), Barua (1963), Kubair et al (1966)) for the case of fully-developed and developing flows. In the present study, the analytical results of Mori and Nakayama (1967) will be used wherever necessary. The following assumptions are made:

1. Flow is fully-developed, i.e. the velocity and temperature profiles remain unchanged in the axial direction up to the bubble detachment position.
2. The core flow is turbulent, i.e. momentum and heat transfer are due to the effective viscosity and conductivity, respectively. Furthermore, the momentum and heat flux eddy diffusivities are equal ($Pr = 1$).
3. The inside wall temperature before the bubble detachment position reaches a value slightly higher than saturation temperature which remains constant beyond this point.
4. Bubbles remain near the wall and are confined to the laminar film.
5. The temperature of water film at the edge of the bubbles region remains at local saturation temperature (Larson et al (1969)).

The velocity and temperature profiles up to the

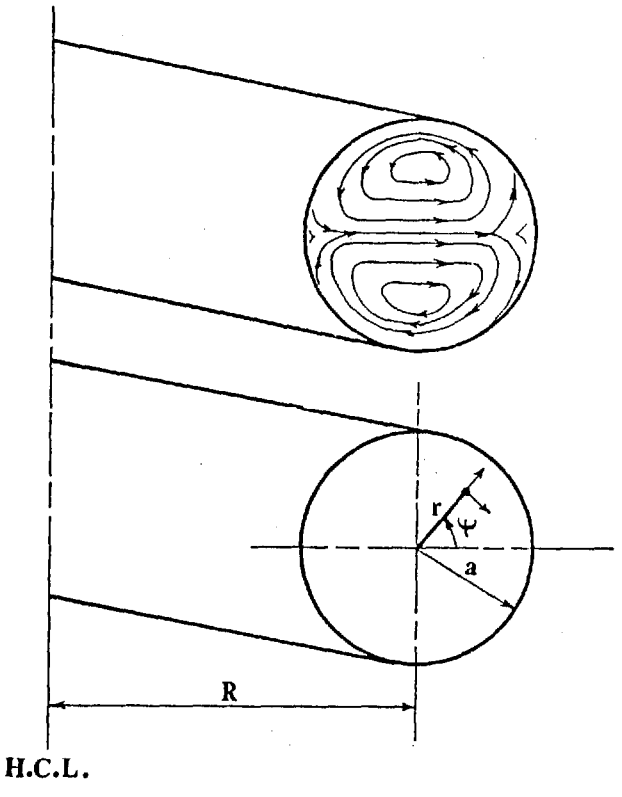


Figure 3.6: Secondary Circulation in Coils

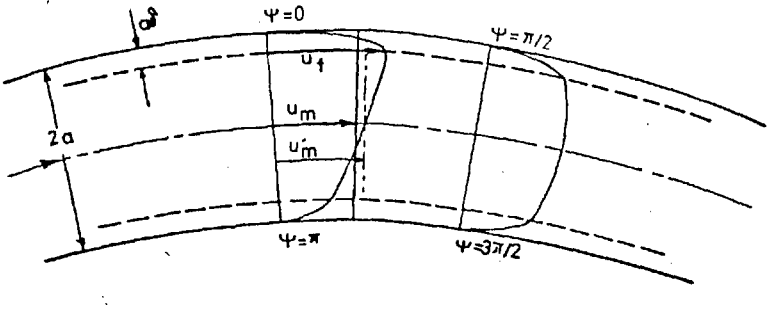


Figure 3.7: Single-Phase Velocity Distributions

point of bubble detachment z_D are given by single-phase flow distributions even though there are some bubbles attached to the wall. Thus, there is a laminar film of thickness $a\delta$ containing attached bubbles and a turbulent core region (Figure 3.7).

Now, Reynolds analogy for heat and momentum transfer is used regarding the inside surface of the laminar film being considered as a tube wall. That is, the tube wall radius is $a\ (1 - \delta)$ instead of a and the mean velocity is $u'_m - u_f$ (the relative velocity of the laminar film u_f and the average of core velocity u'_m). Then, on the basis that $(\dot{q}''/\tau)_f$ is only a function of ψ (Figure 3.6), and due to the second assumption, the Reynolds analogy is written as follows:

$$\frac{\dot{q}''_f}{\tau_f} = c_{pc} \frac{T_f - T'_m}{u_f - u'_m} \tag{3.31}$$

Defining the following dimensionless quantities:

$$\eta = \frac{r}{a} \tag{3.32}$$

$$U = \frac{u\ a\ \rho}{\mu} \tag{3.33}$$

$$U^{*2} = \left(\frac{a}{\nu}\right)^2 \frac{\tau}{\rho} \tag{3.34}$$

$$Q'' = \frac{\dot{q}''}{G\ \Delta\ H_{in}} \tag{3.35}$$

$$Re = \frac{2a\ G}{\mu} \tag{3.36}$$

$$\theta = \frac{T_w - T}{\Delta\ T_{in}} \tag{3.37}$$

Then, equation (3.31) can be written as follows:

$$\frac{Q''_f}{U^{*2}_f} = \frac{2}{Re} \frac{\theta'_m - \theta_f}{U_f - U'_m} \tag{3.38}$$

According to Mori et al (1967a,b) the velocity and temperature profiles of the core can be described by the following equations:

$$U = A + \frac{C}{D} \eta \cos \psi \tag{3.39}$$

$$\frac{\theta}{\theta_m} = N e^{\alpha_o/D \, (A \eta \cos \psi + C/2D \, \eta^2 \cos^2 \psi)} \tag{3.40}$$

where the different coefficients in the above equations are expressed by the following relations when $1/(2m - 1)$ power law is assumed for turbulent velocity profile:

$$A = \frac{Re}{2} \frac{1}{1 - (1/m) \delta} \tag{3.41}$$

$$C = \frac{\lambda_m}{16} \left(\frac{(2m - 1)^2}{m (4m - 1)}\right)^{(2m-1)/m} Re^{(2m-1)/m} \delta^{-1/m} \left(1 + \frac{2m - 1}{m} \delta\right) \tag{3.42}$$

$$D = D_m \left(Re^m \left(\frac{\alpha}{R}\right)^{\frac{1}{2}}\right)^{1/(m+1)} \tag{3.43}$$

$$\delta = \delta_m \left(Re \left(\frac{\alpha}{R}\right)^{m/2}\right)^{-1/(m+1)} \tag{3.44}$$

$$\alpha_o = \left(\alpha_m Pr^{1-k} Re \, \delta^{(1/m)} A^{-(m-1)/m} - \frac{m - 1}{m} \frac{C}{2D^2}\right)^{-1} \tag{3.45}$$

$$N = \left(1 + \frac{3C \alpha_o}{8D^2} + \frac{\alpha_o A^2}{8D^2}\right)^{-1} \tag{3.46}$$

According to Mori et al (1967), if $m = 4$, then:

$$\lambda_m = 0.316 \ , \ D_m = 0.0852 \ , \ \delta_m = 0.2566 \ , \ \alpha_m = 10.93 \ , \ k = 1/3 \qquad (3.47)$$

and if $m = 5$:

$$\lambda_m = 0.184 \ , \ D_m = 0.0613 \ , \ \delta_m = 0.04242 \ , \ \alpha_m = 16.42 \ , \ k = 0.4 \qquad (3.48)$$

The core mean velocity and temperature are as follows:

$$U'_m = \frac{1}{\pi \ (1 - \delta)^2} \int_{\eta=0}^{1-\delta} \int_{\psi=-\pi}^{\pi} U \ \eta \ d\eta \ d\psi \qquad (3.49)$$

Employing equation (3.39):

$$U'_m = \frac{1}{\pi \ (1 - \delta)^2} \int_{\eta=0}^{1-\delta} \int_{\psi=-\pi}^{\pi} \left(A + \frac{C}{D} \eta \ cos \ \psi\right) \eta \ d\eta \ d\psi \qquad (3.50)$$

which gives:

$$U'_m = A \qquad (3.51)$$

and the mixed mean temperature of the fluid in the core region is:

$$T'_m = \frac{1}{\pi \ a^2 \ (1 - \delta)^2 \ u'_m} \int_{r=0}^{a(1-\delta)} \int_{\psi=\pi}^{\pi} u \ T \ r \ dr \ d\psi \qquad (3.52)$$

which becomes:

$$\frac{\theta'_m}{\theta_m} = \frac{1}{\pi \ U'_m \ (1 - \delta)^2} \int_{\eta=0}^{1-\delta} \int_{\psi=-\pi}^{\pi} U \ \theta \ \eta \ d\eta \ d\psi \qquad (3.53)$$

The temperature field in the core region, equation (3.40), may be expanded as:

$$\frac{\theta}{\theta_m} = N \left\{1 + \frac{\alpha_o A}{D} \eta \cos \psi + \frac{\alpha_o}{2D^2} (C + \alpha_o A^2) \eta^2 \cos^2 \psi + \right.$$

$$\left. + \frac{\alpha_o^2 A}{D^3} \left(\frac{C}{2} + \frac{\alpha_o A^2}{3}\right) \eta^3 \cos^3 \psi + \ldots\ldots \right\} \qquad (3.54)$$

Substituting equations (3.39) and (3.54) into (3.53), and by taking into account the terms $\eta^2 \cos^2 \psi$ in the expansion, it follows:

$$\frac{\theta'_m}{\theta_m} = \frac{N}{\pi U'_m (1 - \delta)^2} \int_0^{1-\delta} \int_{-\pi}^{+\pi} \left[A + \left(\frac{C}{D} + \frac{\alpha_o A^2}{D}\right) \eta \cos \psi + \right.$$

$$\left. + \frac{\alpha_o A}{2D^2} (3C + \alpha_o A^2) \eta^2 \cos^2 \psi \right] \eta \, d\eta \, d\psi \qquad (3.55)$$

Carrying out the integration, the following relation is obtained:

$$\theta'_m = M \theta_m \qquad (3.56)$$

where $$M = N \left\{1 + \frac{\alpha_o}{8D^2} (3C + \alpha_o A^2) (1 - \delta)^2\right\} \qquad (3.57)$$

Inserting equations (3.51) and (3.56) into equation (3.38) gives:

$$\frac{Q''_f}{U^{*2}_f} = \frac{2}{Re} \frac{M \theta_m - \theta_f}{U_f - A} \qquad (3.58)$$

The friction velocity U^{*2}_f is given by Mori and Nakagama (1967) as follows:

$$U^{*2}_f = \frac{C}{2} + B A^{(m-1)/m} \delta^{-(1/m)} \frac{C}{D} \cos \psi \qquad (3.59)$$

where $$B = \frac{\lambda}{2^{3+(1/m)}} \cdot \frac{2m - 1}{m} \left(\frac{(2m - 1)^2}{m (4m - 1)}\right)^{(2m-1)/m} \qquad (3.60)$$

Assuming that the interface between the region of attached bubbles and the core has the temperature of the water film (Larson and Tong (1969)), thus:

$$\theta_f = \theta_{sat} \tag{3.61}$$

$$U_f = A + \frac{C}{D}(1 - \delta)\cos\psi \tag{3.62}$$

as

$$\theta_m = \theta_{sat} + \theta_{sub} \tag{3.63}$$

where

$$\theta_{sub} = \frac{T_{sat} - T_m}{\Delta T_{in}} \tag{3.64}$$

Then, substituting equations (3.59), (3.61), (3.62) and (3.63) into equation (3.58), the heat flux at the interface between the film and the core as a function of ψ becomes:

$$Q''_f(\psi) = \frac{2M}{Re}\left(\theta_{sub} - \left(\frac{1}{M} - 1\right)\theta_{sat}\right) F(\psi) \tag{3.65}$$

where

$$F(\psi) = \frac{C/2 + B\,A^{(m-1)/m}\,\delta^{-(1/m)}\,C/D\cos\psi}{C/D\,(1 - \delta)\cos\psi} \tag{3.66}$$

Now, the mean value of $Q''_f(\psi)$ around the periphery of the tube can be found from equation (3.65):

$$\overline{Q}''_f = \frac{1}{2\pi}\int_{\psi=-\pi}^{\psi=\pi} Q''_f(\psi)\,d\psi \tag{3.67}$$

Carrying out the integration:

$$\overline{Q}''_f = \frac{2B\,A^{(m-1)/m}\,\delta^{-(1/m)}}{Re\,(1 - \delta)} M\left(\theta_{sub} - \left(\frac{1}{M} - 1\right)\theta_{sat}\right) \tag{3.68}$$

The criterion for the inception of the bubble detachment may be written as (Larson et al (1969)):

$$\bar{Q}''_f = \frac{1}{1-\delta} Q'' \tag{3.69}$$

Combining equations (3.41), (3.44), (3.68) and (3.69), and rearranging, the subcooling at which bubble detachment occurs can be obtained as follows:

$$\theta_{sub} = \frac{\delta_m^{1/m} (1 - \frac{1}{m}\delta)^{(m-1)/m}}{2^{1/m} B M} \left[Re \left(\frac{a}{R}\right)^{-\frac{1}{2}}\right]^{1/(m+1)} Q'' - (1 - \frac{1}{M}) \theta_{sat} \tag{3.70}$$

With reference to equation (3.35), we have:

$$Q'' = \frac{\dot{q}''}{G \Delta H_{in}} = \frac{1}{4Z_o} \tag{3.71}$$

where

$$Z_o = \frac{Z_1}{d} \tag{3.72}$$

Also, the energy balance along the tube neglecting the energy content of the wall voidage will give:

$$T_m - T_i = \frac{4Z_D}{d} \cdot \frac{\dot{q}''}{G} \tag{3.73}$$

defining

$$Z_D^* = \frac{Z_D}{Z_1} \tag{3.74}$$

Equation (3.73) can be rearranged as:

$$\theta_{sub} = 1 - Z_D^* \tag{3.75}$$

Hence, the length at which bubble detachment occurs can be obtained by combining equations (3.70), (3.71) and (3.75) as follows:

$$z_D^* = 1 - \frac{\delta_m^{1/m}\,(1 - \frac{1}{m}\,\delta)^{(m-1)/m}}{2^{2+1/m}\,M\,B}\left[Re\,(\frac{a}{R})^{-\frac{1}{2}}\right]^{1/(m+1)}\frac{1}{z_o} - (1 - \frac{1}{M})\,\theta_{sat} \qquad (3.76)$$

The value of M (equation (3.57)) has been computed and found to be a weak function of δ at different Reynolds number and (a/R) (Figure 3.8). It can be approximated by the following relation:

$$M = 1 - 0.18\,\delta \qquad (3.77)$$

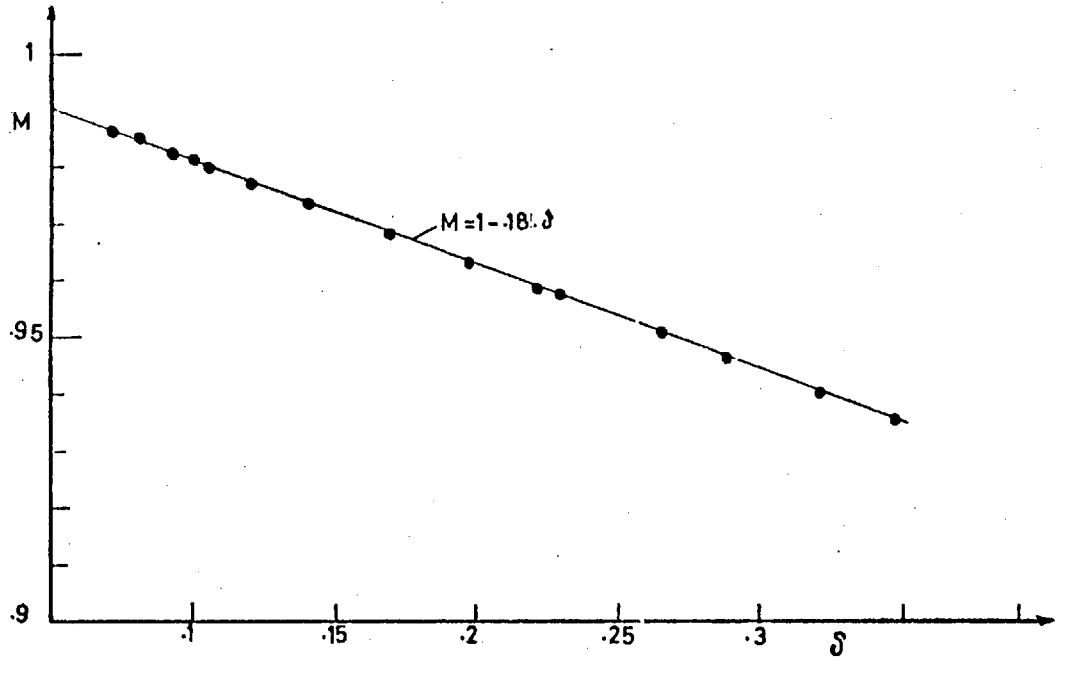


Figure 3.8: Variation of Parameter M

The value of M varies between 0.95 and 1. Therefore, the order of magnitude of the term $(1 - 1/M)$ is 10^{-2} and also as the wall superheat θ_{sat} is of the order of magnitude 10^{-2}, then the order of magnitude of the term $(1 - 1/M)\,\theta_{sat}$ is very much less than unity, hence this term can be neglected compared to the other terms in equation (3.76). Thus:

$$Z_D^* = 1 - \frac{\delta_m^{1/m} \left(1 - \frac{1}{m}\delta\right)^{(m-1)/m}}{2^{2+1/m} \cdot B \left(1 - 0.18\,\delta\right)} \left[Re \left(\frac{a}{R}\right)^{-\frac{1}{2}}\right]^{1/(m+1)} \frac{1}{Z_o} \qquad (3.78)$$

Mori and Nakayama (1967) have studied the forced convective heat transfer in curved pipes, and it has been shown that the heat transfer coefficient for water agreed with the experimental values for $m = 5$. Accordingly, we chose $m = 5$ and then equation (3.78) becomes:

$$Z_D^* = 1 - 4.28 \frac{(1 - 0.2\,\delta)^{0.8}}{1 - 0.18\,\delta} Re^{1/6} \left(\frac{a}{R}\right)^{-1/12} \frac{1}{Z_o} \qquad (3.79)$$

The following approximation can be made within the practical values of $0.05 < \delta < 0.3$:

$$\frac{(1 - 0.2\,\delta)^{0.8}}{1 - 0.18\,\delta} \simeq 1.003 \qquad (3.80)$$

Thus, from equations (3.80) and (3.79), we have:

$$Z_D^* = 1 - 4.3\, Re^{1/6} \left(\frac{a}{R}\right)^{-1/12} \frac{1}{Z_o} \qquad (3.81)$$

In summary, the subcooling and the position of the bubble detachment at a given heat flux, inlet mass velocity and temperature, are predicted as follows:

1. Find Reynolds number from equation (3.35) where the fluid properties are calculated for the average temperature between inlet and saturation.
2. Evaluate the subcooling as follows:

$$\theta_{sub} = 4.3\, Re^{1/6} \left(\frac{a}{R}\right)^{-1/12} \frac{1}{Z_o} \qquad (3.82)$$

3. If $\theta_{sub} > 1$, the bubble detachment occurs at inlet to the tube.
4. If $\theta_{sub} < 1$, calculate the bubble detachment position from equation (3.81).

A comparison with some available experimental results by other investigators, e.g. Carver et al (1964) and Owhadi (1966), and a discussion of relevant results is given in Chapter 5.

3.7.2.4 Vapour generation function

Beyond point z_D vapour generation starts while the liquid core temperature is less than saturation temperature. Assume a separated two-phase model as shown in Figure 3.9 and consider an infinitesimal control volume enclosing the vapour layer, then the macroscopic mass balance may be written as:

$$\rho_v u_1 A_1 + \dot{m}''_f P_1 \Delta z = \rho_v u_2 A_2 \qquad (3.83)$$

where P_1 is the periphery and $\dot{m}''_f$ is the average liquid mass flux across the liquid-vapour interface. u and A refer to the average vapour velocity and cross-section, respectively, and indices 1 and 2 refer to inlet and outlet conditions, respectively. The conservation of energy for control volume is:

$$-\rho_v H_v (A_1 u_1 - A_2 u_2) = (P \dot{q}'' - P_1 \dot{q}''_f) \Delta z + \dot{m}''_f H_l P_1 \Delta z \qquad (3.84)$$

Combining equations (3.83) and (3.84), the mass of generated vapour may be found as follows:

$$\dot{m}''_f = \frac{P \dot{q}'' - P_1 \dot{q}''_f}{P_1 (H_v - H_l)} \qquad (3.85)$$

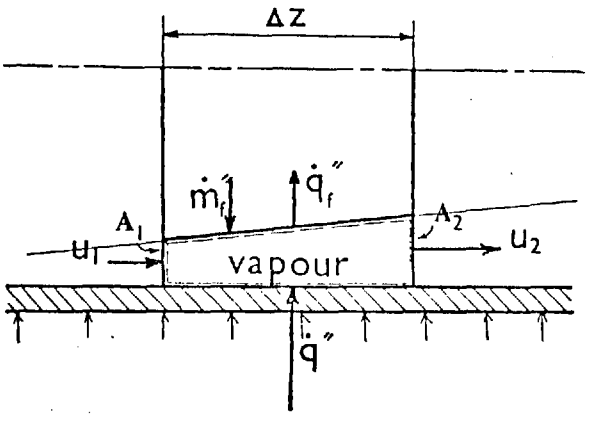


Figure 3.9: A Control Volume Model of Vapour Phase in the Subcooled Boiling Region

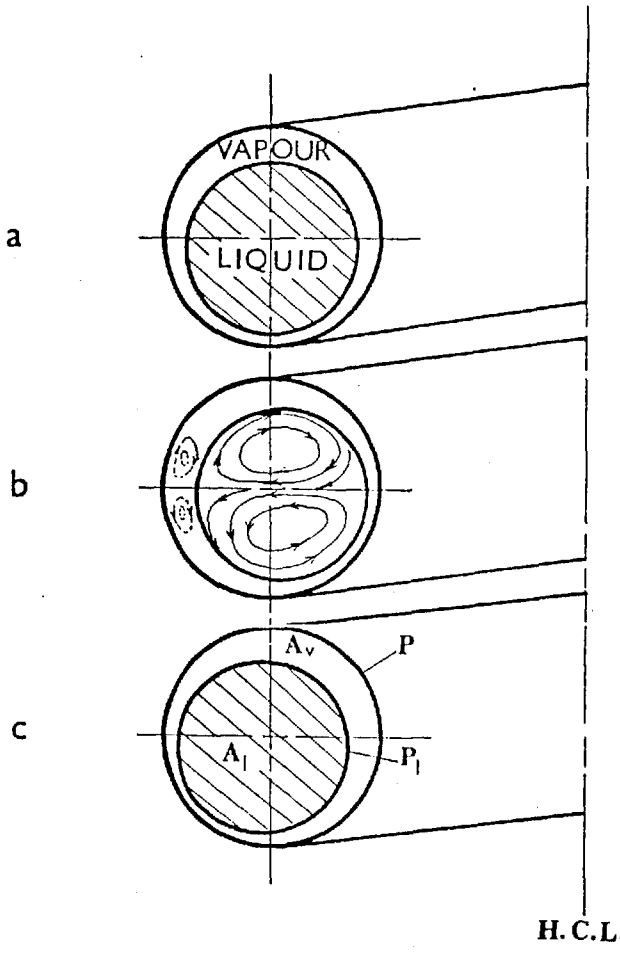


Figure 3.10: Possible Concentration of Vapour Phase in the Subcooled Boiling Region

The vapour generation rate in terms of cross-section average value can be written as:

$$\Upsilon = \frac{P_1 \dot{m}''_f}{A} \tag{3.86}$$

Consider the case of fully-developed nucleate boiling inside helically coiled tubes; and assume that the bubble generation exists all around the periphery of the cross-section. As in the case of horizontal or vertical tube flow boiling (Tong (1965)), assume that the detached bubbles travel at lower velocity than the core stream and they remain within a layer near the wall (Jiji (1962)).

Assuming that the centrifugal and gravity forces will only shift the core as shown in Figure 3.10, then:

$$\frac{P_1}{P} = \left(\frac{A - A_v}{A}\right)^{\frac{1}{2}} = (1 - \alpha)^{\frac{1}{2}} \tag{3.87}$$

Substituting equations (3.85) and (3.87) into equation (3.86), and rearranging yields:

$$\Upsilon = \frac{4\,\dot{q}''}{d\,H_{fv}} \left\{\frac{1 - (1 - \alpha)^{\frac{1}{2}}\,\dot{q}''_f/\dot{q}''}{1 + (H_f - H_l)/H_{fv}}\right\} \tag{3.88}$$

$\dot{q}''_f$ is the heat flux through the liquid-vapour interface and it is considered as follows:

$$\dot{q}''_f = h_f\,(T_{sat} - T_l) \tag{3.89}$$

where h_f is the heat transfer coefficient between vapour and liquid core. It is assumed to be equal to the heat transfer coefficient at the bubble growth position which can be obtained by combining equations (3.71), (3.82)

and (3.89) as follows:

$$h_f = 0.058\, Re^{5/6}\, Pr\, (\frac{d}{D})^{1/12}\, \frac{k_l}{d} \qquad (3.90)$$

It should be mentioned that equation (3.88) is less valid as the void fraction increases. However, as the void fraction and liquid core temperature T_l increases downstream, the value of $\dot{q}''_f$ decreases and approaches zero when the liquid core temperature reaches the saturation temperature (equation (3.89)). Therefore, such a model is not influenced by high values of void fraction. When thermal equilibrium is attained, $H_l = H_f$, vapour generation from equation (3.89) becomes identical to the thermodynamic quality.

3.7.3 Bulk Boiling Boundary

The bulk boiling boundary is established when the enthalpy of the liquid phase equals:

$$H_l = H_f \qquad (3.91)$$

Beyond this position, thermal equilibrium is attained between the two phases and the steam quality may be identified as follows:

$$x = \frac{H_v - H_f}{H_{fv}} \qquad (3.92)$$

3.7.4 Annular Flow and Dryout Boundary

The most interesting feature of helically-coiled tubes is the occurrence of the dryout at the relatively very high quality region as

compared with straight tubes (Carver et al (1964); Naitoh et al (1974)). Such behaviour is most beneficial in practice and it enables the design of low cost boilers with high outlet steam quality.

It is understood that fluid particles inside coiled tubes are mostly affected by three forces, namely, gravitational, centrifugal and drag forces caused by the secondary circulation. The magnitude of the forces depends on the system parameters and geometry. The most probable flow pattern before the dryout commences would be expected to be annular flow. The thickness of the annular film, under imposed forces, would be different around the periphery of the tube and so would be the dryout vapour quality.

It is postulated that when the effects of gravitational and centrifugal forces are dominant, e.g. low mass velocity or large coil diameter, the thicker liquid film would be established at outer and lower surfaces of the tube depending on the balance of gravitational and centrifugal forces. Therefore, the dryout is expected at the opposite sides between the top and inside surfaces as reported by Carver et al (1964). As the secondary circulation effects become more important, it drags the liquid film from the outer position to the inside surface of the coiled tube (Lacey (1970); Banarjee (1967)). The film breaks up at the outside positions (Kozeki (1970)). At high mass velocities and small coil diameters, the effect of secondary circulation becomes large compared to the centrifugal forces and gravity. Hence, it disturbs the liquid film and originates liquid droplets which are sharply deposited to the outer surface by the centrifugal forces. Therefore, the inside and outer surfaces are supplied with more liquid than the top and bottom positions and it results in lower dryout vapour quality at the top and bottom positions as reported by Owhadi (1966,1968) and Kozeki et al (1970).

In any case, the secondary circulation effect in helically-coiled tubes is strong enough to give higher average dryout vapour quality than in a straight tube as reported by Carver (1964), Misopolski (1969), Bell (1969), Shires (1971) and Crain (1973).

The effect of mass velocity and heat flux on the dryout vapour quality has been reported by Carver et al (1964), Kozeki (1970), Duchatelle (1973) and Naitoh et al (1974), and it is concluded that the critical vapour quality decreases on increasing the mass velocity and the wall heat flux. However, the reverse effects have also been reported by Duchatelle (1973). The effect of pressure on the dryout vapour quality has been investigated by Naitoh et al (1974). It is found that the critical vapour quality decreases as pressure is increased. They have correlated the critical vapour quality as a function of heat flux and pressure as follows:

$$x_{cr} = 1.0 - (0.612\ p^{0.186} - 1.195)\ \dot{q}'' \times 10^{-3} \qquad (3.93)$$

where p is pressure in bars

$\dot{q}''$ is heat flux in kW/m^2

$$51 < p < 173 \text{ bars}$$

$$360 < G < 1400 \text{ kg/m}^2\text{s}$$

$$58 < \dot{q}'' < 640 \text{ kW/m}^2$$

Other dimensional correlations have been given by Ruffel (1974) in terms of the coil dimensions for the top and inside positions of the tube as follows:

For the top position:

$$x_{cr} = 1 - \frac{0.13\ D/100\ d}{(G/10^3)^{1.5}} \left(\frac{\dot{q}''}{100}\right)^{0.75(G/10^3)^{0.5}} \tag{3.94}$$

and for the inside position:

$$x_{cr} = 1 - 10^{-4} \left\{4 \times \dot{q}'' + 0.109 \times 10^{-3}\ G^2\ \left(\frac{D}{d}\right)^{0.5}\right\} \tag{3.95}$$

$\dot{q}''$ in kW/m^2 and G in kg/m^{2}s:

$$300 < G < 1800 \text{ kg/m}^2\text{s}$$

$$0.06 < \dot{q}''/G < 0.34 \text{ kJ/kg}$$

It should be mentioned that the definition of the dryout point, average critical vapour quality and the processes of experimental data differ for different investigators and mostly they are affected by personal interpretation and observations.

In the present work, equations (3.93), (3.94) and (3.95) have been compared with the available experimental results of Carver et al (1964) and Kozeki (1970) as shown in Tables 3.1 and 3.2. It appears that equation (3.95) predicts the average dryout vapour quality better than equations (3.93) and (3.94) at mass velocities less than 1000 kg/m s. But at higher mass velocities, the average values of two predictions from equations (3.94) and (3.95) are taken into account, and give better prediction than equation (3.93) does.

In the present study, we apply equation (3.95) to define the critical dryout vapour quality, as it is more reasonable at the low mass velocities which are involved in the stability analysis. However, in the

Table 3.1: Comparison of data of Carver et al (1964) and Kozeki et al (1970) with dryout correlations

Source	P (bar)	G (kg/m²s)	$\dot{q}''$ (kW/m²)	D/d	x_{cr}		
					Experiment	Equation (3.95)	Equation (3.93)
Kozeki et al (1970)	21	325	165	40	0.93	0.926	Not valid
	21	486	165	40	0.96	0.917	
Carver et al (1964)	179	678	325	38	0.79	0.83	0.866
	179	678	325	38	0.65	0.77	0.795

Table 3.2: Comparison of data of Carver et al (1964) with dryout correlation

Source	P (bar)	G (kg/m²s)	$\dot{q}''$ (kW/m²)	D/d	x_{cr}		
					Experiment	Average Equations (3.94) & (3.95)	Equation (3.93)
Carver et al (1964)	179	1355	442	38	0.8	0.789	0.817
		1355	473	38	0.79	0.782	0.8
		1897	407	38	0.77	0.76	0.832
		1897	460	38	0.76	0.74	0.81
		1897	477	155	0.68	0.47	0.8
		1897	694	155	0.49	0.34	0.71
		1355	442	155	0.63	0.55	0.817

computer program "HOB", provision has been made for the use of any other correlations.

3.7.5 Onset of Superheating

The superheated region is normally assumed to commence at the point where the bulk fluid enthalpy reaches the saturated value of vapour enthalpy at local pressure:

$$H = H_v \tag{3.96}$$

3.8 HEAT TRANSFER COEFFICIENTS IN DIFFERENT REGIMES IN HELICALLY-COILED TUBES

3.8.1 Liquid Phase

The fluid flow inside helically-coiled tubes is considered turbulent and it is believed that the forced convection heat transfer is most dominant inside the tube. This can be explained by the high mass velocity and the secondary circulation of fluid in coils of once-through boilers.

The correlation for heat transfer coefficient in terms of dimensionless groups is given by Seban and McLaughlin (1963), and it is confirmed experimentally by many other investigators (Owhadi (1966); Crain (1973); Mori (1967):

$$\frac{Nu_c}{Nu_s} = \left[Re\ (\frac{d}{D})^2\right]^{1/20} \tag{3.97}$$

$$Nu_s = 0.023\ Re^{0.8}\ Pr^{0.4} \tag{3.98}$$

Therefore, it is assumed that the complete mixing of the fluid exists at any cross-section and the liquid bulk temperatures remain constant at each section. Furthermore, the temperature differences between the tube wall and the bulk of liquid are, in practice, typically less than $20^{o}C$. Hence, in calculating equation (3.97), liquid transport properties are taken to be appropriate to the bulk temperature at local pressure.

3.8.2 Two-Phase Heat Transfer Coefficient

Boiling flow inside helically coiled tubes has concerned a number of researchers who have attempted to examine the flow phenomena

locally. Experimental evidence has revealed that the two-phase heat transfer coefficient varies at different positions around the periphery of the tube, and it is higher than those of straight tubes under similar conditions. This has been interpreted as due to the effect of secondary circulation of flow, gravity and centrifugal forces as discussed before.

The information about the average heat transfer coefficient at each cross-section is limited to low pressure systems. Owhadi et al (1966,1968) have reported an experimental investigation of boiling flow at low pressures in helically-coiled tubes. Circumferential average heat transfer coefficient has been correlated in terms of the Lockhart-Martinelli (1949) parameter as follows:

$$\frac{h_{tp}}{h_{lc}} = f\left(\frac{1}{X}\right) \tag{3.99}$$

where h_{lc} is the value of heat transfer coefficient if the liquid phase alone was considered inside the coil and it is given by equation (3.97). The Lockhart-Martinelli parameter is approximated as follows:

$$X = \left(\frac{1-x}{x}\right)^{0.9} \left(\frac{\rho_v}{\rho_l}\right)^{0.5} \left(\frac{\mu_l}{\mu_v}\right)^{0.1} \tag{3.100}$$

Owhadi et al (1966,1968) have confirmed that the heat transfer coefficient was increasing along the tube at medium vapour mass quality ranges, but the experimental data scattered in low and high quality ranges.

In the other report by Crain (1973), the ratio of the heat transfer coefficient to a heat transfer coefficient calculated as if only the vapour were flowing in the tube, has been correlated against the Lockhart-Martinelli parameter for higher quality ranges up to 90 per cent.

This correlation is supposed to complement the Owhadi et al investigation and the present author has compared these two correlations in an attempt to fit a polynomial for both sets of data for quality ranges of 0 to 90%. It is found that the two sets of data from Owhadi (1966) and Crain (1973) exhibit large discrepancies at medium quality ranges of their experimental results.

Kozeki et al (1970) have reported the investigation of helically-coiled tube once-through boilers at pressures of 5-21 bars where a constant temperature primary fluid was employed for heating the tubes. It was noticed that the local heat transfer coefficients were less likely to be affected by mass flow rate, vapour quality and pressure. The average heat transfer coefficient, unlike the Owhadi correlation, was not altered with the increase of vapour quality. Kozeki attributed the discrepancy to the differences of test conditions. Later, Kozeki (1973) correlated the heat transfer coefficient applying the Lockhart-Martinelli parameter which was compared to the Schorck and Grossman (1959) empirical equation.

It appears to the author that there is a lack of certainty about the use of the existing heat transfer correlations in helical tubes, even for low pressure systems, and consequently, the application of these correlations is open to question at high pressures. Therefore, it is considered preferable to use heat transfer correlations for straight tubes at high pressures. Then the overall steady-state performance of the helical tubes are examined under the application of such correlations.

A series of experimental programmes has been conducted at Babcock and Wilcox Limited at high pressures. The two-phase heat transfer correlation of Jens-Lottes (1951), which is modified by Thom et al (1965), has been employed in the process of steady-state performance

of the rigs. It has been shown (Ruffel (1974)) that the prediction of tube wall temperatures, length of boiling boundaries and vapour exit conditions agree very well with the experimental values.

Therefore, in the present investigation, the following correlation of tube wall temperature is considered to be valid for both subcooled and bulk boiling regions:

$$T_w = T_{sat} + J\, e^{-mp}\, \dot{q}''^{n} \tag{3.101}$$

where p is absolute pressure in bars, $\dot{q}''$ is the heat flux in kW/m^2 and T is in degrees C. Then, the case:

$$J = 4.45 \quad , \quad m = -1/62 \quad , \quad n = 0.25 \tag{3.102}$$

corresponds to the correlation of Jens and Lottes, while the case:

$$J = 0.71 \quad , \quad m = -1/86.874 \quad , \quad n = 0.5 \tag{3.103}$$

resembles the correlation of Thom et al.

We have also examined the heat transfer correlation by Chen (1963). The Chen correlation is extended up to dryout point. It is found that the use of either Chen or Thom et al has no significant effect on the steady-state performance nor on the transient oscillations.

3.8.3 Post Dryout Heat Transfer

Post dryout heat transfer is entered when the liquid film on the heated surface finally disappears as a result of liquid evaporation and droplet entrainment. Experimental evidence of straight tube post

dryout region has revealed that the flow pattern is basically one of droplets being carried along in a vapour phase which can be superheated. Similar phenomena would be expected to occur in helically-coiled tubes to some extent.

Maddock and Lacey et al (1974), in their air-water experiments, have examined the annular film and the droplets behaviour. It is postulated that the droplets originating from the inside film are affected by the secondary circulation, centrifual and drag forces. The large droplets or the droplets near the outer side of the tube cross-section are rapidly deposited onto the surface while the small droplets would be influenced by the drag forces which would result in a higher residence time. On the other hand, small droplets should quickly evaporate. Therefore, droplets, as compared to the case of straight tubes, are not likely to penetrate very far downstream into the superheated region.

The vapour superheating, in the dry wall region, increases the complexity of the analysis, and additional information of droplets (e.g. droplet population and sizes) can be incorporated with the proposed model of Bennett et al (1968) and Bailey et al (1973) to overcome this difficulty.

Fortunately, in coiled steam generators, the distance between the dryout point and the onset of the superheated section tends to be short (Carver et al (1964); Owhadi (1966); Naitoh et al (1974)). One can therefore assume that heat is transferred to the vapour-liquid mixture by a forced convection mechanism and furthermore the bulk vapour phase does not become superheated. Following this assumption, then one of the heat transfer correlations for straight tubes (e.g. Bishop (1965)) may be employed with proper modification for use in helically-coiled tubes.

For the film of boiling water in the post dryout region at the ranges of 18 < p < 215 bars and 100 < G < 2000 kg/m^{2}s, Miropolski and Pikus (1969) have suggested the following expression:

$$Nu = c\, Re^{0.8}\, Pr_w^{0.8} \times b \tag{3.104}$$

where

$$Re = \frac{G\, d_i}{\mu_v} \tag{3.105}$$

and

$$b = Y \{x + \frac{\rho_v}{\rho_l} (1 - x)\}^{0.8} \tag{3.106}$$

$$Y = \frac{\rho_l}{\rho_v} \{1 - (1 - \frac{\rho_v}{\rho_l})\, x^{0.2}\} \tag{3.107}$$

$$c = 0.017\ (1 + 1.59\, \frac{d}{D}) \tag{3.108}$$

and where the physical properties in the vapour Prandtl number are evaluated at the wall temperature, otherwise the saturation values are used.

Nevertheless, unlike the situation of straight tubes, in the case of coiled tubes, the rise in the tube metal temperature with the initiation of the dryout is gradual and small, as has been experienced by many investigators (Cumo (1972); Kozeki (1970); Miropolski (1969)). Therefore, similar assumptions to those of Ruffel (1974) are made, i.e. that the film resistance beyond the dryout point increases linearly with vapour quality from the value of the nucleate boiling at the onset of the dryout to the K per cent of the value of the dry saturated vapour. The value of K = 70% is recommended by Ruffel (1974) in agreement with the experimental results of Babcock and Wilcox Limited.

In the computer code, other options are provided to replace

the present assumption with the heat transfer coefficients of the form given in equations (3.104) to (3.108).

3.8.4 Convective Heat Transfer to Vapour Phase

When the fluid has become nearly dry vapour, it behaves once more as a single-phase fluid and obeys similar laws to the liquid phase. The single-phase heat transfer coefficient of the following form is employed beyond the superheated boundary:

$$Nu_s = K\, Re^m\, Pr^n \tag{3.109}$$

A comprehensive review of the dry steam heat transfer coefficients has been carried out by Bailey (1970) and for pressure ranges of 150-210 bars, the correlation of Bishop et al (1964) is recommended where the constants of equation (3.109) are:

$$K = 0.0073 \quad , \quad m = 0.886 \quad , \quad n = 0.61 \tag{3.110}$$

At pressure ranges of 20-100 bars, Heineman's correlation (1960) can be used where:

$$K = 0.0133 \quad , \quad m = 0.84 \quad , \quad n = 1/3 \tag{3.111}$$

This correlation has been used successfully in the Babcock and Wilcox test rigs as reported by Ruffel (1974).

The fluid properties in the recommended correlations are based on the film temperature. However, it has been quoted (Bailey (1970)) that the Bishop et al correlation slightly underestimates the experimental

values of the heat transfer coefficient, and the bulk temperature is replaced for assessing the fluid properties. This improves to some extent this discrepancy.

It is appropriate to mention that the local values of heat transfer coefficient can vary around the periphery of the curved tube. This has been noticed by Miropolski et al (1969) who found that the heat transfer rate could become less than the value of the straight tube at the inside of the curved tubes.

3.9 SUMMARY AND REMARKS

A summary of the relevant heat transfer correlations and the transition boundaries is given in Table 3.3. The correlations are empirically deduced from experimental results and they should be applied to situations outside those of their formulation with great care.

The correlations have been developed for steady-state conditions, and in the next chapter they will be employed in solutions of equations (3.1), (3.3), (3.8), (3.11), (3.14) and (3.16) which describe the dyanmics of a once-through steam generator. In the dynamic calculation, the situation is, therefore, regarded as a quasi-steady condition where the steady-state correlations are assumed to be valid at each time interval.

Table 3.3: Summary of the heat transfer and transition boundary relationships for helically coiled tubes

Heat Transfer Regions and Transition Boundaries	Source	Correlations P (bars), $\dot{q}''$ (kW/m^2), G (kg/m^{2}s), T (^{o}C)	Range of Original Experiments
Single-phase liquid	Seban-McLaughlin (1963)	$\frac{Nu_c}{Nu_{st}} = \left(Re\ (d/D)^2\right)^{0.05}$ $Nu_{st} = 0.023\ Re_b^{0.8}\ Pr_b^{0.4}$	$17 < D/d < 104$ $12 < Re < 65000$
Transition to subcooled boiling	Developed in the present study	$\theta_{sub} = 4.3\ Re^{1/6}\ (\frac{a}{R})^{-1/12}\ \frac{1}{z_o}$ $z_o = G\ \Delta\ H_i/4\dot{q}''$	Satisfactory agreement with experimental data at 179 and 1-2 bars
Subcooled boiling HTC	1. Thom et al (1965)	$\Delta T_{sat} = 0.71\ e^{-p/86.874}\ \dot{q}''^{0.5}$	$51.7 < p < 138$ $2BD < \dot{q}'' < 600$ water-steam only
	2. Jens-Lottas (1951)	$\Delta T_{sat} = 4.45\ e^{-p/62}\ \dot{q}''^{0.25}$	$7 < p < 172$, $\dot{q}'' < 12500$ $11 < G < 10500$ water-steam
Transition to bulk boiling		$H_1 = H_f$	
Two-phase nucleate boiling heat transfer coefficient	1. Thom et al (1965) 2. Jens-Lottas (1951)	As subcooled boiling region	
	3. Chen (1963)	$h_{TP} = h_{NcB} + h_c$ $h_c = 0.023\ \left(\frac{G(1-x)d}{\mu_f}\right)^{0.85}\ \left(\frac{c_p}{k}\right)_f^{0.4}\ .\ \left(\frac{d}{D}\right)^{0.1}\ \frac{k_f}{d}\ .\ F$ $h_{NcB} = 0.00122\ \frac{k_f^{0.79}\ c_{pf}^{0.45}\ \rho_f^{0.49}}{\sigma^{0.5}\ \mu_f^{0.29}\ H_{fv}^{0.24}\ \rho_v^{0.25}}\ .$ $\Delta T_{sat}^{0.24}\ \Delta p_{sat}^{0.75}\ .\ S$ $F = Fun.(1/X_{tt})\quad ,\quad S = Fun.(Re_{TP})$	$1 < p < 35$ $6.2 < \dot{q}'' < 2400$ $x < 71\%$

Table 3.3 (continued)

Heat Transfer Regions and Transition Boundaries	Source	Correlations p (bars), $\dot{q}''$ (kW/m^2), G (kg/m^{2}s), T (^{o}C)	Range of Original Experiments
Dryout position	Ruffel (1974)	$x_{cr} = 1 - 10^{-4} \left(4\dot{q}'' + 0.109 \times 10^{-3} G^2 \left(\frac{D}{d}\right)^{0.5}\right)$	$300 < G < 1800$ $0.06 < \dot{q}''/G < 0.34$ $48 < D/d < 186$ water-steam
Post dryout heat transfer coefficient	1. Miropolishi and Dikus (1969)	$Nu = A\, Re^{0.8}\, Pr_w^{0.8}.\, B$ $A = 0.017\ (1 + 1.59\ \frac{d}{D})$ $B = \frac{\rho_l}{\rho_v}\left(1 - (1 - \frac{\rho_v}{\rho_l})\, x^{0.2}\right)\left(x + \frac{\rho_v}{\rho_l}\,(1 - x)\right)^{0.8}$	$98 < p < 215$ $100 < G < 2000$ water-steam only
	2. Ruffel (1974)	Linear increase of resistance with x up to k% of dry steam	
Transition to superheat		$H = H_v$	
Single-phase vapour (steam)	1. Heineman (1960)	$Nu = 0.0133\ Re_f^{0.84}\ Pr_f^{1/3}$	$20 < p < 104$ $190 < G < 1100$ $150 < \dot{q}'' < 910$ $2.4 < d < 8.5$ mm
	2. Bishop et al (1964)	$Nu = 0.0073\ Re_f^{0.866}\ Pr_f^{0.61}$	$162 < p < 215$ $680 < G < 3400$ $240 < \dot{q}'' < 2570$ $2.5 < d < 5.1$ mm

CHAPTER 4

NUMERICAL TECHNIQUES AND SIMULATION PROGRAM

4.1 INTRODUCTION

This chapter summarises the governing differential equations involved in the simulation and describes the mathematical manipulation necessary for the solution process.

The continuous space discrete time (CSDT) technique is employed in the numerical integration of the resulting set of first order non-linear partial differential equations. Iteration techniques are set up for coupling of the primary and the secondary variables, and for compatability between the inlet mass velocity and system pressure drop. The boiling boundaries are treated more rigorously to overcome the discontinuous behaviour of variables at these positions.

The numerical methods applied together with the solution procedure are discussed. The general strategy of the simulation program is outlined; a brief description of its individual subroutines is given.

4.2 REVIEW OF GOVERNING EQUATIONS

The steam generator is represented by a single helically-coiled tube of length L containing flowing water/steam, with an outer concentric tube of counter flowing primary gas (Figure 3.1).

The mathematical model of the system, which was presented in Chapter 3, is as follows:

The primary flow:

$$\frac{\partial T_g}{\partial t} - u_g \frac{\partial T_g}{\partial z} + \frac{\pi d_o h_p}{\rho_g A_g C_{pg}} (T_g - T_w) + \dot{q}''_{loss} = 0 \qquad (3.1)$$

The tube wall:

$$\frac{\partial T_w}{\partial t} - \frac{\pi d_o h_p}{m_w C_w} (T_g - T_w) + \frac{\pi d_i h_s}{m_w C_w} (T_w - T) = 0 \qquad (3.3)$$

$$\dot{q}'' = h_s (T_w - T) \qquad (3.7)$$

The secondary flow:

$$\frac{\partial \rho_1}{\partial t} + \frac{\partial G}{\partial t} = 0 \qquad (3.8)$$

$$\frac{\partial \rho_2}{\partial t} + G \frac{\partial x}{\partial z} + x \frac{\partial G}{\partial z} = 0 \qquad (3.11)$$

$$\frac{\partial G}{\partial t} + 2 v_1 G \frac{\partial G}{\partial z} + G^2 \frac{\partial v_1}{\partial z} + \rho_1 g \sin \beta + \frac{P}{A} \tau_w + \frac{\partial p}{\partial z} = 0 \qquad (3.14)$$

$$\frac{\partial H_1}{\partial t} + G \frac{\partial H}{\partial z} + H \frac{\partial G}{\partial z} - v_2 G \frac{\partial p}{\partial z} = \frac{P}{A} \dot{q}'' \qquad (3.16)$$

These equations are written in one-dimensional space, z, in the direction of secondary flow. z varies from the inlet $z = 0$ to the outlet

$z = L$ and t between 0 and ∞.

Three important conditions are:

i) At $z = 0$, boundary conditions are applied to the temperature and pressure of the secondary flow.

ii) The boundary conditions on the gas flow and temperature are applied at the outlet of the steam generator ($z = L$) at which the interaction between the vapour and gas is terminated.

iii) Finally, a certain given pressure drop is imposed between the inlet and the outlet of the steam generator.

4.3 NUMERICAL METHODS

It has been shown by Carling (1965), Brereton et al (1967), and Noronha (1968) that the continuous space discrete time (CSDT) technique is much more suited to solving the two-point boundary value problem of a once-through boiler, heated by primary flow. In this scheme (CSDT), the time derivatives are replaced by appropriate finite difference approximations and the resulting equations of the primary and the secondary sides are integrated in space at every time step by one of the numerical techniques of ordinary differential equations.

Therefore, by introducing normal first order backward difference schemes to substitute time derivatives, i.e. $\partial T/\partial t = (T - T^*)/\Delta t$, the set of partial differential equations (3.1), (3.3), (3.7), (3.8), (3.11), (3.14) and (3.16) are written as follows:

The primary flow:

$$\frac{\partial T_g}{\partial z} = \left(\frac{\pi d_o h_p}{\rho_g A_g C_{pg}} + \frac{1}{u_g \Delta t}\right) T_g - \frac{\pi d_o h_p}{\rho_g A_g C_{pg}} T_w - \frac{1}{u_g \Delta t} T_g^* \qquad (4.1)$$

z varies between 0 and L. Equation (4.1) is written with the same spatial variable, z, in the direction of the secondary flow. A transformation of this variable, namely $z' = L - z$, must be made before equation (4.1) can be integrated in the direction of the primary flow as discussed later. Thus, equation (4.1) becomes:

$$\frac{\partial T_g}{\partial z'} = -\left(\frac{\pi d_o h_p}{\rho_g A_g C_{pg}} + \frac{1}{u_g \Delta t}\right) T_g + \frac{\pi d_o h_p}{\rho_g A_g C_{pg}} T_w + \frac{1}{u_g \Delta t} T_g^* \qquad (4.2)$$

where z' goes from 0 to L.

The tube wall:

(a) The secondary side heat transfer coefficient is not a function of $\dot{q}''$ (single-phase region):

$$T_w = \frac{\pi d_o h_p T_g + \pi d_i h_s T + \frac{m_w C_w}{\Delta t} T_w^*}{\pi d_o h_p + \pi d_i h_s + \frac{m_w C_w}{\Delta t}} \tag{4.3}$$

$$\dot{q}'' = h_s (T_w - T) \tag{4.4}$$

(b) The secondary side heat transfer coefficient is a function of $\dot{q}''$ (two-phase region):

$$T_w = T_{sat} + J e^{-m.p} \dot{q}''^n + \left[\frac{d_i}{2 k_w} ln \frac{d_o + d_i}{2d_i}\right] \dot{q}'' \tag{4.5}$$

$$\dot{q}'' = \frac{\pi d_o h_p}{\pi d_i} T_g + \frac{m_w C_w}{\pi d_i \Delta t} T_w^* - \left[\frac{\pi d_o h_p}{\pi d_i} + \frac{m_w C_w}{\pi d_i \Delta t}\right] T_w \tag{4.6}$$

The secondary flow:

$$\frac{\partial G}{\partial z} = -\frac{\rho_1}{\Delta t} + \frac{\rho_1^*}{\Delta t} \tag{4.7}$$

$$\frac{\partial x}{\partial z} = -\frac{x}{G}\frac{\partial G}{\partial z} + \frac{\gamma}{G} - \frac{\rho_2}{G \Delta t} + \frac{\rho_2^*}{G \Delta t} \tag{4.8}$$

$$-\frac{\partial p}{\partial z} = 2 v_1 G \frac{\partial G}{\partial z} + G^2 \frac{\partial v_1}{\partial z} + \frac{P}{A} \tau_w + \rho_1 g \sin \beta + \frac{G}{\Delta t} - \frac{G^*}{\Delta t} \tag{4.9}$$

$$\frac{\partial H}{\partial z} = \frac{P}{A} \dot{q}'' - \frac{H}{G}\frac{\partial G}{\partial z} - \frac{H_1}{G \Delta t} + v_2 \frac{\partial p}{\partial z} + \frac{H_1^*}{G \Delta t} \tag{4.10}$$

z varies between 0 and L.

All parameters refer to the new time step ($t = I.\Delta t$) except those with '*' which refers to the previous time step.

The unknown parameters are T_g, T_w, $\dot{q}''$, G, p, x and H which describe the dynamic state of the system.

Values of h_p and h_s are given by equations (3.4) and (3.5), respectively. In the two-phase regions, the heat transfer coefficient (equation (3.101)) is a function of the local heat flux, $\dot{q}''$; therefore, the tube wall temperature, T_w, and the heat flux, $\dot{q}''$, are calculated from the simultaneous solution of equations (4.5) and (4.6) by Newton's method (Conte (1971)). Values of ρ_1, ρ_2, v_1, v_2, H_1 and τ_w are given by equations (3. 9), (3.12), (3.15), (3.17), (3.18) and (3.22), respectively. In the case of thermal non-equilibrium, subcooled boiling region, the enthalpy of the liquid is deduced from the knowledge of the vapour quality, x, and the mixed mean enthalpy, H, by rearranging equation (3.20) as follows:

$$H_l = \frac{H - x\,H_v}{1 - x} \tag{4.11}$$

Temperatures can be found from the supplied state equations in the form of:

$$T = Fun\ (p,H) \quad \text{or} \quad T_{sat} = Fun\ (p) \tag{4.12}$$

Finally, liquid and vapour physical properties are found in a similar manner as a function of local pressure and temperature from supplied functions.

In Appendix B, it has been shown that the backward difference approximation of time derivatives produces a stable time solution in the

case of a linear heat exchanger, and this approximation has also been used successfully for the non-linear case of the present study.

The resulting set of first order non-linear differential equations (4.2), (4.7), (4.8), (4.9) and (4.10) is presented in the form of a gradient of an individual state variable, expressed in terms of the remaining variables and their gradients at time t and $t - \Delta t$. Following Brereton and Carling (1967), a second order predictor corrector method is adopted for the integration of equations (4.2), (4.7), (4.8), (4.9) and (4.10) along the axial direction (Z).

At each time step, I, values of system variables are predicted at the nodal point $n.\Delta Z$ from the knowledge of previous nodes by using Euler open type formula (Conte (1965), McCracken and Dorn (1965)):

$$F_k\,(n,I) \;=\; F_k\,(n-2,I) + 2\,\Delta Z\,\frac{\partial F_k}{\partial Z}\,(n-1,I) \qquad (4.13)$$

where F_k is a system variable (H, G, x, p, T_g), $k = 1, 2, \ldots, 5$ and $\partial F_k/\partial Z$ is the gradient of the system variable (k) calculated from the right hand side of equations (4.2), (4.7), (4.8), (4.9) and (4.10).

Then the fluid temperature and densities are calculated from the state equations. Estimates of the void fraction (α) are made from equations (3.29) or (3.30). Also, the tube wall temperature, T_w, and the heat flux, $\dot{q}''$, are evaluated from a pair of equations (4.3) and (4.4) or (4.5) and (4.6) due to the predicted values. The results are used in the modified Euler closed type correction formula as follows:

$$F_k^{(i)}\,(n,I) \;=\; F_k\,(n-1,I) + \frac{\Delta Z}{2}\left[\frac{\partial F_k^{(i-1)}}{\partial Z}\,(n,I) + \frac{\partial F_k}{\partial Z}\,(n-1,I)\right] \qquad (4.14)$$

The predicted formula (4.13) provides a first approximation $F_k^{o}(n,I)$

which is used in the correction formula to get a better estimate of $F_k(n,I)$. An iterative procedure is evolved by the successive application of the corrector formula (4.14) and subsequent testing for convergence. The convergence is achieved when the difference between two successive iterations i and $i-1$, is within a specified positive tolerance, ε_k:

$$\left| \frac{F_k^i(n,I) - F_k^{i-1}(n,I)}{F_k^i(n,I)} \right| < \varepsilon_k \tag{4.15}$$

The accuracy that can be expected on each length step (ΔZ) is limited by the error of the corrector formula (4.14), and by the step size ΔZ. The value of ε_k is typically 10^{-4}, and the number of iterations never exceeds two with a proper choice of length step ΔZ. Values of ΔZ and Δt must be a compromise between the desired accuracy and minimum computing time. In the case of a counterflow heat exchanger with an imposed pressure drop on the secondary side, the time step Δt is related to the residence time of a pressure wave (L/C) to travel along the boiler (Bosgra and Buis (1970)), and it is therefore chosen to be:

$$\Delta t > \frac{L}{C} \tag{4.16}$$

where C is the sonic velocity which is typically 150-300 m/s for water/steam. The length step ΔZ is limited by the convergence of iterations of corrector formula (4.14). Accordingly (Conte (1965) and McCracken (1965)), ΔZ is taken such that:

$$\Delta Z < 2\, u_{in}\, \Delta t$$

Given a solution at time $t = t_1$, the solution of partial differential equations can be sought at time $t = t_1 + \Delta t$ by the technique outlined.

4.4 GENERAL CALCULATION PROCEDURE

The nature of counter flow heating is such that conservation equations of each side (primary and secondary sides) have to be integrated in opposite directions to avoid numerical instability (Carling (1965)). This requires iteration techniques to be set up for coupling of the primary and the secondary temperatures, also for compatability between the imposed pressure drop and calculated inlet mass velocity.

To carry out the calculation at any time step, equations of the secondary flow (equations (4.7) to (4.10)) and the tube wall (equations (4.3) to (4.6)) are integrated in parallel along the tube ($Z = 0$ to L) by using a predetermined primary temperature distribution, e.g. values of previous time step. Subsequent knowledge of a new wall temperature distribution enables re-calculation of the primary temperature distribution; the gas energy equation (4.2) is integrated from $Z = L$ to $Z = 0$. An iterative sequence is evolved by the alternative calculation of the secondary side and the tube wall temperatures, and subsequent evaluation of the primary temperature until the variables become compatible. i.e. The difference between two successive calculations of gas temperature and water/steam enthalpy becomes less than a prescribed tolerance.

In order to start the steady-state calculations, an estimate of the primary temperature distribution is necessary. Initially, the gas temperature distribution is considered to be uniform and equal to, e.g. the inlet gas temperature. Once the steady-state distributions are found, the distribution of the gas temperature from the previous time step is taken as the initial estimate for the new time in the dynamic calculation.

In the procedure outlined, it was assumed that the inlet mass

velocity of the secondary flow was known and no restriction on the pressure drop was applied. However, in view of the third boundary condition (section 4.2), if the system pressure drop is specified, the secondary side equations become a boundary value problem. Consequently, the inlet mass velocity must be matched accordingly via an extra iteration which accompanies the temperature-enthalpy iteration. The inlet mass velocity is iterated until the assigned accuracy between the calculated and imposed pressure drop is achieved. The iteration technique employed here is described in section 4.5.

Carling (1965) has investigated the convergence of the temperature-enthalpy iteration for a linear counter flow heat exchanger with known inlet mass velocity, and he concluded that the procedure outlined could always be convergent if:

$$\frac{k}{k + \frac{1}{u_{in}\,\Delta t}}\ \beta < 1 \qquad (4.17)$$

where k and u_{in} are the heat transfer characteristics and the inlet velocity of the secondary side, respectively. The coefficient β depends on heat transfer characteristics, k, and velocity of the primary flow. The value of β is always less than unity (Carling (1965)).

From equation (4.17) it is evident that the solution converges for any positive values of the inlet mass velocity. However, in the stability analysis, the inlet mass velocity may oscillate with increasing amplitude and this may result in reverse flow in some highly unstable systems. The numerical procedure cannot tolerate such complex behaviour. Therefore, the inlet mass velocity is examined at the beginning of each time step and the calculation is terminated when the inlet mass velocity

is about to reverse.

The technique outlined above has been successfully used with no difficulty so far. Experience indicates that convergence is rapid; usually three iterations are required to achieve errors less than 0.001 T_{sat} for temperatures and 0.001 Δp_s for system pressure drops.

The following steps summarise the sequence of iteration procedures at the current time $(I.\Delta t)$:

1. Estimate a distribution for gas temperature:

$$T_g^i\ (n,I) \;=\; T_g\ (n,I-1) \qquad n \;=\; 1,\ 2,\ \ldots,\ N$$

where N is the total length step along the tube; n and I are the current steps of length and time, respectively. i is the number of iterations.

2. Estimate the inlet mass velocity, $G(1,I)$, from equation (4.18) as given in section 4.5.

3. Solve equations of the secondary flow (equations (4.7) to (4.10)) and the tube wall (equations (4.3) and (4.4) or (4.5) and (4.6)) by the numerical technique of section 4.3. This results in:

$$H^{(i)}\ (n,I)\ ,\ G\ (n,I)\ ,\ x\ (n,I)$$
$$p\ (n,I)\ ,\ T_w\ (n,I)\ ,\ \Delta p\ (t)\ ,\ n \;=\; 1,\ 2,\ \ldots,\ N$$

4. Check convergence of the inlet mass velocity by comparing the calculated and imposed pressure drop, i.e.

$$\left|\ \Delta p\ (t) - \Delta p_s\ (t)\ \right| \;<\; \varepsilon$$

If convergence criterion is not satisfied, find a new value of the inlet mass velocity from equation (4.21) as described in section 4.5. Go to step 3.

5. Solve energy equation of the primary side (equation (4.2)) by the numerical technique of section 4.3 to find:

$$T_g^{(i)}(n,I) \quad , \quad n = N, N-1, \ldots, 1$$

6. Check for convergence of temperature and enthalpy, i.e.

$$\left| H^{(i)}(n,I) - H^{(i-1)}(n,I) \right| < \varepsilon_H$$

$$\left| T_g^{(i)}(n,I) - T_g(n,I) \right| < \varepsilon_T$$

If convergence criteria are not satisfied, go to step 3.

7. Start the calculation of the new time step from step 1.

The principal block diagram of the computation procedure is illustrated in Figure 4.1.

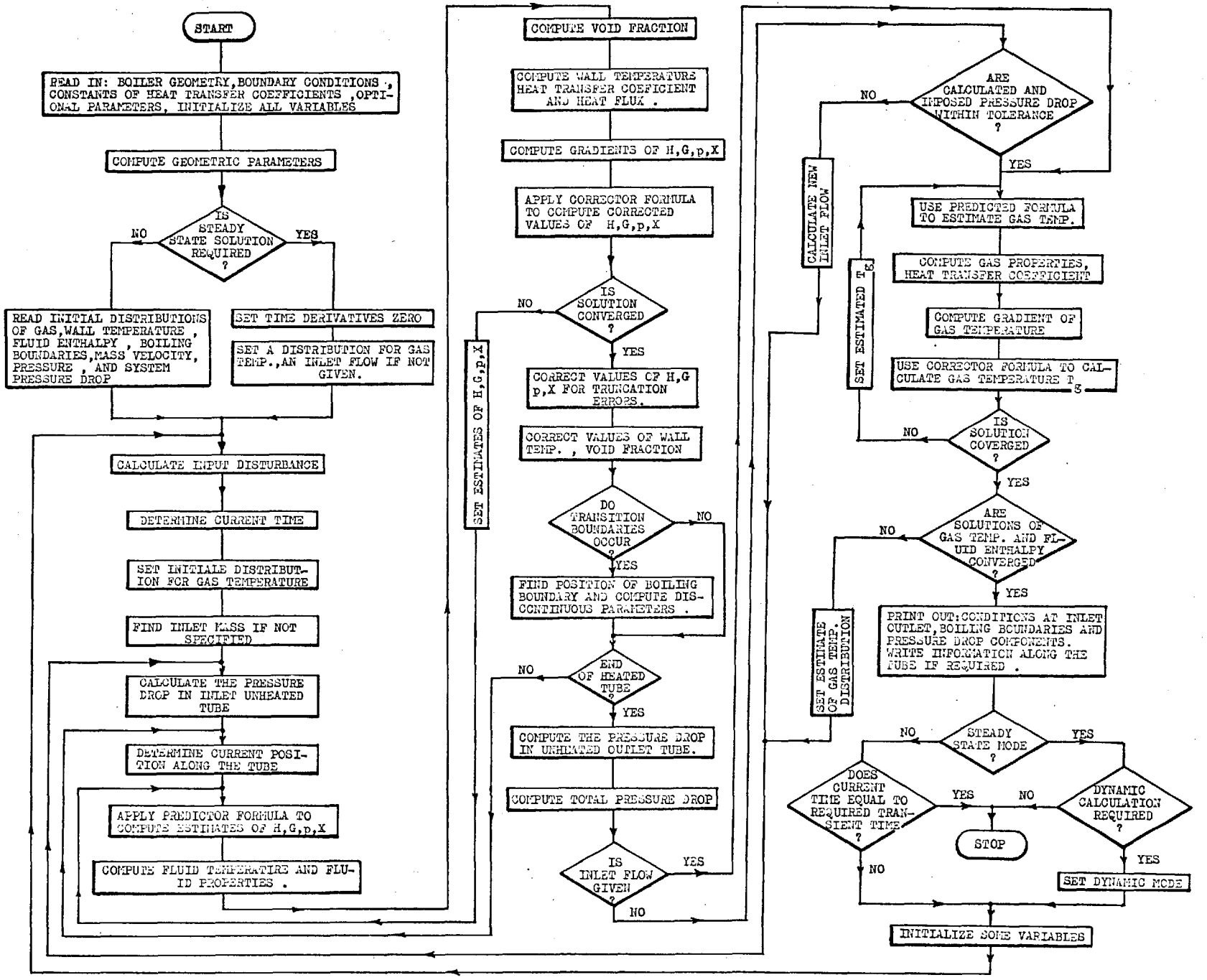


FIG.4-1 FLOW DIAGRAM SHOWING OVERALL SEQUENCE OF COMPUTATIONS

4.5 ITERATION PROCEDURE FOR THE INLET MASS VELOCITY

For a given pressure drop as a system boundary condition, the inlet mass velocity is a dependent parameter, and under certain operating conditions (heat flux, inlet subcooling and pressure) it has at least one value which satisfies the momentum conservation law.

The momentum equation is, as mentioned, integrated with respect to the axial coordinate to obtain the pressure distribution and hence some means are required to evaluate the appropriate time varying inlet mass velocity. A simple iteration technique based on the secant method (Conte (1965)) has been adopted as described below.

As a first approximation, the inlet mass velocity at $t + \Delta t$ is set to be:

$$G\ (o, t + \Delta t) = G\ (o, t) + \beta \left(\frac{\partial G}{\partial t}\right) \Delta t \tag{4.18}$$

where

$$\frac{\partial G}{\partial t} = \frac{G\ (o, t) - G\ (o, t - \Delta t)}{\Delta t} \tag{4.19}$$

and

$$0 < \beta < 1$$

The weighting factor, β, is chosen so as to give a reasonable and positive value for $G\ (o, t + \Delta t)$

The pressure drop, which is calculated from the momentum conservation law, Δp at $t + \Delta t$, is compared to that of the imposed boundary condition, Δp_s at $t + \Delta t$. If the result is not within the tolerance:

$$\left| \Delta p\ (t + \Delta t) - \Delta p_s\ (t + \Delta t) \right| < \varepsilon \tag{4.20}$$

then the next estimate for $G^{i+1}\ (o, t + \Delta t)$ is made according to:

$$G^{i+1}\ (o, t + \Delta t) = G^{i}\ (o, t + \Delta t) - \frac{\Delta p^{i}\ (t + \Delta t) - \Delta p_{s}\ (t + \Delta t)}{\left.\frac{\partial\ \Delta p}{\partial G}\right|_{t+\Delta t} - \left.\frac{\partial \Delta p_{s}}{\partial G}\right|_{t+\Delta t}} \qquad (4.21)$$

where $$\left.\frac{\partial\ \Delta p}{\partial G}\right|_{t+\Delta t} = \frac{\Delta p^{i}\ (t + \Delta t) - \Delta p^{i-1}\ (t + \Delta t)}{G^{i}\ (o, t + \Delta t) - G^{i-1}\ (o, t + \Delta t)} \qquad (4.22)$$

and i in the above equations refers to the number of iterations performed.

The entire process is carried out with the temperature-enthalpy iteration as explained before, and the tolerance $\varepsilon = 0.001\ \Delta p_{s}$ is usually achieved in about three iterations.

4.6 TRANSITION BOUNDARIES

System parameters may possess discontinuous features at transition boundaries due to the changes in the characteristics of thermo-fluid flow.

The density variation at the bulk boiling and superheater boundaries causes discontinuities in the slope of the fluid mass velocity, temperature, and pressure distributions.

The change of the mechanism of the heat transfer occurs at the onset of the subcooled boiling, dryout, and superheater boundaries, and therefore it induces discontinuous behaviour on the heat flux and the tube wall temperatures.

In spite of the fact that most of the system parameters remain continuous at transition boundaries, their derivatives do not exist (Knowles et al (1973)). At the onset of the subcooled boiling, the inside temperature of the tube wall exhibits a slight drop. The reverse behaviour may happen at the dryout boundary, although the jump of the wall temperature at the dryout is suppressed in the helically-coiled tubes.

The discontinuous behaviour of the system parameters is undesirable in any numerical treatments, and, indeed, it complicates the problem at those intervals containing any discontinuity. For example, the conservation of mass in the form of:

$$\frac{\partial \rho}{\partial t} + \frac{\partial G}{\partial z} = 0 \tag{4.23}$$

is not applicable within a control volume of Figure 4.2, which contains a phase transition at z_o. The derivatives $\partial\rho/\partial t$ and $\partial G/\partial z$ are numerically non-existent at the transition point z_o. However, system parameters and their derivatives exist and are continuous upstream of the discontinuous

point z_o. The continuity law may be written for the upstream of the transition point as follows:

$$\left.\frac{\partial \rho}{\partial t}\right|^{-\varepsilon} + \left.\frac{\partial G}{\partial z}\right|^{-\varepsilon} = 0 \qquad (4.24)$$

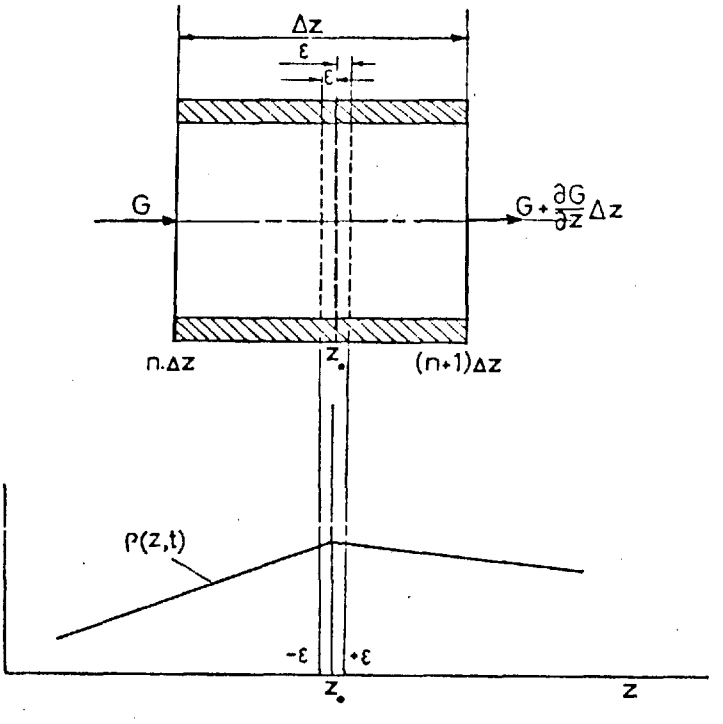


Figure 4.2

In a similar manner, the continuity equation of the downstream of z_o is:

$$\left.\frac{\partial \rho}{\partial t}\right|^{+\varepsilon} + \left.\frac{\partial G}{\partial z}\right|^{+\varepsilon} = 0 \qquad (4.25)$$

This method can be applied to any other conservation law and it

requires the computation of the derivatives at the upstream and the downstream of the transition boundary.

4.6.1 Method of Approximation of the Time Derivatives

Consider a moving transition boundary (Figure 4.3). The boundary which was located at position P at time $(I-1)\Delta t$ moves to a position T during the time interval Δt. Assume that the position of T is known, and its distance from the boundary of a control volume between the nodes $(n-1)$ and (n) is equal to $k_2\Delta z$. The approximate time derivation of a system parameter f at the upstream of T is:

$$\left.\frac{\partial f}{\partial t}\right|_T^{-\varepsilon} = \frac{f|_T^{-\varepsilon} - f|_{T'}^{-\varepsilon}}{\Delta t} \tag{4.26}$$

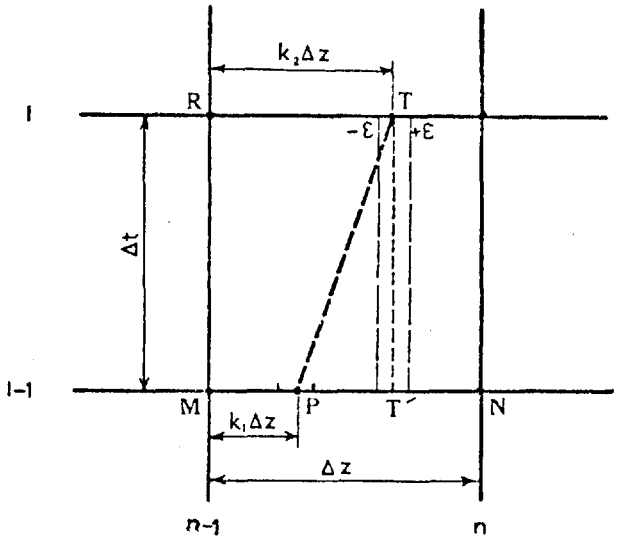


Figure 4.3

The value of $f|_{T'}^{-\varepsilon}$ may be related linearly to the known information of the previous time as:

$$f|_{T'}^{-\varepsilon} = \lambda\, f|_P^{-\varepsilon} + (1-\lambda)\, f|_M \tag{4.27}$$

The Taylor series expansion about points P and T' at a fixed time $(I-1)\Delta t$ may be written as follows:

$$f|_{T'}^{-\varepsilon} = f|_M + k_2\,\Delta z\,\left.\frac{\partial f}{\partial z}\right|_M + \frac{1}{2}\,k_2^2\,\Delta z^2\,\left.\frac{\partial^2 f}{\partial z^2}\right|_M + \ldots. \tag{4.28}$$

$$f|_P^{-\varepsilon} = f|_M + k_1\,\Delta z\,\left.\frac{\partial f}{\partial z}\right|_M + \frac{1}{2}\,k_1^2\,\Delta z^2\,\left.\frac{\partial^2 f}{\partial z^2}\right|_M + \ldots. \tag{4.29}$$

Inserting equations (4.28) and (4.29) into equation (4.27) and neglecting the second and higher order derivatives, yields:

$$\lambda = \frac{k_2}{k_1} \tag{4.30}$$

Substituting equations (4.27) and (4.30) into equation (4.26), the time derivative of the upstream region can be approximated as:

$$\left.\frac{\partial f}{\partial t}\right|_{T'}^{-\varepsilon} = \frac{\frac{k_2}{k_1}\left(f|_T^{-\varepsilon} - f|_P^{-\varepsilon}\right) + \left(1 - \frac{k_2}{k_1}\right)\left(f|_T^{-\varepsilon} - f|_M^{-\varepsilon}\right)}{\Delta t} \tag{4.31}$$

Similarly, the approximate time derivatives at downstream can be related to the known information of the previous time step as:

$$\left.\frac{\partial f}{\partial t}\right|_{T'}^{+\varepsilon} = \frac{f|_T^{+\varepsilon} - f|_{T'}^{+\varepsilon}}{\Delta t} \tag{4.32}$$

where

$$f|_{T'}^{+\varepsilon} = \eta\, f|_P^{+\varepsilon} + (1 - \eta)\, f|_N \tag{4.33}$$

with

$$\eta = \frac{1 - k_2}{1 - k_1} \tag{4.34}$$

In this manner, therefore, it is possible to evaluate the time derivatives of the upstream and the downstream of transition points in terms of system parameters at time steps *(I-1)* and *(I)*.

The method is applicable for small movement of the transition boundary relative to that of the previous time step. This can be achieved by decreasing Δt and increasing Δz. The final computer program is arranged in such a way that transition boundaries are not allowed to move faster than $2\Delta z$ at any time step Δt. When a transition point at the time $(I-1)\Delta t$ coincides with the nodal point $n\ \Delta z$ ($k_1 = 0$ or 1), the same technique is proceeded at the next time step as shown in Figure 4.4, where points M and N are taken to be at $(n-1)\Delta z$ and $(n+1)\Delta z$. In this case, the value of λ remains unchanged but the value of η is altered to:

$$\eta = \frac{2 - k_2}{2 - k_1} \tag{4.35}$$

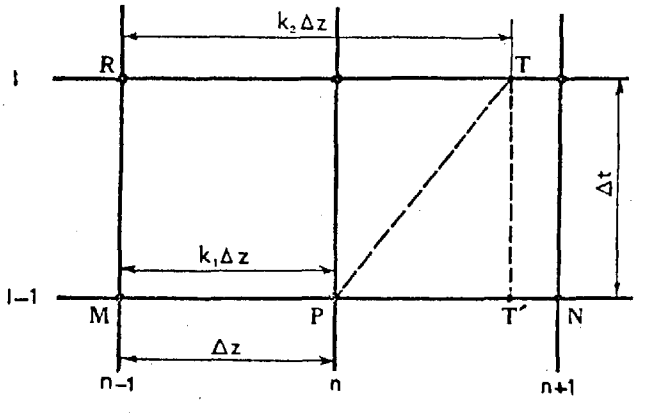


Figure 4.4

4.6.2 Position of the Transition Boundary

To find the position of the transition point (k_2 in equation (4.31)) and system parameters, $f|_T^{\pm\varepsilon}$, a linear iteration method has been used under the assumption that the fluid enthalpy remains continuous at the transition boundary.

As a first guess, the length of the transition boundary is estimated from:

$$k_2 = \frac{H_{corr} - H\ (n-1,I)}{H\ (n,I) - H\ (n-1,I)} \tag{4.36}$$

H_{corr} is the enthalpy of the transition point which is calculated from appropriate equations, e.g. Table 3.3. $H\ (n,I)$ is the enthalpy of the nodal point where the enthalpy first exceeds the value of H_{corr}. Then the system parameters are evaluated using equations (4.31) and (4.32), and a pair of predictor-corrector formulae similar to equations (4.13) and (4.14) in which the length step is replaced by $k_2\Delta z$. The newly generated H_T and H_{corr} are compared, and if the difference $|\ H_T - H_{corr}\ | < \varepsilon$ is not acceptable, a new value of k_2 is produced from:

$$k_2^{i+1} = \frac{H_{corr}^{i} - H\ (n-1,I)}{\frac{\Delta z}{2}\left(\frac{\partial H^{i}\ (n,I)}{\partial z} + \frac{\partial H\ (n-1,I)}{\partial z}\right)} \tag{4.37}$$

The procedure is iterated for values of $i = 1, 2, 3, \ldots$ onwards. Experience shows that the sequence of the procedure converges rapidly in two iterations for a value of $\varepsilon = 0.0005\ H_v$.

4.6.3 Remarks

Numerical methods, discussed in the preceding sections, have been successfully employed for the prediction of system parameters. Solutions are produced by the application of the steady-state correlations

for heat transfer coefficients, the dryout vapour quality, etc., at each increment of the time step. It is noticed that the use of steady-state correlations at some transition boundary requires further restrictions to overcome certain discrepancies.

The first of these requirements is imposed on the conditions of the downstream region of the subcooled boiling boundary, i.e. at each new time step once the boiling starts, the generation of vapour is considered to continue downstream, and the heat transfer mechanism will take place due to the nucleate boiling.

The second restriction is explained as follows: Experience suggests that the steady-state correlations induce discontinuous behaviour in the tube wall temperature at the dryout boundary when it moves downstream as shown in Figure 4.5. The steady-state two-phase heat transfer coefficient (equation (3.101)) over-rates values of the tube wall temperature and heat flux at the nodal point (n,I) of Figure 4.5. i.e. When the value of heat flux at (n,I) is substituted back into the dryout correlation (equation (3.95)), it reveals that the dryout has already occurred at very low or negative quality region. In the other attempt, when the slope of the heat flux is controlled by the information obtained from the upstream region, it generates a tube wall temperature lower than the local saturation temperature and hence invalidates the boiling heat transfer correlation (equation (3.101)).

It is believed that the longitudinal heat conduction is an important factor in modelling of the tube wall at the dryout boundary. The theoretical model of Thompson (1970) can be beneficial in doing so. Also, when saturation liquid film moves through the hot wall, existence of a vapour film may cause a lower heat transfer coefficient than the one predicted from the steady-state two-phase heat transfer correlation.

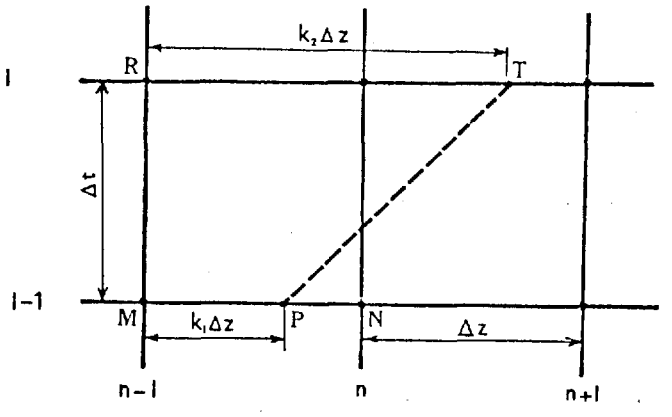


Figure 4.5

The movement of the dry boundary and the tube wall temperature are modelled by the control of the heat transfer coefficient at the position *(n,I)* for Figure 4.5, and it is assumed not to exceed the heat transfer coefficient of the upstream node, e.g. position *(n - 1,I)*.

4.7 COMPUTER PROGRAM

A computer program has been developed to determine the dynamic behaviour of a helically-coiled tube steam generator, heated by a counter flow primary gas. The simulation program is based on the theoretical model given in chapter 3, and the numerical procedure as described in sections 4.3 to 4.6. The governing partial differential equations of section 4.3 are solved in conjunction with additional algebraic equations for heat transfer coefficient, friction factor, etc. In the dynamic calculation, the situation is, therefore, regarded as a quasi-steady condition where the steady-state physical correlations are valid during each time interval.

The program calculates a number of important aspects of the steady-state and dynamic performance of the steam generator. Particular attention is focused on the dynamic stability of the system.

The general structure of the program is sufficiently flexible to be adapted to certain conditions, e.g. constant heat flux systems (electrically heated test rigs), heating by a parallel-flow primary gas.

The computer program includes 20 individual subroutines, each of which performs a specific task. The subroutines and their inter-relationships are described in section 4.7.3.

The program has been developed in FORTRAN IV language on a CDC 6400 computer. The storage required is 20 to 25 k words and the running time varies between 5 to 8 seconds per time step, depending on the mode of operation and step size.

4.7.1 Input Data and Disturbances

The steady-state and dynamic calculations require the following data to be specified by the user:

1. Geometrical dimensions of the boiler tube.
2. Physical properties of the tube metal and the primary flow if it is not carbon dioxide.
3. Characteristics of inlet valve and unheated tubes.
4. Integration step sizes.
5. Modes of calculation (steady-state, transient, both).
6. Type of input disturbance if dynamic calculation is required.
7. Required time of dynamic calculation.
8. Operational conditions, e.g. inlet subcooling, inlet enthalpy or pressure, and inlet mass velocity or system pressure drop of the secondary flow. Also, inlet mass velocity and temperature of the primary flow.
9. Optional parameters, e.g. exponents of heat transfer coefficients, output requirement.

The stability of the system may be investigated by disturbing steady-state conditions. The disturbance can be applied at the inlet of the primary flow (power disturbance), or at the inlet of the secondary flow to investigate effects of subcooling, mass velocity, and system pressure.

Disturbances are of the form of a ramp or sinusoidal functions. A ramp can be applied in one of the following forms where G is assumed to be one of the input parameters, e.g. inlet mass velocity.

$$G\,(O,t) = G\,(O,t_o)\left[1 + \beta\,(1 - e^{-\Omega(t-t_o)})\right] \quad , \quad t > t_o \qquad (4.38)$$

or

$$G\,(O,t) = G\,(O,t_o)\left[1 + \beta\,\Omega\,(t - t_o)\right] \quad , \quad \frac{1}{\Omega} > t > t_o \qquad (4.39a)$$

$$G\,(0,t) = G\,(0,t_o)\,(1+\beta) \quad , \quad t > \frac{1}{\Omega} \tag{4.39b}$$

Equations (4.38) and (4.39) provide a means of imposing a ramp-type disturbance starting at time t_o, the size of which is β times the inlet mass velocity at time t_o. Therefore, the transient step response is sought as the primary means for obtaining information on system stability. The equation:

$$G\,(0,t) = G\,(0,t_o)\,[1+\beta \sin \omega\,(t-t_o)] \quad , \quad t_1 > t > t_o \tag{4.40}$$

is used to impose a sinusoidal variation on the input starting at $t = t_o$. The amplitude of oscillation is β times the initial condition at time t_o. It may, therefore, be employed to determine the frequency response of the system. This oscillation can be applied over a finite interval of $t_1 - t_o$ which is a convenient way to excite the system, and hence, to investigate system instabilities and its degree of damping.

4.7.2 Outputs

The program calculates the distribution of the system parameters along the tube at each time step. These parameters consist of temperatures (the primary side, the secondary side, and the tube wall), enthalpy, mass flow rate, pressure, vapour quality, void fraction, heat transfer coefficient, heat flux to the secondary flow, and lengths of boiling boundaries.

One is often not interested in the space variations at the duration of transition (time calculations). These may be obtained if users so desire. However, only small amounts of information are written

out at each step, mainly inlet, outlet, conditions of boiling boundaries, and the pressure drop of different regions and their components. At certain positions along the boiler, which the user can identify, system parameters are written on a tape for further processing. These values may be written out at every $k\ \Delta t$ time where k is defined by the user. Then the next time step integration is proceeded until the required time period of the dynamic calculation is reached.

The stored data of different time on the tape are then plotted on graphs to give a time history of the parameters. Each graph contains a plot of the inlet mass velocity in addition to the required parameter in order to get a comparison of the phase lag and relative amplification of the parameters.

4.7.3 General Description of Subroutines

The name "HOB" is given to the assembly of all routines associated with the calculation of the dynamic behaviour of a helical tube once-through boiler. The subroutines and their inter-relationship are briefly as follows:

Subroutines for equations of state:

These contain equations of state of the secondary flow. Most of these routines have originally been written for water/steam at Babcock and Wilcox of the United Kingdom. The subroutine is modified in some cases, and they are converted into SI units. Different properties can be obtained by specifying pressure, p, and enthalpy, H, or temperature, T, as follows:

SUBROUTINE WATSPH(p,H,T,SPH)		given p and H, temperature and specific
SUBROUTINE STESPH(p,H,T,SPH)		heat of water or steam are sought
FUNCTION PERSAT(T)	:	calculate saturation pressure
FUNCTION TSL(p)	:	calculate saturation temperature
FUNCTION HL(p,T)		calculate enthalpies of water (HL)
FUNCTION HV(p,T)		or steam (HV)
FUNCTION VL(p,T)	:	specific volume of water
FUNCTION VV(p,T)	:	specific volume of steam
FUNCTION VISL(p,T)	:	viscosity of water
FUNCTION VISV(p,T)	:	viscosity of steam
FUNCTION CONL(p,T)	:	conductivity of water
FUNCTION CONV(p,T,VV)	:	conductivity of steam
FUNCTION SURF(T)	:	surface tension of water

SUBROUTINE VOIDS(x,p,void):

This calculates the void fraction from the information of the vapour quality, x, and the local pressure, p, due to equations (3.29) and (3.30). It also calculates some useful quantities given by equations (3.9), (3.12), (3.15) and (3.17).

SUBROUTINE FRICT:

This performs the calculation of the friction factor for helical tubes (equation (3.25)) and the two-phase friction multiplier (equations (3.26) to (3.28)). Any other up-dated correlation may be replaced in the routine.

SUBROUTINE DEFS(U1,U2,U3):

This calculates gradients of mass velocity, pressure, and enthalpy from equations (4.7), (4.9) and (4.10), respectively. It uses the information of the previous time step (U1,U2,U3). It finds the slope of the different components of pressure drop (gravitational, frictional, and accelerational), and it calls FRICT in so doing.

SUBROUTINE GEN(U4):

The vapour generation function (equation (3.88)) and its gradient (equation (4.8)) are calculated from the information of the previous time step (U4). This routine is called when thermal non-equilibrium exists in the subcooled boiling region.

SUBROUTINE WALL(U5,T_g):

This calculates heat transfer coefficients of the secondary side, and it embodies the differential equation for the temperature of the tube metal employing equation (4.3). The heat flux into the secondary flow is estimated from equation (4.4). When the formula of the boiling heat transfer coefficient is supplied as a function of local heat flux, the routine applies an iteration technique based on Newton's method to perform the calculation of the wall temperature and the heat flux from equations (4.5) and (4.6).

SUBROUTINE CHEN:

This calculates the two-phase heat transfer coefficient of Chen (1963) given in Table 3.3. Polynomials are being fitted to the F and S parameters of the Chen correlation. It is called by subroutine WALL if the user requires.

SUBROUTINE FASE:

Three versions of this routine, namely FASE1, FASE2 and FASE3, are written for different regions along the tube to prevent complexity of the computer programming.

These subroutines embody a numerical integration due to equation (4.14) to produce values of $G^{i}(n,I)$, $H^{i}(n,I)$, $x(n,I)$ and $p(n,I)$ They call subroutines VOIDS, WALL, DEFS and different functions of state equations. The routines perform the iteration of the predictor formula. If the number of the iterations exceeds a value of "NPC", which is set by the user (normally taken to be five), it stores a numeric message for the final checking and continues the integration. The final checking of the spatial increments is performed in the subroutine MAIN.

SUBROUTINE FINAL:

This routine estimates the error of the predictor-corrector pair and it improves the accuracy of the integration procedure. It also evaluates the maximum error of the enthalpy distribution between two successive "temperature-enthalpy iterations" from:

$$\text{ERR} = \left| H^{i}(n,I) - H^{i-1}(n,I) \right| \quad , \quad n = 1, 2, \ldots, N \qquad (4.41)$$

The value of "ERR" is stored and then it is passed to the subroutine MAIN for the examination of the convergence of the "temperature-enthalpy". This routine is called by subroutines FASE at each spatial increment.

SUBROUTINE PREPAR:

This prepares and stores different information for the next time step (U1,U2,U3,U4,U5). It is called by subroutine HYDRO as soon as

the calculation of each spatial increment ends.

SUBROUTINE DISC:

This calculates the slope of the different parameters at discontinuous boundaries. It is called by subroutine BOND twice for the calculation of the conditions of the upstream and the downstream of each transition boundary.

SUBROUTINE BOND:

This embodies the integration of the secondary flow parameters at discontinuous boundaries. It performs the iteration which was discussed in section 4.6, and it calls subroutines DISC, VOIDS, DEFS, and GEN in doing so. This subroutine may be called maximum four times for a complete integration of the boiler tube where the subcooled liquid enters and the superheated vapour leaves the boiler. The length of boiling boundaries and some useful information at boundaries are calculated by this routine.

SUBROUTINE DET:

This detects the transition of boiling boundaries. It calculates the appropriate values of enthalpy of transition boundaries from the relevant equations (Table 3.3). It is called by subroutine HYDRO at each spatial increment until the superheater boundary is detected.

SUBROUTINE HYDRO:

This is the main program for the calculation of the secondary flow parameters. It initialises different parameters, and it

calls subroutines FASE, DET and PREPAR repeatedly until an integration of the secondary flow parameters from the inlet of the boiler to the outlet is completed. It calculates different components of the pressure drop, and also the pressure drop of different regions (single-phase liquid, two-phase, and single-phase vapour) are estimated at each time step.

A check of the inlet mass velocity is performed due to equation (4.20). The difference between the calculated and given pressure drops is stored, and is passed to the subroutine MAIN for the convergence test. This subroutine stops the program when the inlet mass velocity is about to reverse.

SUBROUTINE COEFF:

This calculates quantities that are fixed during the computation of the system parameters. It is called once by the MAIN routine.

SUBROUTINE IBC:

The subroutine calculates boundary conditions of the boiler and also the input functions. The type of input disturbance may be a ramp or sinusoidal function according to the requirement of the user. When the system pressure drop is given as one of the boundary conditions, an estimate of the inlet mass velocity is made according to equations (4.18) and (4.19). The other form of input functions may be supplied by the user. This routine is called by subroutine MAIN at the beginning of the integration of each new time step.

SUBROUTINE TAICAL:

This routine provides the calculation of the pressure drop in

the inlet and outlet unheated tubes. The tube geometry can be straight or helically-coiled. The friction factor of Moody is used to calculate the pressure drop of a straight tube. This is called twice by subroutine HYDRO at every time step. The roughness and geometry of the tubes should be provided.

SUBROUTINE GEAT(πG,HH):

Given the primary side temperature and pressure, this routine calculates the primary flow physical properties and heat transfer coefficient as given by equation (3.2).

Physical properties of carbon dioxide are used in this routine. They are written as polynomial functions of pressure and temperature in the range of $150^{o}C < T < 800^{o}C$.

SUBROUTINE GAS:

This routine calculates the primary flow temperature $T_g^i(n,I)$ for any distribution of the tube metal temperature which is given to it. The integration of the primary temperature is traced on the opposite direction of the secondary flow, and as it is generated at each spatial increment, the maximum error with the previous value of the "temperature-enthalpy iteration" is calculated from:

$$\text{ERRG} = \left| T_g^i(n,I) - T_g^{i-1}(n,I) \right| \quad , \quad n = 1, 2, \ldots, N \qquad (4.42)$$

The value of ERRG is later passed on to subroutine MAIN for the examination of the convergence criteria.

SUBROUTINE MAIN:

This is the master routine of the complete program. It calls COEFF and it initialises the different parameters. Given the boiler length and the number of mesh points, it calculates the spatial increment.

The steady-state calculation starts by putting IST=0 which cancels time derivative terms in dynamic equations. If the steady-state is not required, it reads the distribution of the initial values of different parameters along the tube for the dynamic calculations and is started by putting IST=1. This routine calls HYDRO and GAS iteratively until the convergence criteria of the inlet mass velocity (equation (4.20)) and the "temperature-enthalpy iteration" (equations (4.41) and (4.42)) are satisfied. Then it calls subroutines of outputs to write some information about system parameters and the accuracy of integration being reached. There is an option to write about the longitudinal distribution of system parameters if the user requires. The useful data which consist of temperature, pressure, mass velocity, vapour quality and void fraction at inlet, outlet and fixed positions along the boiler, particularly the upstream and the downstream of transition boundaries, are stored for each time increment. This information is later used for plotting or further analysis.

Then the time is increased and certain variables are up-dated for the next integration.

Besides the subroutines described, special subroutines are written to permit a graphical presentation of the output data using the graphical facilities of the Imperial College of Science and Technology of the University of London.

CHAPTER 5

EVALUATION OF SIMULATION RESULTS (STEADY-STATE)

This chapter demonstrates the performance characteristics of a once-through steam generator under steady-state conditions. The usefulness of the program in studying the steady-state behaviour of the boiler, and in understanding the effects of various design parameters on the performance characteristics, is also discussed.

The study reported here is basically divided into three objectives, namely:

i) Validation of the prediction of the onset of subcooled boiling in helically-coiled tube boilers via comparisons with available experimental results.

ii) Evaluation of the steady-state predictions; longitudinal distribution of the system variables along the coiled tube are studied and discussed.

iii) Study of the static characteristics of the system, and the conditions that raise the potential of the static instability.

5.1 EVALUATION OF THE ONSET OF SUBCOOLED BOILING

In Chapter 3, a theoretical study was made for predicting the subcooled boiling flow inside helically-coiled tubes. A criterion of the onset of subcooled boiling was derived in terms of dimensionless quantities as follows:

$$Z_D^* = 1 - 4.3\, Re^{1/6} \left(\frac{a}{R}\right)^{-1/12} \frac{1}{Z_o} \tag{3.81}$$

A discussion and comparison of predictions with available experimental results are given in the following section.

5.1.1 Experimental Location of the Onset of Subcooled Boiling

It was reported by Carver et al (1964), in their experiments at a pressure of 170 bars (2600 psi), that the inlet temperature to test sections was kept subcooled as far as possible. Furthermore, they presented the longitudinal temperature of the tube surface at fairly small intervals; their experimental results have therefore been chosen for comparison. The test sections which were electrically heated consisted of two coils of 0.4 m (16 in) and 1.6 m (65 in) with a 1 cm (0.42 in) ID tube. The wall temperature was measured at 14 cm (6 in) intervals along the heated length of the test sections. Six thermocouples were spaced at 60^o intervals around the circumference every 14 cm. There was a 30^o displacement between two successive thermocouple stations along the tube. This staggered arrangement of thermocouples made it possible to locate the position of the onset of subcooled boiling around the tube circumference more accurately. The inside wall temperature and heat transfer coefficients were calculated and tabulated for each longitudinal and angular position.

In the present study, to locate the onset of subcooled boiling, the longitudinal distribution of the inside wall temperature for each angle is plotted along the length of the coiled tube, e.g. Figures 5.1 and 5.2. It can be seen that the inside wall temperature increases to a value greater than the saturation temperature, and then remains constant. At some points, it drops slightly and then increases again. The position of the onset of subcooled boiling is considered to be the average of the two thermocouple positions where the constant wall temperature drops to a lower value.

For some experiments, the wall temperature drops between the two thermocouple positions (12 in) and no temperature variation can be seen in the longitudinal distribution (Figures 5.1 and 5.2). In these cases, the longitudinal distribution of the heat transfer coefficient is taken into account as well as the fact that the heat transfer coefficient increases to a higher order relative to the previous position, while the temperature is constant. The average of the two positions is regarded as the onset of subcooled boiling (Figure 5.3).

In this manner, the position of the onset of subcooled boiling can be established for any of the twelve angular locations. Now, one can define and calculate an 'average' position of the onset of subcooled boiling for each test by dividing the sum of the positions of the onset of subcooled boiling obtained for each of the twelve angles by twelve.

The tests which are chosen for comparison are given in Table 5.1, together with the values of Z_D and the subcooling θ_{sub} at Z_D predicted from equations (3.81) and (3.82), respectively.

The first position where data recording starts is 7.6 cm (3 in) from the start of heat addition (taken as the inlet). It is

believed that, for some runs, the subcooled boiling occurs before this point. This is noticed from the water and wall temperatures and the value of the heat transfer coefficient (e.g. cases 1, 2, 3 and 9 in Table 5.1). In such a case, the subcooled boiling position is regarded at the inlet, however, and it can be within 7.6 cm from the inlet, e.g. case 8 in Table 5.1, where the onset of the subcooled boiling position occurs at such intervals due to the prediction.

The accuracy of detection of the position of the onset of subcooled boiling as outlined above could be ± 15.2 cm (± 6 in).

For low pressure systems, Owhadi (1966,1968) investigated forced convection boiling inside a helically-coiled tube of 1.25 cm (0.492 in) ID at pressures near atmospheric in two coils of 25 cm (9.86 in) and 52 cm (20.57 in) diameters and 3 m (10 ft) length. Temperature measurements were made at four circumferential locations at each of nine stations along the tube. The main part of Owhadi's investigation was concerned with the two-phase heat transfer coefficient. The water inlet temperature was arranged to be near saturation temperature to cover the required vapour quality at exit for a certain imposed heat flux. However, four runs were made to investigate single-phase heat transfer. In all cases, subcooled boiling occurred near the exit and resulted in higher heat transfer coefficients for those points. Two further runs were conducted under heat fluxes higher than the single-phase runs to examine the subcooled boiling heat transfer.

Therefore, six runs have been chosen for comparison. Positions of the onset of subcooled boiling have been established as outlined above from the longitudinal temperature and heat transfer distributions produced by Owhadi (1966). The results are given in Table 5.2.

5.1.2 Comparison and Discussion

The predictions and experimental values of the onset of subcooled boiling are given in Tables 5.1 and 5.2, and are compared in Figures 5.4 and 5.5. As seen from the Tables and Figures, the present analysis compares favourably with the experimental results for water at high and low pressures and wide ranges of coil diameters, heat fluxes and mass flow rates. The deviations, considering the range of accuracy of the experimental values, are less than 10 per cent.

Also, Figure 5.6 presents the onset of subcooled boiling at each angular location. The maximum error is 20 per cent. In fact, this discrepancy is expected since the present analysis predicts the circumferential averaged position of the onset of subcooled boiling. The onset of subcooled boiling differs around the periphery of the tube, and it first occurs at points 270 to 0^{o} for most of the experiments (Figures 5.1 and 5.2).

Bearing in mind the accuracy of the experimental data, we may conclude that equation (3.81) agrees well with the experimental results for the water/steam system. The analysis has been carried out for liquids having $Pr \simeq 1$ and it therefore excludes liquid metal flows which have low Prandtl numbers.

A further attempt has also been made by considering a different power for the velocity profile in the analysis, the value of $m = 5$ in equation (3.78) being replaced by 4. Employing the quantities given by relations (3.48), the calculation yields:

$$Z_D^* = 1 - 3.6\, Re^{0.2} \left(\frac{a}{R}\right)^{0.1} \frac{1}{Z_o} \qquad (5.1)$$

Comparison of predictions due to equation (5.1) with the

experimental results are shown in Figure 5.7. It is seen that this formula underestimates all the experimental values. The discrepancies are caused by inadequate consideration of the velocity profile in the analysis.

Table 5.1: Comparison with data of Carver et al (1964)

Case	Data of Carver et al (1964) Run Number - To	$\frac{a}{R} \times 100$	G (kg/m^{2}s)	$\dot{q}''$ (kW/m^2)	H_i (kJ/kg)	Z_1 (cm)	$Z_{D_{exp}}$ (cm)	Prediction θ_{sub} Equation (3.82)	Prediction Z_D (cm)	% DEV
1	30536 - 30787	1.31	1352.2	394.4	1674.5	50	AI*	1.64	AI	-
2	30788 - 31039		1352.2	441.7	1674.5	42.2	AI	1.13	AI	-
3	31436 - 31687		675.4	318.6	1674.5	31.5	AI	1.43	AI	-
4	32414 - 32587		375.7	271.3	339.6	512.8	470	0.072	476	+ 1.3
5	32588 - 32767		375.7	312.3	337.3	446.6	409	0.082	410	-
6	32768 - 32947		375.7	350.2	323.3	402.1	355	0.093	365	+ 2.6
7	34238 - 34369	0.33	1900.1	567.9	1670	53	AI	1.15	AI	-
8	34370 - 34555		1900.1	694.1	1644.5	62.4	AI	0.979	1.3	-
9	35292 - 35479		1356.2	517.4	1653.8	52.9	AI	1.09	AI	-
10	35666 - 35851		1356.2	640.5	1567.7	92.3	34.3	0.624	34.8	+ 2.0
11	35852 - 35935		678.1	315.5	1153.7	334	287	0.148	284	- 1.0
12	35936 - 36037		678.1	397.5	1132.8	274	229	0.179	225	- 1.5
13	36038 - 36223		678.1	470.1	1158.3	222.2	171	0.222	173	+ 0.8
14	36224 - 36361		678.1	593.1	783.8	291.5	239	0.166	243	- 2.4
15	36362 - 36547		678.1	388.1	1602.6	59.7	7.5	0.86	8.3	-
16	36548 - 36613		381.1	397.5	304.7	368.3	328	0.114	326	- 0.5
17	36614 - 36703		381.1	482.7	309.4	302.2	267	0.139	260	- 2.4
18	37706 - 37795		381.1	425.9	314	341.5	300	0.123	299	- 0.5
19	37796 - 37885		381.1	441.7	309.4	330.4	296	0.127	288	- 2.5

* At inlet to the tube

Table 5.2: Comparison with data of Owhadi (1966)

Run Number	$\frac{a}{R} \times 100$	G (kg/m^{2}s)	$\dot{q}''$ (kW/m^2)	T_i (^{o}C)	Z_1 (cm)	$Z_{D_{exp}}$ (cm)	Prediction		% DEV
							θ_{sub} Equation (3.82)	Z_D (cm)	
24		324.5	106.3	50.1	200	167.6	0.162	167	-
25	4.99	363.6	48.9	53.7	451.7	NSB*	0.073	418.6	GTL**
26		97.4	24.6	40.1	311.5	284.5	0.084	285.4	+ 0.3
124		316.4	107.9	48.6	197.7	171.4	0.163	165.3	- 3.5
125	2.39	342.1	25.3	83.0	301.9	266.7	0.112	268.1	+ 0.5
126		99.2	26.2	43.0	283.4	255.3	0.093	257	+ 0.6

* No subcooled boiling

** Greater than the tube length

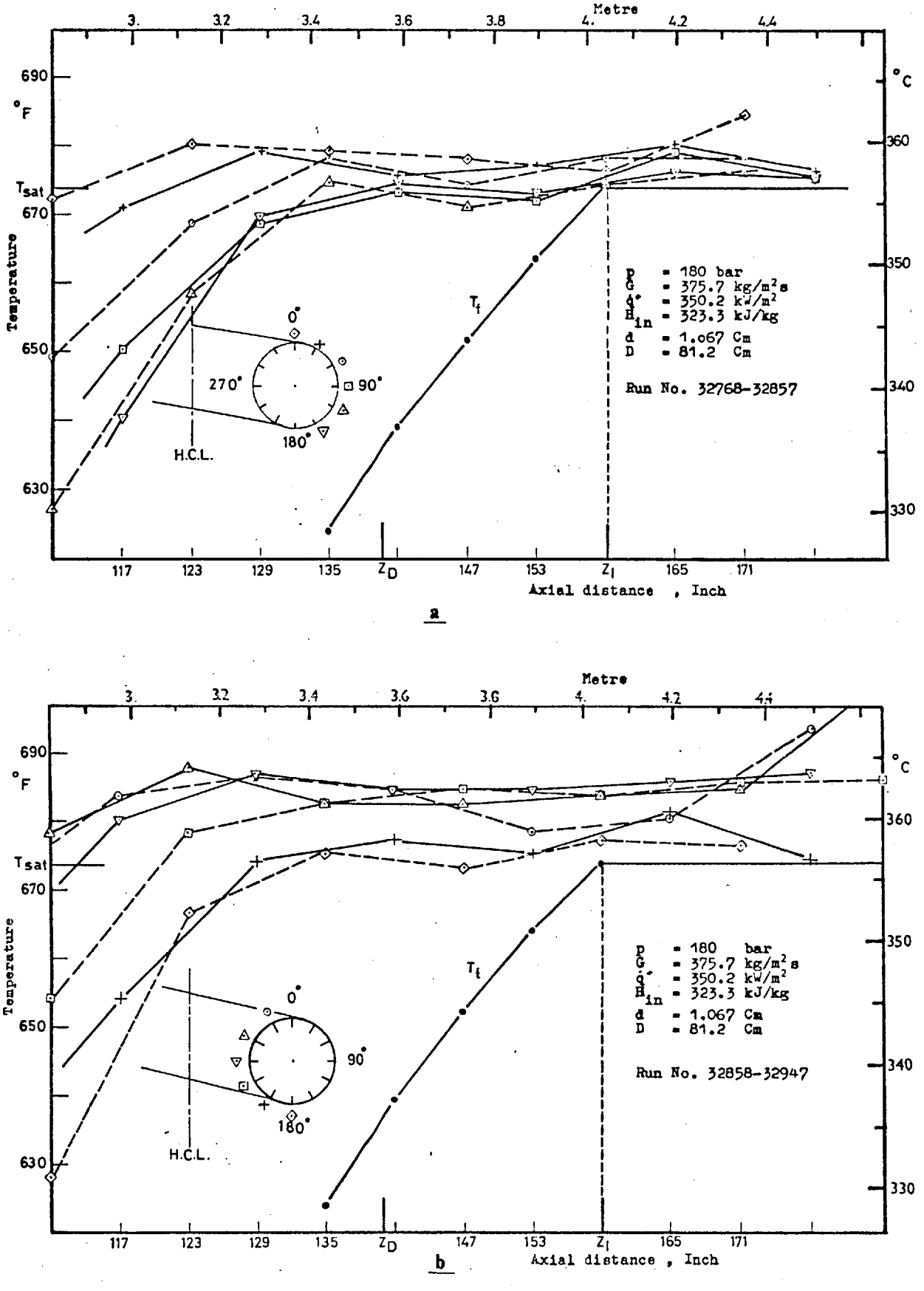


Figure 5.1: Experimental values of axial distribution of inside wall temperature at different circumferential positions (from Carver et al (1964))

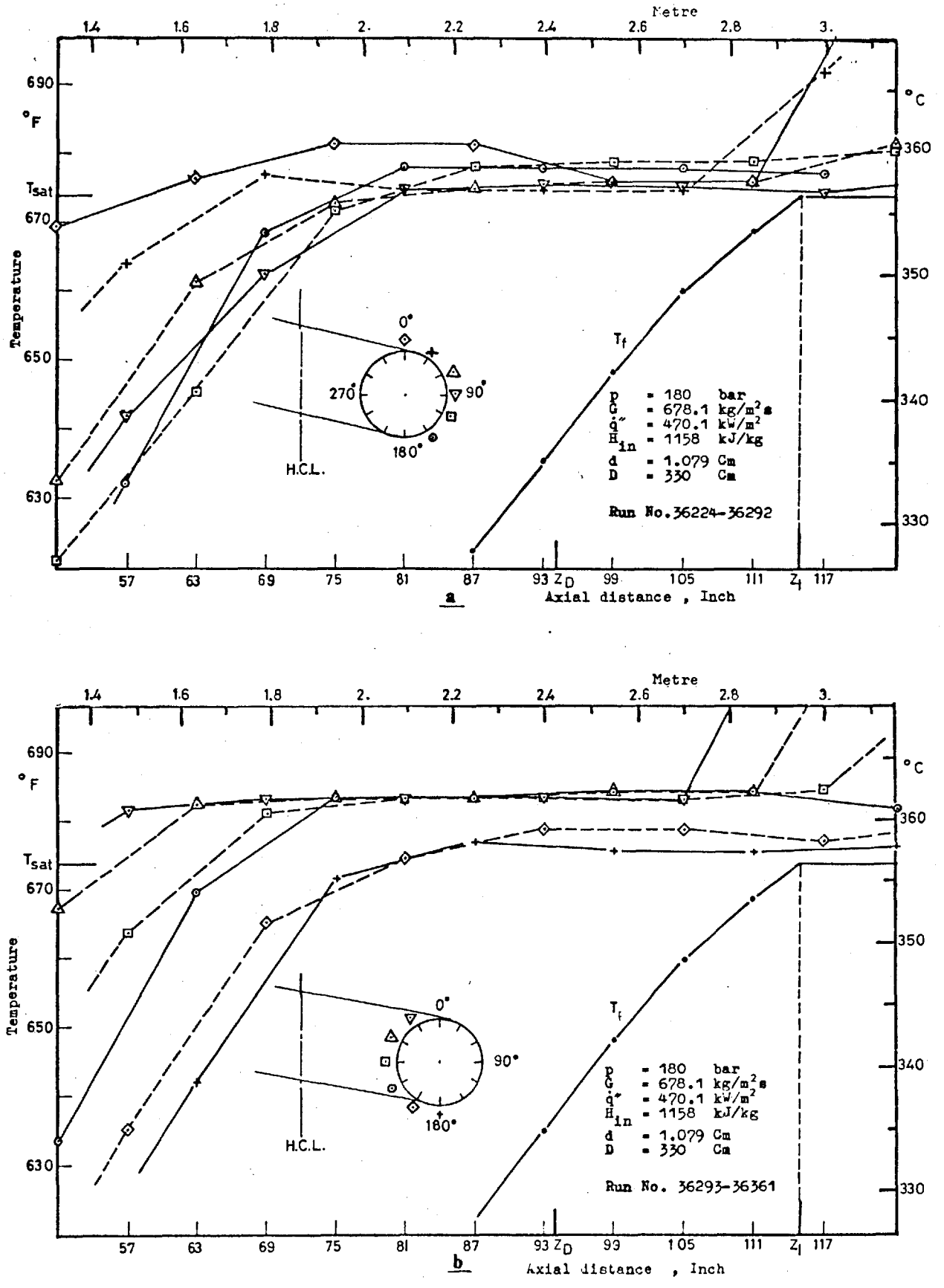


Figure 5.2: Experimental values of axial distribution of inside wall wall temperature at different circumferential positions (from Carver et al (1964))

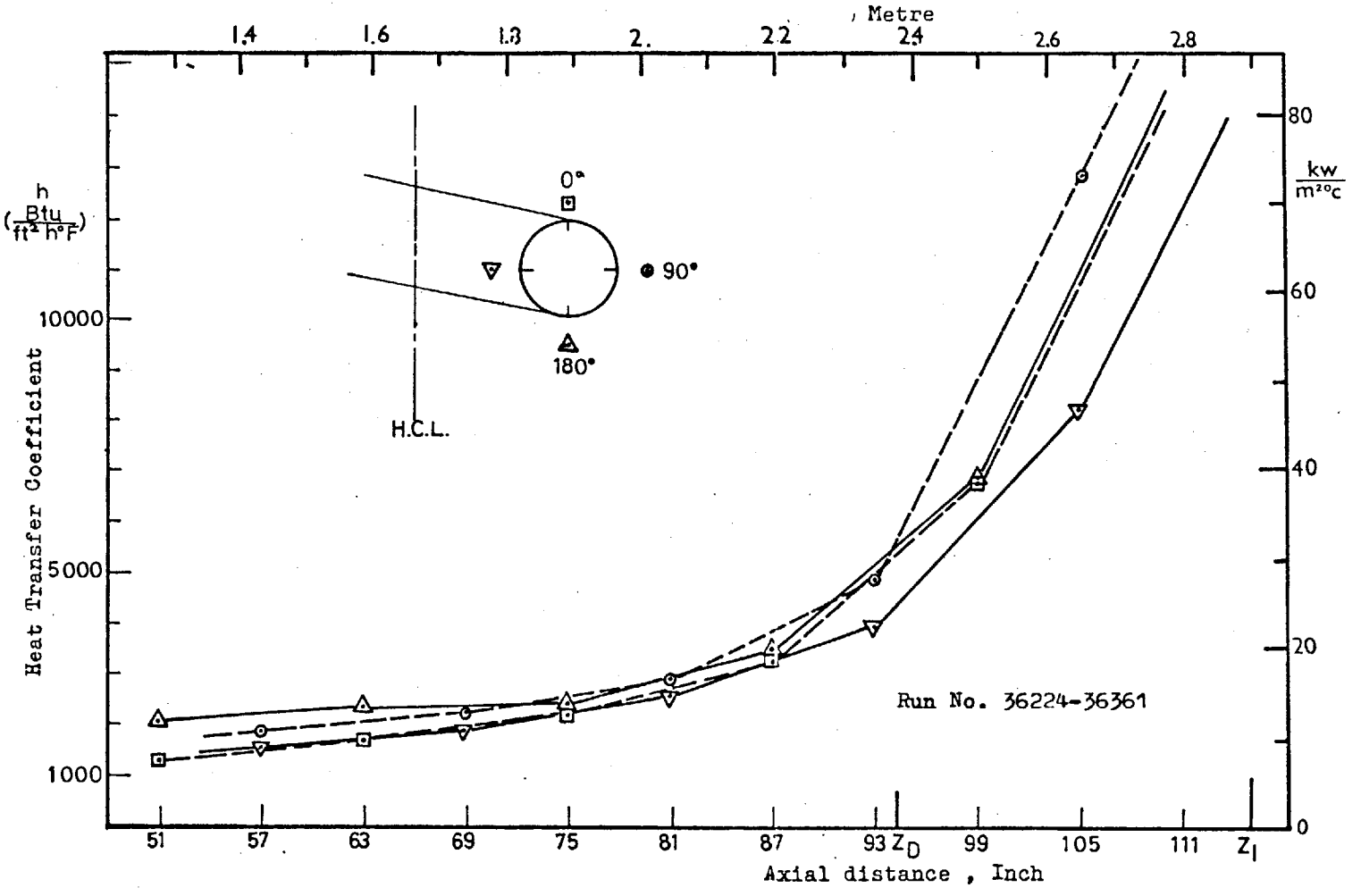


Figure 5.3: Axial distribution of heat transfer coefficient at different circumferential positions in the subcooled boiling region (Carver et al (1964))

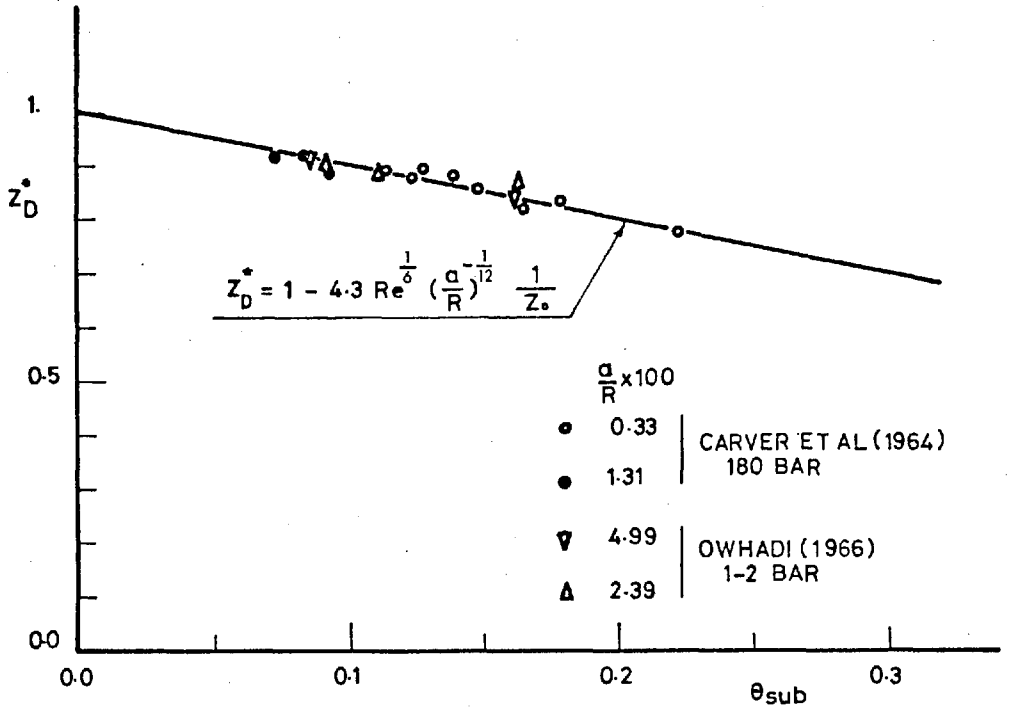


Figure 5.4: Comparison of prediction and experiment

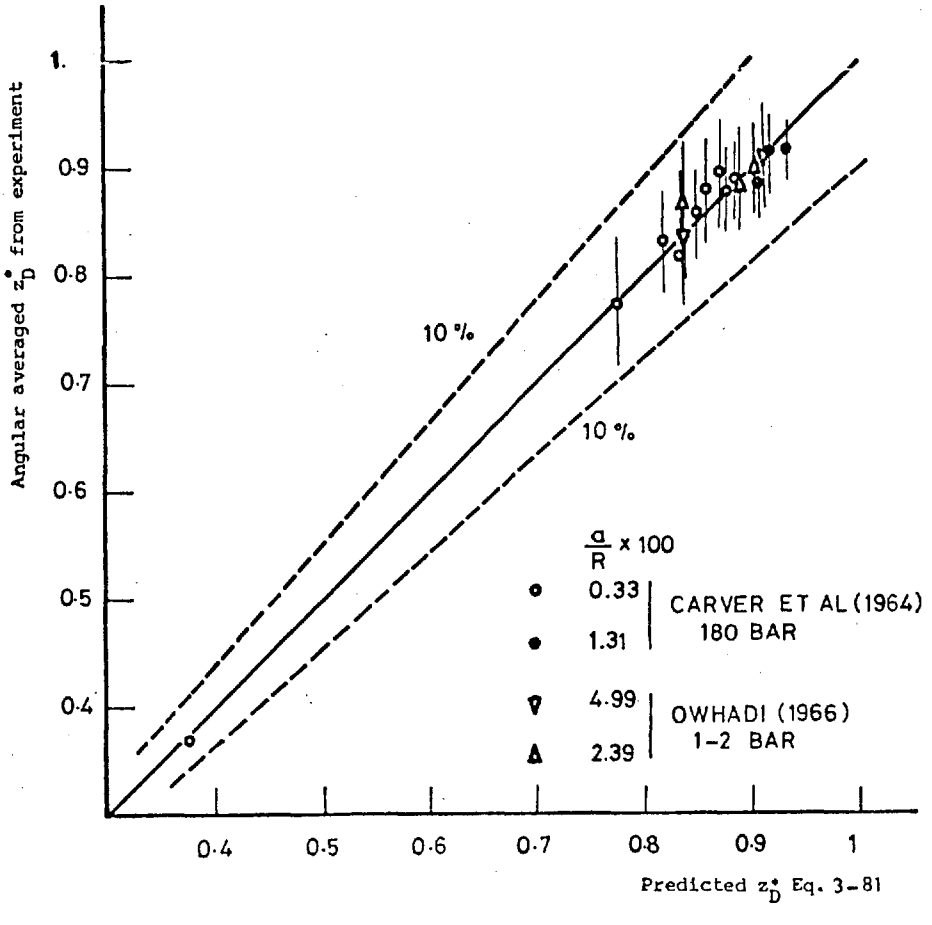


Figure 5.5: Comparison of prediction and experiment

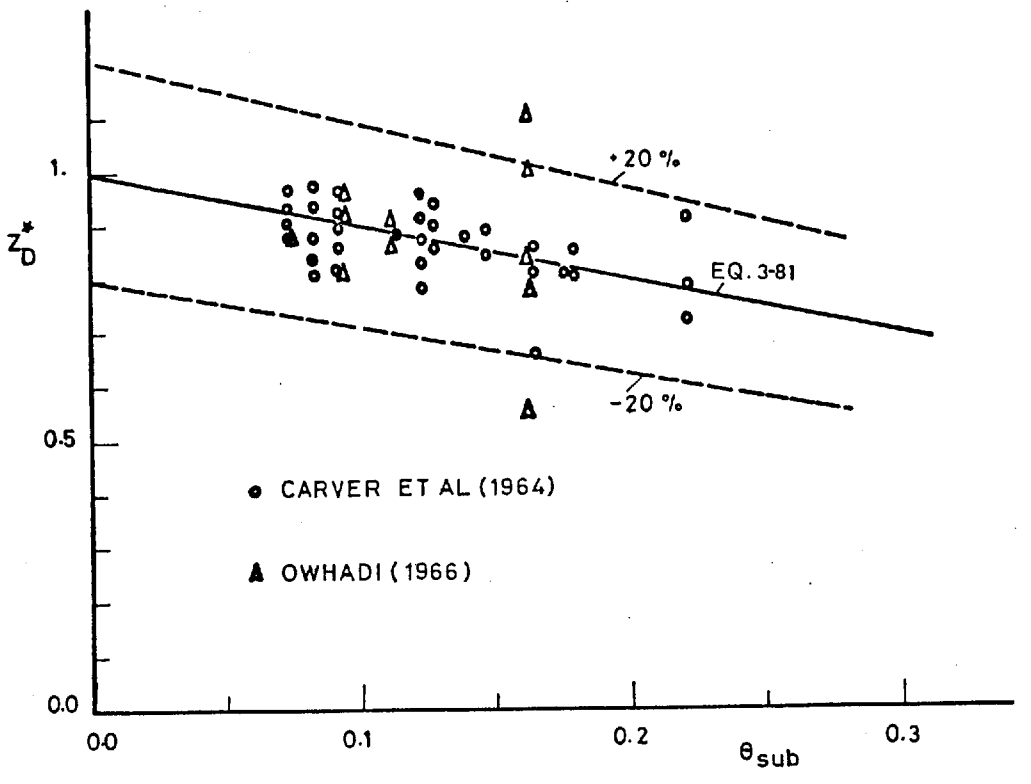


Figure 5.6: Comparison of prediction and experimental results

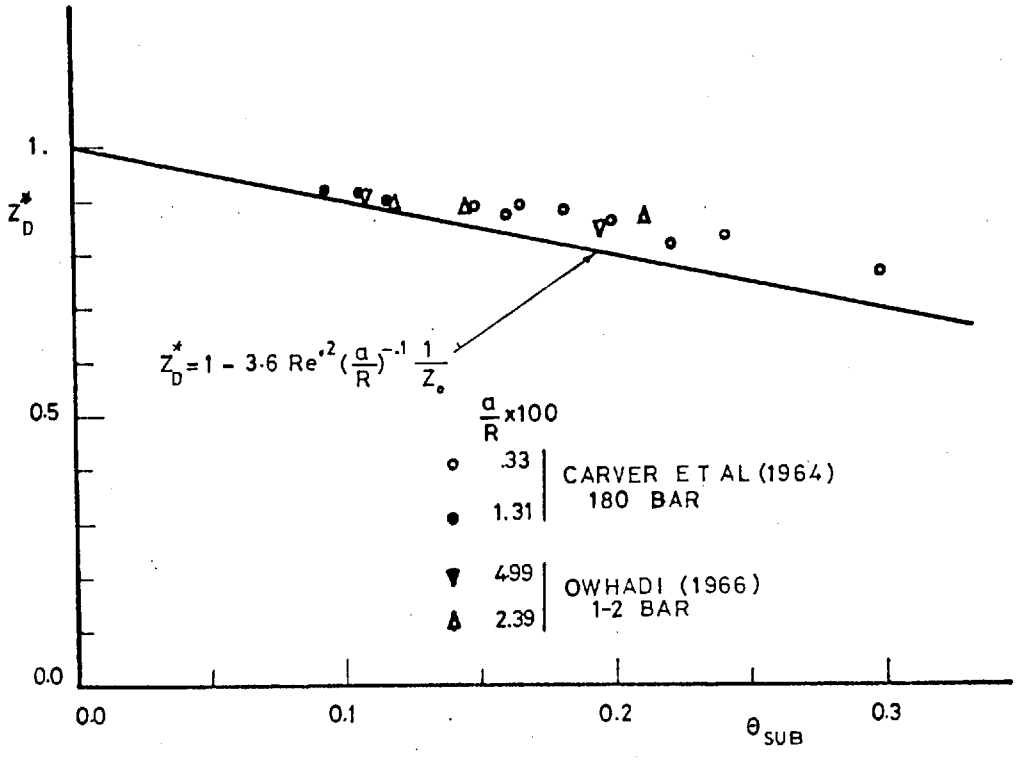


Figure 5.7: Comparison of prediction due to equation (5.1) with experimental results

5.2 STEADY-STATE RESULTS

5.2.1 Axial Distribution of Temperatures

The calculated distributions of the secondary flow temperature T, the tube wall temperature T_w, the primary flow temperature T_g, vapour quality x, and void fraction α are plotted on Figure 5.8 as a function of the distance along the tube. Figure 5.10 shows a typical variation of the same quantities at the subcooled boiling region. It can be seen that the longitudinal distribution of temperatures of the secondary flow and the tube wall (Figure 5.8) at the subcooled and superheater regions are approximately exponential. The steepest parts occur at the entrance of the subcooled region and at the onset of superheater. This is important in the dynamic analysis; any small disturbance of the system may induce large temperature oscillations at these regions as will be shown in Chapter 6. A typical calculated heat transfer coefficient and heat flux along the tube are illustrated in Figure 5.9.

In the following sections, some aspects of the steady-state performance of the boiler are investigated. The sensitivity of the axial distribution of the system variables and operation conditions to certain parameters and experimental correlations is studied and discussed.

5.2.2 Heat Flux Distribution

Axial heat flux distribution is illustrated in Figure 5.9. The heat flux is largest at the entrance of the subcooled and at the onset of superheater; it decreases along the subcooled and superheater regions. Local heat flux in these regions is coupled to the secondary side due to the heat transfer coefficients and temperatures of either side. Heat transfer coefficients (Figure 5.9) in the subcooled and

superheater do not exhibit appropriate changes with temperature; hence, the heat flux distribution in the subcooled and superheater is mainly controlled by changes of temperature difference between the primary and the secondary sides.

In the evaporator region, the two-phase heat transfer coefficient of Thom et al (1965) is used in the calculation. Such a nucleate boiling heat transfer relationship gives large increases in heat flux for very small increases in the temperature differences between the tube wall and two-phase flow. Consequently, the inside wall temperature is unlikely to rise more than about $5^{o}C$ above the local saturation temperature at a pressure of 75 bar (Figure 5.10). In the case of a counter flow heat exchanger, the primary flow temperature increases along the secondary flow direction, with a nearly constant heat transfer coefficient between the primary fluid and the inner wall of the tube. It follows that since the temperature of the secondary fluid in the evaporator is constant (saturation temperature), the heat flux must rise along the evaporator region until the dryout location is approached as shown in Figure 5.9. Figures 5.11 and 5.12 demonstrate the axial distribution of different parameters at 150 bar under the application of the heat transfer coefficients of Jens-Lottes (1951) and Thom et al (1965). No differences are noticeable for the axial distribution of heat flux, vapour quality, and temperatures (Figure 5.11), except the wall temperature which is slightly lower for Thom et al (1965) correlations.

The nucleate boiling heat transfer coefficient (e.g. Jens-Lottes (1951)) is strongly dependent on heat flux but it is unaffected by changes in flow rate. In order to investigate the effect of secondary flow rate, the heat transfer correlation of Chen (1963), which

is dependent on the two-phase Reynolds number, is extended to higher vapour qualities than 70% and to pressures greater than 35 bar which are limits of Chen's correlation. The results are plotted in Figure 5.13 where a comparison of three different heat transfer correlations is shown. Again, no differences in the heat flux distribution are noticeable under different correlations. Similar comparisons are made at low pressures; Figure 5.14 is plotted at 30 bar where the inlet condition of the primary flow is kept unchanged as that of Figures 5.12 and 5.13; and Figure 5.15 is produced at 10 bar and different inlet conditions.

From the foregoing demonstration, the following concluding remarks can be made:

i) Unlike the single-phase and superheater regions, where the heat flux is controlled by the heat transfer characteristics of both the primary and the secondary flows, the heat flux distribution in the two-phase region is strongly controlled by the temperature and heat transfer coefficient of the primary side.

ii) The heat flux decreases along the tube at the subcooled region and it reaches a minimum as the subcooled boiling takes place. Then it increases to a maximum at the dryout boundary. The values of the local heat flux and hence the maximum and minimum are dependent on the system pressure at fixed primary conditions. For the same inlet conditions of the primary flow, the maximum and minimum values of the heat flux are greater for low pressure systems than those of high pressure systems.

iii) The different two-phase heat transfer correlations, namely, Thom et al (1965), Chen (1963) and Jens-Lottes (1951), do not alter the distribution of heat flux at high pressure systems within the applicability of the correlations. At low pressures, the heat flux distribution is slightly affected under the use of different correlations. This is more significant for the Jens-Lottes correlation than for the other two.

5.2.3 Subcooled Boiling Region

The liquid temperature T, the inside temperature of the tube wall T_{w_i}, vapour quality x and void fraction α along the subcooled boiling region are plotted in Figures 5.10 and 5.16 to 5.19 at different conditions. When the generation of bubbles starts, the inside tube wall temperature is somewhat superheated (Figure 5.17), while the liquid temperature is subcooled. As the subcooled boiling continues, the liquid temperature increases monotonically until, at some point (bulk boiling boundary), thermal equilibrium is attained and the temperatures of the liquid and the vapour become identical to the local saturation temperature.

There is an overshoot present in the tube wall temperature at the onset of subcooled boiling (Figures 5.16 and 5.17). This can be explained by the change of the mechanism of the heat transfer as boiling takes place. The magnitude of this overshoot depends largely upon the distribution of the nucleation centres on the heating element and hence on the subcooled boiling heat transfer coefficient. A high heat transfer coefficient (low pressure or high heat flux) produces less tube

wall superheat downstream of the onset of subcooled boiling; therefore, a higher overshoot is expected (Figures 5.17 and 5.19). Figures 5.16 and 5.17 are plotted for different primary flow rates at the same pressure. At low heat flux (Figure 5.16), the changes in temperature and void fraction are gradual and the overshoot in wall temperature is almost suppressed. At high heat flux, the reverse effects are noticed in Figure 5.17. As the heat flux is increased, more nucleation centres are activated; hence, a higher overshoot in the tube wall temperature is sought, and the vapour void distribution becomes steeper downstream of the subcooled boiling region (Figure 5.17.

The overshoot in the wall temperature becomes smaller at high pressure as shown in Figures 5.18 and 5.19.

When applying the present model, the length of the subcooled boiling region with thermal non-equilibrium becomes longer as the heat flux increases (Figures 5.16 and 5.17). This is displayed in Figure 5.20 where the ratios of the boiling boundaries to the tube lengths are plotted as a function of the primary flow rate.

In the preceding discussion, Smith's correlation (1970) was employed to find the void distribution. Trials were made using the void correlation of Massena (1960). The void correlation should not affect the axial temperature distributions of the primary side, the secondary side and the tube wall as shown in Figures 5.21 and 5.22; but the void distribution varies with different correlations. At low pressures, the difference of the void distribution is considerable when different correlations are used in the calculation (Figures 5.16 and 5.21). However, at high pressures, the effects are small and negligible due to the low density ratio of liquid and vapour phases. The void distribution affects the components of the pressure drop in the evaporator

region. This is shown in the following section.

5.2.4 Pressure Drop Distribution

The axial pressure drop distribution is illustrated in Figures 5.23 and 5.24 at pressures of 74.6 and 30 bar, respectively. The pressure gradient varies along the tube due to the variation of the effective density. The slope of the pressure drop curve is constant at the subcooled region where the velocity and the density of the liquid are nearly constant. It becomes variable along the evaporator due to the change of effective density or vapour void. It appears that the pressure gradient reaches a maximum at high vapour quality region, until the superheating starts.

In a boiling flow where the outlet condition is operating at high vapour quality or superheated conditions (Figures 5.23 to 5.25), a high portion of the total pressure drop in the tube occurs in the upstream region of the outlet. Since, in the two-phase or superheater region, the density decreases and velocity increases compared to the economiser. This behaviour is undesirable and unavoidable in once-through boilers, and it reduces the stability of the system as will be discussed later.

Effects of two-phase heat transfer correlations (Thom et al (1965), Chen (1963), and Jens-Lottes (1951)) on the pressure drop distribution are shown in Figure 5.24. At low pressures, the total pressure drop due to Jens-Lottes (1951) correlations is less than those calculated using Chen (1963) and Thom et al (1965) correlations. This is essentially due to the difference in the length of the evaporator (Figure 5.14) which causes the pressure drop distribution at the superheater region to be shifted by the difference of the evaporator

pressure drops. At high pressures, the effect of different heat transfer correlations on the pressure drop distribution is not pronounced (Figure 5.23).

The change of the axial distribution of the void fraction affects the different components of the evaporator pressure drop. As discussed in section 5.2.3, the distribution of void fraction differs from one correlation to another, particularly at low pressures. This results in different pressure drop curves as shown in Figure 5.25. It can be seen that the pressure drop, calculated by Smith's (1970) void correlation, is greater than the pressure drop due to Massena's (1960) correlation at similar operating conditions. The pressure drop deviation due to two correlations increases at high void fractions due to the differences shown in Figure 5.21. Beyond the superheater boundary, the pressure gradients are unchanged and the pressure drop curve is shifted by the difference of the evaporator pressure drops. The total pressure drop and its components along the economiser, evaporator and superheater are illustrated in Figure 5.26 as a function of the primary flow rate (different heat flux) for the void correlations of Smith (1970) and Massena (1960) at a pressure of 10 bar. It can be seen that the differences between the total pressure drops are due to the differences of evaporator pressure drops. This is illustrated in Figure 5.27 to investigate the effect of accelerational, gravitational and frictional components of pressure drop. It shows the importance of two-phase frictional pressure drop; hence, the correlation of the two-phase frictional multiplier. At low pressures, although small deviations of the void distribution (due to different correlations) have little effect on the accelerational and gravitational pressure drops, differences in the frictional pressure drop are magnified. Hence, the

compatability of the two correlations, the two-phase frictional multiplier and the void fraction, is necessary to predict a reliable system pressure drop as similar to, for example, those of the experimental values. The two-phase frictional multiplier, which is used in this analysis, was produced by Ruffel (1974) using the correlation of Massena (1960) for high pressure systems.

The foregoing discussion leads to the conclusion that the void fraction relationship is an important factor in the evaluation of pressure drop components; and, although the void correlations of Smith (1970) and Massena (1960) with the two-phase frictional multiplier of Ruffel (1974) produce similar results at high pressures, e.g. 74 bar, caution should be exercised when attempting to use the different correlations at low pressures.

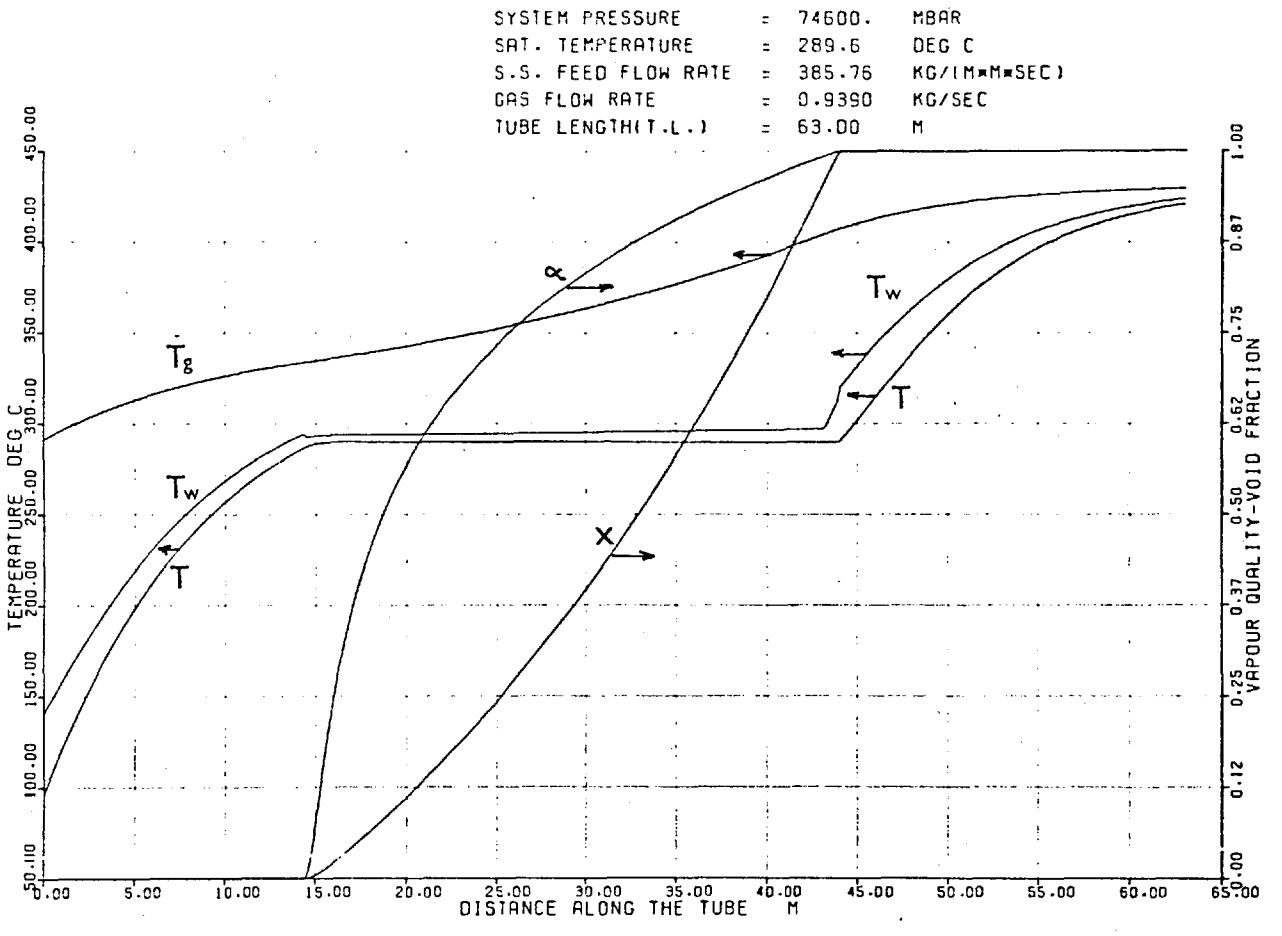


FIG.(5.8)- TEMPERATURES.VAPOR QUALITY AND VOID DISTRIBUTION ALONG THE TUBE

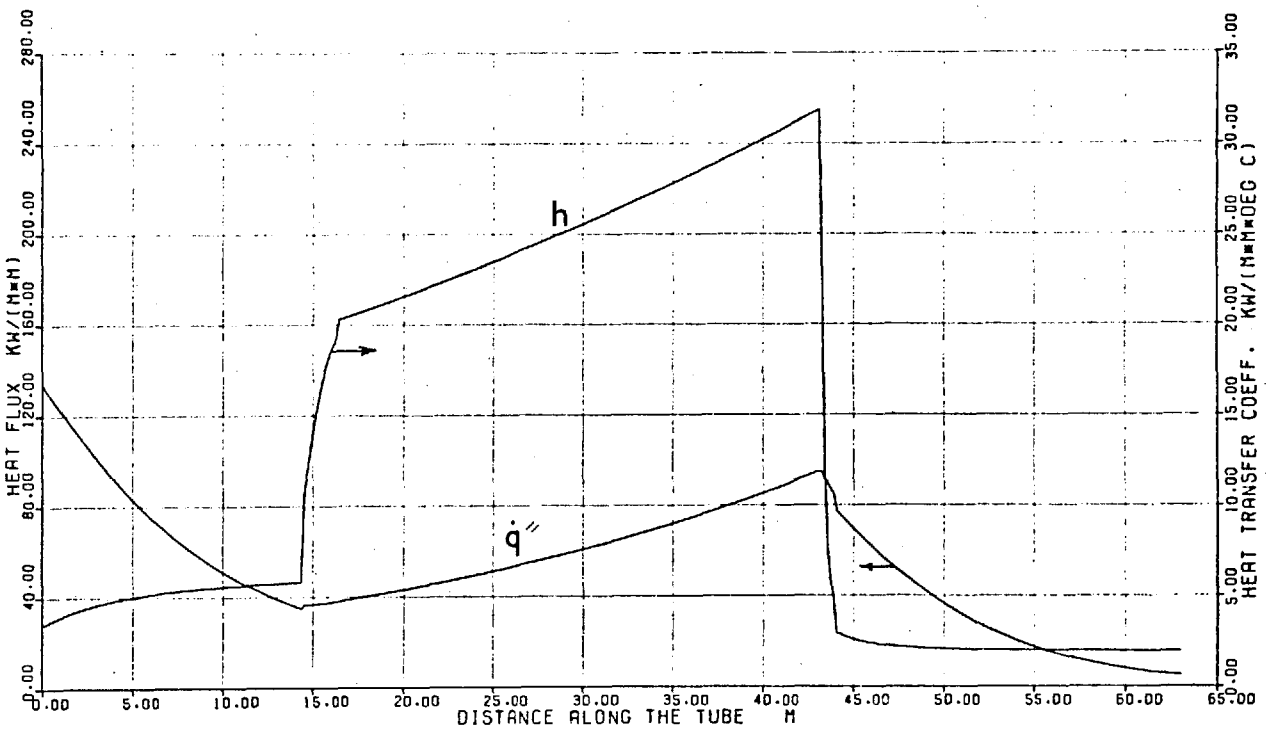


FIG.(5.9) - HEAT FLUX AND HEAT TRANSFER COEFFICIENT DISTRIBUTION ALONG THE TUBE

SYSTEM PRESSURE = 74600. MBAR
SAT. TEMPERATURE = 289.6 DEG C
S.S. FEED FLOW RATE = 385.76 KG/(M*M*SEC)
GAS FLOW RATE = 0.9390 KG/SEC
TUBE LENGTH(T.L.) = 63.00 M

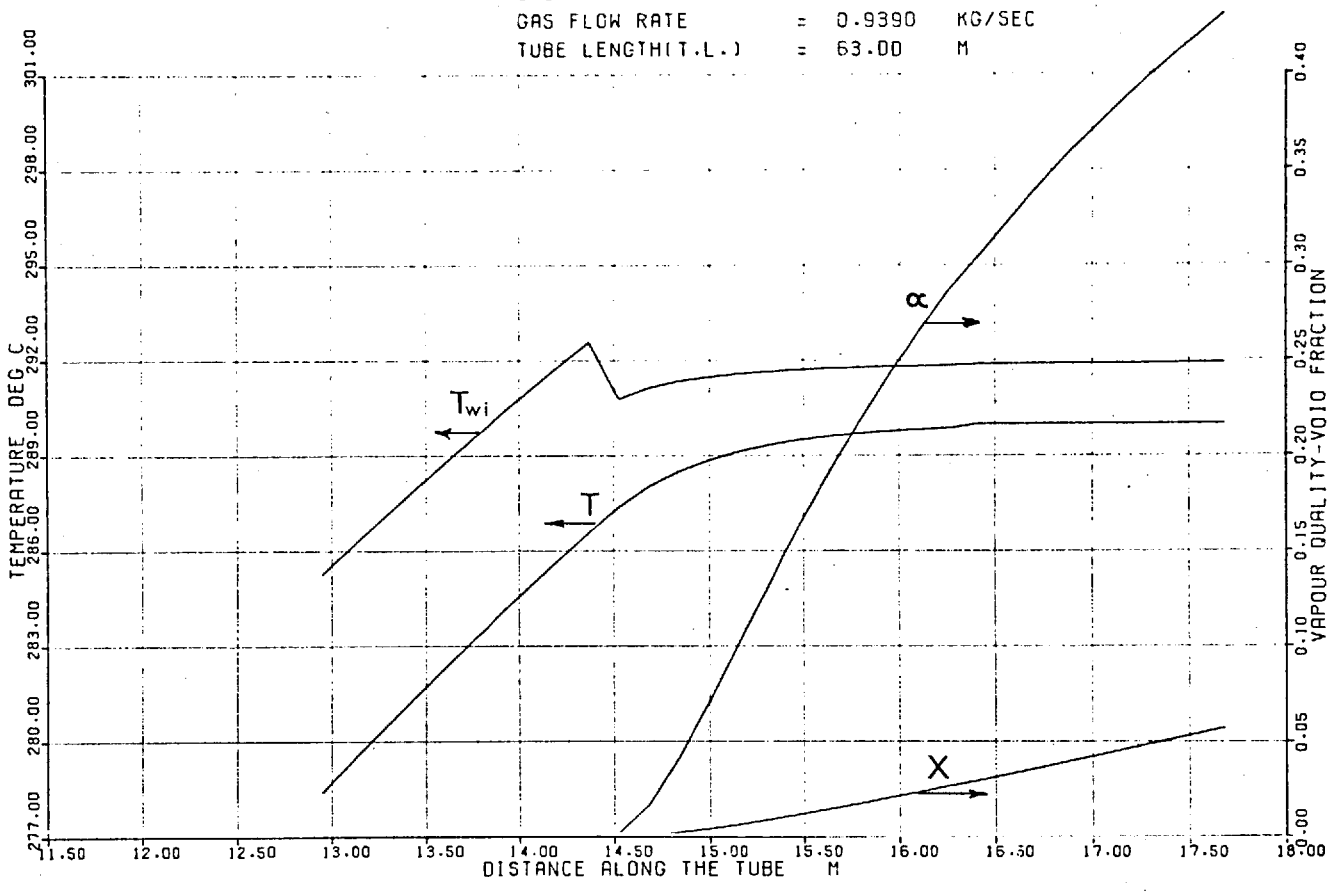


FIG.(5-10) - AXIAL TEMPERATURE , VOID AND QUALITY DISTRIBUTION AT SUBCOOLED BOILING REGION

SYSTEM PRESSURE = 150000. MBAR
SAT. TEMPERATURE = 341.8 DEG C
S.S. FEED FLOW RATE = 385.76 KG/(M*M*SEC)
GAS FLOW RATE = 0.9390 KG/SEC
TUBE LENGTH(T.L.) = 63.00 M

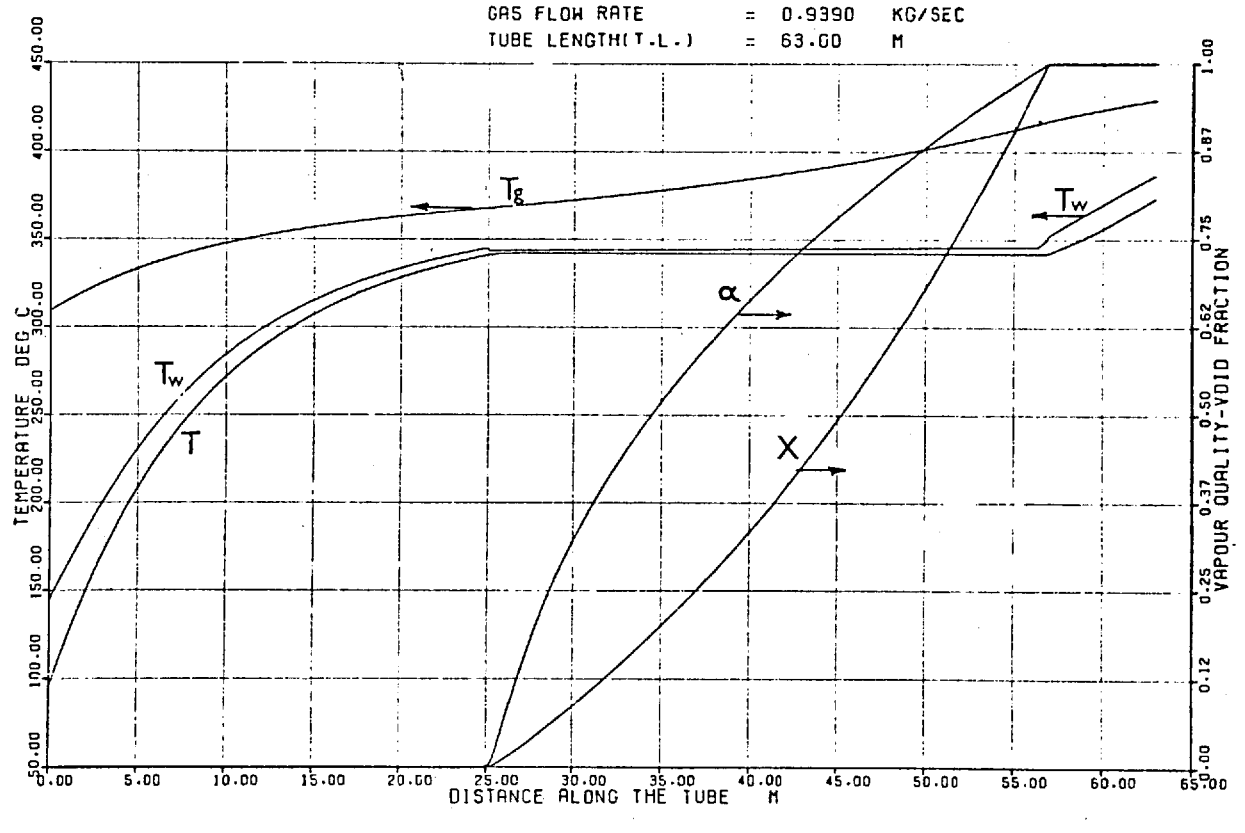


FIG.(5-11) - TEMPERATURES,VAPOR QUALITY AND VOID DISTRIBUTION ALONG THE TUBE

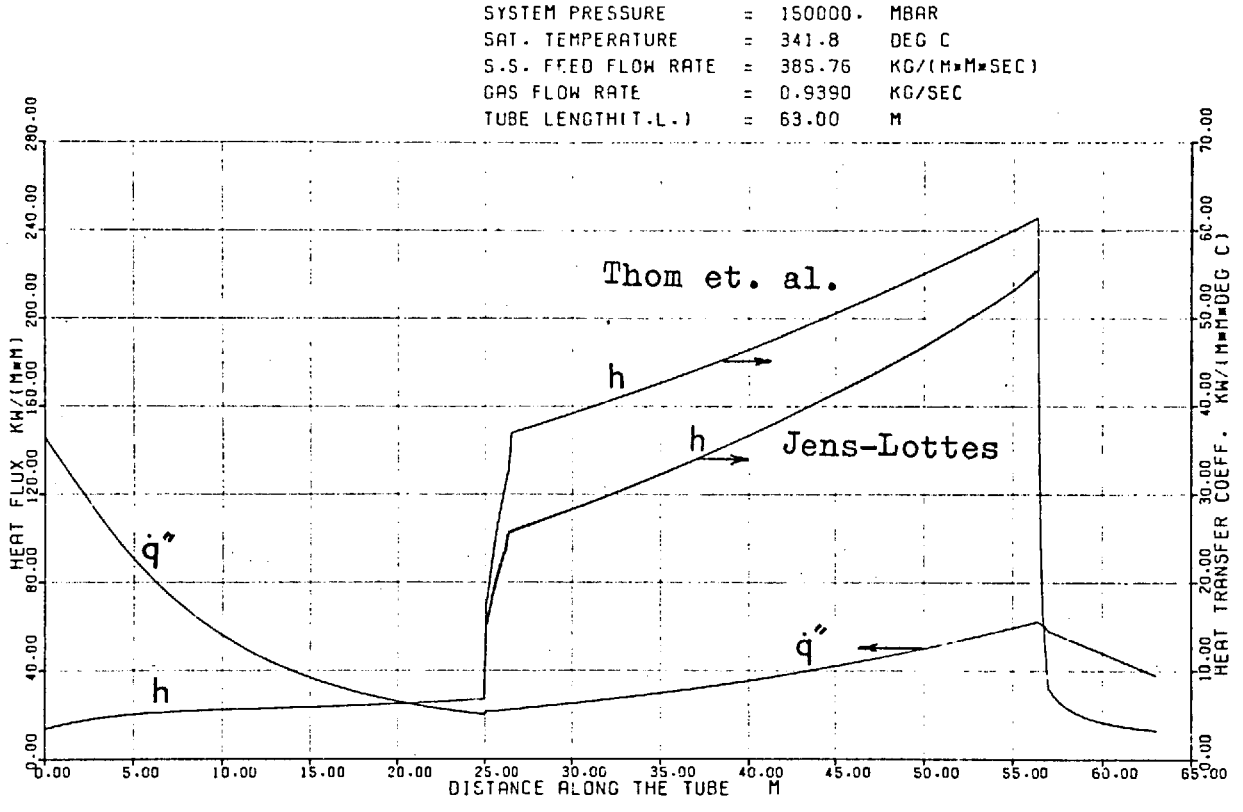


FIG.(5-12) - HEAT FLUX AND HEAT TRANSFER COEFFICIENT DISTRIBUTION ALONG THE TUBE

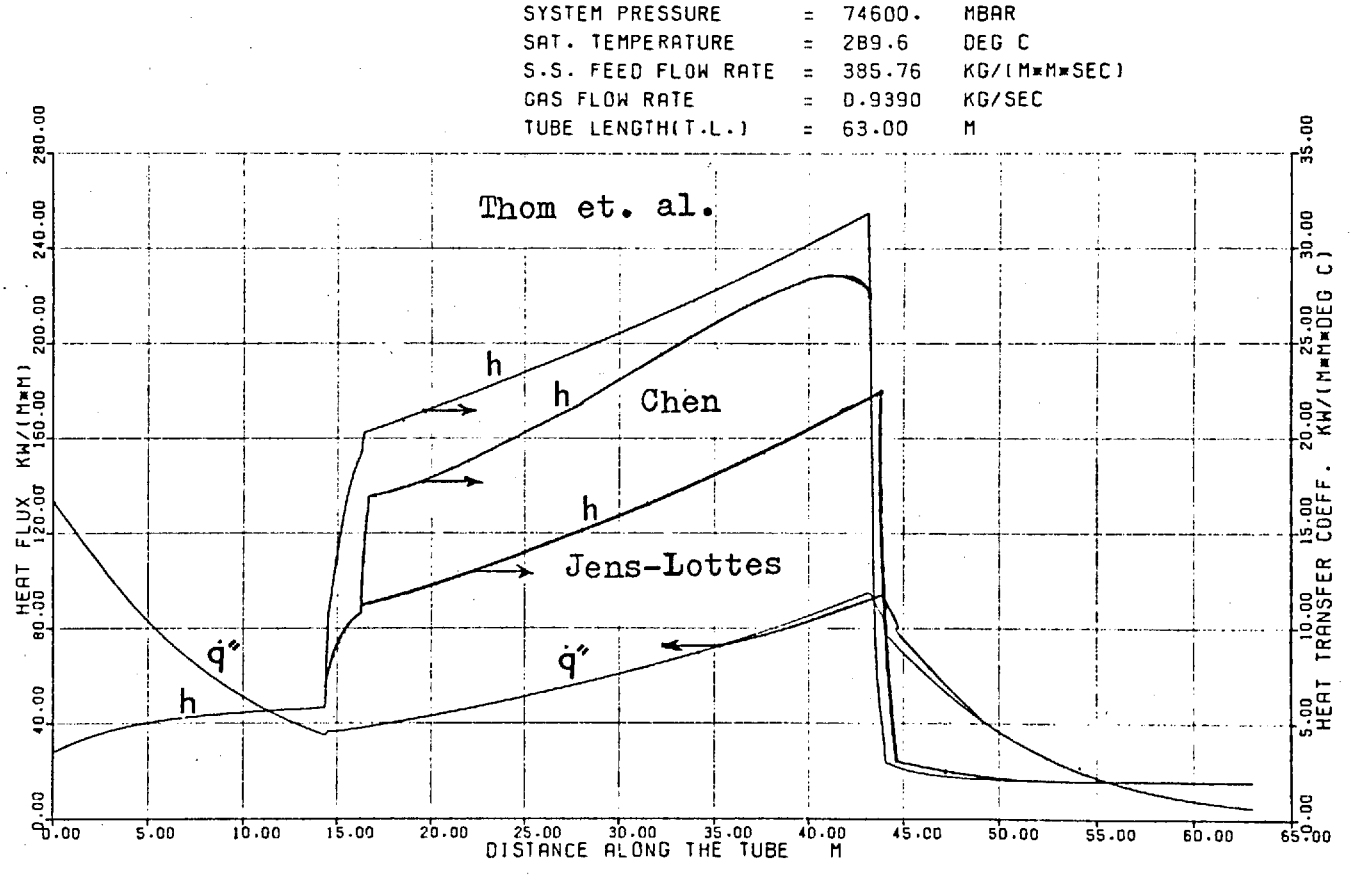


FIG.(5-13) - HEAT FLUX AND HEAT TRANSFER COEFFICIENT DISTRIBUTION ALONG THE TUBE

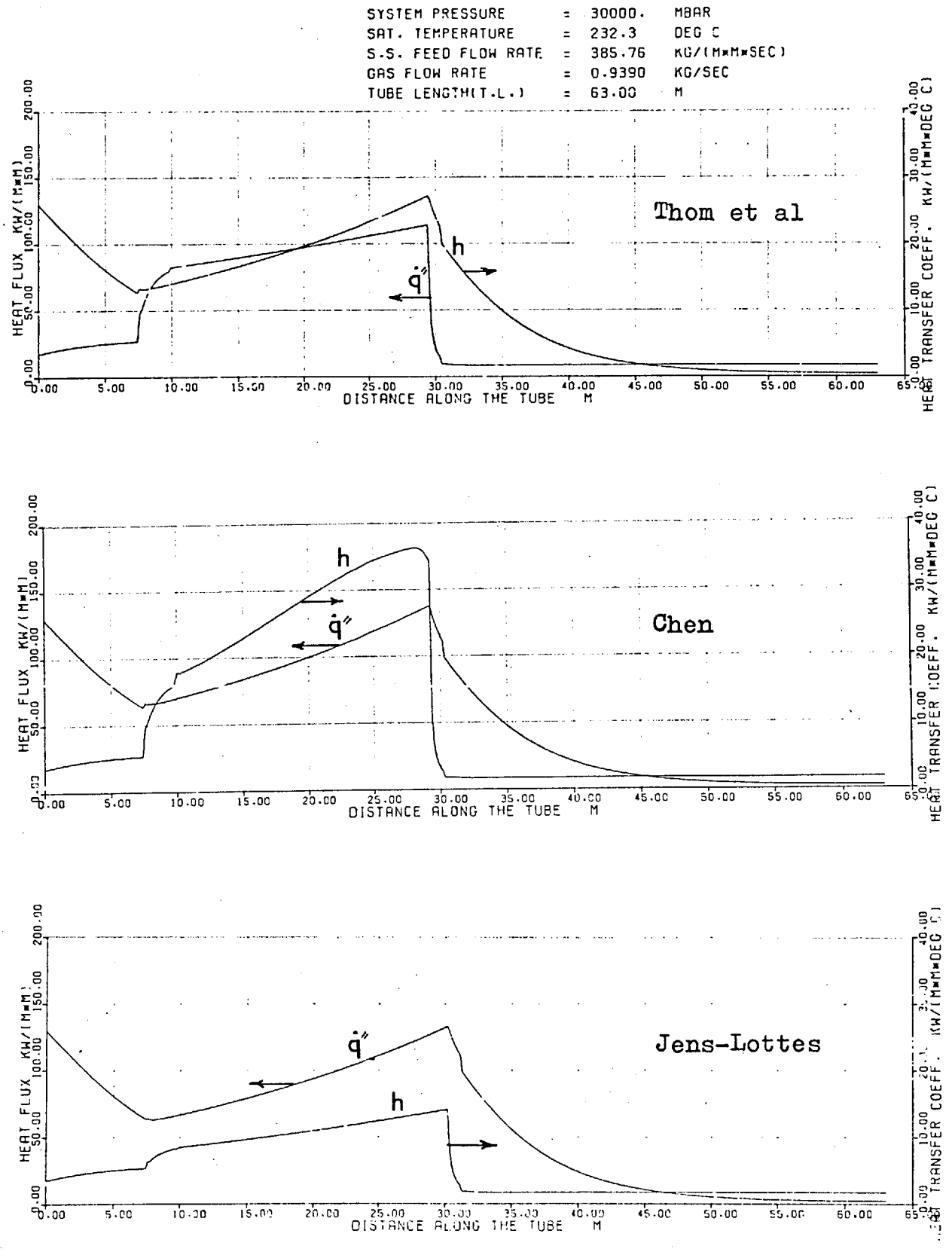


FIG.(5.14) - HEAT FLUX AND HEAT TRANSFER COEFFICIENT DISTRIBUTION ALONG THE TUBE

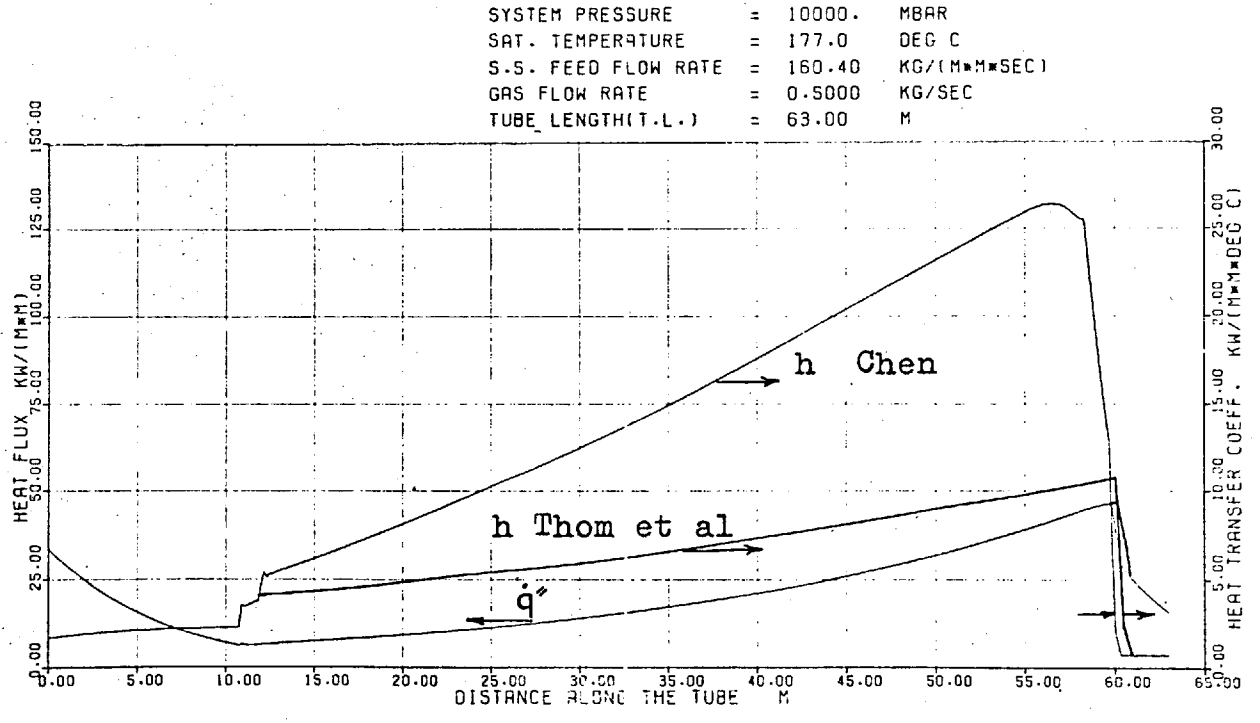


FIG.(5-15) - HEAT FLUX AND HEAT TRANSFER COEFFICIENT DISTRIBUTION ALONG THE TUBE

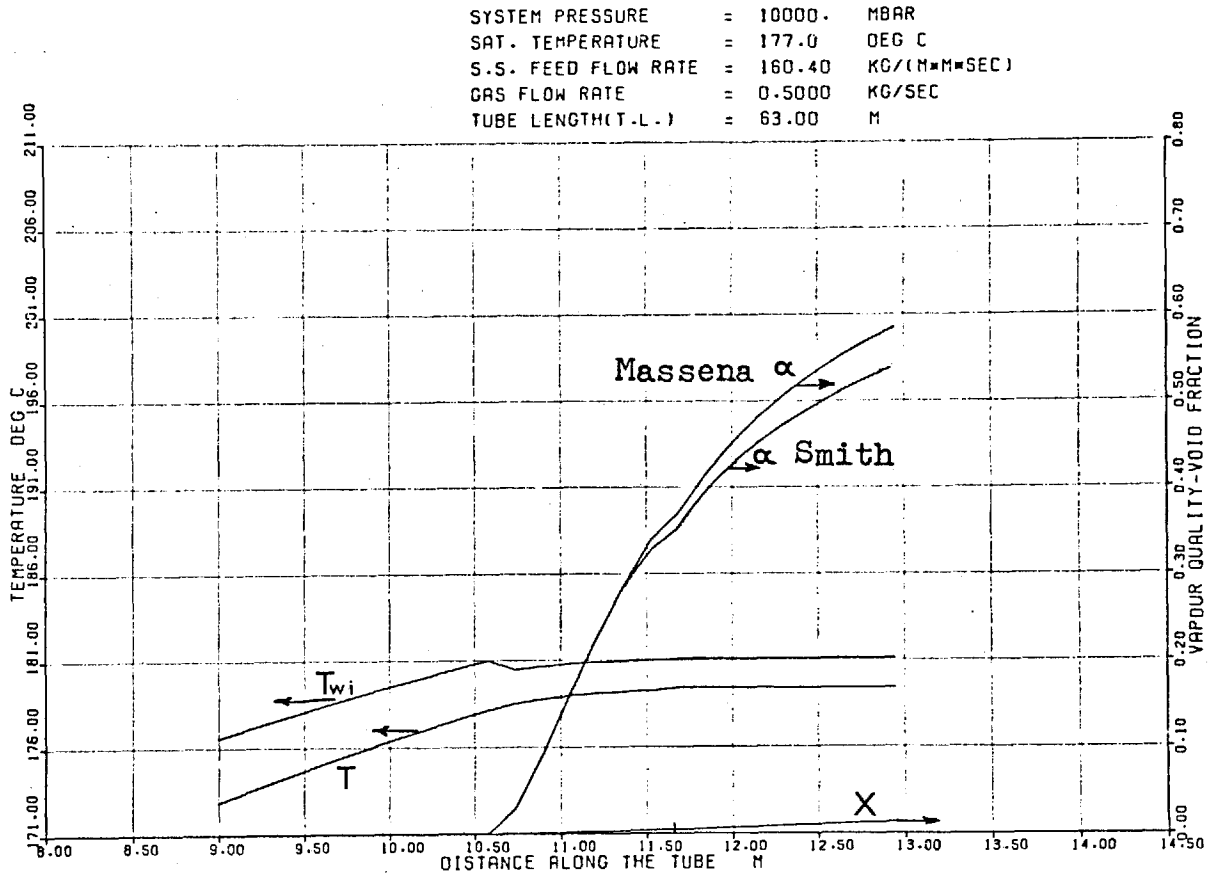


FIG.(5.16) - AXIAL TEMPERATURE , VOID AND QUALITY DISTRIBUTION AT SUBCOOLED BIOLING REGION

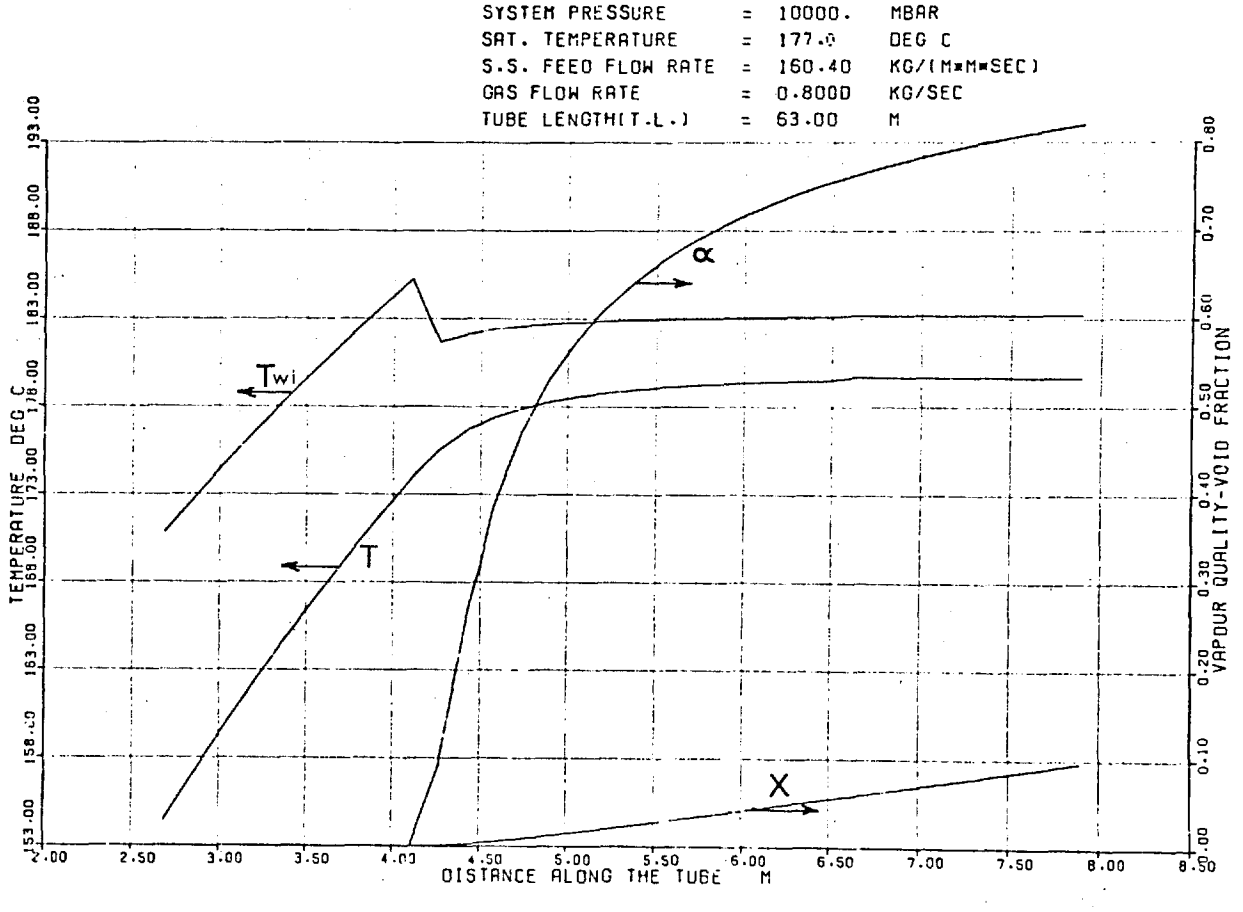


FIG.(5.17) - AXIAL TEMPERATURE , VOID AND QUALITY DISTRIBUTION AT SUBCOOLED BIOLING REGION

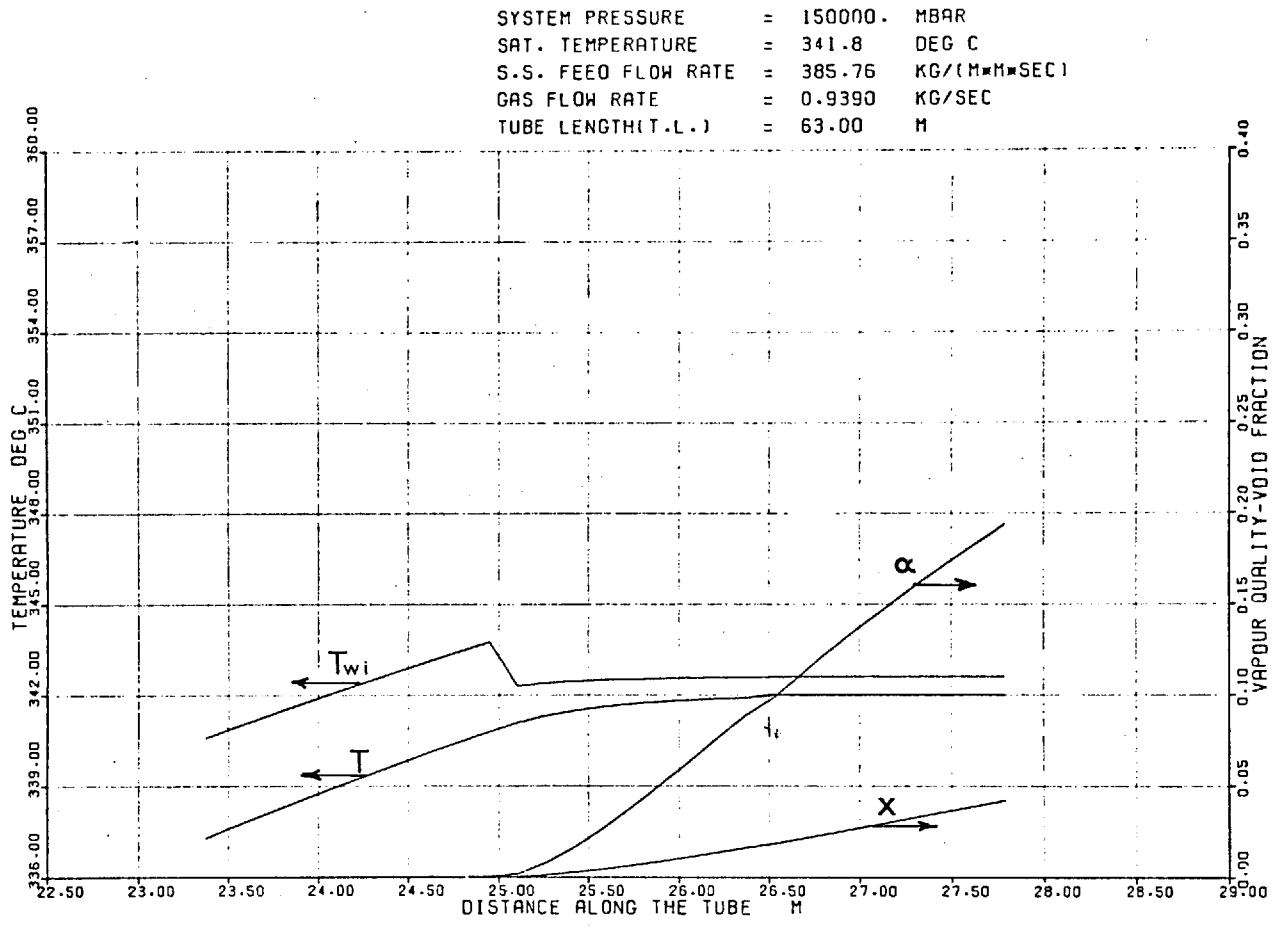


FIG.(5.18) - AXIAL TEMPERATURE , VOID AND QUALITY DISTRIBUTION AT SUBCOOLED BIOLING REGION

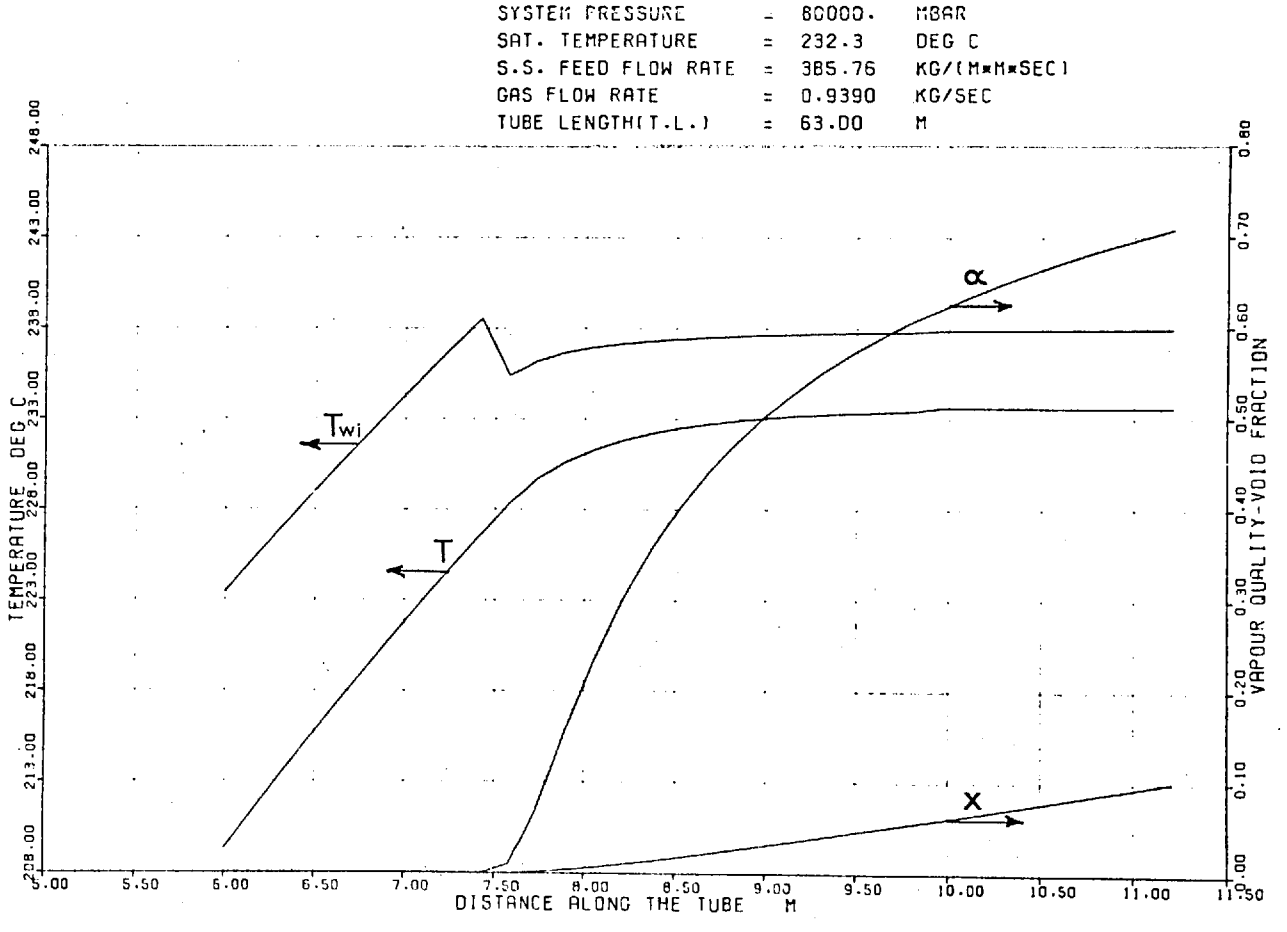


FIG.(5.19) - AXIAL TEMPERATURE , VOID AND QUALITY DISTRIBUTION AT SUBCOOLED BIOLING REGION

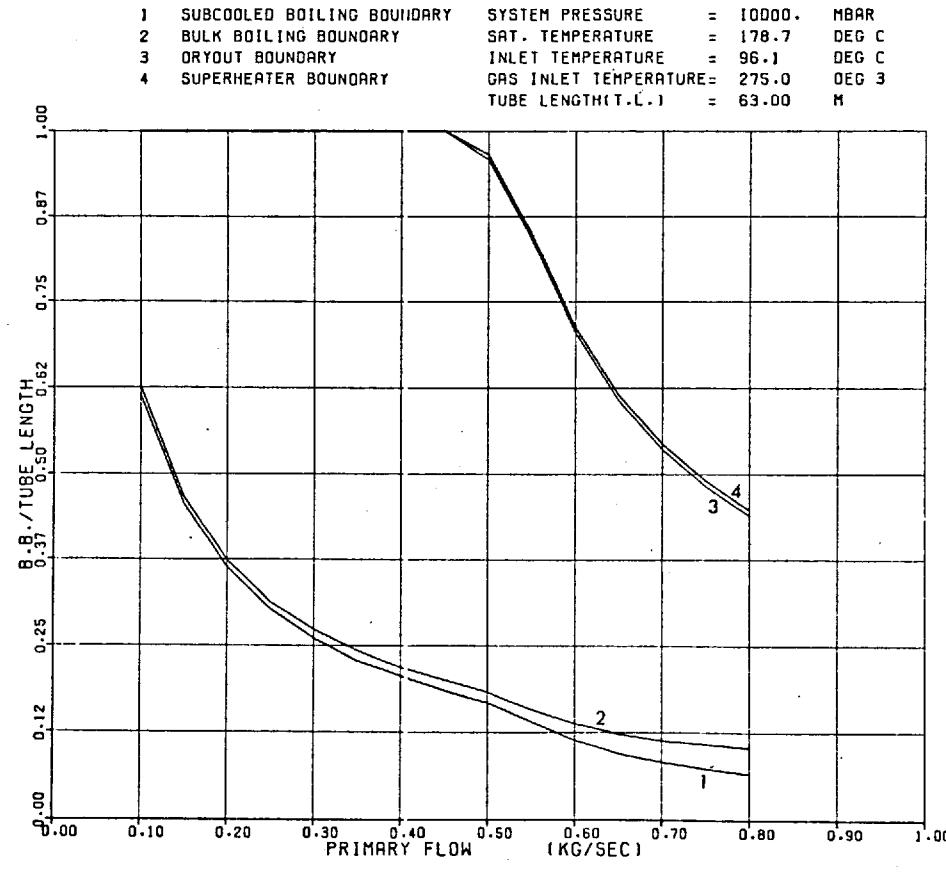


FIG.15.201 - BOILING BOUNDARIES MOVEMENTS

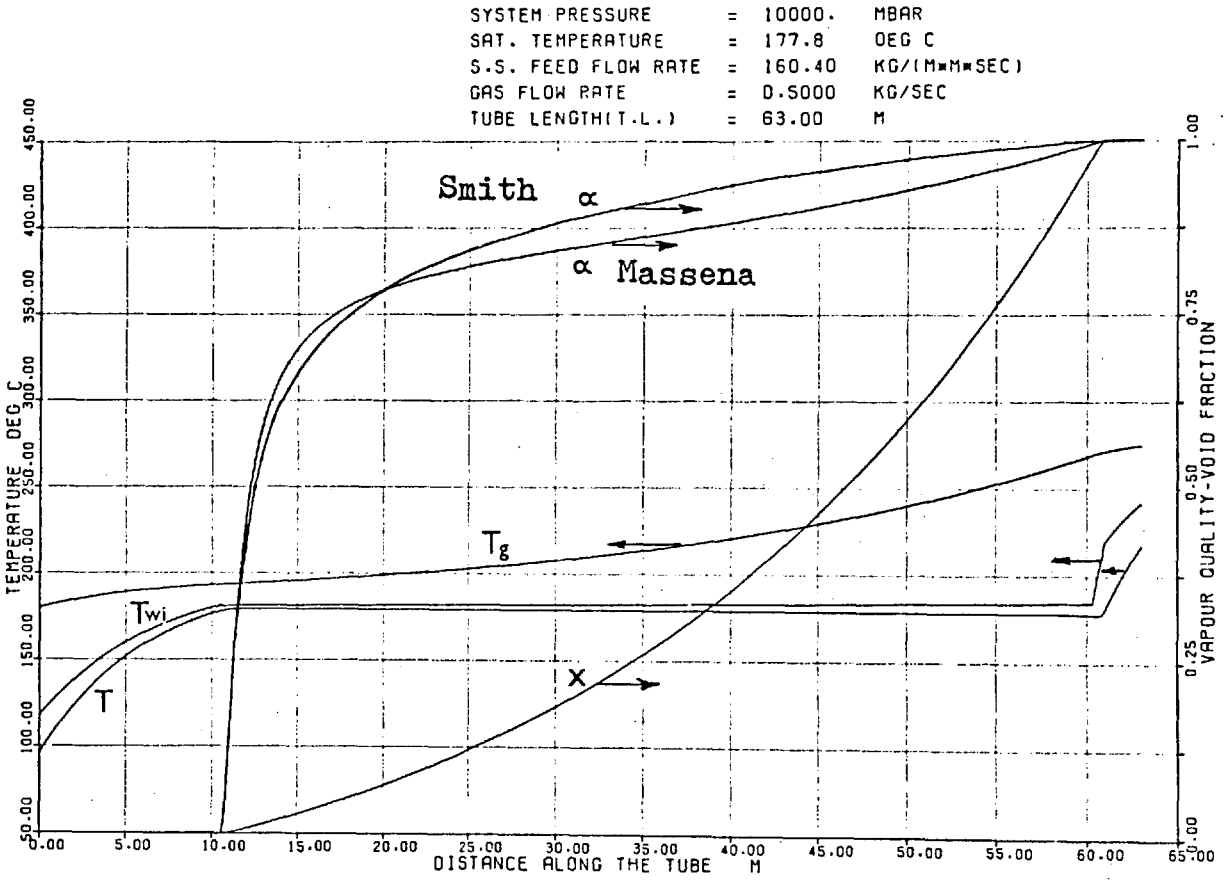


FIG.(5.21) - TEMPERATURES, VAPOR QUALITY AND VOID DISTRIBUTION ALONG THE TUBE

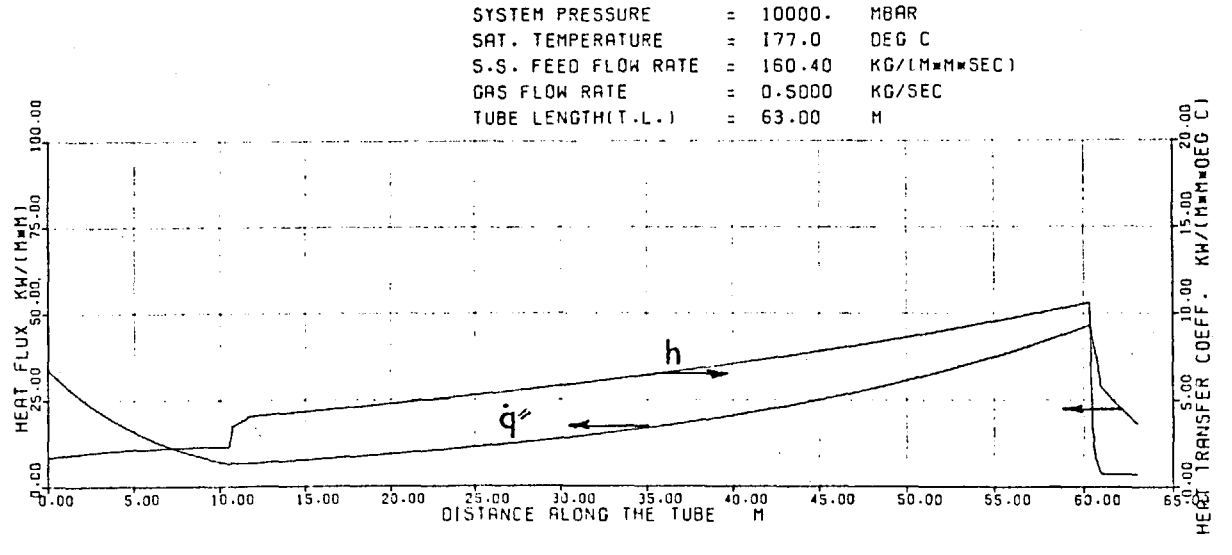


FIG.(5.22) - HEAT FLUX AND HEAT TRANSFER COEFFICIENT DISTRIBUTION ALONG THE TUBE

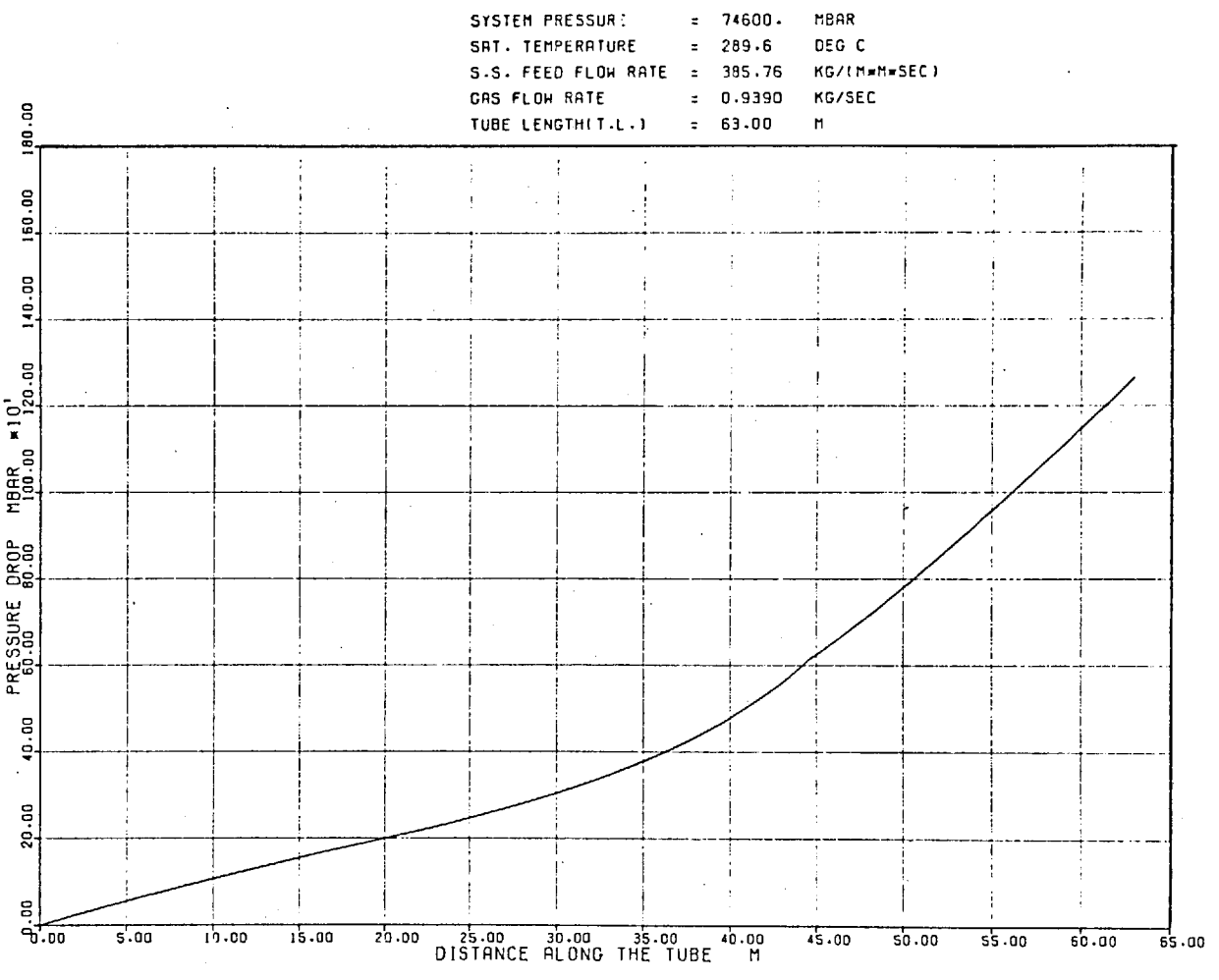


FIG.(5.23) - PRESSURE DROP DISTRIBUTION ALONG THE TUBE

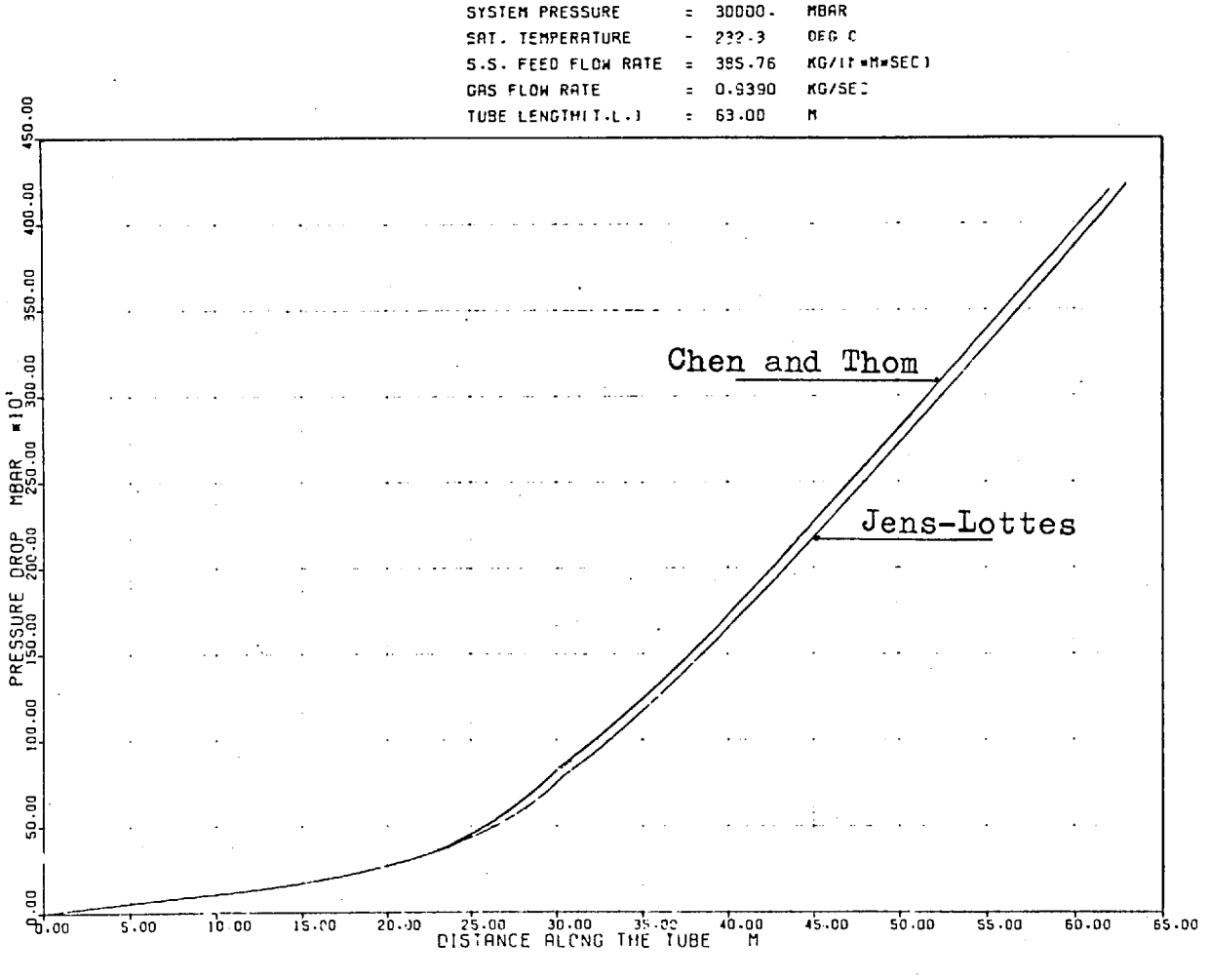


FIG.(5.24) - PRESSURE DROP DISTRIBUTION ALONG THE TUBE

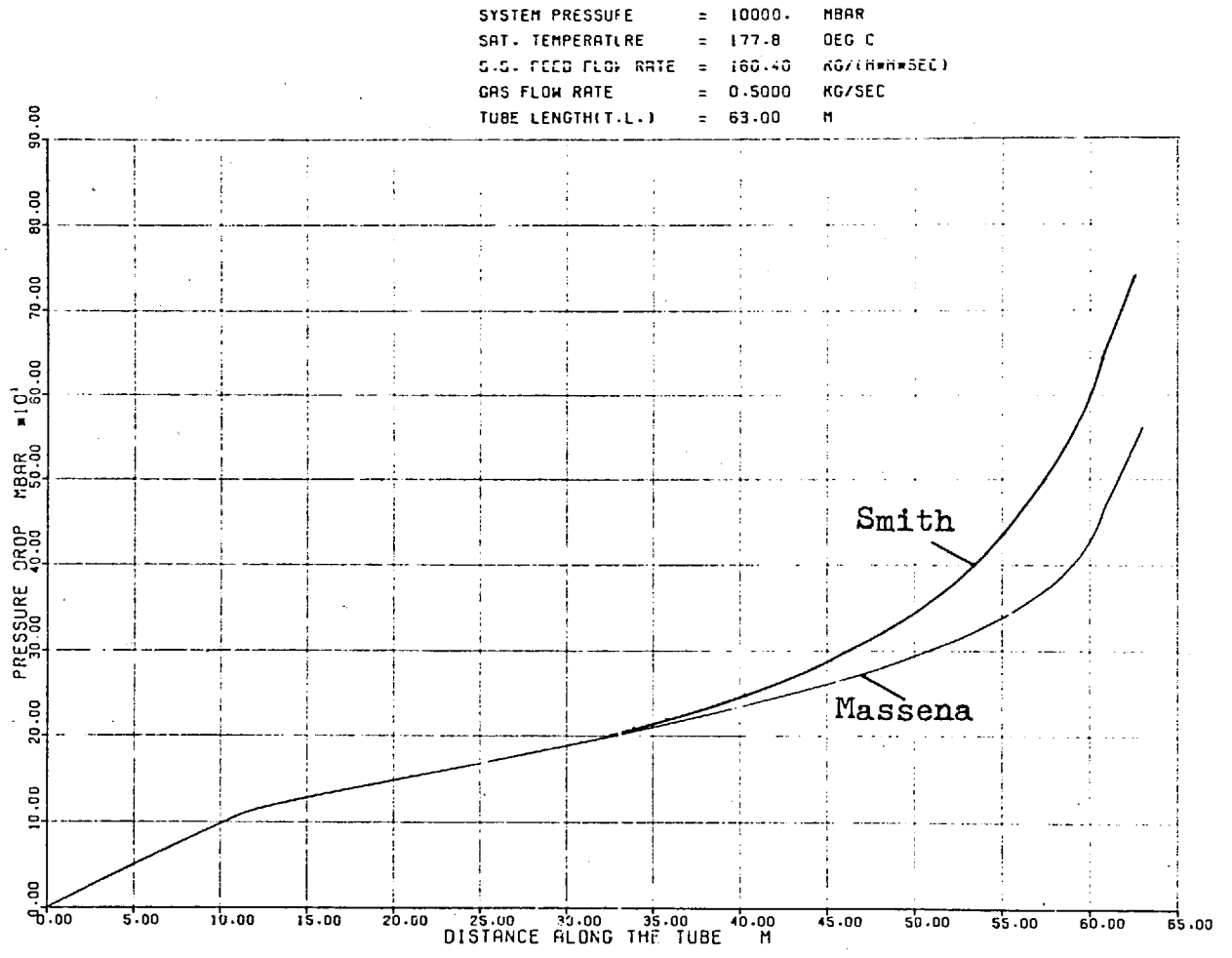


FIG.(5.25) - PRESSURE DROP D STRIBUTION ALONG THE TUBE

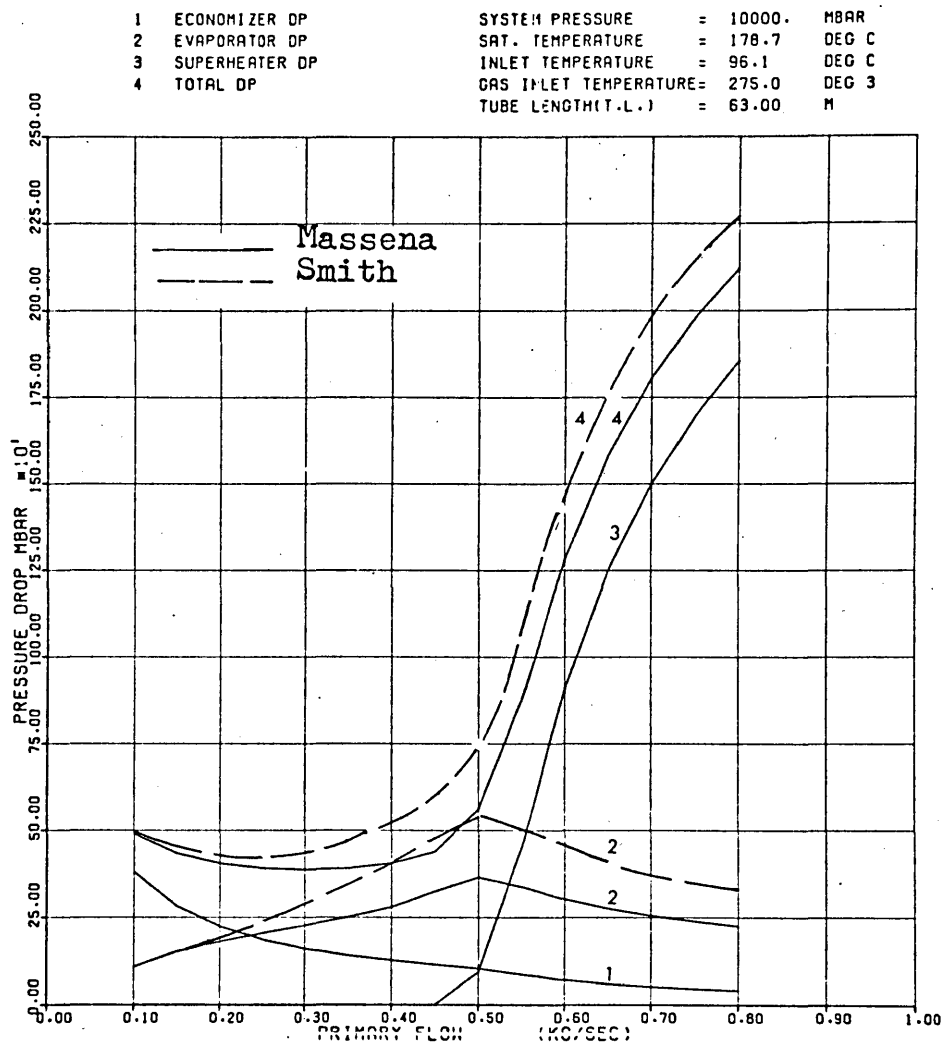


FIG.(5.26) - PRESSURE DROP OF DIFFERENT REGIONS

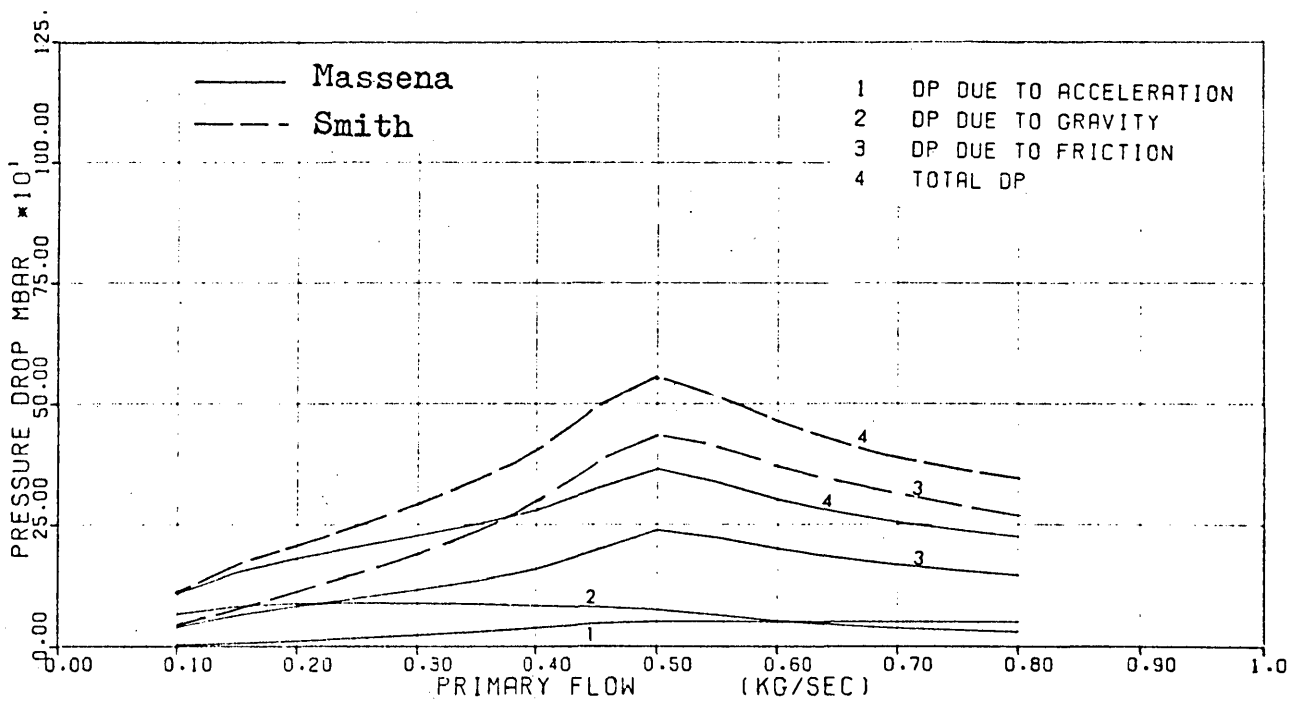


FIG.(5.27) - DIFFERENT COMPONENTS OF EVAPORATOR PRESSURE DROP

5.3 STATIC STABILITY RESULTS

5.3.1 Pressure Drop/Mass Velocity Characteristic

The predicted water/steam pressure drop versus inlet mass flow rate is plotted in Figure 5.28 for a typical set of operating conditions of an actual industrial test rig.

Inlet mass velocity is increased from a low value while the other parameters are kept unchanged. The pressure drop is calculated from the inlet where the heating starts up to the outlet. No effects of the inlet gagging and the inlet or outlet unheated tubes are taken into account.

Figure 5.28 shows a maximum and a minimum in the internal characteristic of the pressure drop-mass velocity curve which exhibits a possibility of static instability at certain mass velocities. In the same figure, different components of pressure drop are illustrated. It shows the dominant effect of the frictional pressure drop and counteractive effects of the gravitational and accelerational pressure drops against the negative slope part of the total pressure drop.

The position of the boiling boundaries and the outlet temperatures are plotted in Figures 5.29 and 5.31, respectively, as a function of inlet mass velocity. It is seen that the negative slope part of the Δp versus G occurs while the outlet condition of the system is superheated vapour. As the inlet mass velocity increases, the boiling boundaries move towards the outlet. The gradients of movements of the dryout and superheater boundaries are greater than those of the subcooled and bulk boiling boundaries (Figure 5.29). Furthermore, the length of the superheater region decreases rapidly and it eventually diminishes as the mass flow increases further.

The overall pressure drop is the sum of the subcooled

(economiser), two-phase (evaporator) and superheater pressure drops (Figure 5.30). These are affected by the mass velocity and the length of each region. As shown in Figure 5.30, the superheater pressure drop increases with increasing mass velocity until a maximum beyond which it decreases due to decreasing length of the superheater region.
The negative slope part of the overall pressure drop-mass flow diagram originates when the resultant superheater pressure drop decreases with increasing mass velocity.

The overall pressure drop Δp can be written as:

$$\Delta p = \Delta p_{sub} + \Delta p_{tp} + \Delta p_{sh} \tag{5.2}$$

The limiting condition for static instability may be defined as:

$$\frac{\partial (\Delta p)}{\partial G} > 0 \tag{5.3}$$

From equations (5.2) and (5.3), the static instability criterion can be rearranged as follows:

$$\frac{\partial (\Delta p_{sub} + \Delta p_{tp})/\partial G}{\partial \Delta p_{sh}/\partial G} > -1 \tag{5.4}$$

When the outlet condition of the system is always superheated vapour with changes in the inlet mass velocity, the numerator of equation (5.4) remains always positive, while the denominator term, $\partial \Delta p_{sh}/\partial G$, may become negative. This arises due to the decreasing length of the superheater with increasing mass velocity or vice versa. Static instability occurs when $\partial \Delta p_{sh}/\partial G$ is negative and its absolute value is greater than the economiser and the evaporator pressure drop gradients

with respect to mass velocity.

The different components of pressure drop in the different regions along the tube (Figure 5.32) show that the pressure drop in the superheater and the evaporator is strongly due to frictional components (Figure 5.32a and b). Therefore, the pressure drop gradients in these regions can vary depending on the values of the length of each region and its movements, mass flow rate, density and the tube geometry and roughness. The stabilising effect of the economiser pressure drop gradient is strongly due to the gravitational pressure drop. The gravity component changes with the movement of the subcooled boiling boundary.

Two comments arise concerning the effect of the tube geometry and the nature of heating on the negative slope part. The friction coefficient in helically-coiled tubes is higher than straight tubes. This would result in a higher pressure drop in the superheater region, hence the slope of the negative part of Δp versus G would be larger than that of a straight tube under similar operating conditions. The slope is further decreased compared to a vertical straight tube due to decreasing gravity in the economiser region.

Secondly, in a system heated by a counterflow gas, due to the coupling of heat flux-flow, the movements of the subcooled boiling boundary is suppressed, while the movements of the superheater boundary is accelerated compared with, for example, a constant heat flux system. (This is explained thoroughly in the next chapter.) These movements would result in a lower pressure drop gradient in the economiser and a larger gradient in the superheater region. Hence, the potential of static stability will be more pronounced in a counterflow heated system compared to a system in which no coupling between the flux-flow exists

(e.g. constant heat flux).

5.3.2 Stable Operating Regions

The outlet temperatures of the primary and secondary flow are plotted in Figure 5.31 as a function of inlet mass velocity. Figures 5.30 and 5.31 show that there are two stable operating regions where the outlet condition is dry superheated vapour. When the system operates at region I of Figure 5.31, the outlet temperature is highly superheated and the system exhibits static instability when the mass flow rate increases. Operation at low outlet superheat is possible at region II (Figure 5.31) where the system becomes sensitive to instability as the inlet mass velocity decreases. This is qualitatively consistent with the experimental results of a sodium heated once-through rig (Figure 5.33a and b) as reported by Waszink and Efferding (1973).

The outlet temperature of the primary flow decreases as mass flow increases (Figure 5.31). The temperature drop on the primary side, therefore, increases at unstable conditions as reported by Moxon (1973). Nevertheless, due to the predictions (Figure 5.31), there exist stable operating conditions which have higher temperature drops on the primary side than that of the unstable case.

Figures 5.34 and 5.35 illustrate the variations of temperature, heat flux and heat transfer coefficient at a point upstream of the subcooled boiling boundary. As the inlet mass velocity increases, the amount of the total heat extraction from the primary side increases, and hence it decreases the level of the primary temperature as shown in Figure 5.34, Curve 1. The model also shows that the temperature at which the subcooled boiling starts (Figure 5.34, Curve 3) increases with

inlet mass flow. Hence, the local heat flux is expected to decrease. On the other hand, any rise in mass flow increases the heat transfer coefficient of the economiser (Figure 5.35, Curve 2). Consequently, the local heat flux is affected by two counteracting parameters which cause the local heat flux to exhibit a minimum as shown by Figure 5.35, Curve 1. The minimum of the local heat flux-mass velocity curve is examined at different operating conditions. For all cases, the negative slope region of Δp versus G falls just before the minimum heat flux where the local temperature difference between the primary and the secondary side is small. The above discussion supports the explanation of Moxon (1973).

In summary, the conditions of the temperature of the primary and the secondary flow most likely to cause static instability are:

i) a high temperature drop on the primary side; and
ii) a small temperature difference between the primary gas and the secondary flow.

5.3.3 Effects of the Primary Side Parameters on the Static Characteristics

5.3.3.1 Effect of mass flow rate

Figures 5.36 to 5.39 illustrate the effect of 10% and 20% reductions of the primary flow on the static characteristics of the system. The negative slope of the pressure drop-mass flow curve is steepened compared to the nominal condition shown in Figure 5.36.

When the primary flow decreases, the total heat input to the secondary side decreases. This lengthens the single-phase

and two-phase regions whereas it shortens the superheater region (Figure 5.37). When plotting the position of the subcooled boiling boundary against mass flow (Figure 5.37), it can be seen that the slope increases as a result of decreasing the primary mass flow rate. Consequently, the stabilising effect of the economiser and evaporator are increased, while the destabilising component of the superheater pressure drop is decreased (Figure 5.38). The stabilising components of pressure drop are mainly due to decreasing frictional pressure drop and increasing the gravitational pressure drop (Figure 5.36).

The above consideration is useful in the early stages of system design. However, if a system is designed to operate at a point A in Figures 5.38 and 5.39 under, for example, constant pressure drop, a reduction in the primary flow rate would move the operating point to B (Figure 5.38), where the condition of the vapour at the outlet is wet as seen in Figure 5.39. Naturally, this behaviour is undesirable from an operational point of view. In practice, this is normally avoided by gagging the inlet mass flow. This shifts the pressure drop-mass flow characteristic upwards.

5.3.3.2 Effect of the primary side heat transfer coefficient and inlet temperature

The reduction of heat transfer rate on the primary side decreases the local heat flux and hence it reduces the negative part of the pressure drop-mass flow curve. This is shown in Figures 5.40 to 5.43 which illustrate the effect of a 50% decrease in the local value of the heat transfer coefficient.

Figure 5.44 illustrates a similar trend when the inlet temperature of the primary flow decreases.

From the point of view of safe operation, any decrease in the primary side heat transfer coefficient (Figure 5.40) or in the inlet temperature (Figure 5.44) may cause static instability if sufficient feed resistance is not provided.

5.3.4 Effects of the Secondary Side Parameters on the Static Characteristics

5.3.4.1 Effect of system pressure

The effect of system pressure is illustrated in Figures 5.45 to 5.50, which are produced at a pressure of 150 bar. The overall pressure drop-mass flow characteristic curve does not possess a negative slope region. At high pressures, the vapour density increases while the liquid density decreases. The latter steepens the economiser pressure drop-mass flow curve, while the former decreases the slopes of the superheater and evaporator pressure drop-mass flow curves. Furthermore, the pressure drops are affected by the changes in the positions of boiling boundaries as shown in Figure 5.46. Consequently, as the system pressure is increased, while all the other conditions are fixed (Figures 5.28 and 5.45), the system shows a monotonic characteristic due to equation (5.4).

The static stability at high pressures is only possible when the primary side flow rate or inlet temperature decreases, or the heat transfer coefficient of the primary flow deteriorates, as shown in Figures 5.47 and 5.48. Here, decrease of the primary flow at a constant system pressure drop would cause the operational point C to move to point D where the outlet superheating is very small.

5.3.4.2 Effect of secondary side heat transfer coefficient

If the heat transfer coefficient of the secondary side increases, the local heat flux will increase, and the length of the economiser and evaporator will decrease. Therefore, the negative slope part will increase. Or, vice versa, any decrease of the heat transfer coefficient would reduce the slope of the negative part of the static characteristic curve (Δp versus G).

Figures 5.51 and 5.52 show a comparison of the static characteristic curves for a 50% difference in the local heat transfer coefficient of the economiser. Figure 5.51 illustrates the effect of heat transfer changes on the movement of the boiling boundary consistent with the above discussion.

Similar effects are displayed in Figure 5.53 for changes of the superheater heat transfer coefficient.

In the above discussions, the two-phase heat transfer correlation of Jens-Lottes (1951) was used to predict the static characteristics. The effect of two-phase heat transfer correlations of Thom et al (1965) and Chen (1963) are illustrated in Figure 5.54. No significant differences in the static characteristics are noticeable at a pressure of 75 bar.

5.3.4.3 Effect of the coil geometry

As the helix diameter decreases, the effects of centrifugal forces and secondary circulation inside the coil increase at a fixed value of the inlet mass flow. Hence, the heat transfer coefficient and the pressure drop increase. Therefore, the negative slope part of the pressure drop-mass flow diagram increases as shown in Figure 5.55. In systems with large coil diameters, the reverse effect

is expected as illustrated in Figure 5.55.

The effect of the helix angle is shown in Figure 5.56. A large angle of inclination results in a high gravitational pressure drop which acts against the negative slope part of the pressure drop-mass flow characteristic curve.

5.3.5 Conclusions

A counterflow gas fired helically-coiled tube once-through steam generator could become statically unstable. This could arise from the shape of the static characteristic curve (Δp versus G) or from gradual changes of the static characteristic curve due to changes of the primary flow conditions.

It has been shown that the pressure drop-mass flow characteristics of such a system could possess a negative slope even at relatively high pressures. This would be due to decreasing the length of the superheater as mass flow increased or vice versa. The pressure drops in the single-phase liquid and two-phase regions would counteract against the negative slope, while superheater pressure drop would give rise to the negative slope of the static characteristic curve.

Two stable operating regions have been recognised. Firstly, at very high outlet superheat where static instability arose as mass velocity increased. Secondly, at low outlet superheat where any decrease of mass flow reduced the potential of the stable operation.

When the system tended to become unstable, the temperature drop of the primary side was high, whereas the temperature difference between the primary and the secondary sides was small.

Effects of certain parameters on the static characteristic curve have been investigated and discussed. It has been shown that the

pressure drop-mass flow curve is affected by variation of the primary flow parameters, changes of the inlet temperature, mass flow rate and deterioration of the heat transfer coefficient of the primary side, which could cause static instability. These will require specific attention from the point of view of the control system, particularly in the area of static stability.

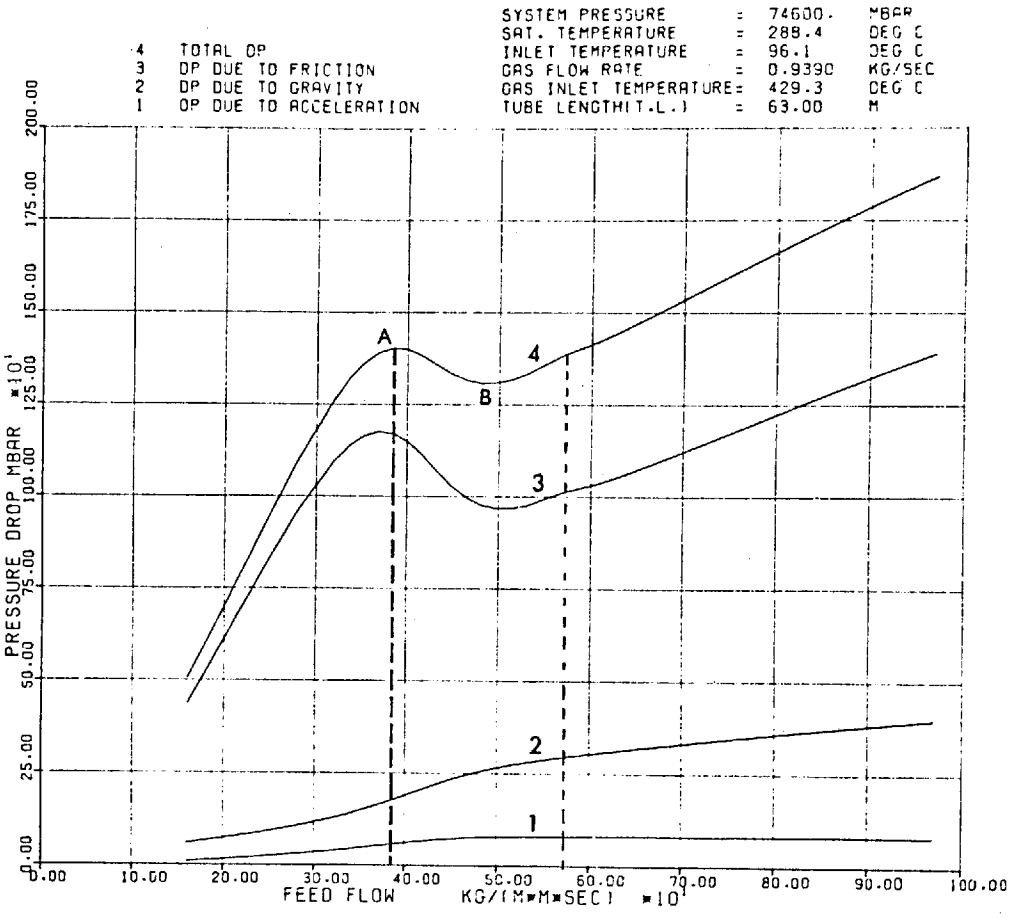


FIG.(5-28) - DIFFERENT COMPONENTS OF PRESSURE DROP VERSUS MASS VELOCITY

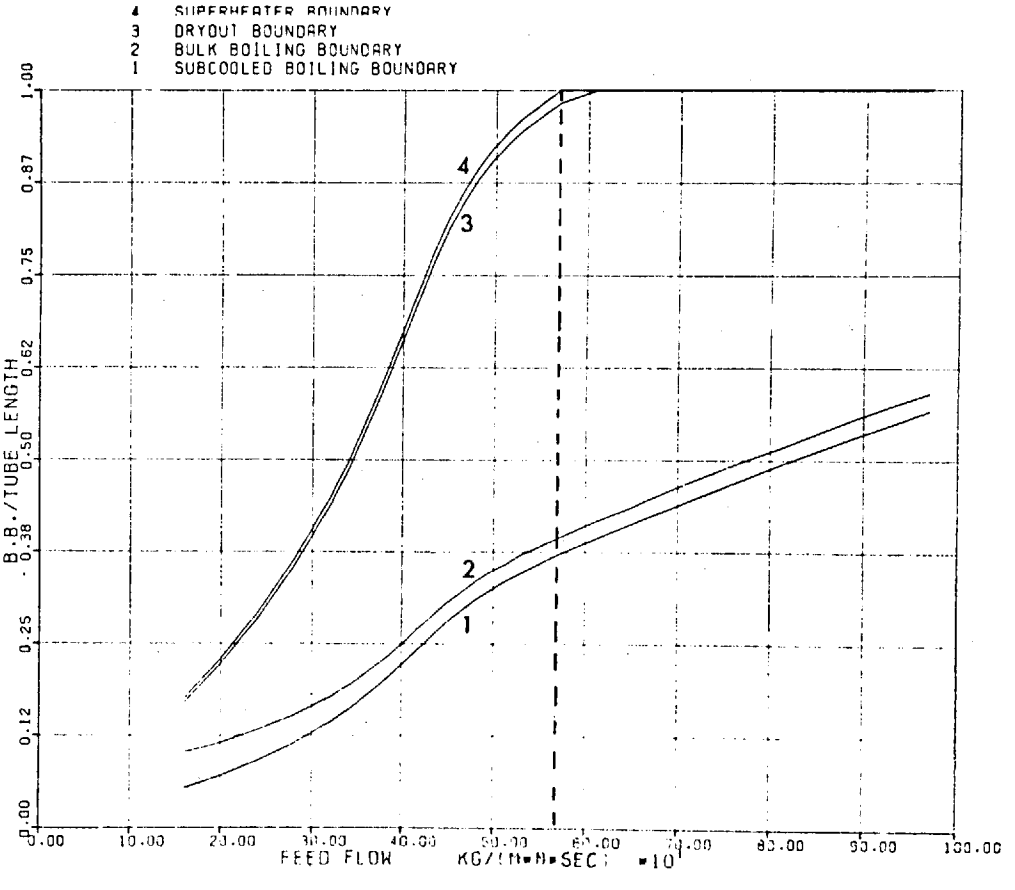


FIG.(5-29) - BOILING BOUNDARIES MOVEMENTS VS MASS VELOCITY

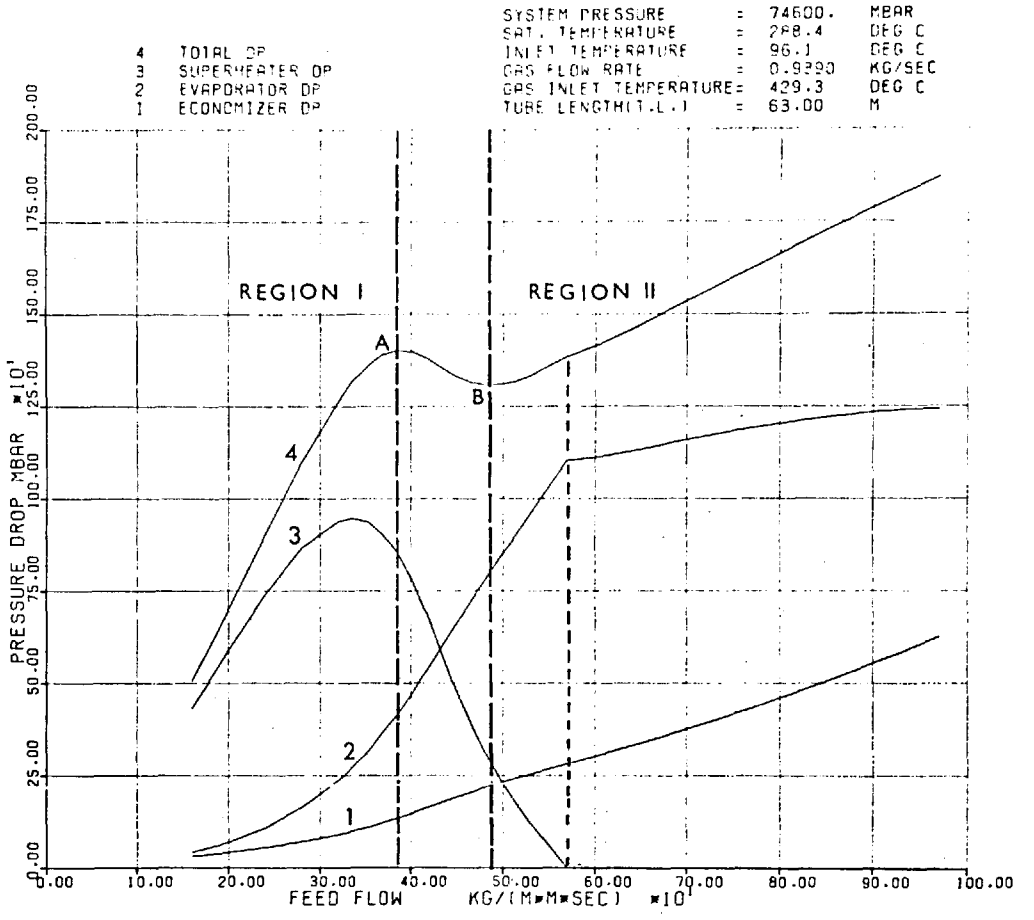


FIG.(5.30) - PRESSURE DROP OF DIFFERENT REGIONS VERSUS MASS VELOCITY

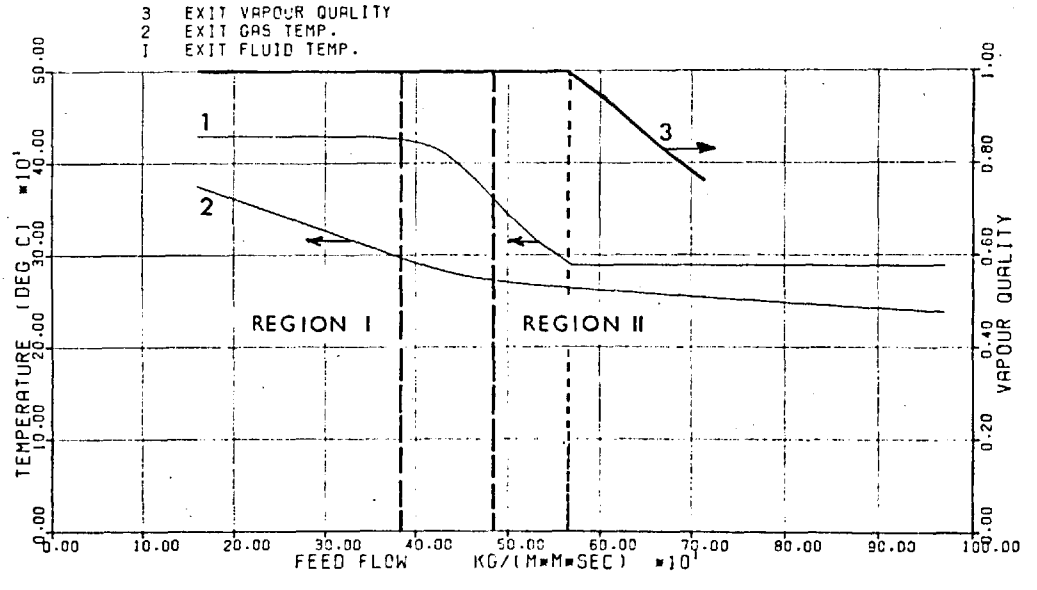
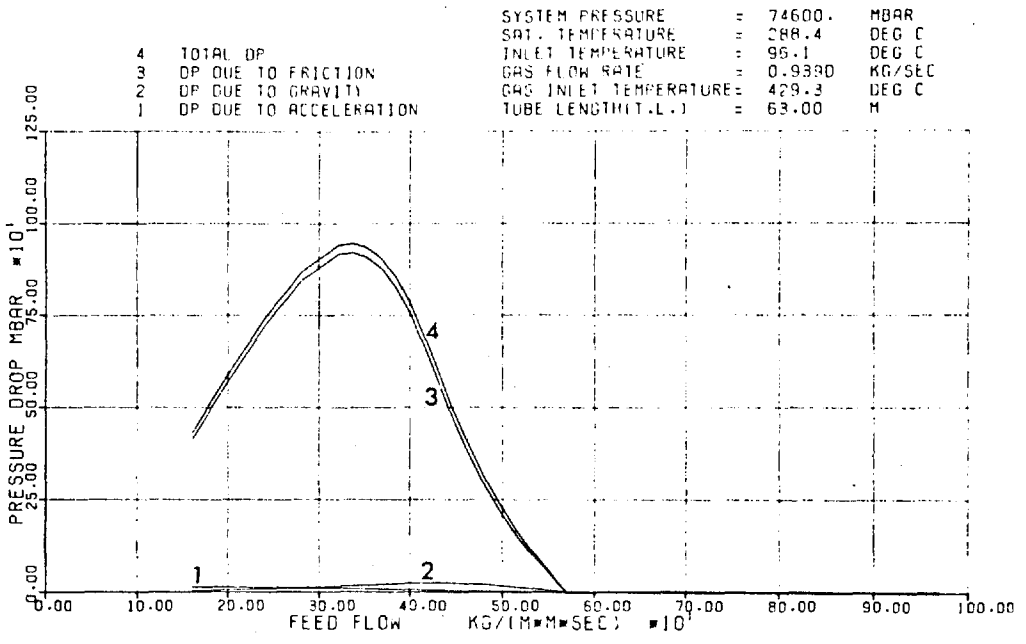
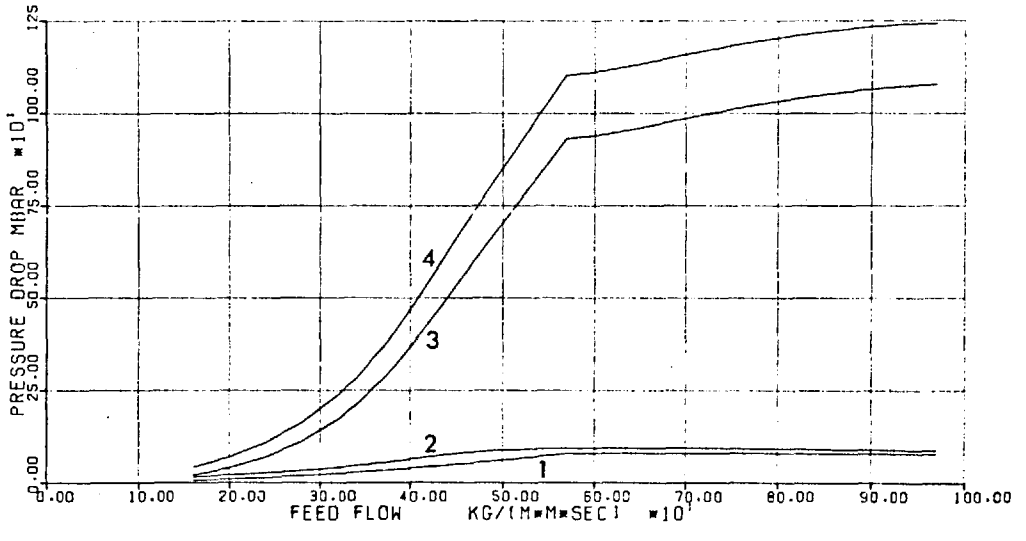


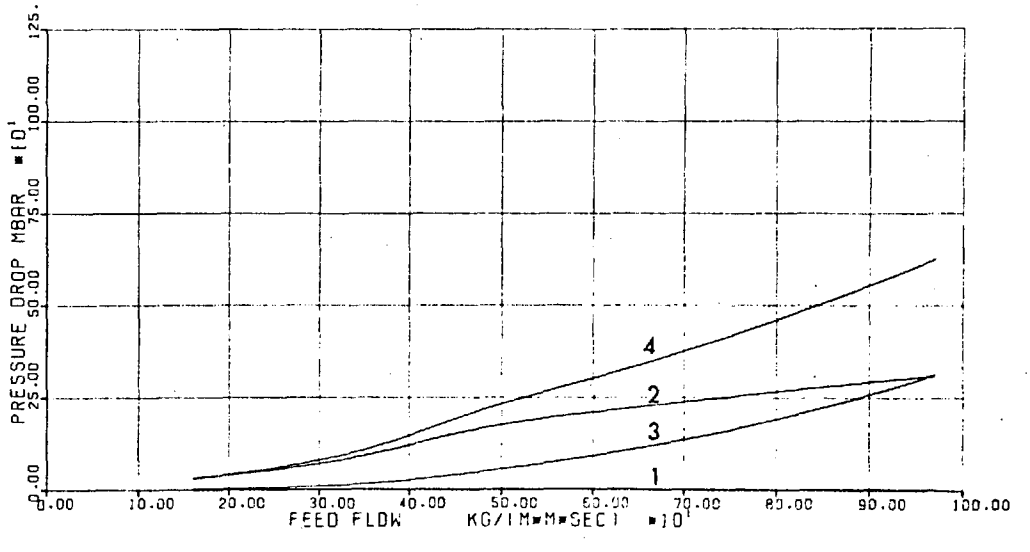
FIG.(5.31) - VARIATION OF EXIT TEMPERATURES AND VAPOUR QUALITY VS MASS VELOCITY



(a) - DIFFERENT COMPONENTS OF SUPERHEATER PRESSURE DROP VS MASS VELOCITY

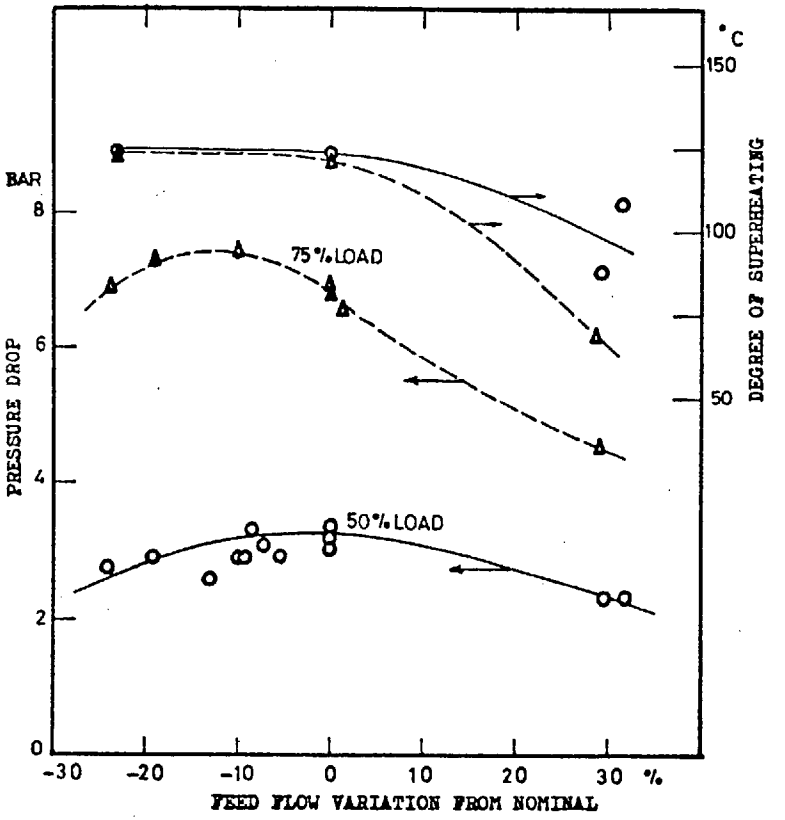


(b) - DIFFERENT COMPONENTS OF EVAPORATOR PRESSURE DROP VS MASS VELOCITY

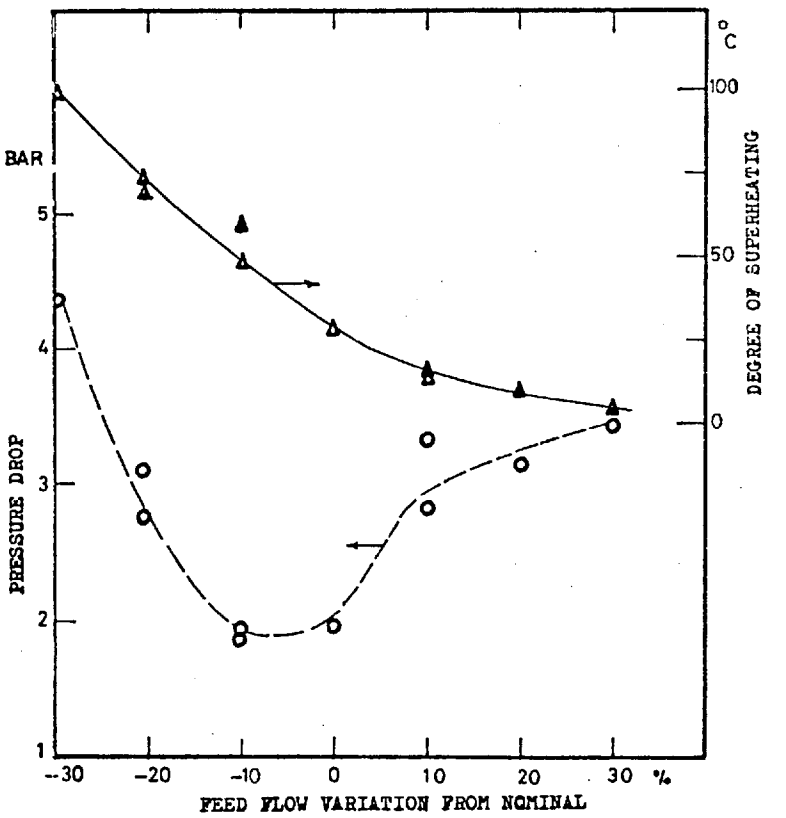


(c) - DIFFERENT COMPONENTS OF ECONOMIZER PRESSURE DROP VS MASS VELOCITY

Figure 5.32: Components of pressure drop of different regions along the tube



(a) Nominal steam outlet is 510 ± 9°C and 165.5 bar



(b) Nominal steam outlet is 16°C and 182.5 bar

Figure 5.33: Water/steam pressure drop versus feed water flow rate; experimental results of Waszink et al (1973)

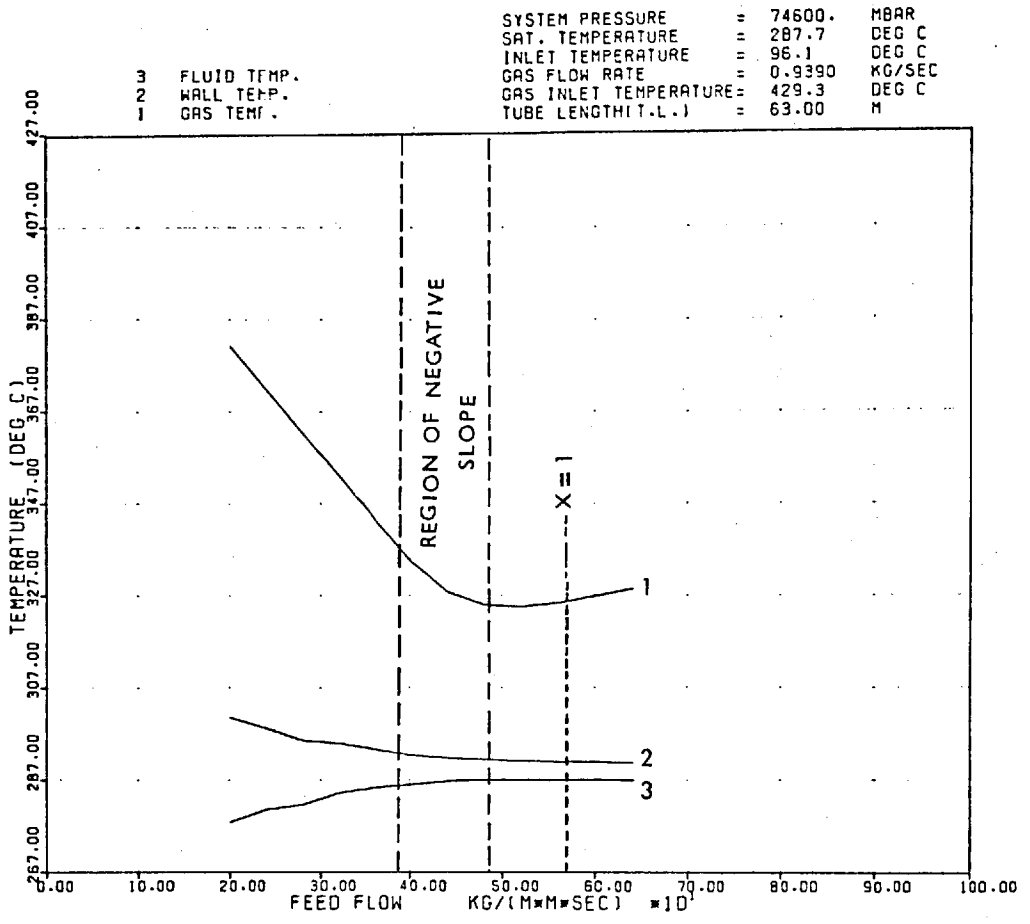


FIG.(5-34) - VARIATION OF TEMPERATURES AT THE ONSET OF SUBCOOLED BOILING VS MASS VELOCITY

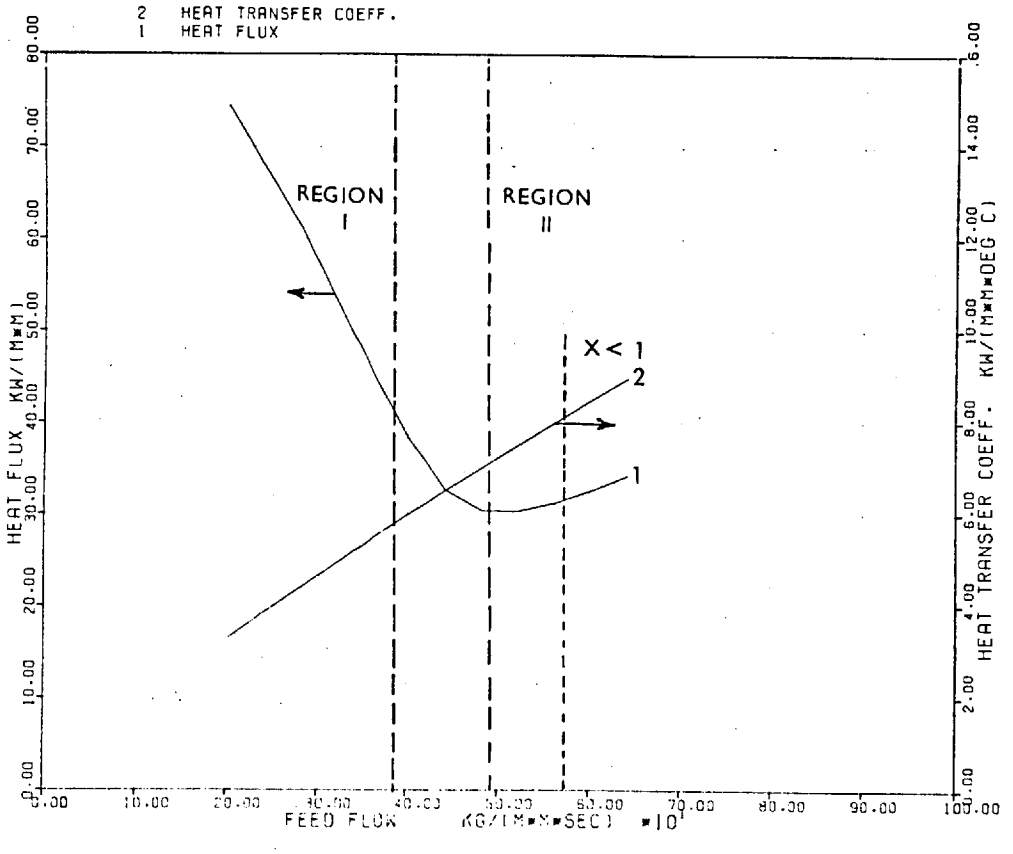


FIG.(5-35) - VARIATION OF HEAT FLUX AND HEAT TRANSFER COEFF. AT ONSET OF SUBCOOLED BOILING VS MASS VELOCITY

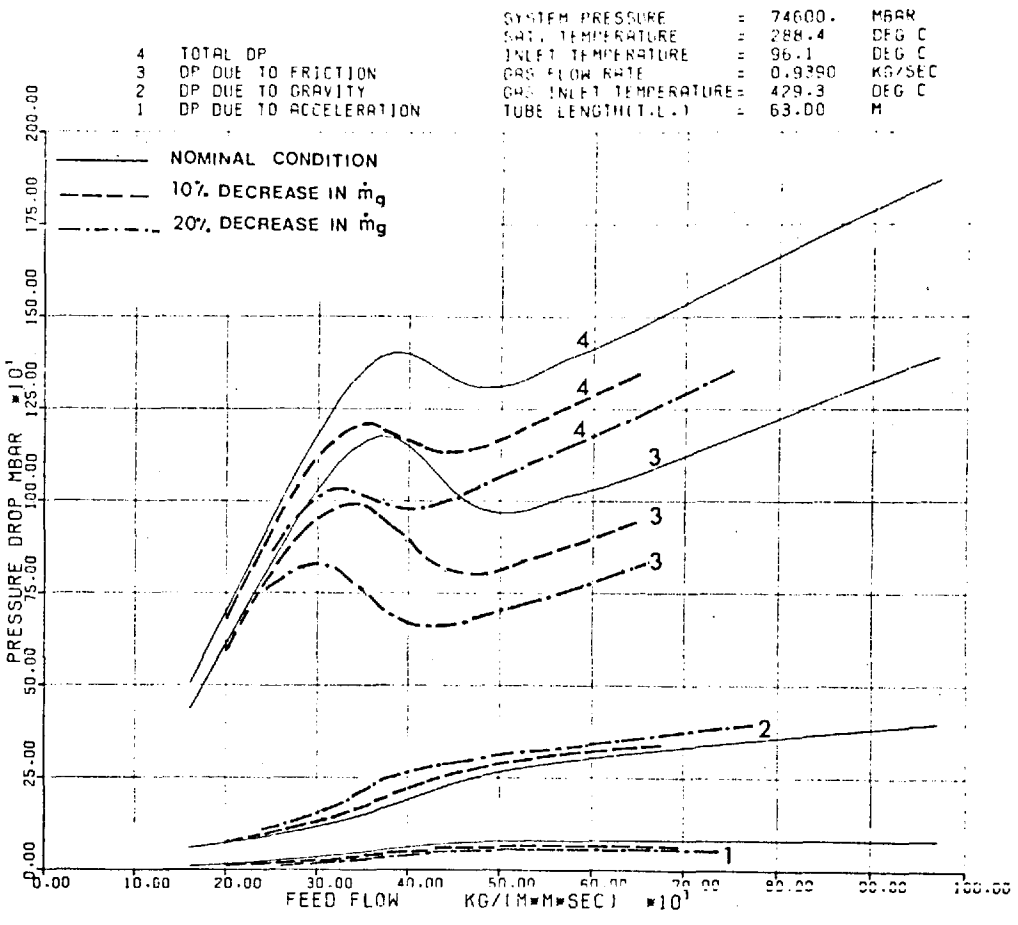


Figure 5.36: Effect of the primary flow rate on the pressure drop components of the static characteristics

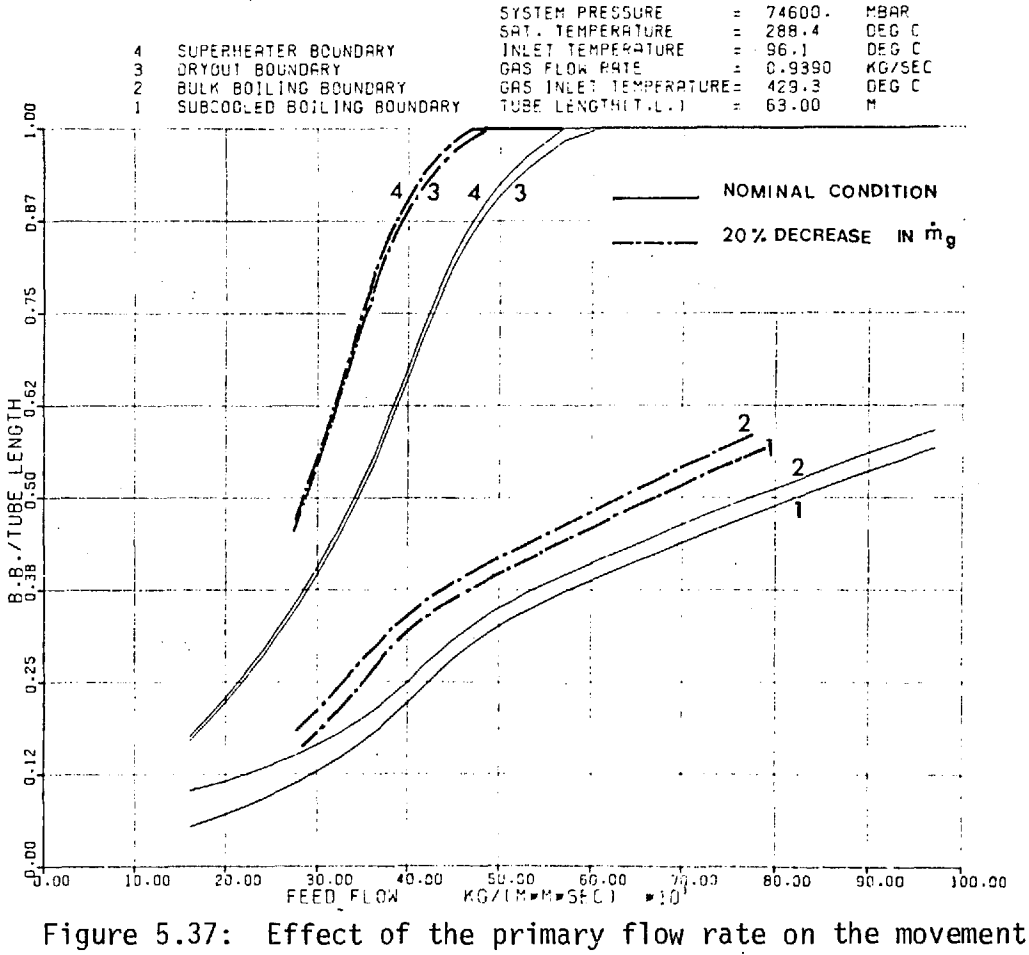


Figure 5.37: Effect of the primary flow rate on the movement of the boiling boundaries versus mass flow

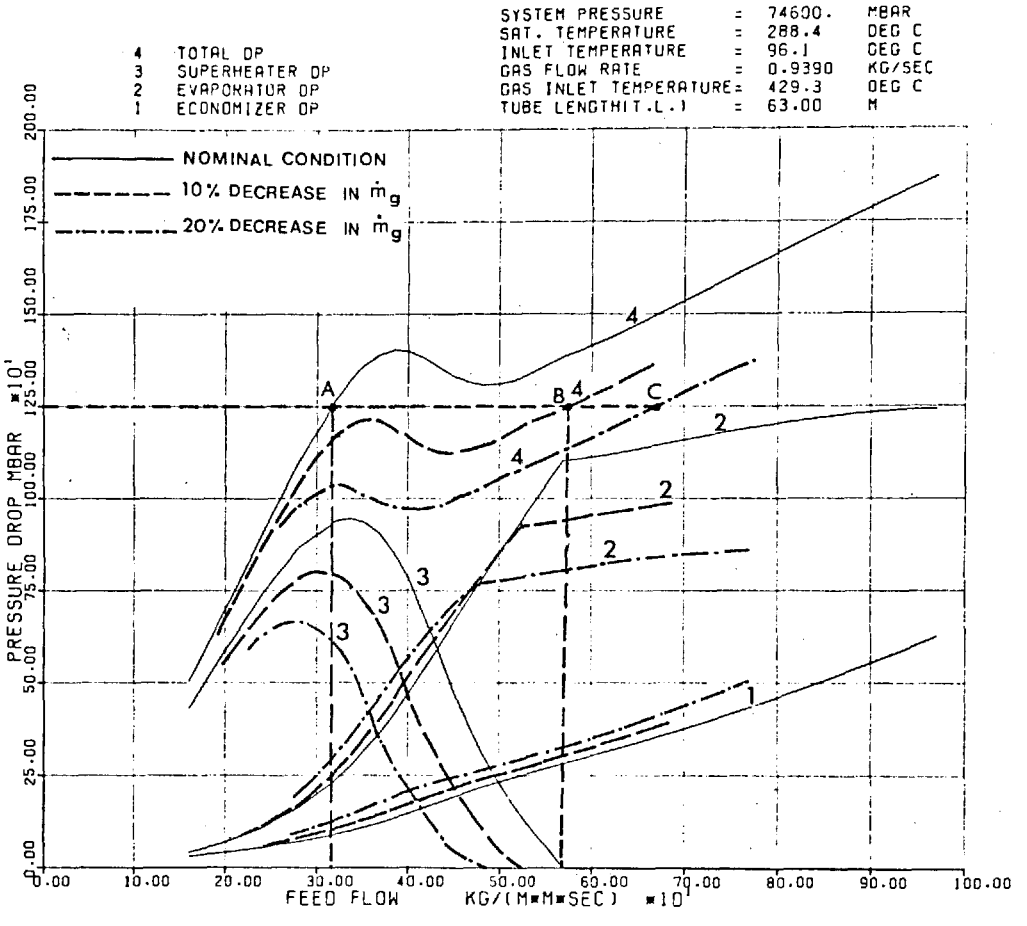


Figure 5.38: Effect of the primary flow rate on the static characteristic curve

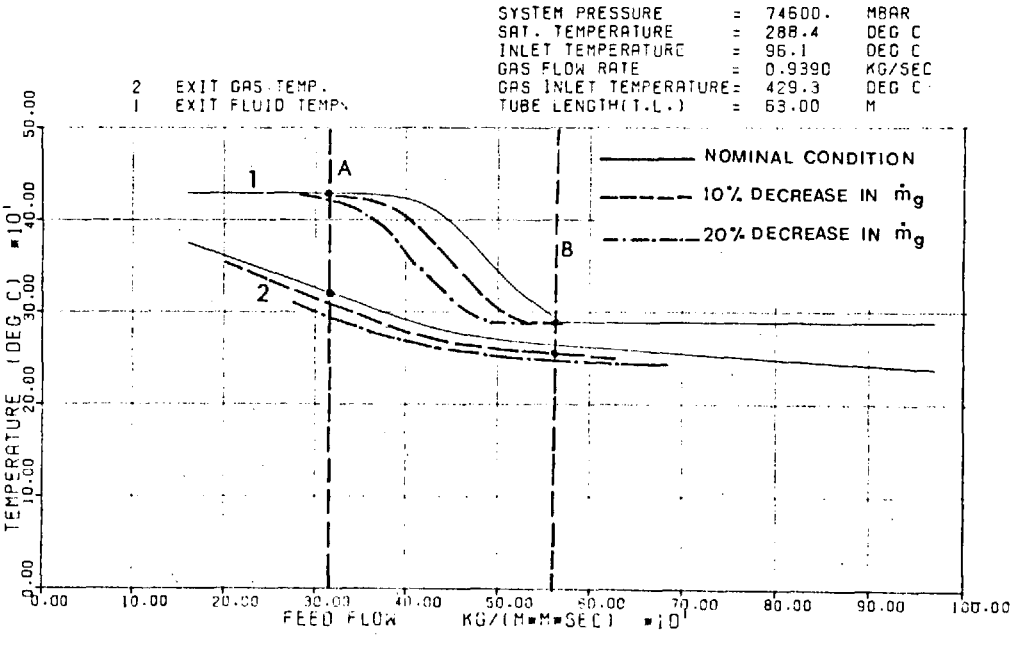


Figure 5.39: Effect of the primary flow rate on the variation of the outlet temperatures versus mass flow

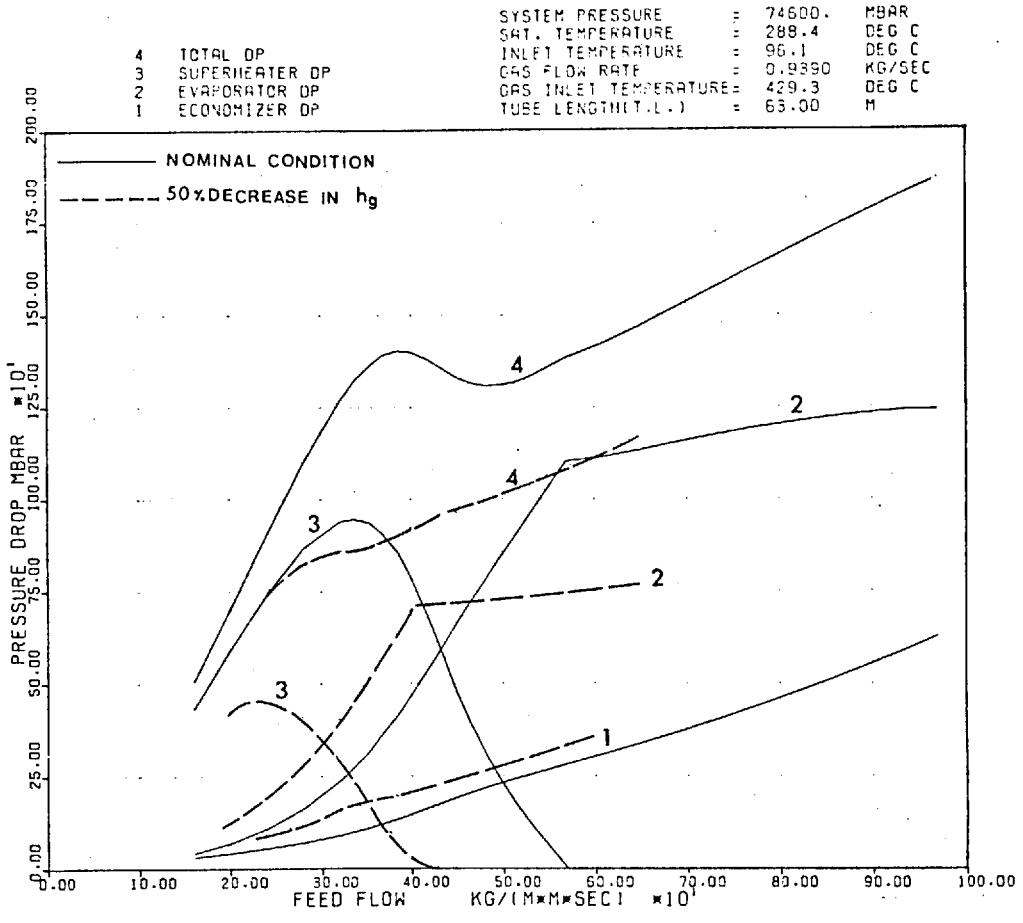


Figure 5.40: Effect of the primary side heat transfer coefficient on the static characteristic curve

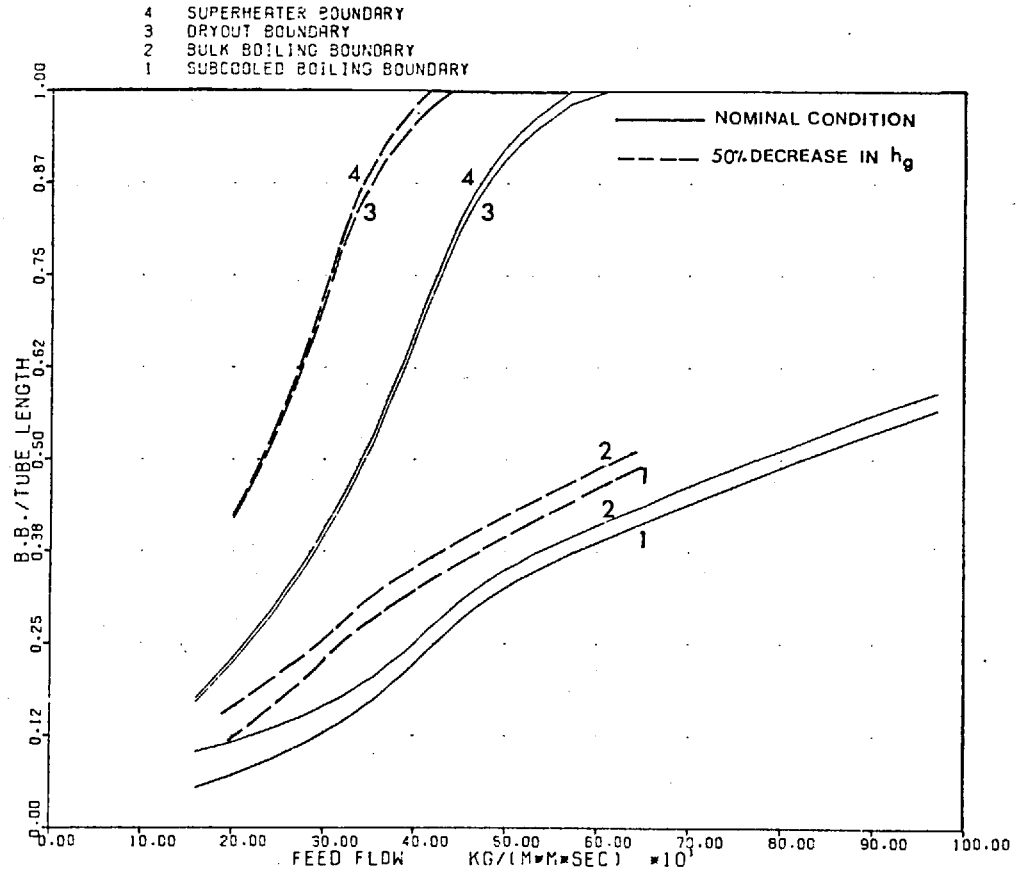


Figure 5.41: Effect of the primary side heat transfer coefficient on the movement of the boiling boundary versus mass flow

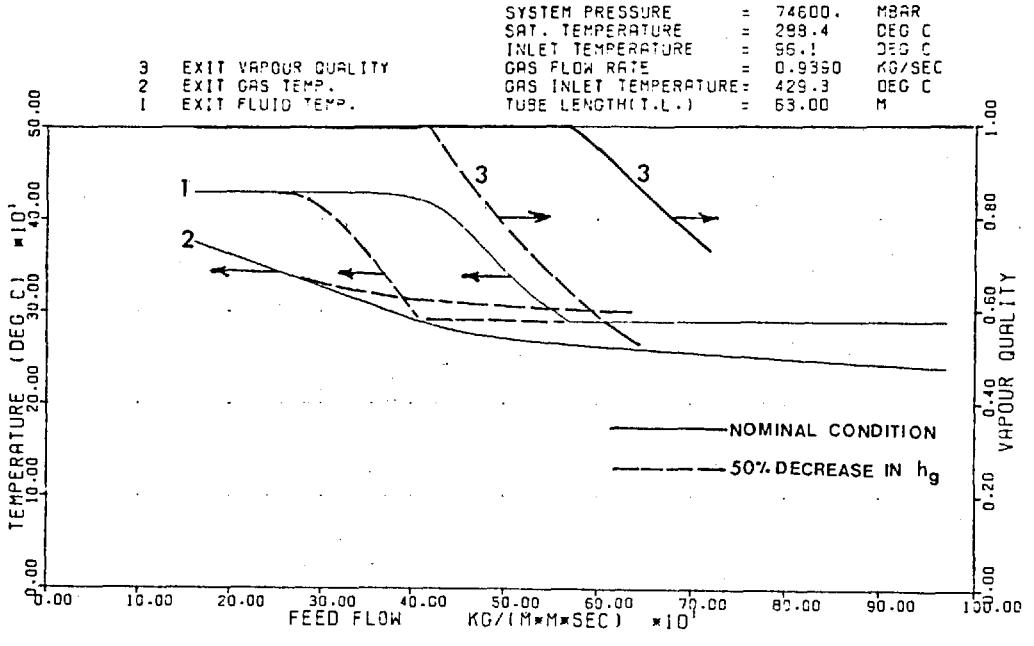


Figure 5.42: Effect of the primary side heat transfer coefficient on the variation of exit temperatures versus mass flow

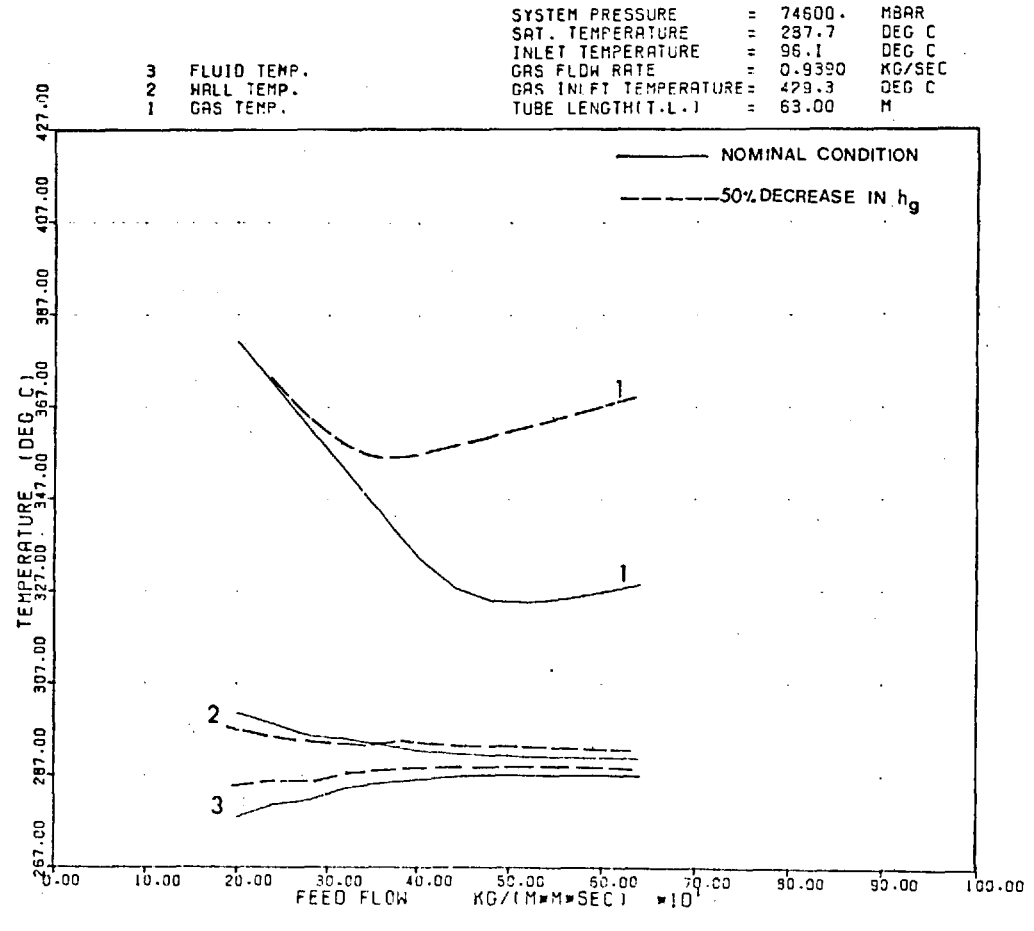


Figure 5.43: Effect of the primary side heat transfer coefficient on the variation of local temperatures versus mass flow

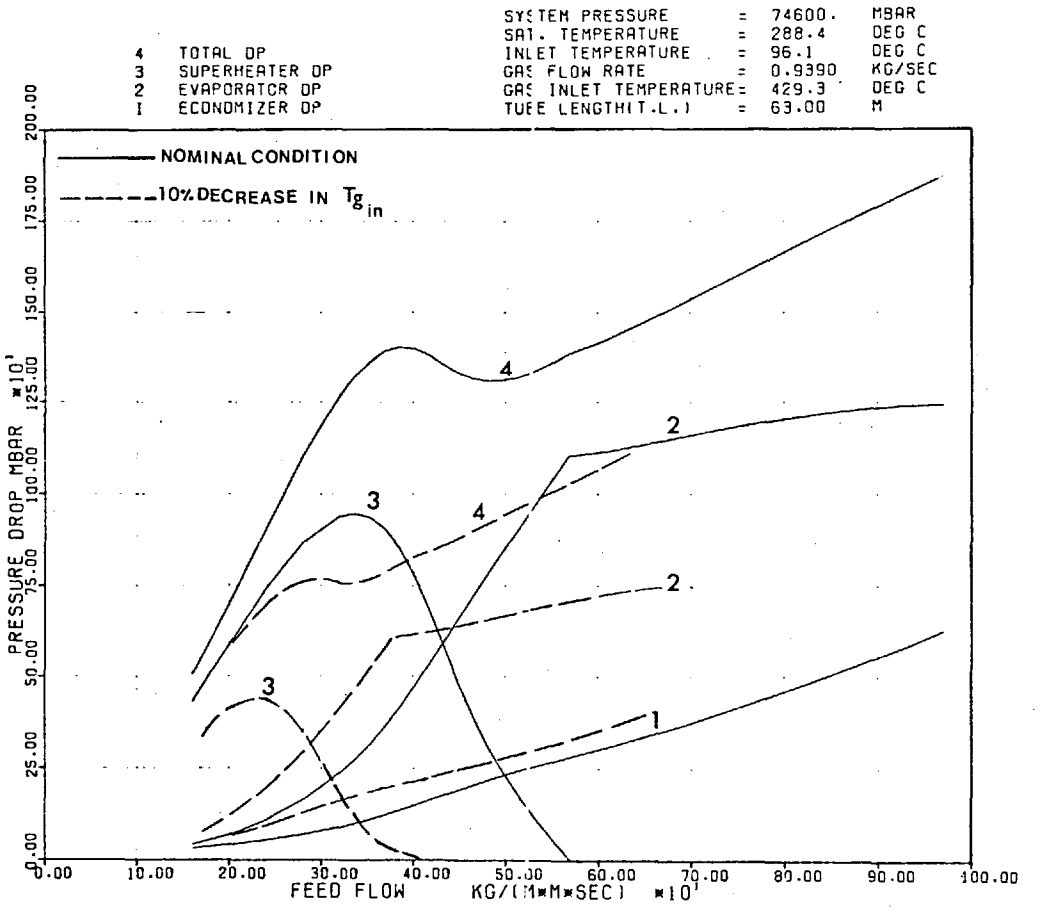


Figure 5.44: Effect of the inlet temperature of the primary flow on the static characteristic curve

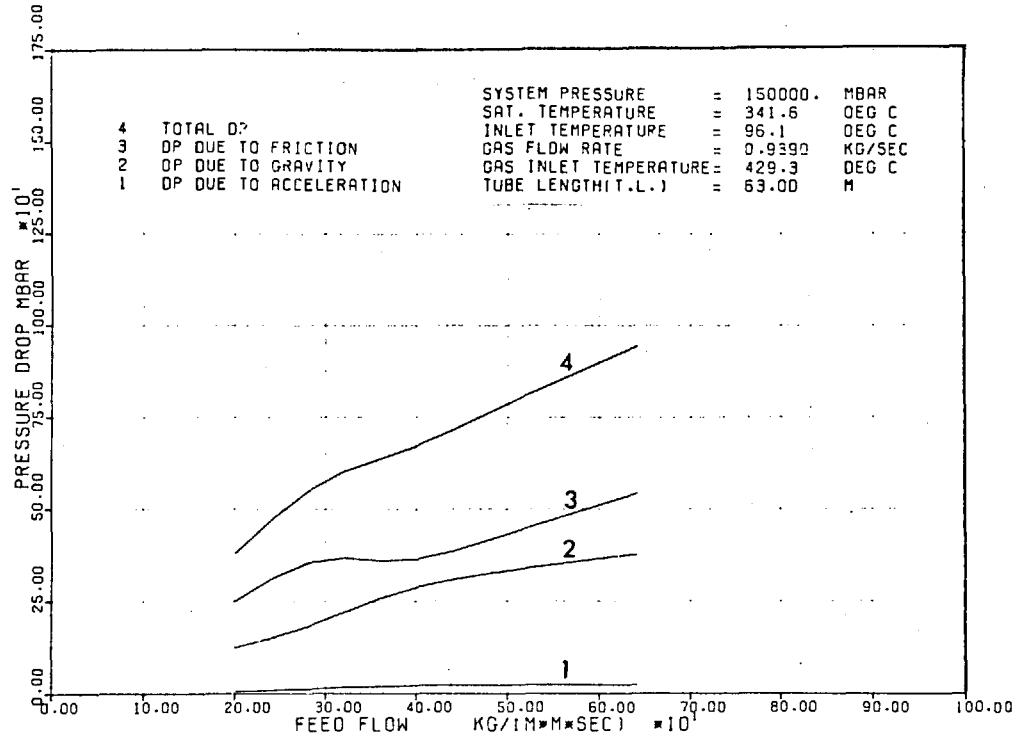


Figure 5.45: Different components of pressure drop versus mass velocity

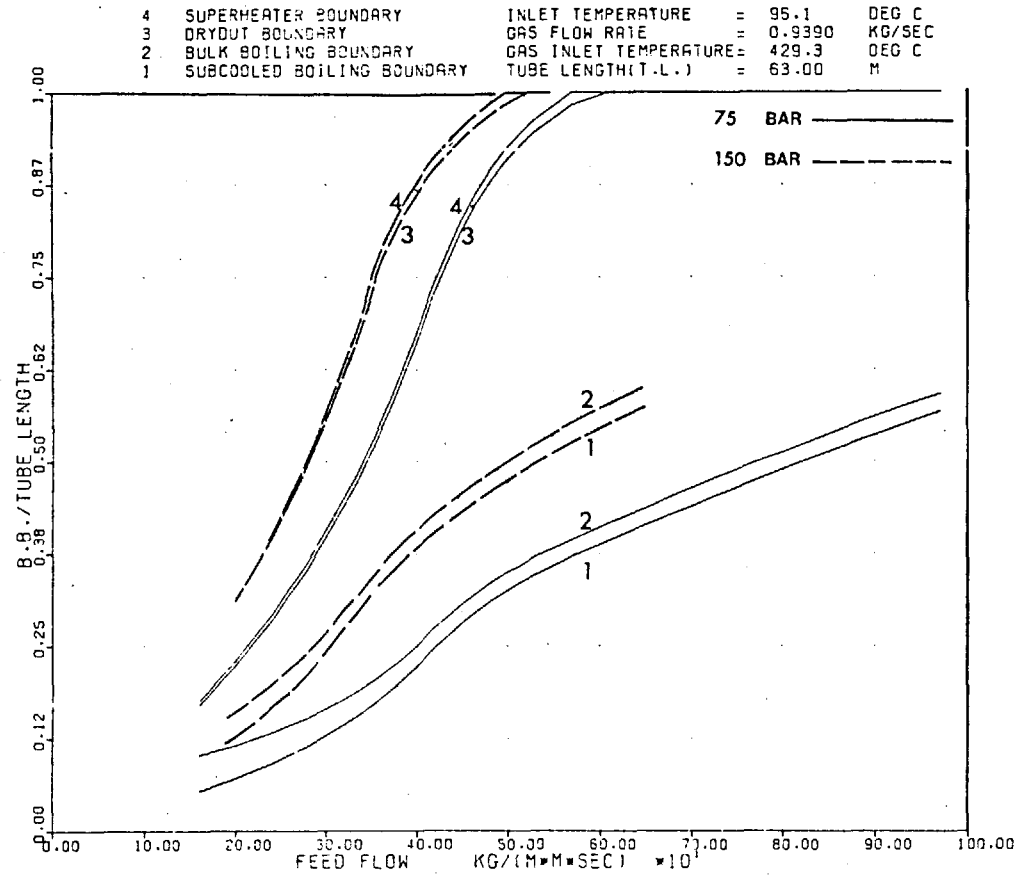


Figure 5.46: Movements of boiling boundaries with mass flow rate at different pressures

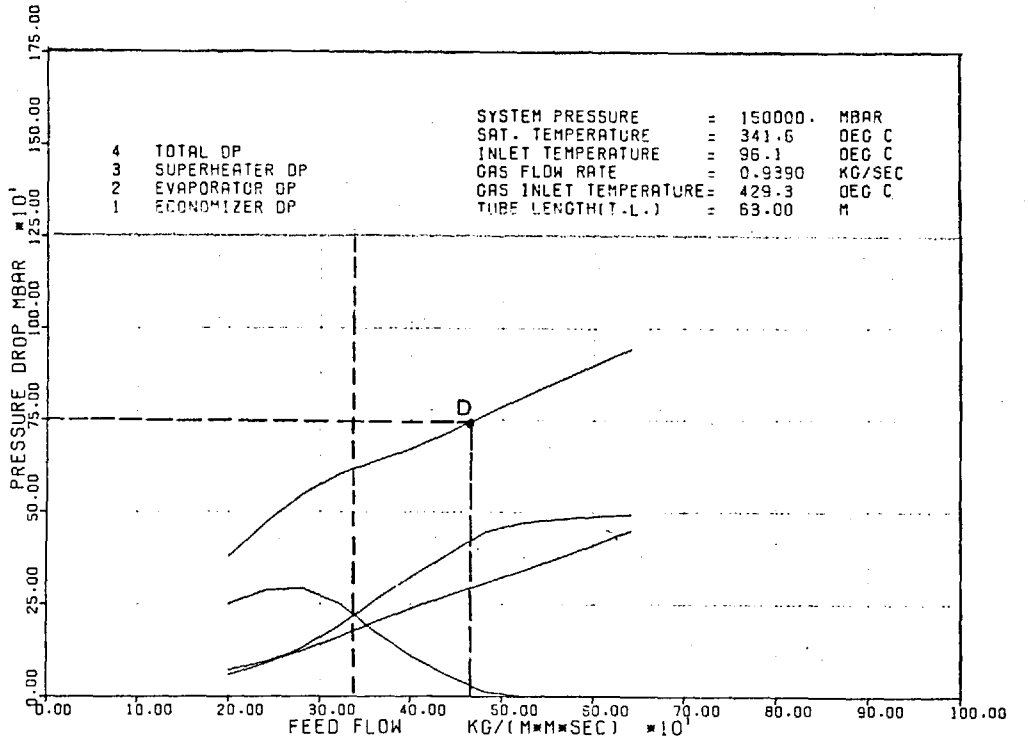


FIG.(5.47) - PRESSURE DROP OF DIFFERENT REGIONS VERSUS MASS VELOCITY

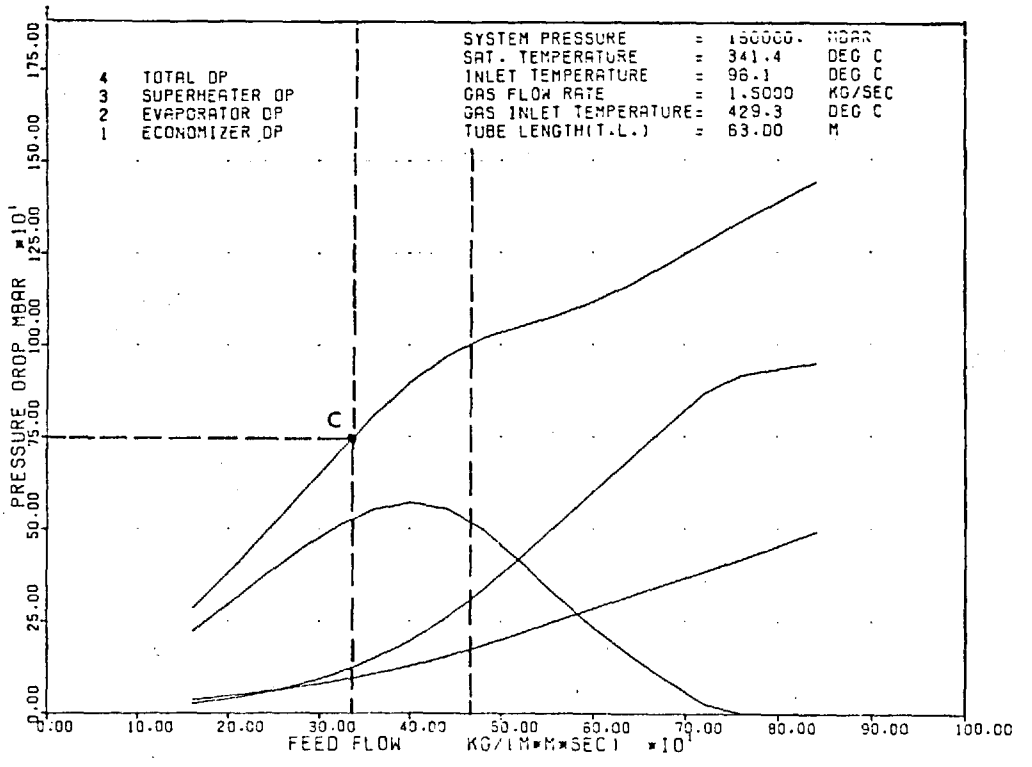


FIG.(5.48) - PRESSURE DROP OF DIFFERENT REGIONS VERSUS MASS VELOCITY

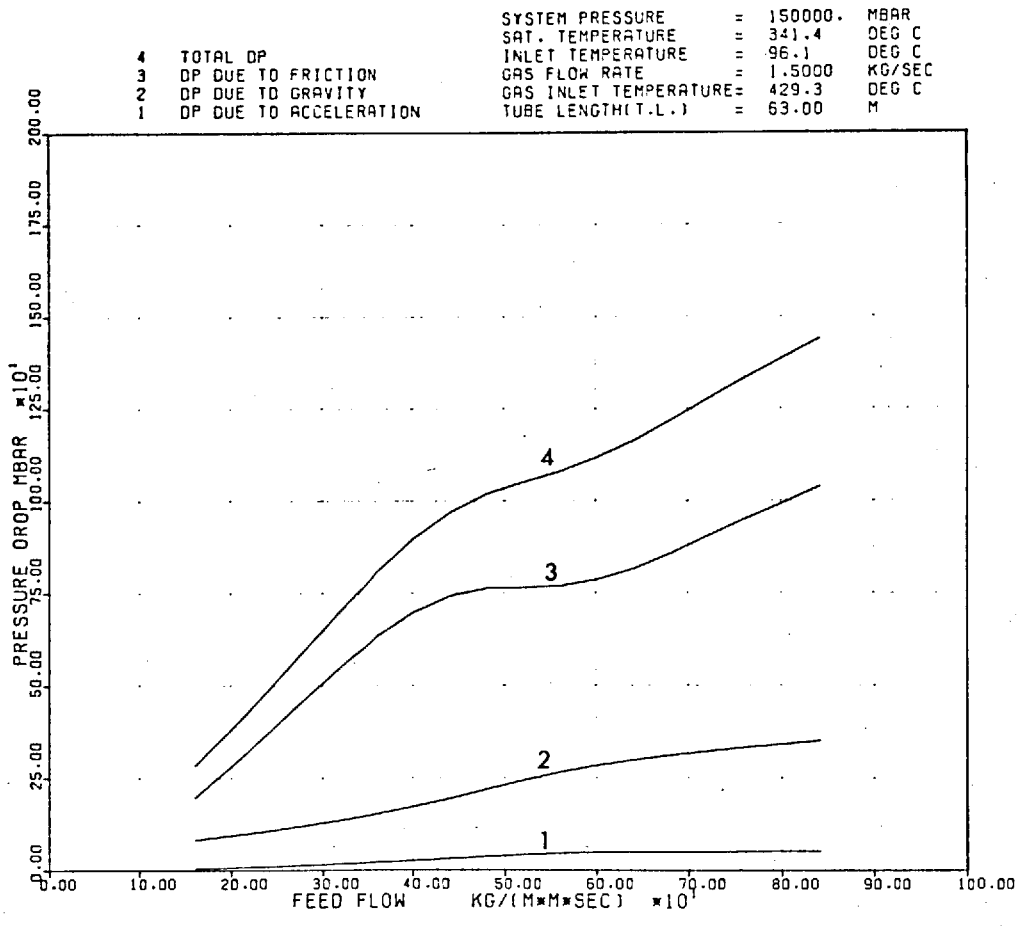


FIG.(5.49) - DIFFERENT COMPONENTS OF PRESSURE DROP VERSUS MASS VELOCITY

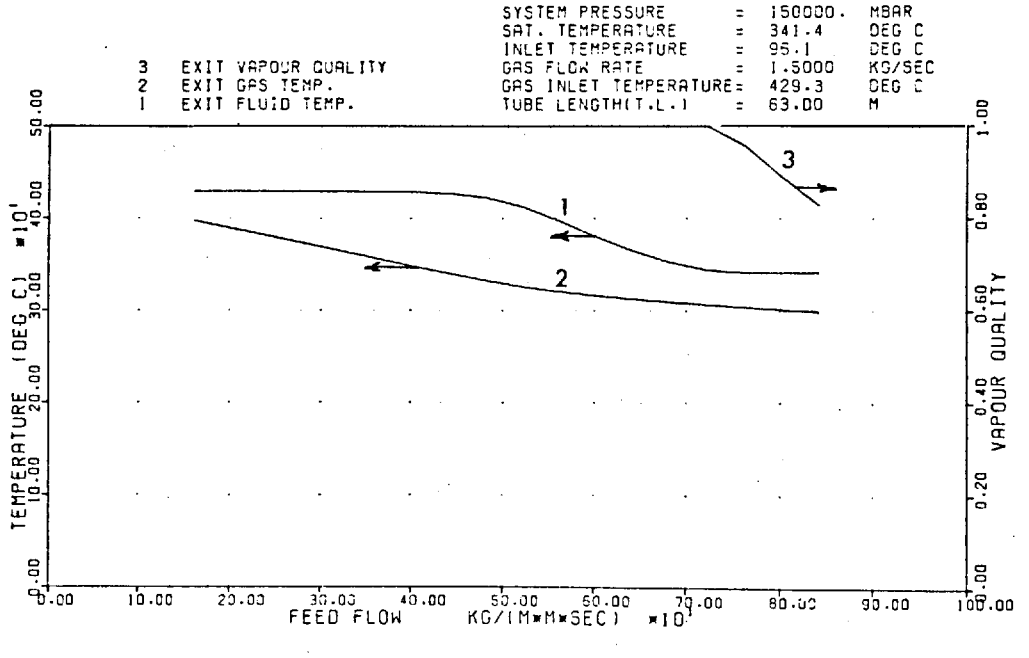


FIG.(5.50) - VARIATION OF EXIT TEMPERATURES AND VAPOUR QUALITY VS MASS VELOCITY

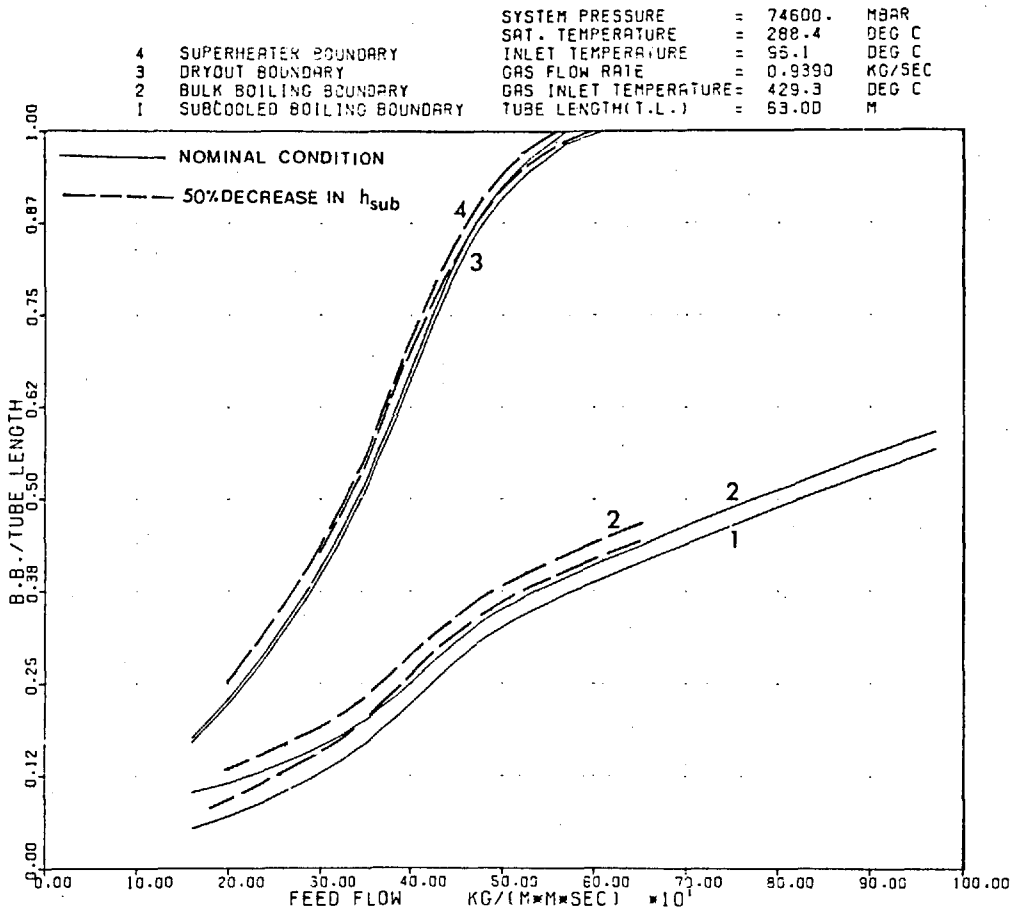


Figure 5.51: Effect of single-phase liquid heat transfer coefficient on the movements of boiling boundaries versus mass flow

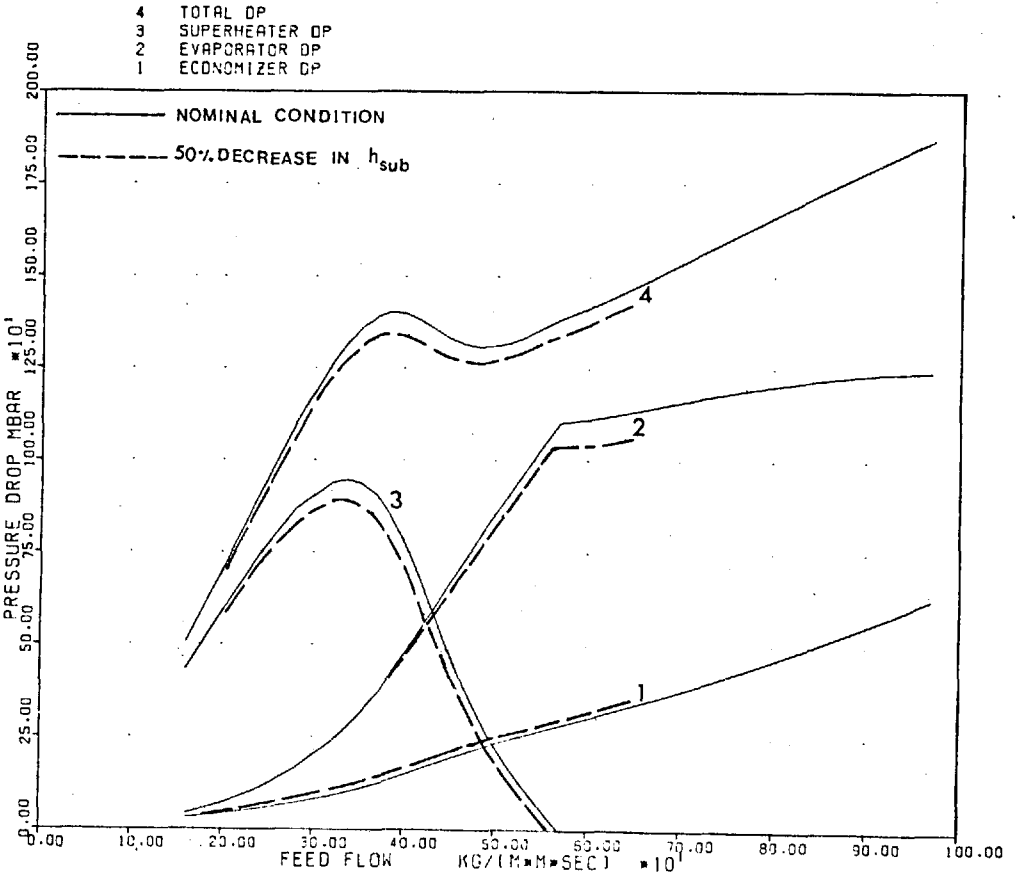


Figure 5.52: Effect of single-phase liquid heat transfer coefficient on the static characteristic curve

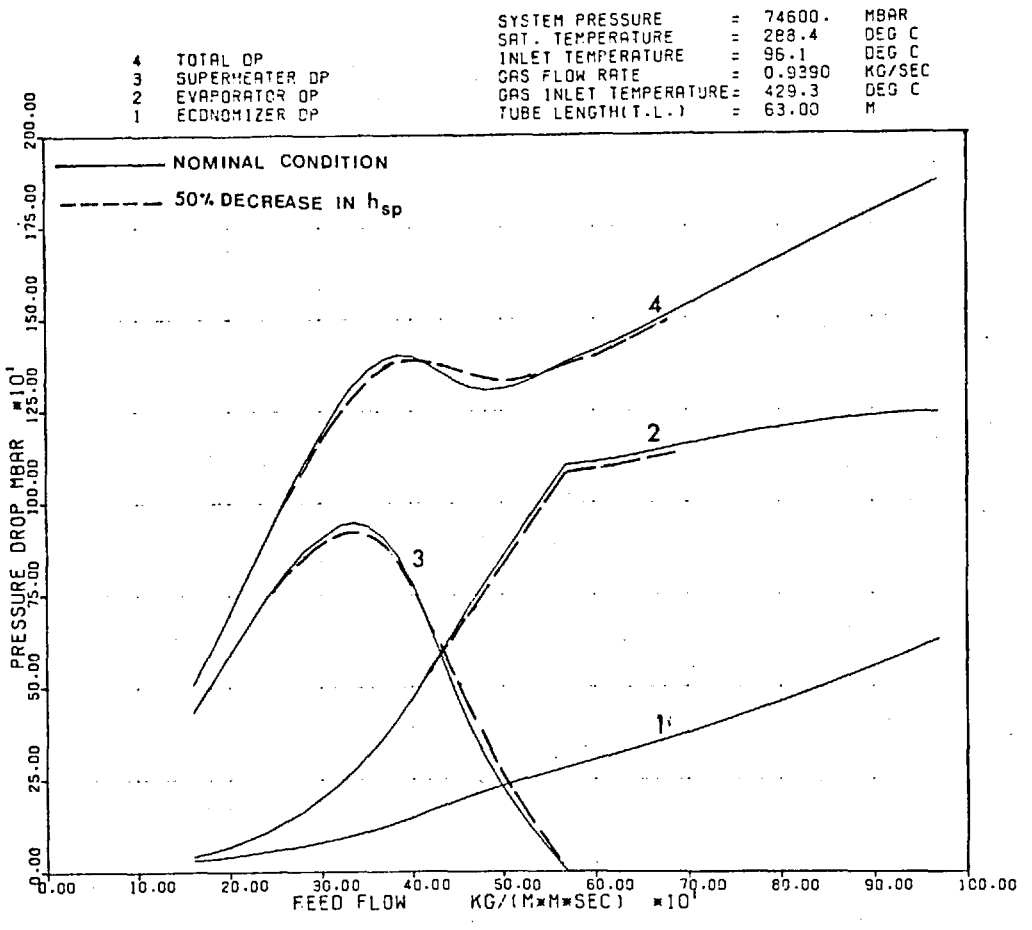


Figure 5.53: Effect of single-phase vapour heat transfer coefficient on the static characteristic curve

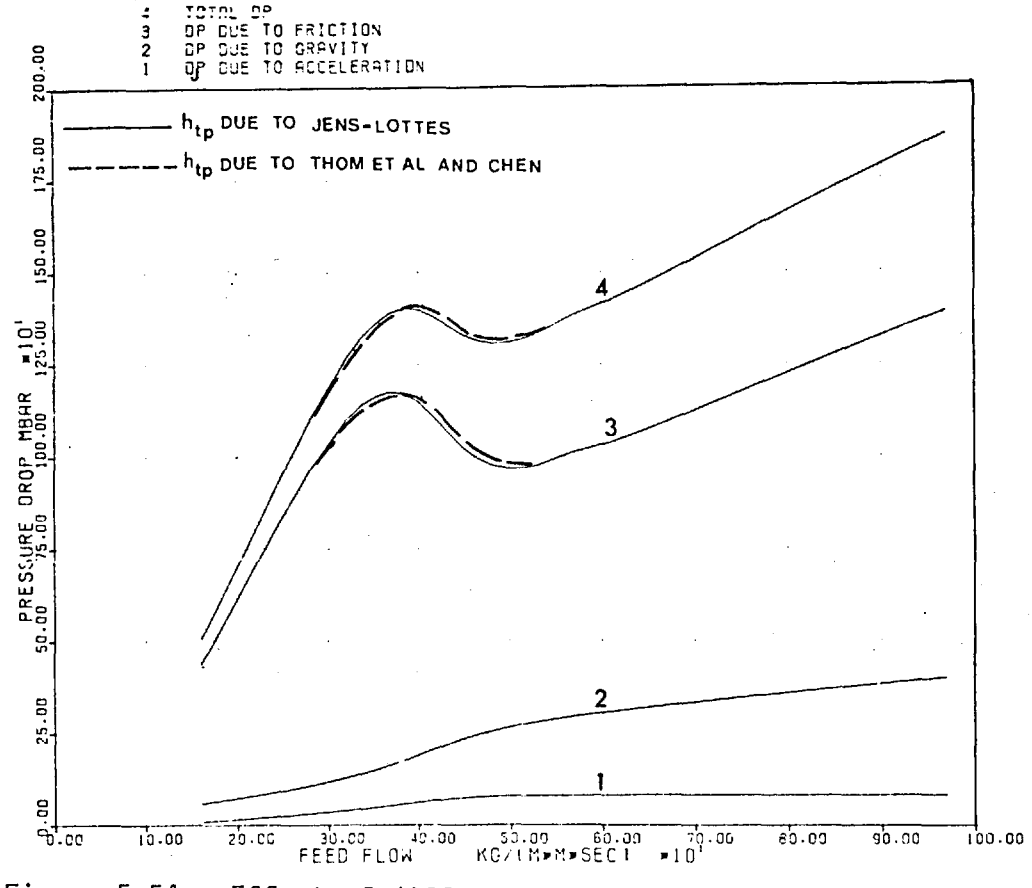


Figure 5.54: Effect of different two-phase heat transfer coefficient on the static characteristic curve

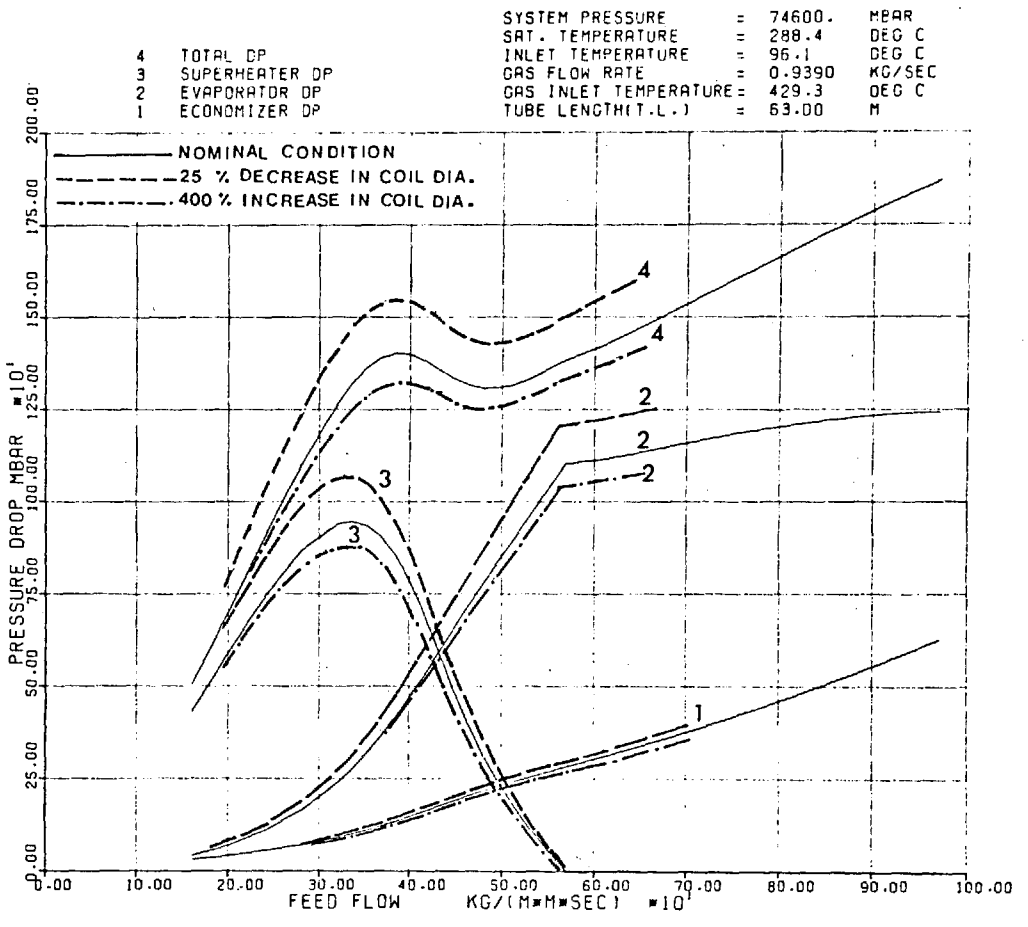


Figure 5.55: Effect of the coil diameter on the static characteristic curve

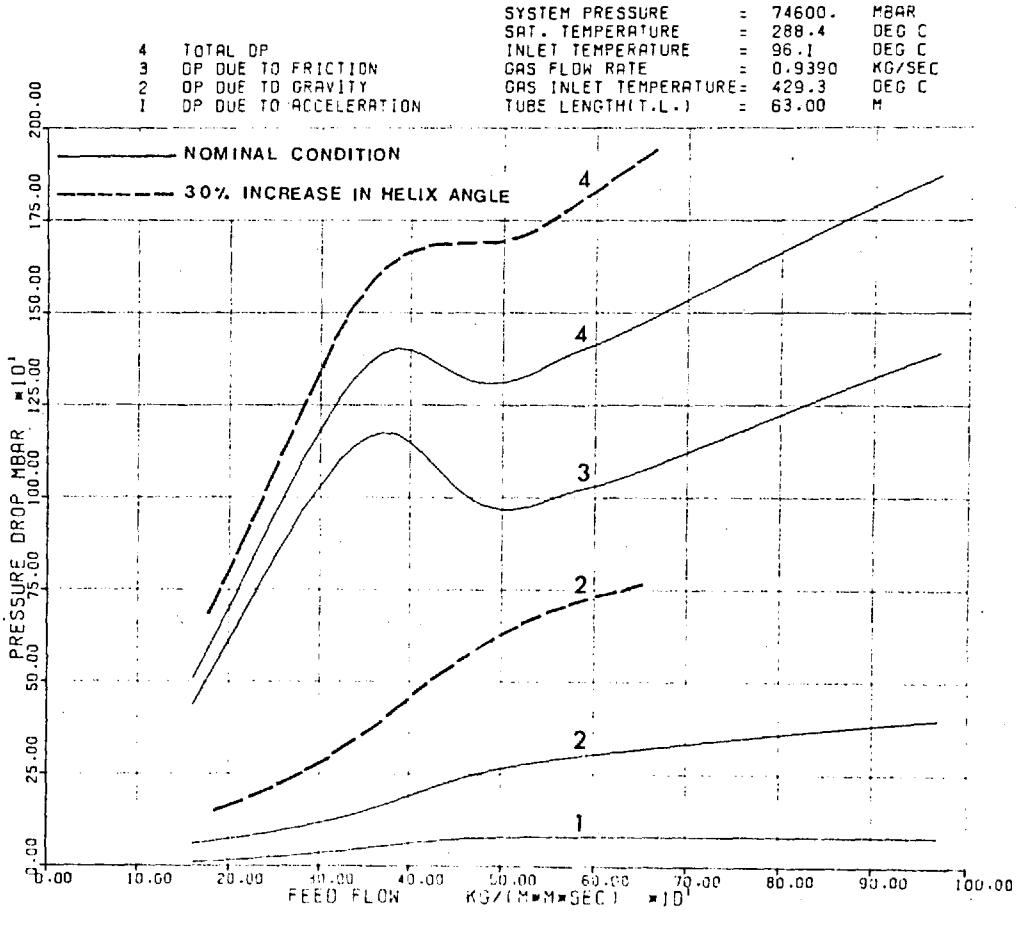


Figure 5.56: Effect of the helix angle on the static characteristic curve

CHAPTER 6

DYNAMIC SIMULATION RESULTS

6.1 INTRODUCTION

In Chapters 3 and 4, the mathematical model of a helically-coiled tube once-through boiler was derived and computerised as a first step in analysing the dynamics of the system. Once such a model is obtained, several methods can be applied for the analysis of the system performance.

Many design criteria are based on the response of the system to changes in initial conditions. These changes are most commonly simulated with simple functions of time, e.g. step function, etc. What type of changes to use for analysing boiler characteristics may be determined by the objective in mind and the form of the input that the boiler will be subjected to most frequently under operation. For instance, if the initial conditions of the boiler are gradually changing with time, e.g. start-up, then a ramp input may be a good approximation of the initial changes.

This chapter is concerned with three kinds of analysis, namely, transient behaviour, frequency response analysis and the examination of self-sustained oscillations when the system is dynamically unstable.

The end conditions of the boiler and the tube wall temperatures are of main interest for the design of the control system, protection of the boiler and reactor metal from thermal cycling, and of particular interest is the dynamic instability. These are investigated using frequency response analysis as a qualitative tool in the design of a once-through boiler. However, the prediction of dynamic instability for a particular operating condition is performed in the investigation of self-sustained

oscillations.

The effect of heat flux-flow coupling nature of a counterflow gas fired boiler is also investigated using the types of input functions mentioned above.

The response of different parameters to a prescribed input function are presented as a function of time. The fluctuations of different parameters are calculated as a ratio of the initial conditions which are referred to as steady-state (SS) solution, and are given in each graph presenting the time history of a parameter.

The dynamic analyses are performed at operational conditions similar to those of an actual industrial gas fired helically-coiled tube test rig for which data have been made available. The computer program can be used for other operating conditions and end constraints with proper modifications of the boundary conditions. However, due to limitations on the available computer time, and the many possible ranges of operational conditions, a number of relevant case studies have been made.

6.2 TRANSIENT RESPONSE ANALYSIS

Analyses are performed with changes of the initial inlet mass velocity of the secondary flow (water). The purpose of this investigation is to determine the transient characteristics of system variables, in particular, the end conditions of the boiler, the movement of the boiling boundaries, the thermal conditions of the tube metal and the distribution of the pressure drop along the boiler.

The inlet mass velocity is increased or decreased stepwise from the initial value by 30% or 50% during a period of 3 to 6 seconds.

6.2.1 Response of Exit Mass Flow and Boiling Boundaries

The response of exit mass velocity to stepwise increase and decrease of the inlet mass velocity is illustrated in Figure 6.1. The response curves show an initial inflexion superimposed upon an exponential response. The initial inflexion is due to the effect of heat flux changes along the boiler as discussed later, while the increasing (or decreasing) part arises directly from the increase (or decrease) of the inlet mass velocity. It is seen that the settling time (the time required for the response to reach to 95% of the final steady-state value, Ogata (1970)) is long compared, for example, with residence time of the secondary flow in the tube.

Boiling boundary movements as a ratio of the tube length are plotted in Figure 6.2. As inlet mass increases (or decreases) stepwise, the length of the liquid phase region (economiser) and the two-phase region (evaporator) increases, and the superheater decreases. The movements of the subcooled and bulk boiling boundaries tend to be slow and gradual (Figure 6.2). These movements arise from the rise of enthalpy in the economiser and changes in the heat flux at the boiling

boundaries. The enthalpy gradient along the economiser is affected by changes of mass velocity and heat flux profile. The heat flux variation, which is coupled to the secondary flow, results partly from changes of the secondary side heat transfer coefficient (the secondary side heat transfer coefficient in the liquid phase region dominates that of the primary side which is gas), and partly from the changes in the temperature difference between the primary and secondary flow (Figure 6.3). As a result of the above consideration, when inlet mass flow increases, the movement of the subcooled boiling boundary (Figure 6.2a) will be reduced by a factor of 5 compared with that in a constant heat flux system. This can be understood with a simple energy balance coupled with a 0.8 power law between the heat transfer coefficient and the mass flow rate. The movement of the boiling boundary will be suppressed even further by the resulting changes of heat flux due to the temperature difference between the primary and the secondary flows (Figure 6.3).

The movements of the dryout and superheater boundaries in Figure 6.2 tend to be relatively fast compared with the subcooled boiling boundary and the case of a constant heat flux system. Changes of the inlet mass flow do not directly affect the two-phase heat transfer coefficient assuming a Jens-Lottes type correlation in the evaporator. Therefore, the heat flux in the evaporator would not be affected by the changes of secondary flow if there was no coupling between the heat flux and the secondary flow, e.g. a constant heat flux system. Nevertheless, the heat flux in the two-phase region reduces due to a decrease in the level of the primary temperature as shown in Figures 6.3a and 6.4a. Therefore, the superheater boundary moves outward not only due to the effects of increasing mass and subcooled boundaries, but also because of decreasing heat flux along the evaporator region.

Responses of the primary temperatures along the evaporator do not occur instantaneously, and they are delayed relative to the inlet mass velocity as seen in Figure 6.4. Therefore, during the delayed period, the heat flux along the evaporator (which is still not affected by the primary temperature) can produce a high rate of vapour generation. This will result in a large gradient for the exit mass velocity with time (Figure 6.1a). As the heat flux in the evaporator eventually decreases with the primary temperature, the vapour generation rate will be suppressed, and hence, the slope of the exit mass velocity as on Figure 6.1a. The slope can be seen to reduce; in some cases, reaching zero after which it increases gradually.

6.2.2 Heat Flux Variations at Boiling Boundaries

The potential of the heat flux-flow coupling, so far, was shown in the previous section and no effects of heat flux variations were considered with time at boiling boundaries.

Variations of the heat flux and the heat transfer coefficient at a fixed position downstream of the initial steady-state boiling boundaries are plotted with time in Figures 6.5 and 6.6. Figure 6.5 reveals that the heat flux at the fixed position (the corresponding temperature profile is identified by the symbol Y in Figure 6.3b) downstream of the initial bulk boiling boundary reduces and drops down, then increases to a maximum beyond which it decreases to the settling value. Almost the reverse behaviour occurs at the superheater boundary (Figure 6.6). These phenomena can be explained in terms of changes of the heat transfer mechanism and the stored energy in the tube metal as follows:

As the subcooled and bulk boiling boundaries move outward

(Figure 6.2a), the heat transfer mechanism at the fixed position (Y) (Figure 6.5) changes from the bulk boiling to the subcooled boiling and finally to the forced convective mechanism. During the transient interval A-B (Figures 6.3b and 6.5), the tube wall temperature is controlled by the two-phase heat transfer mechanism (Jens-Lottes correlation is used in the analysis). It remains nearly constant in time, i.e. negligible stored energy in the tube, and slightly higher than saturation temperature as shown in Figure 6.3b. The heat flux, therefore, decreases due to the decrease of the heat transfer coefficient (Figure 6.5) and it drops to a minimum value when the subcooled boiling boundary is just passing the fixed position (Y). A high reduction in the heat transfer coefficient is accompanied by a slight rise in the tube wall temperature (Figure 6.3b), which increases to a maximum. Consequently, the heat flux increases to a maximum but is delayed relative to the maximum of the wall temperature due to the tube wall inertia (the time constant, $(\rho\ C_p\ v/h\ A)$, of the tube wall increases by a factor of 10 when two-phase heat transfer changes to forced convective mechanism). Finally, as the subcooled boiling boundary eventually moves away from the position (Y), the tube wall temperature and heat flux decreases to the new steady values (Figure 6.5).

Similar arguments can be made for a fixed position downstream of the initial position of the superheater boundary. In this case, the mechanism of heat transfer changes from forced convective vapour phase to two-phase boiling when the boundary moves outward and passes a fixed position. The tube wall temperature reduces and drops to a value slightly greater than the saturation temperature (Figure 6.4b). It, therefore, results in a high heat flux due to high stored energy in the wall. Therefore, the two-phase heat transfer coefficient which depends

on heat flux increases (Figure 6.6). Hence, the wall temperature reduces until the superheater boundary moves further downstream of the fixed position and the inertia effects die down.

Consequently, at the boiling boundaries, the discontinuous behaviour of heat fluxes, which result from changes of the heat transfer mechanism and the tube wall temperature, both counteract against the variation of heat flux profile along the tube arising from the increasing mass flow rate.

6.2.3 Response of Outlet Temperature

The outlet temperatures of the primary and the secondary flows are plotted in Figure 6.7 in response to different stepwise changes of inlet mass velocity. When the inlet mass flow increases (or decreases), the heat extraction from the primary flow increases (or decreases). Therefore, the temperature level of the primary flow (Figures 6.3a and 6.4a), and hence the outlet temperature of gas decreases (or increases) as shown in Figure 6.7.

The outlet vapour temperature does not change for any disturbance of Figure 6.7. This is due to the long superheater (Figure 6.2), in which the temperature increases exponentially along the tube (Figure 5.8). This is consistent with the experimental results of a helically-coiled tube steam generator as reported by Kozeki et al (1970) and also with the data of a sodium heated once-through rig given by Waszink et al (1973). When the length of the superheater is short (Figure 6.8a), the outlet temperature of the secondary flow decreases (Figure 6.8c) as the inlet mass velocity increases (Figure 6.8b). This can occur most likely when the new operating point falls near or on the negative slope of the static characteristics of the system (Figures 5.28

to 5.31).

6.2.4 Response of Pressure Drop

The response of pressure drop distribution to step increase in inlet mass velocity is displayed in Figures 6.9 to 6.11 for different operational conditions. The total pressure drop increases rapidly and then slowly. At the latter stages of the response, it decreases gradually to a steady value. Figures 6.9a and 6.10a show that the variation of the total pressure drop is controlled predominantly by the frictional component, the accelerational and gravitational pressure drops being small in comparison with the frictional pressure drop. The subcooled liquid region constitutes most of the gravitational component (Figure 6.11b), while the accelerational pressure drop mostly occurs due to the density changes in the two-phase region (Figure 6.11a). The contributions of different regions along the boiler to the total pressure drop are displayed in Figures 6.9b and 6.10b.

When the inlet mass flow increases, the pressure drop in the economiser rises slightly because of the gravity effect arising from the movement of the subcooled boiling boundary (Figures 6.9b and 6.10b). The pressure drop in the evaporator and superheater changes mostly due to variations of friction pressure drop which is a function of the changes of exit mass velocity and the movement of the superheater boundary. As the inlet mass flow increases, the superheater boundary moves towards the outlet, and the mass velocity, e.g. at the end of the evaporator, increases. Therefore, the pressure drop in the evaporator increases monotonically (Figures 6.9b and 6.10b). In the superheater, there are two competing effects on the pressure drop:

i) outward movement of the superheater boundary reduces the length of the superheater and hence decreases the superheater pressure drop; and

ii) the increase of exit mass velocity gives rise to pressure drop.

Consequently, when inlet mass increases, the superheater pressure drop increases instantly due to the increase of the exit mass. When the effect of decreasing the length of the superheater eventually becomes dominant, the pressure drop decreases gradually as shown in Figures 6.9b and 6.10b.

It appears that the response of the total pressure drop to the increase of inlet mass flow arises predominantly from the evaporator and superheater, and it increases rapidly at the early stage of the transient time, and then it decreases gradually to the settling value.

It is appropriate to notice that when inlet mass flow increases, there are conditions for which the settling value of the pressure drop is lower than the initial value as shown in Figure 6.10. This phenomenon has been observed experimentally by Akgawa et al (1972) for a helically-coiled tube steam generating rig. Such a phenomenon can be related to the static characteristics of the system as discussed in section 5.3.1 (Figures 5.28 and 5.30). This condition most likely occurs when the superheater is short and the outlet vapour superheating is low and sensitive to the mass flow variations (Figures 5.29 and 5.31).

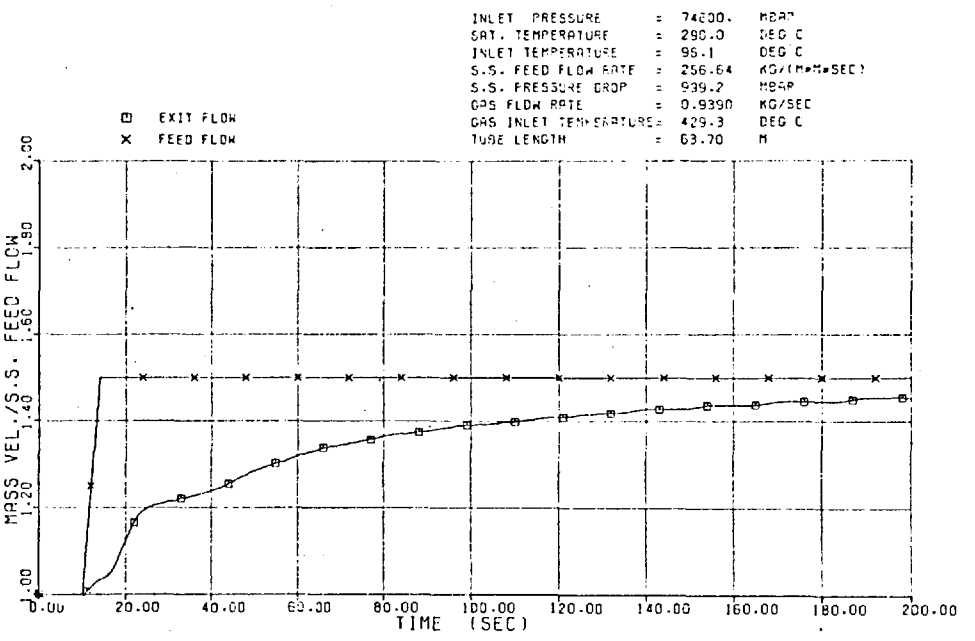


FIG.(6.1a) RESPONSE OF EXIT MASS VELOCITY TO STEP INCREASE IN FEED FLOW

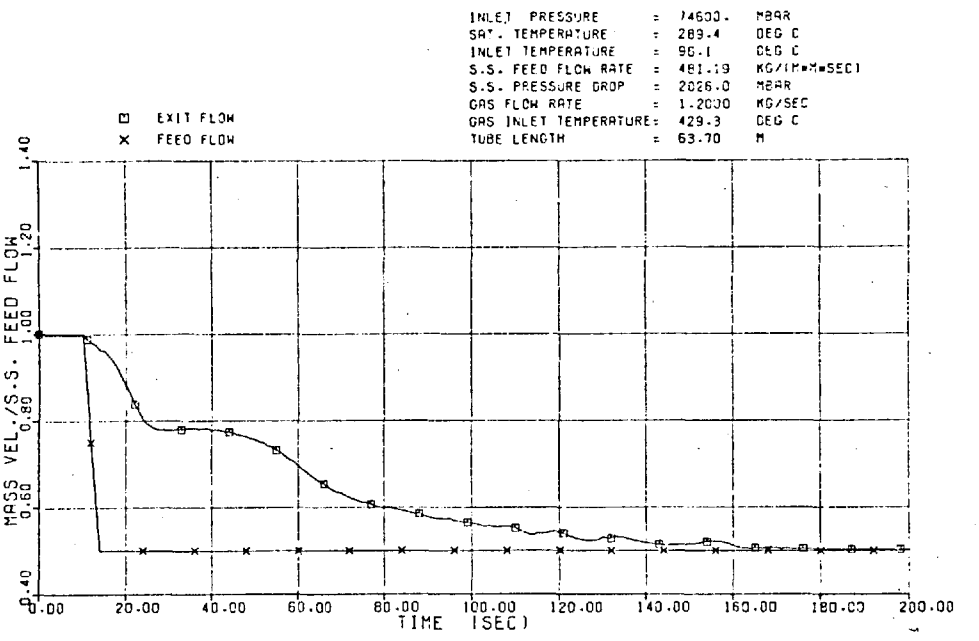


FIG.(6.1b) RESPONSE OF EXIT MASS VELOCITY TO STEP DECREASE IN FEED FLOW

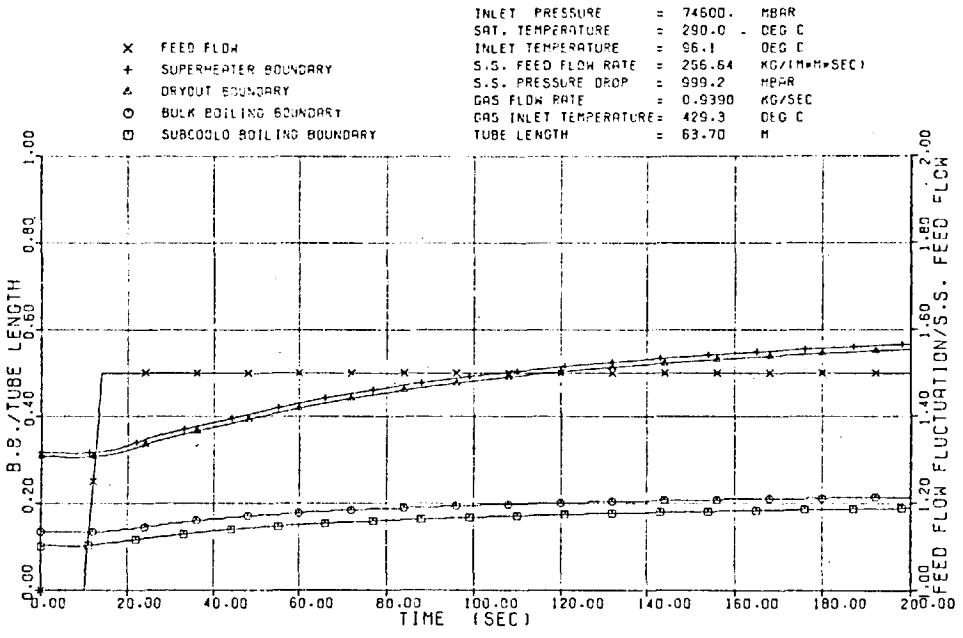


FIG.(6.2a) BOILING BOUNDARIES RESPONSE TO STEP INCREASE IN FEED FLOW

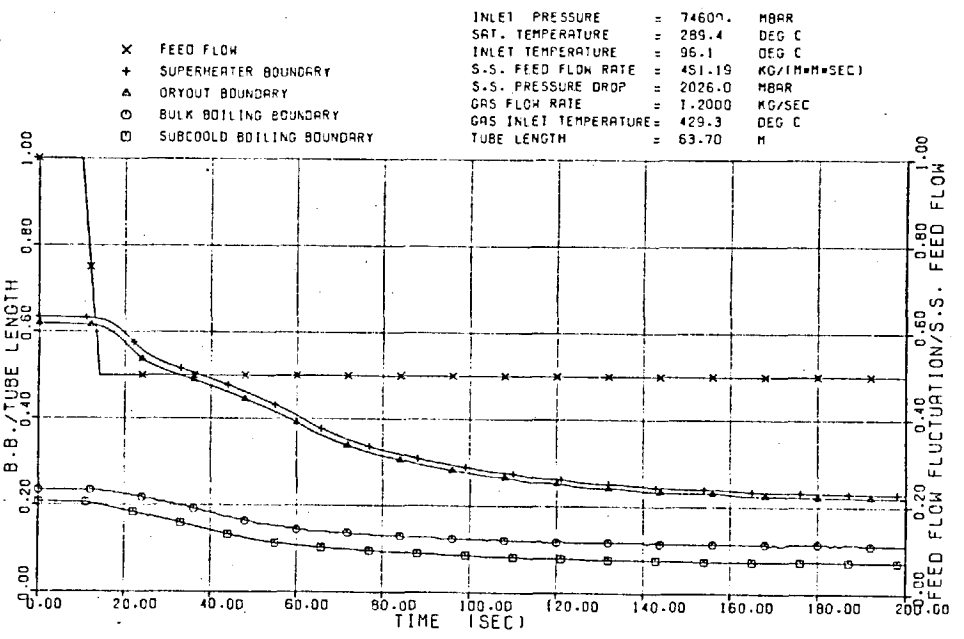


FIG.(6.2b) BOILING BOUNDARIES RESPONSE TO STEP DECREASE IN FEED FLOW

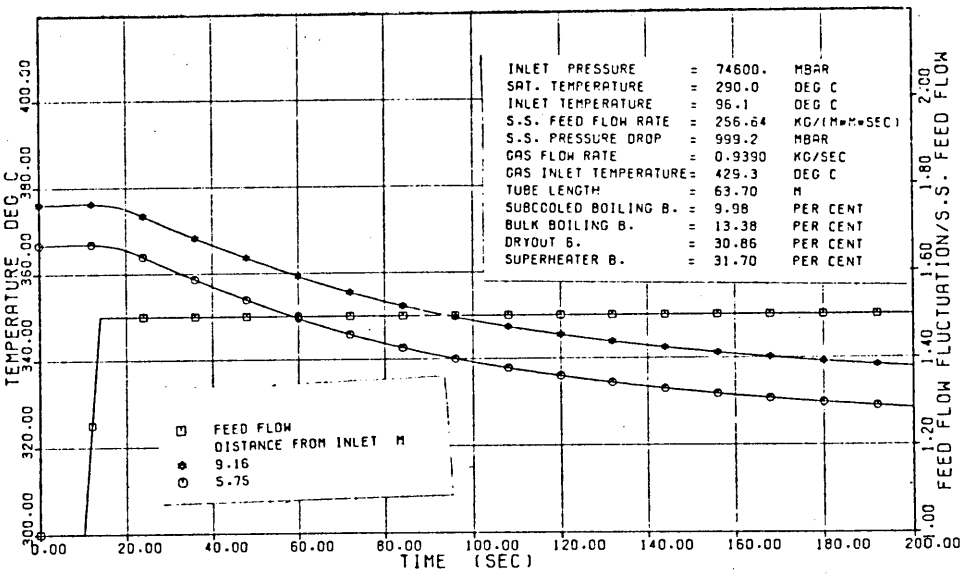


FIG.(6.3a) PRIMARY FLUID TEMPERATURES AT FIXED POSITIONS NEAR SUBCOOLED AND BULK BOILING BOUNDARIES

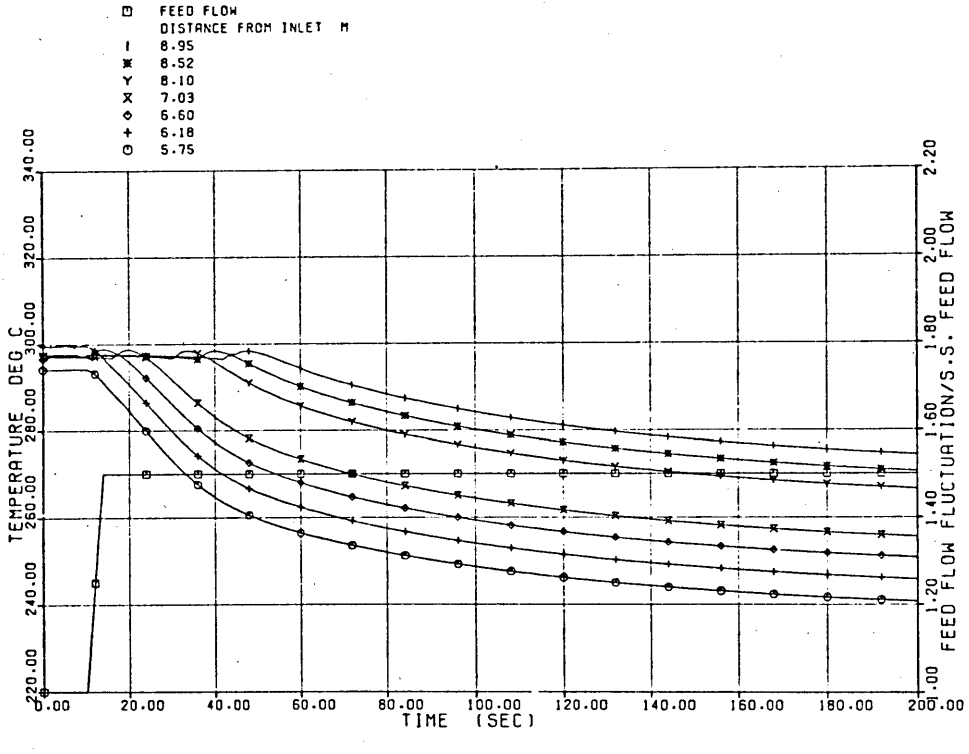


FIG.(6.3b) TUBE WALL TEMPERATURES AT FIXED POSITIONS NEAR SUBCOOLED AND BULK BOILING BOUNDARIES

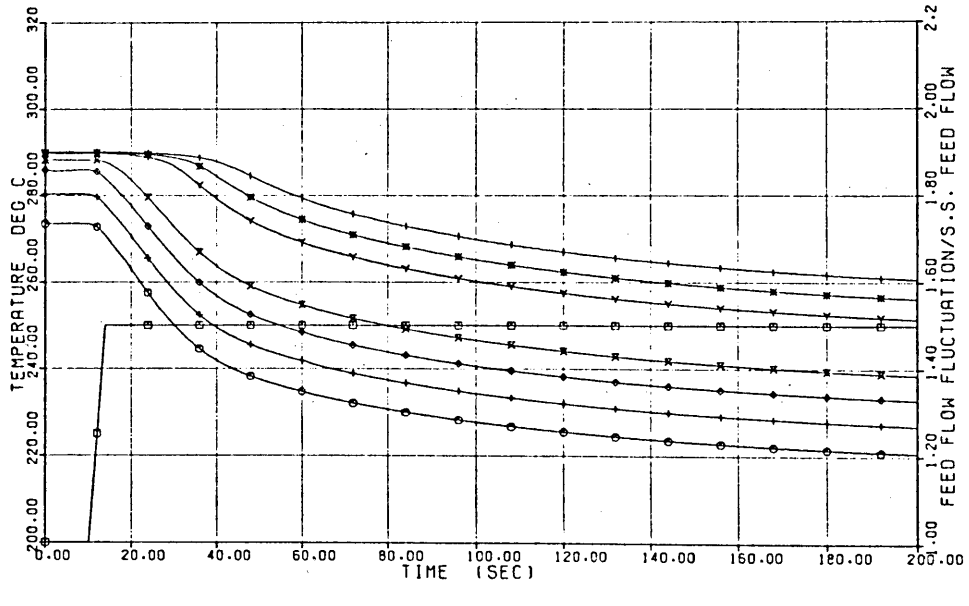


FIG.(6.3c) FLUID TEMPERATURES AT FIXED POSITIONS NEAR SUBCOOLED AND BULK BOILING BOUNDARIES

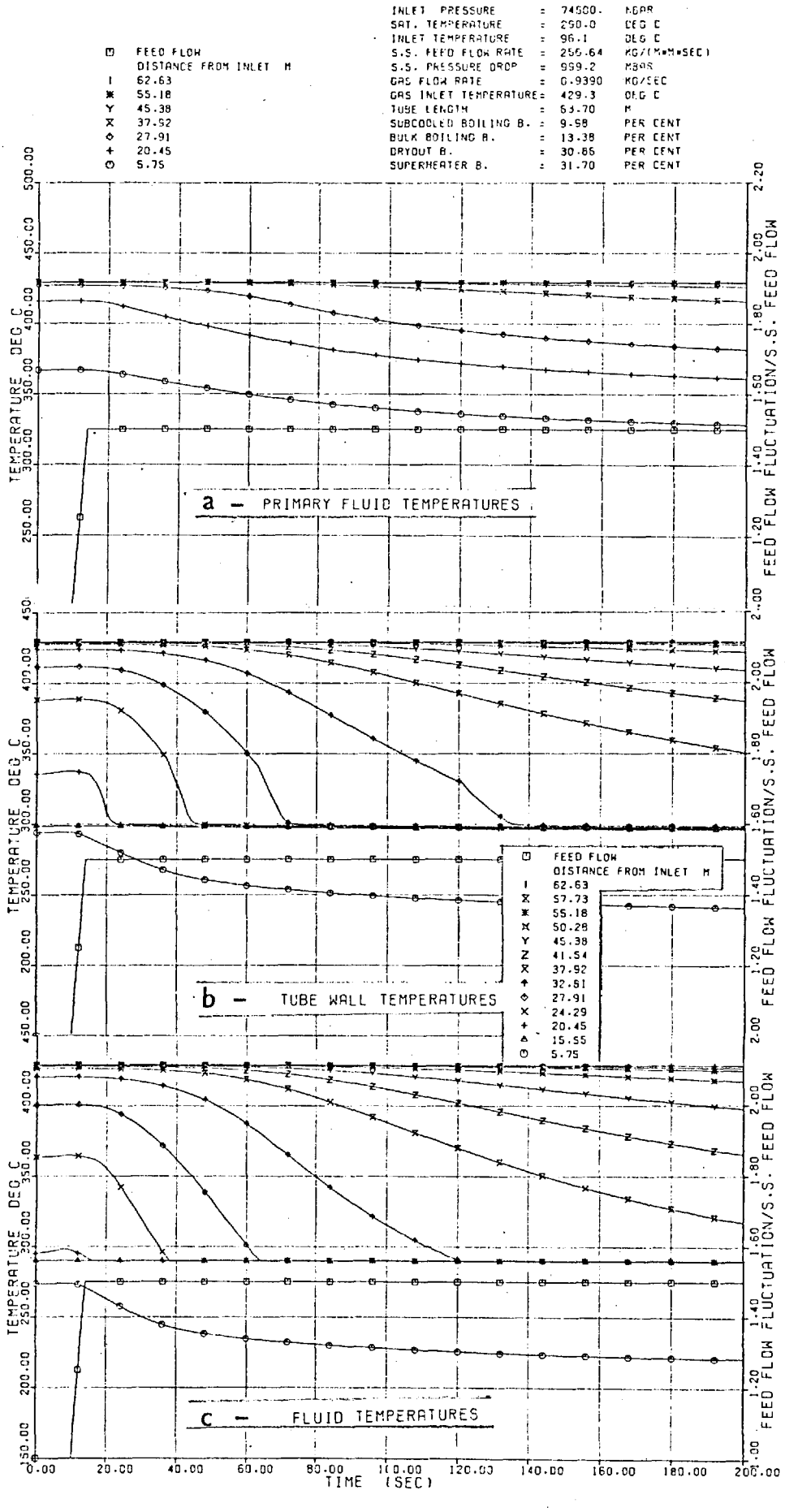


Figure 6.4: Variation of temperatures at fixed positions along the tube

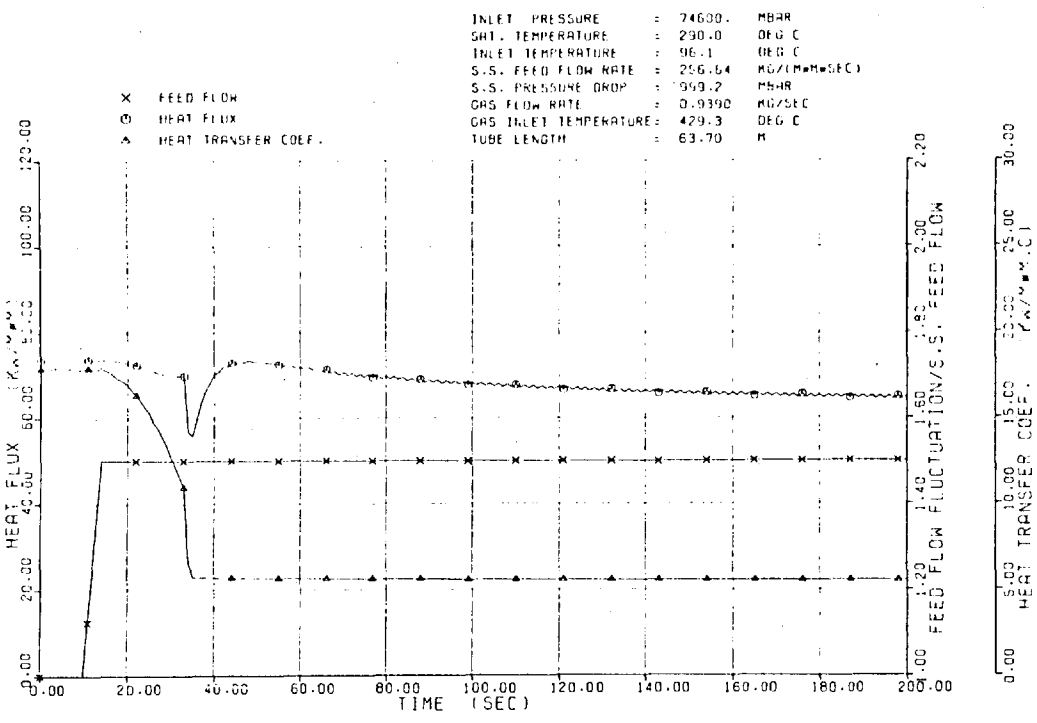


FIG.(6.5) VARIATION OF HEAT FLUX AND HEAT TRANSFER COEFFICIENT AT BULK BOILING BOUNDARY

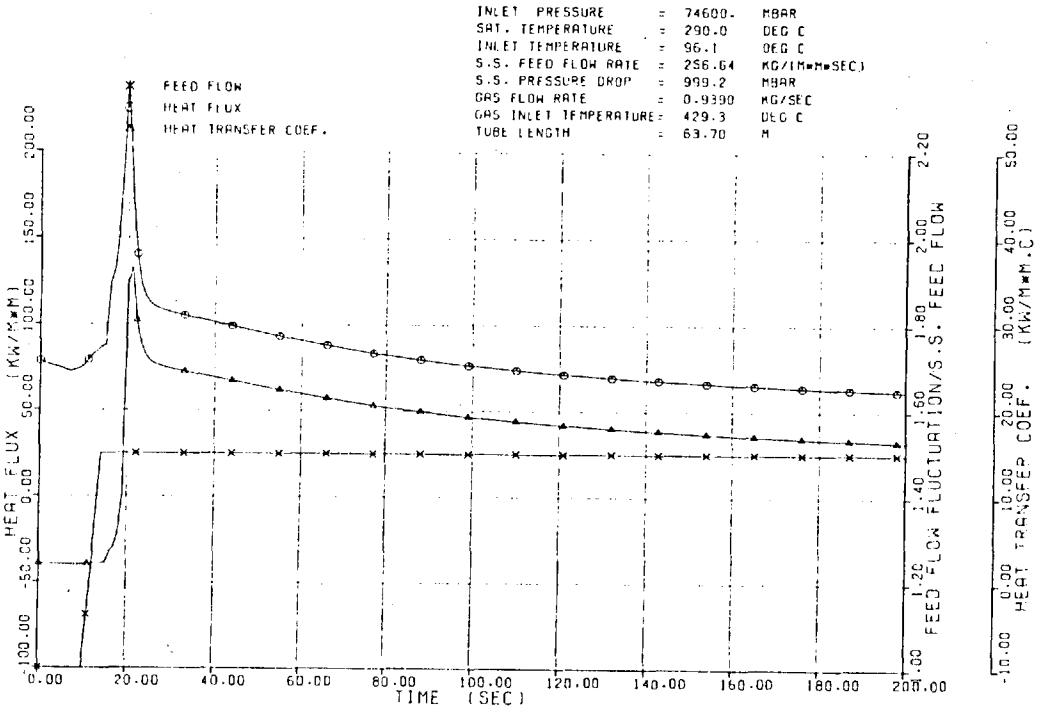


FIG.(6.6) VARIATION OF HEAT FLUX AND HEAT TRANSFER COEFFICIENT AT SUPERHEATER BOUNDARY

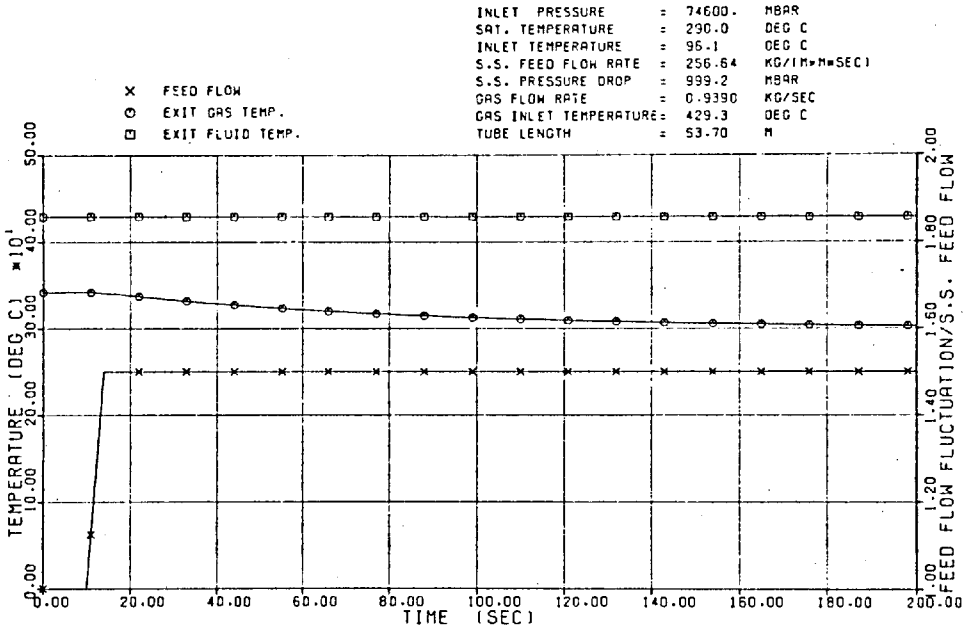


FIG.(6.7a) RESPONSE OF EXIT TEMPERATURES TO STEP INCREASE IN FEED FLOW

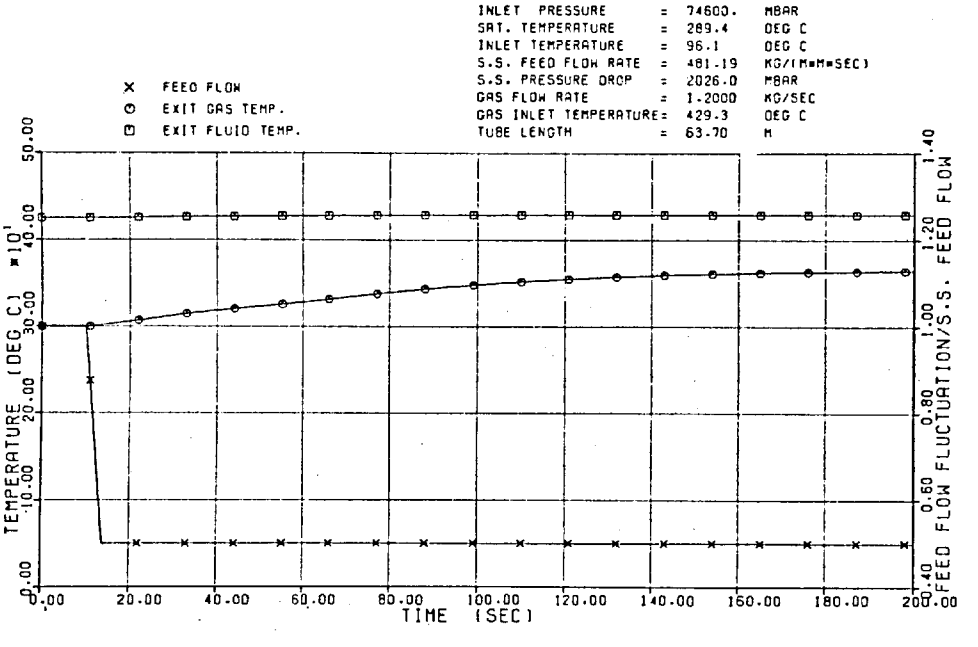


FIG.(6.7b) RESPONSE OF EXIT TEMPERATURES TO STEP DECREASE IN FEED FLOW

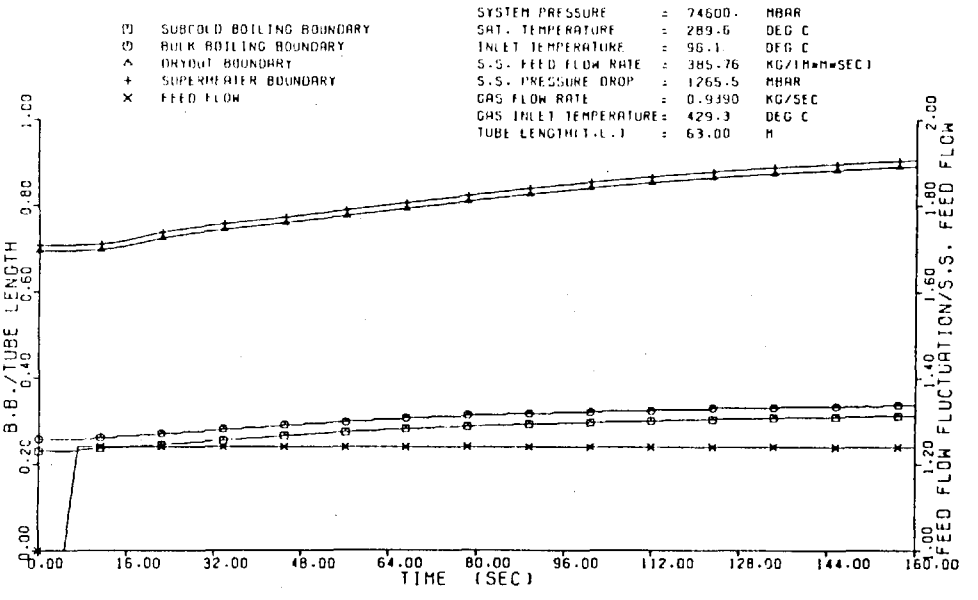


FIG.(6.8a) BOILING BOUNDARIES RESPONSE TO STEP INCREASE IN FEED FLOW

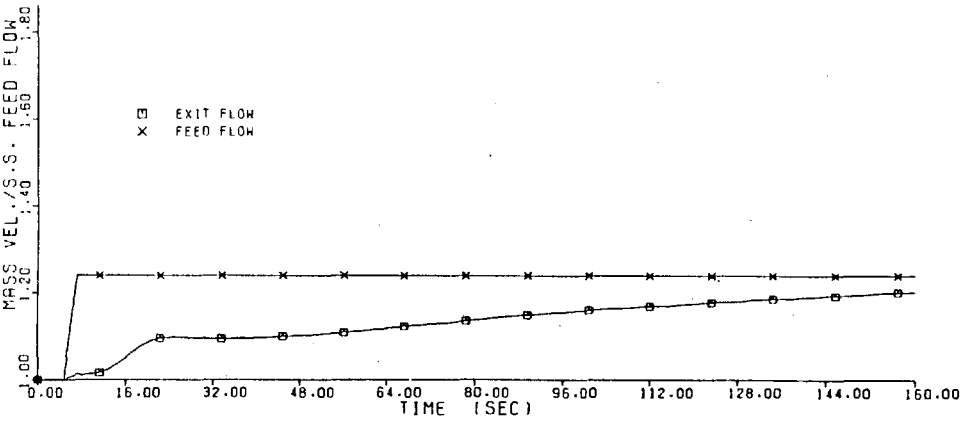


FIG.(6.8b) RESPONSE OF EXIT MASS VELOCITY TO INLET MASS EXCITATION

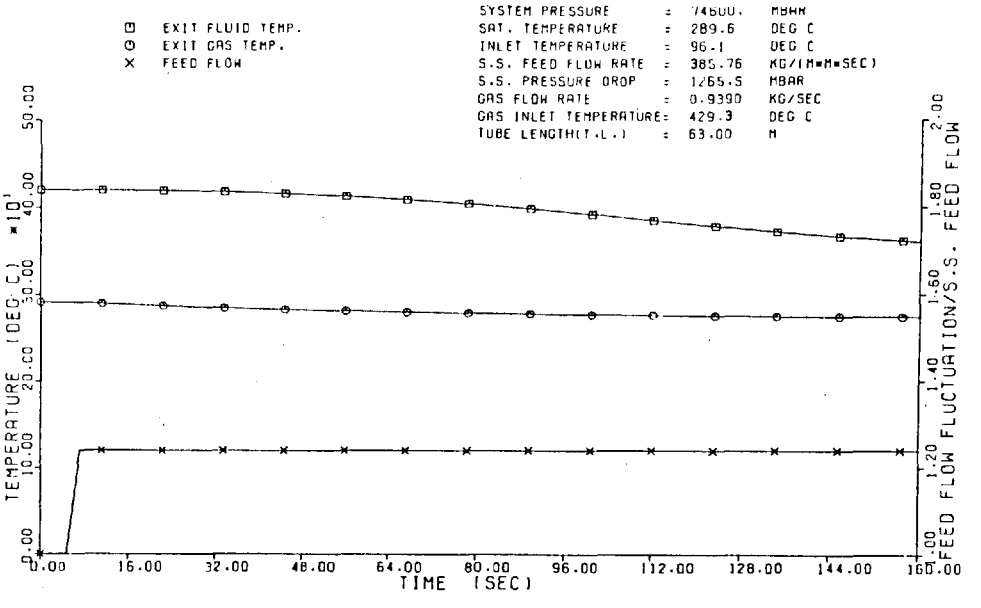


FIG.(6.8c) RESPONSE OF EXIT TEMPERATURES TO INLET MASS EXCITATION

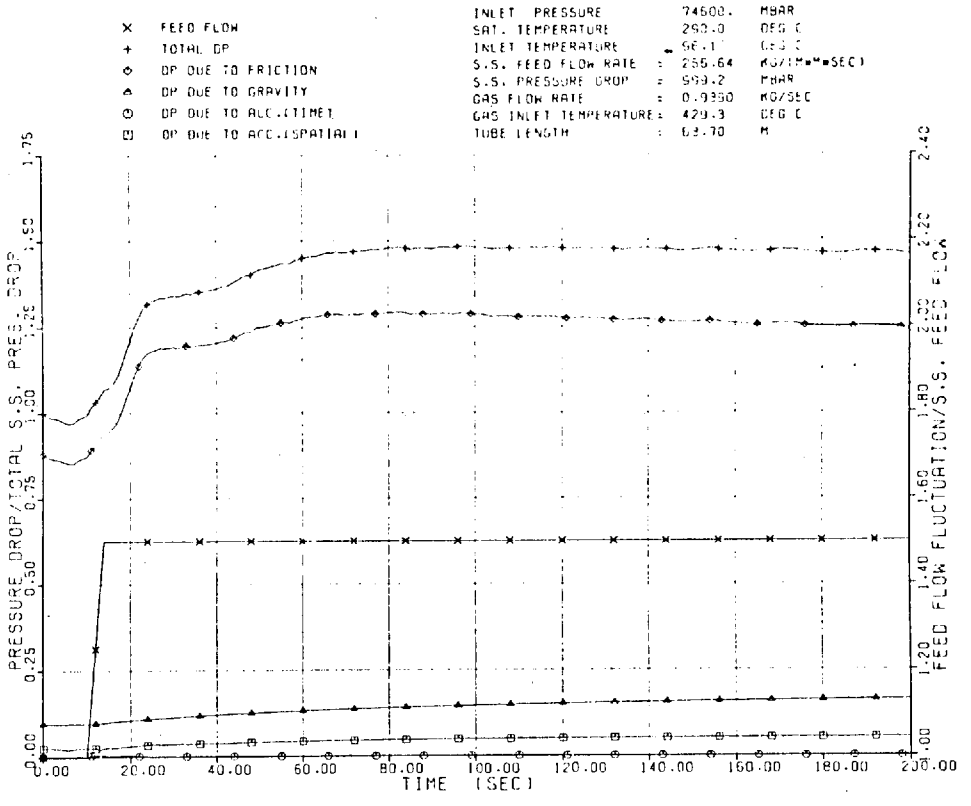


FIG.(6.9a) DIFFERENT COMPONENTS OF PRESSURE DROP

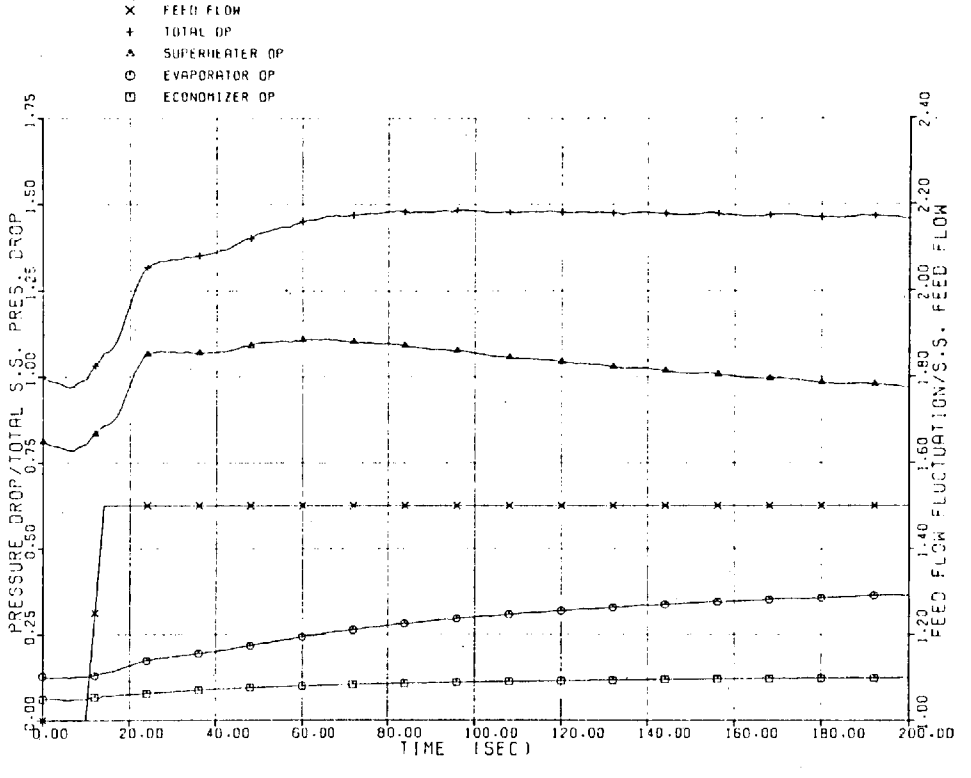


FIG.(6.9b) PRESSURE DROP OF DIFFERENT REGIONS ALONG THE TUBE

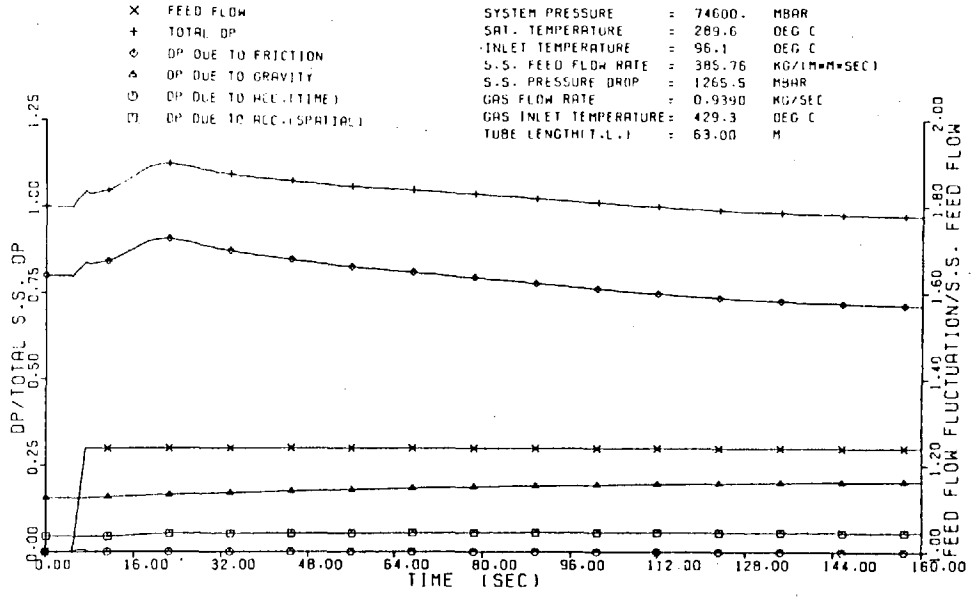


FIG.(6.10a) DIFFERENT COMPONENTS OF PRESSURE DROP

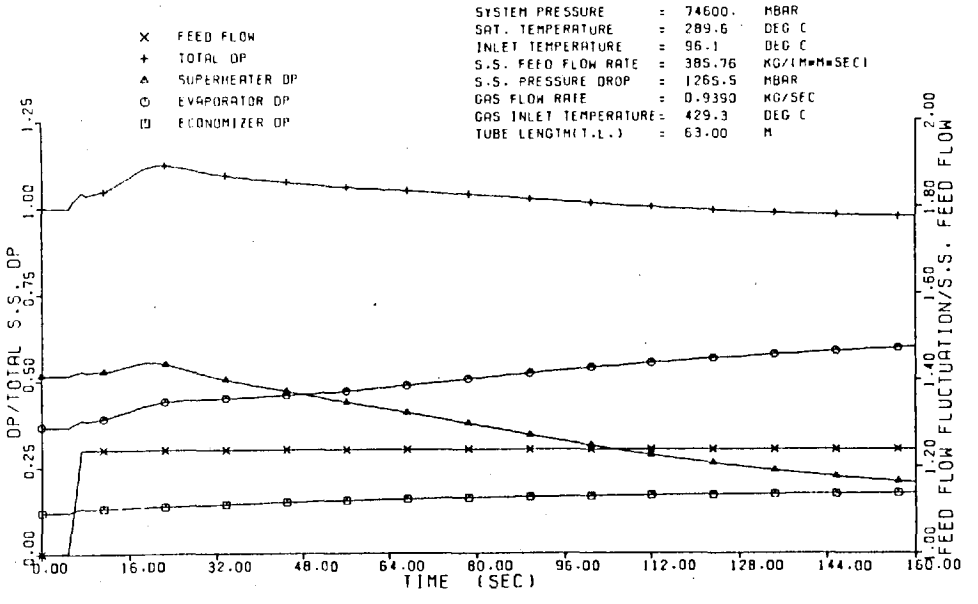


FIG.(6.10 b) PRESSURE DROP OF DIFFERENT REGIONS ALONG THE TUBE

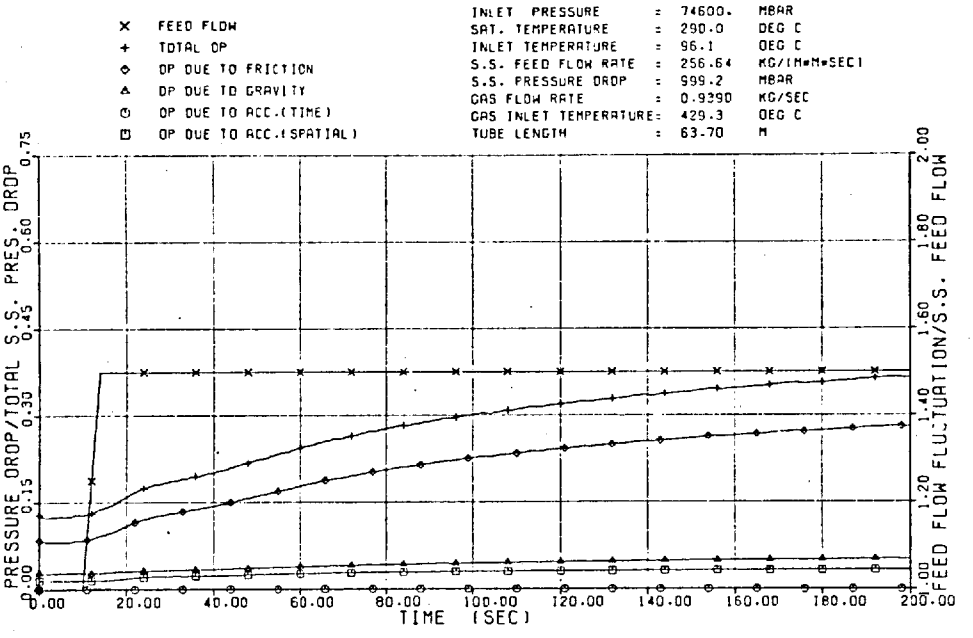


FIG.(6.11a) DIFFERENT COMPONENTS OF EVAPORATOR PRESSURE DROP

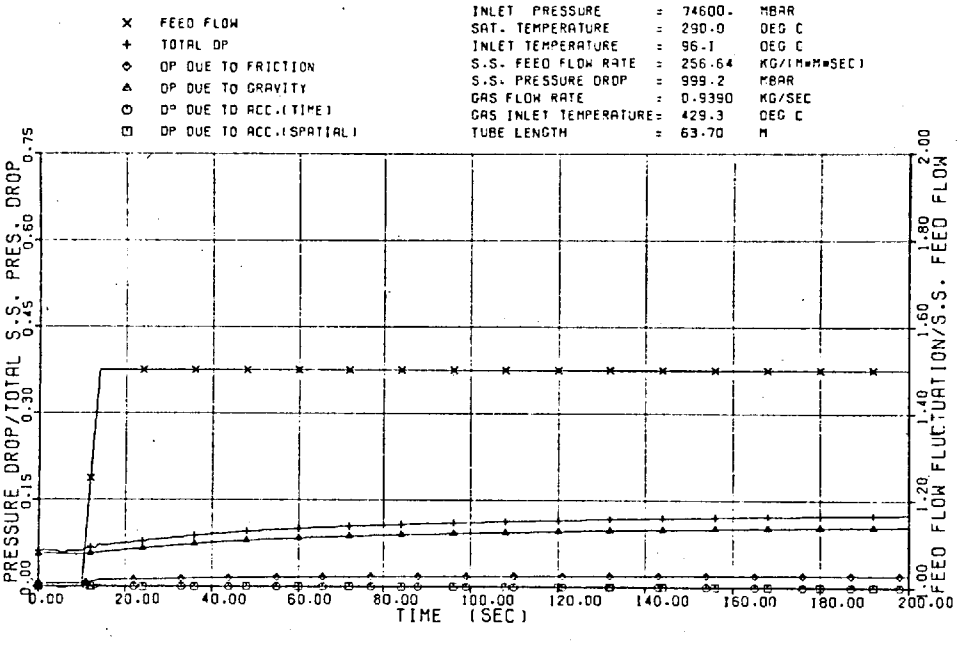


FIG.(6.11b) DIFFERENT COMPONENTS OF ECONOMIZER PRESSURE DROP

6.3 FREQUENCY RESPONSE ANALYSIS

In the following sections, the frequency response of a once-through boiler to inlet mass velocity oscillations is carried out using the digital computer program. It is shown that the analysis leads to useful information about the dynamic behaviour of the system. In particular, the dynamic stability of a once-through steam generator is investigated and an assessment of the inlet resistance is made as a means of stability of the system.

6.3.1 Operating Conditions

The frequency response calculation is made for two operating conditions similar to two experimental cases which have been carried out in an industrial research laboratory. The operational conditions, together with some useful results of steady-state calculation, are summarised in Table 6.1.

The analysis excludes other external elements (e.g. unheated tubes at the inlet and outlet, etc.), which are required to maintain the given inlet velocity. However, inlet gagging is included to increase the stability of the system as will be shown later. This is achieved by vectorial addition of a term proportional to the square of the inlet mass velocity and the total pressure drop of the tube.

6.3.2 Characteristics of the Input and the Output Variables

It is assumed that the system is excited, for example, by controlling a pump with a sinusoidal signal corresponding to a desired fluctuation in the inlet mass flow. Therefore, the inlet mass velocity is varied with respect to time (t) by the following relationship:

Table 6.1: Steady-state conditions for frequency response analyses

	Parameters and Units	Test Condition Number (1)	Test Condition Number (2)
Primary Flow	Total flow (kg/s)	0.939	0.467
	Inlet temperature (^{o}C)	429.3	438
	Outlet temperature (^{o}C)	296	281.5
	Local heat loss (%)	0	12.5
Secondary Side	Flow rate (kg/s)	0.0481	0.0241
	Flow rate (kg/m^{2}s)	385.7	193.2
	Inlet temperature (^{o}C)	96	84
	Outlet temperature (^{o}C)	427	437
	Inlet pressure (bar)	74.6	78
	Outlet pressure (bar)	73.2	77.4
	Length of economiser (subcooled) (m)	13	13.1
	Length of evaporator (subcooled boiling and two-phase) (m)	26.2	23.5
	Length of superheater (m)	24.1	27.1

$$G(0,t) = G(o,o)\left[1 + a\ sin\ \frac{2\pi}{T}\ t\right] \qquad (6.1)$$

where $G(0,0)$ is the initial steady-state value of inlet mass velocity, and T is the period of oscillations in seconds. The other inlet operational conditions are kept constant.

The resulting perturbation of the output parameters, e.g. pressure drop, exit mass velocity, temperatures, etc., are obtained at intervals Δt at different frequency, $\omega = 2\pi/T$ Rad/s, and they are plotted as a function of time (t). As shown in Figures 6.12 and 6.13, every figure includes oscillations of the inlet flow to give a common time reference for comparison.

The output variables (for example, shown in Figures 6.12 and 6.13) vary smoothly with time. This implies that an adequate numerical approximation is used in the numerical solution of the governing equations.

As seen in Figures 6.12 and 6.13, it appears that the oscillations of different parameters are most likely sinusoidal. Therefore, the amplitude of the oscillations is calculated by estimating the peak-to-trough difference in the parameters of interest. Also, phase difference with the inlet mass velocity oscillations is calculated from the ratio of the time interval between peaks in the two waves to the total period of the oscillations. These characteristics of variables are used in the construction of frequency response curves as discussed in the following sections.

6.3.3 Response of Exit Mass Velocity

Responses of the outlet mass velocity for the two conditions

of Table 6.1 are given in polar coordinates (Nyquist diagram) in Figures 6.14 and 6.15. The ratio of the amplitude of the exit mass velocity to inlet mass oscillations is the distance from the origin to the locus curve. The angle, measured clockwise from the positive real axis, is the phase lag of the exit mass velocity fluctuation with respect to the inlet flow oscillation.

As frequency increases, the amplitude vectors of the outlet mass flow rotate in a clockwise direction for both conditions of Figures 6.14 and 6.15. At some frequencies, the amplitude vectors encircle certain points on the complex plane, and hence they pass through a minimum value beyond which the vectors rotate again in a clockwise direction as the frequency increases. At high frequencies, the phase lag generally increases with frequency, and the loci curves encircle the origin of the complex plane (Figures 6.14 and 6.15). This trend of the exit mass velocity is in agreement with the frequency response results of Moxon (1973) for a helically-coiled tube once-through steam generator heated by a primary flow (Figure 2.19).

The curves of Figures 6.14 and 6.15 show that the real part of the dynamic response is negative (phase angle between -90 and -270^{o}) over a considerable range of frequencies at each operating condition of Table 6.1. Bearing in mind that a large fraction of the total pressure drop between the inlet and outlet of the tube occurs in the evaporator and the superheater regions (without inlet gagging), the existence of negative exit mass flow oscillations implies that there is a potential for dynamic instability as will be discussed later.

The residence time of the fluid in the economiser (the time required for a particle to travel from the inlet of the boiler to the onset of the subcooled boiling region) is believed to make an important

contribution to the dynamics. The subcooled or economiser residence time is obtained by dividing the subcooled length by the liquid velocity. The effect of the residence time can be seen by comparing the response curves of the exit mass velocities in Figures 6.14 and 6.15. The test conditions have nearly equal subcooled lengths (Table 6.1) with residence times of 28.2 and 56.6 seconds. In agreement with these values, the amplitude vector in Figure 6.15 rotates with frequency comparatively faster than the one in Figure 6.14, which has a shorter residence time than that of Figure 6.15. For example, the exit mass velocity loci cross the negative real axis (-180^{o} phase angle) nearly at a frequency of 0.315 Rad/s in Figure 6.14 and at a frequency of about 0.19 Rad/s in Figure 6.15. This is in agreement with the experimental analysis of the water-heated helically-coiled tube once-through boiler rig of Babcock and Wilcox as reported by Moxon (1973). The calculation of these experimental data show that the residence time in the economiser is about 3.5 seconds, and the exit velocity should, therefore, cross the negative real axis at a rather high frequency which is at about 1 Rad/s as shown in Figure 2.19.

At low frequencies, it is noticed that the amplitude vector encircles a region which is far from the origin of the complex plane, and the vector passes through a minimum value. That is, the oscillations of exit mass velocity are damped at certain frequencies less than the corresponding frequency at -180^{o} phase angle. Figures 6.14 and 6.15 show that the frequency at which the minimum of the amplitude vector occurs varies with the subcooled residence time. This frequency is less than the corresponding frequency to the subcooled residence time, and it is lower for systems having longer residence times. For instance, the minimum of the amplitude of the exit mass velocity nearly occurs at a

frequency of 0.05 Rad/s for Figure 6.14 and at 0.031 Rad/s for Figure 6.15 with the corresponding frequencies to the economiser residence time of 0.22 and 0.11 Rad/s, respectively. In agreement with this trend, Moxon's data (1973) show a minimum amplitude at a frequency between 0.5 and 1 Rad/s with the subcooled residence time of 3.5 seconds (1.79 Rad/s) as shown in Figure 2.19.

In the preceding examples, the exit mass velocity vector encircles a point in the positive region of the polar coordinate (-270 to -90^{o} phase angle) due to the long subcooled residence time. However, at low subcooled residence time, the velocity vector may encircle a point in the negative part of the polar coordinates as for the data of Moxon (Figure 2.19).

Frequency response analyses of constant heat flux systems, as, for example, given by Davies and Potter (1967) and Moxon (1973) do not exhibit the above behaviour of the exit mass velocity. For a constant heat flux system, the exit mass velocity vector rotates around the origin (Figure 2.18) even at low frequencies, which correspond to a positive response in a similar system with flux-flow coupling. It appears that the encirclement of a point other than the origin of the complex plane by the velocity vector is one of the characteristics of systems heated by a primary flow. A system in which the heat source is a primary flow becomes more stable and because of the flux-flow coupling, the encirclement of the origin shifts to another point in the complex plane.

6.3.4 Effect of Flux-Flow Coupling

The above trend of the frequency response of the exit mass flow can be interpreted in terms of the flux-flow coupling in the

economiser and evaporator as carried out in the following paragraph. But before considering the rôle of flux-flow coupling, let us consider the effect of the compressibility of the superheater on the exit mass velocity oscillations.

Figure 6.16 illustrates a comparison of mass velocities at the inlet, outlet and boiling boundaries at different frequencies. It can be seen that changes of densities in the economiser and superheater make a small contribution to the magnitude and phase shift of the outlet velocity. The mass velocity oscillations at the onset of the superheater, which have almost the same amplitude and phase as the exit velocity oscillations, are greatly damped and lag behind the oscillations of the mass velocity at the onset of subcooled boiling boundary. This is due to the vapour generation and changes of density along the evaporator.

As shown in Figure 6.16, the oscillations of mass velocity at the inlet of the economiser are slightly damped and are transmitted almost instantaneously to the evaporator inlet. The oscillations of the mass velocity along the economiser give rise to the heat flux perturbation (Figure 6.17) which is affected by the secondary side heat transfer coefficient. (It is proportional to the local mass velocity due to equation (3.98).) The secondary side temperature oscillations (Figure 6.18) are therefore affected by the oscillations of mass velocity and heat flux. Comparison of Figures 6.17 and 6.18 shows that the oscillations of mass velocity give rise to enthalpy oscillations, while the heat flux oscillations suppress them. In fact, the phase angle between the oscillations of the heat flux and mass velocity in the economiser is very small and it is nearly unchanged at low and high frequencies as shown in Figures 6.17a and b. That is, the phase angle of the heat flux in the economiser is strongly affected by the heat

transfer coefficient rather than the temperature difference between the fluid and the tube wall. The temperature difference nearly remains unchanged with time due to a small phase angle between the fluid temperature (Figure 6.18) and the tube temperature (Figure 6.19). (The time constant of the tube metal is small compared to the lowest period of oscillations in this study.) Therefore, the oscillations of the heat flux remain nearly in phase with mass velocity oscillations, and this damps down the enthalpy oscillations caused by the mass velocity fluctuations.

The above argument ceases to be valid at a point near the initial subcooled boiling boundary, particularly at low frequencies at which the fluctuations of the subcooled boiling boundary are large compared to that of high frequency oscillations as shown in Figures 6.20a and b. The reason is due to alternative changes of the heat transfer mechanism at points near the boiling boundary as discussed in section 6.2.2. The heat flux-flow coupling in the economiser acts to reduce the variation of the boiling boundary position which would otherwise occur in a constant heat flux system.

These oscillations, namely, inlet mass velocity, heat flux and boiling boundary position, change the rate of vapour generation along the evaporator. Consequently, changes in the mass velocity at the end of the evaporator occur, these being then transmitted to the boiler exit. These responses to flow changes do not occur instantaneously. Therefore, at a certain frequency, the oscillations of the exit mass velocity become out of phase with the inlet oscillations as shown in Figure 6.16a.

Let us now consider the rôle of heat flux couplings along the evaporator in bringing the oscillations of flow at the onset of

superheater. In the evaporator, temperatures of fluid and the tube wall, and the two-phase heat transfer coefficient are apparently constant and independent of the secondary flow, respectively. (Jens-Lottes type correlations are used in the analysis.) However, oscillations of the primary temperature, due to coupling of flux-flow in the economiser, are transmitted to the evaporator region (Figure 6.21). The oscillation of primary temperature in the evaporator, therefore, affects the local heat flux and hence the heat transfer coefficient. Consequently, the oscillation of mass velocity at the onset of the superheater is, further, influenced by changes of the heat flux in the evaporator region. The damping effect of flux-flow coupling, particularly, is more pronounced at low frequencies, since the response of the primary temperature to flow changes is slow as shown in section 6.2. Therefore, at low frequencies, the amplitude of the primary temperature oscillations in the economiser is large enough to be transmitted to the evaporator region (Figure 6.22b). As frequency increases, the amplitude of temperature oscillations decreases (Figure 6.22a), and moreover oscillations are damped down when transmitted to the evaporator as shown in Figure 6.21a).

Therefore, at low frequencies, the effect of flux-flow coupling in the economiser and the evaporator is sufficiently strong to damp down the mass velocity oscillations as frequency increases. At certain frequencies, the damping effect of flux-flow coupling reduces with frequency, and the coupling effect in the evaporator diminishes. This causes the exit mass velocity oscillations to grow in amplitude and phase angle as shown in Figures 6.14 and 6.15.

6.3.5 Pressure Drop Oscillations

The pressure drop oscillations and the different components of pressure drop at different regions along the boiler are shown in Figures 6.23 to 6.26.

The economiser pressure drop (Figures 6.24c and 6.26c) is largely due to the hydrostatic effects which lag behind the oscillations of the inlet mass velocity because of changes in the subcooled boiling boundary (Figure 6.20). The frictional pressure drop in this region is small (without inlet gag) as compared to the total pressure drop.

In the evaporator region (Figures 6.24b and 6.26b), the accelerational pressure drop increases while the gravity reduces due to changes of effective density along the tube. The frictional pressure drops constitute a large part of the pressure drops in the evaporator and the superheater regions. Comparison of Figures 6.16, 6.20, 6.24 and 6.26 shows that the phase angles of frictional pressure drops in the evaporator and the superheater are controlled by the perturbations of corresponding mass velocities and the superheater boundary.

It appears that the contributions of components of pressure drops to the total pressure difference between the inlet and outlet, do not have similar responses. For example, hydrostatic effects are mainly important at the economiser. Accelerational pressure loss increases in the evaporator, while frictional effects are distributed along the boiler. As illustrated in Figures 6.23a and 6.25b, there are larger phase lags associated with the frictional pressure drop than with hydrostatic and accelerational effects.

The phase lag (Figure 6.26) increases particulary when the oscillations of the outlet mass velocity (Figure 6.16a) become out of phase with inlet perturbations.

The total pressure drop is a vectorial summation of the pressure drop components in different regions along the boiler (Figures 6.23 and 6.25). Therefore, as illustrated in Figure 6.25, the system may oscillate at a frequency such that the pressure drops at the superheater and the evaporator are out-of-phase with that of the economiser. At this condition, the total pressure drop can oscillate out of phase with inlet mass velocity (Figure 6.25), which is a necessary condition for instability. Or, the system can show an unchanged total pressure drop (Figure 6.33b) while having oscillatory mass velocities and pressure drop components. Any disturbance of the system at this particular frequency, therefore, can lead to oscillatory flow with no net increase in pressure drop.

At very low frequencies, as shown in Figure 6.27, the pressure drop oscillations may possess two peaks for a period of the inlet mass velocity. The oscillations of the outlet mass velocity (Figure 6.16c) at the frequency corresponding to Figure 6.27 show a small phase lag with inlet mass oscillations; this rejects the possibility of dynamic instability. Figure 6.27a shows that the superheater pressure drop increases when the inlet mass velocity decreases, and it causes a second peak in the total pressure drop oscillations. This behaviour is a typical characteristic of static instability as discussed in Chapter 5. The high peak of the pressure drop oscillations is due to the dynamic effects while the second peak results from the static characteristics of the system (Δp versus G). In fact, the operational condition of Figure 6.27 is statically unstable as will be discussed later.

6.3.6 Stability Implication

The discussion of the previous section suggests that the frequency response of the pressure drop to inlet mass velocity variations is a useful method for stability calculation. The present section is concerned with the relevance of the frequency response to the stability of the system.

Let us consider a system of Figure 6.28 consisting of a single heated tube with a certain internal dynamic characteristic. The system operates between two headers in parallel with, for example, a by-pass tube having a certain external dynamic characteristic.

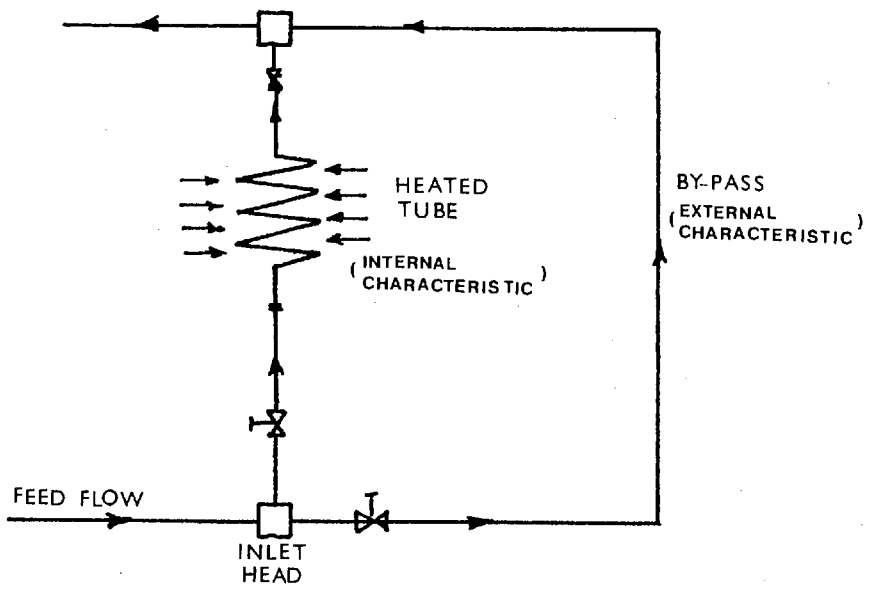


Figure 6.28: A system of a single heated tube parallel to a by-pass

Any disturbance, e.g. the feed flow, will induce a perturbation in the pressure drop between the two headers due to the internal dynamic characteristics of the system. These perturbations will affect the inlet flow of the heated tube through the external dynamic characteristics of the system (e.g. feedback effect of by-pass line). A block diagram

corresponding to this system is shown in Figure 6.29.

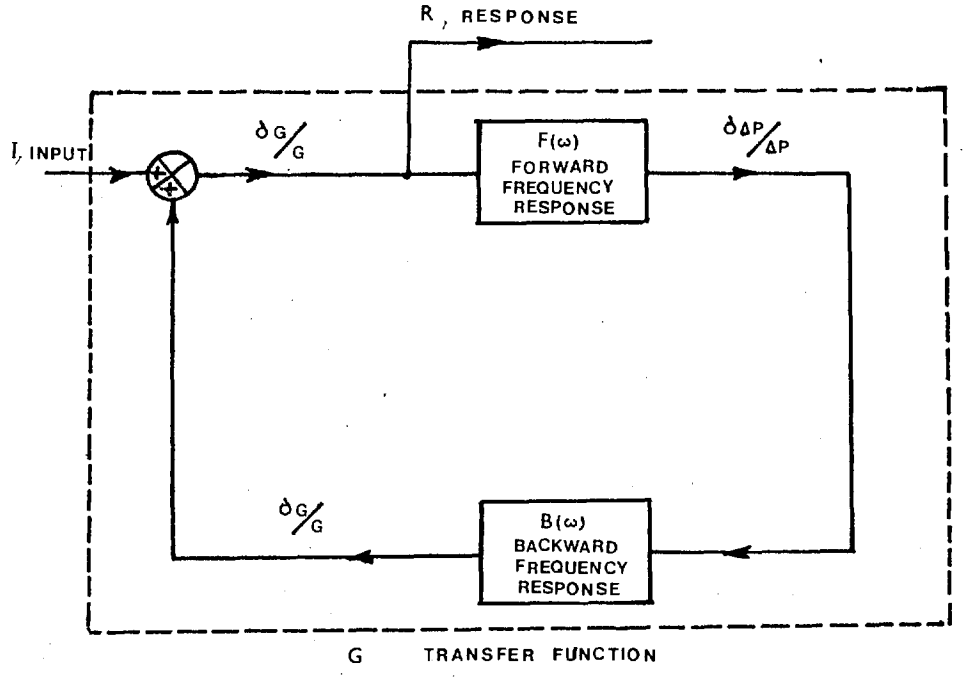


Figure 6.29: Block diagram of the system shown in Figure 6.28

The closed loop of Figure 6.29 consists of a forward transfer function, $F(\omega)$, due to the internal characteristics of flow in a heated tube; a backward transfer, $B(\omega)$, due to the external characteristics of flow in the by-pass line; and a summing point at which the feedback is compared to the input. Following Beckmann et al (1973) and Bailey et al (1971), it is assumed that $F(\omega)$ and $B(\omega)$ are related to the internal and external characteristics, respectively, as follows:

$$F(\omega) = \left(\frac{\partial\ \Delta p}{\Delta p} \Big/ \frac{\partial G}{G}\right)_{int} \tag{6.2}$$

and

$$B(\omega) = \left(\frac{\partial G}{G} \Big/ \frac{\partial\ \Delta p}{\Delta p}\right)_{ext} \tag{6.3}$$

Then, the response of the closed loop system may be written as:

$$R = I + B(\omega)\ F(\omega)\ R \tag{6.4}$$

Hence, the transfer function is:

$$\frac{R}{I} = \frac{1}{1 - B(\omega)\ F(\omega)} \tag{6.5}$$

Therefore, the stability threshold becomes:

$$B(\omega)\ F(\omega) = 1 \tag{6.6}$$

It is now assumed that the feedback function is that of a constant pressure drop ($\partial\Delta p = 0$) between the inlet and outlet headers (a very large by-pass flow or a bank of parallel tubes). It follows that:

$$\frac{1}{B(\omega)} = \left(\frac{\partial\ \Delta p}{\Delta p} \Big/ \frac{\partial G}{G}\right)_{ext} = 0 \tag{6.7}$$

Then, from equations (6.6) and (6.7), the stability criterion becomes:

$$\left(\frac{\partial\ \Delta p}{\Delta p} \Big/ \frac{\partial G}{G}\right)_{int} = 0 \tag{6.8}$$

Therefore, the stability can be investigated by plotting the open loop frequency response, in the form of equation (6.8), in a polar coordinate (Nyquist diagram). However, in this case the critical point becomes zero (origin of the complex plane) rather than -1 in Nyquist criteria. That is, for the stability of the system, the pressure drop response must not encircle the point (0,0) in the clockwise direction

with increasing frequency (ω).

The frequency response of the pressure drop in the form of equation (6.8) not only enables us to investigate the dynamic stability, but it can also predict the static stability, i.e. the value of equation (6.8) becomes zero or negative at very low frequencies.

As a final remark, equation (6.8) is developed for a system having positive nominal pressure drops. Therefore, in some cases in which, for example, the hydrostatic effects between the tube inlet and the inlet header are large and act against the pressure drop, the value of Δp in equation (6.8) should be modified to account for the effect of gravity.

6.3.7 Frequency Response of Pressure Drop

The open loop frequency response of pressure drop to inlet flow variations, which determines the internal characteristics of flow, is shown in Figures 6.30 and 6.31 for the two operating conditions of Table 6.1. No effects of inlet gagging are taken into account.

The data of Figure 6.30 corresponds to the test condition No. 1 in Table 6.1. It is taken at an operating point on the negative slope region of the steady-state pressure drop-mass flow curve (point A in Figure 5.28). As it would be expected, the pressure drop response shown in Figure 6.30 starts with a -180^{o} phase angle at very low frequencies, confirming the static instability operating conditions. An illustration of the pressure drop oscillations is given in Figure 6.27 for different regions along the boiler.

Figure 6.31 is obtained at an operating point in the positive slope region of the steady-state pressure drop-mass flow curve. Frequency responses of this operating point indicate that the real part

of the pressure drop is positive at very low frequencies, which confirms the static stable conditions.

The curves of Figures 6.30 and 6.31 show that the real part of the response vector is negative over a wide range of frequencies, and the response loci encircle the point (0,0), which implies dynamically unstable conditions as discussed in the previous sections.

At low frequencies, the phase angle of the pressure drop response increases with frequency (Figures 6.30 and 6.31) until the response loci encircle a point on the complex plane. Then, with a further increase of frequency, the internal dynamic characteristic vectors rotate around the point (0,0) in a clockwise direction. This trend of frequency response curve is in agreement with the frequency response results of a sodium heated once-through steam generator rig as reported by Waszink and Efferding (1974).

The frequency at which the response curve crosses the negative real axis is the resonant frequency of the system at that particular operating condition. That is, any disturbance of the flow of the system, caused by a bandwidth of noise which is inherent in any actual system, will be amplified at the resonant frequency. Crossings on negative real axes of Figures 6.30 and 6.31 are nearly at frequencies of 0.32 and 0.19 Rad/s, respectively. These results are promising in comparison with the experimental results of Babcock and Wilcox (Appendix A). The experiments showed inlet mass flow oscillations of periods of 22 and 37 seconds for operating conditions of Figures 6.30 and 6.31, respectively. Although in the analysis of Figures 6.30 and 6.31, effects of inlet and outlet unheated tubes are not accounted for (due to incompleteness of the available set of experimental data), the discrepancies between the predicted frequencies and experimentally

observed oscillations are small and encouraging. It can be seen that neglecting the inlet and outlet tubes will not strongly affect the frequency of the oscillations if the amplitudes of the pressure drops in either tube are nearly equal. This can be conceived from the fact that the inlet and outlet tubes counteract one another, i.e. the inlet tube stabilises while the outlet tube destabilises the system. For example, as shown in Figures 6.32a and b, the effect of increasing the inlet resistance which simulates an inlet unheated tube, has small effect on the resonant frequency. However, the amplitude of the oscillations would be influenced with resistance at inlet or outlet as shown in Figure 6.32. The magnitude of the internal dynamic characteristics at -180^{o} is a measure of the amplitude of the oscillations as will be discussed later.

The effect of the economiser residence time can be seen by comparing the frequency response of the internal dynamic characteristics in Figures 6.30 and 6.31. The resonant frequency of the system with shorter residence time (Figure 6.30) is greater than the system of Figure 6.31 which has longer economiser residence time. Also, the magnitude of the oscillations at -180^{o} is affected by the subcooled residence time, and there is a larger amplitude for Figure 6.31 than for Figure 6.30.

6.3.8 Onset of Instability

In the preceding discussion, the operating conditions considered were proved to be unstable. It was noticed that the magnitude and phase angle of the pressure drop was largely due to the evaporator and superheater pressure drop oscillations. When these oscillations at a particular frequency were added to the other components

of pressure drop, they yielded an oscillatory total pressure drop which was out of phase with respect to the inlet velocity oscillations.

The above consideration suggests that any increase of the in-phase component of pressure drop with respect to the inlet mass velocity oscillations can decrease the out-of-phase contributions of the two-phase and superheater pressure drops. Hence, the magnitude of the total pressure drop oscillations at -180^{o} will be suppressed. This would correspond practically, for example, to the boiler being fed through an inlet resistance orifice (gagging).

The stabilising effect of inlet gags is illustrated in Figures 6.33 and 6.34 for the case in which the oscillations of the superheater pressure drop are out-of-phase with the inlet mass flow perturbations. The resistance of an inlet gag is always in-phase with the inlet velocity perturbation (Figures 6.33 and 6.34). Therefore, when its magnitude exceeds the out-of-phase contribution of the evaporator and particularly the superheater (Figure 6.34a), the oscillations of the total pressure drop are dominated by the in-phase components of pressure drop resulting in a positive response of the pressure drop.

The frequency response of the operating conditions of Table 6.1 is displayed in Figure 6.35 for an inlet gag of constant 0.3 m^3/kg (corresponding pressure drop is 0.3 × (inlet mass velocity)^2). Comparison of Figures 6.30, 6.31 and 6.35 shows that the response curves with inlet gagging are shrunk and shifted to the positive real axis far from zero, and both conditions become dynamically stable.

Figures 6.36 and 6.37 illustrate the frequency response of the internal dynamic characteristics at different gag resistance. It can be seen that, as the gag resistance is progressively reduced from a

value corresponding to a stable condition, response curves are shifted to the left of the real axis. Finally, a point is reached at which there is zero (or negative) pressure drop response to an oscillation in the inlet flow at a particular frequency. This corresponds to the onset of instability. If the gagging is further reduced, then the system is unstable but the response of the pressure drop to an imposed inlet flow oscillation would move away from zero as shown in Figures 6.33a, 6.36 and 6.37. Consequently, for a given boiler and steady-state operating condition, the magnitude of the boiler internal dynamic characteristics at -180^{o} is then a measure of the amount of the inlet gag resistance needed for the threshold of stability. Inlet gag resistances larger than this value would permit stable operation of the boiler at this particular operating condition. Gag resistances equal to or less than the value of the onset of instability would result in self-sustained or unbounded inlet flow oscillations. The frequency of the onset of oscillation would then correspond to the perturbation frequency for which the boiler pressure drop response moves away from zero.

Comparison of Figures 6.36 and 6.37 reveals that the operating condition No. 1 in Table 6.1 (Figure 3.36) is less unstable than condition No. 2 (Figure 3.37); and the size of the inlet resistance to stabilise the system with a long subcooled residence time and superheater (Figure 6.37) is greater than for the system with less residence time and superheater length (Figure 6.36).

Finally, the magnitude of the internal dynamic characteristics at -180^{o} and zero frequency (if there is any) is a measure of the amount of inlet resistance required for static stability. As discussed, the operating condition of Figure 6.36 is liable to static stability.

Figure 6.36 shows that the amount of inlet resistance required for dynamic stability is less than the value required to prevent the static stability; and installing an inlet resistance necessary for static stability is sufficient to overcome the dynamic instability for this particular condition.

6.3.9 Responses of Temperatures

Typical oscillations of the outlet temperatures of the primary and the secondary flows are shown in Figure 6.38 at two different frequencies. Also, frequency responses of the exit temperature to inlet mass oscillations are given in Figure 6.39. The exit temperatures show considerable amplitude and phase lag at low frequencies. With increasing frequency, the amplitude decreases rapidly and the phase lag increases. The amplitude of temperature oscillations reaches values of less than $1^{o}C$ for steam and gas at frequencies of 0.052 and 0.35 Rad/s, respectively (Figure 6.39). It appears that the effect of outlet temperature fluctuations is more pronounced at low frequencies. High frequencies are perhaps of less interest from the point of view of stress analysis (thermal fatigue).

However, this is sometimes misleading in the sense that there can be considerable oscillations in the tube wall temperatures at boiling boundaries, though the oscillations of outlet temperatures are very small as illustrated in Figure 6.40. It can be seen that the oscillations at the onset of superheater, which is discussed later, are damped when transmitting exponentially (e.g. Figure 5.8) along the superheater. Therefore, when the superheater region is long enough to damp down the oscillations of the superheater inlet, the temperature oscillations at the exit become small and negligible.

Oscillations of the tube wall temperatures along the boiler (Figure 6.40b) occur mostly in the economiser and superheater regions where the heat flux-flow coupling is due to forced convective heat transfer mechanisms. The amplitude of oscillations of the wall temperatures never exceeds the temperature oscillations of the secondary flow almost everywhere along the tube, except at the region near to the dryout and superheater boundaries. In this region, the oscillations of the tube wall temperature may be twice as much as those of steam at the same positions (Figure 6.41). Figure 6.42 displays the variation of the heat flux and heat transfer coefficient at a fixed position between the dryout and superheater boundaries (the corresponding temperature oscillation in Figure 6.41 is at 38.99 m). This phenomenon is caused by the oscillations of the dryout and superheater boundaries, superimposed on the effect of velocity oscillations. As it was observed in section 6.2, the cyclic variations of temperature (Figure 6.41) and heat flux (Figure 6.42) are caused by alternative changes of the heat transfer mechanism from forced convective to two-phase boiling when the dryout and superheater boundaries oscillate. Figure 6.43 displays the oscillations of the temperature of the dryout-superheater region at a high frequency near to the resonant frequency of the system. It can be seen that the wall temperature oscillation can be up to $20^{o}C$, although the outlet temperatures of steam and gas are suppressed as shown in Figure 6.38a.

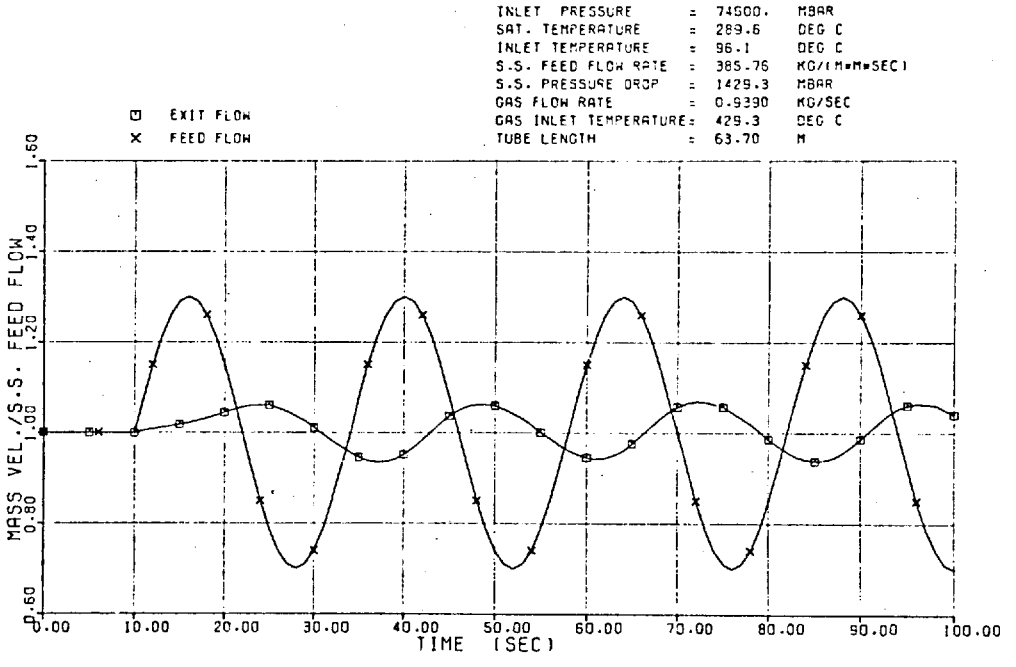


FIG.(6.12a) RESPONSE OF EXIT MASS VELOCITY TO INLET MASS EXCITATION

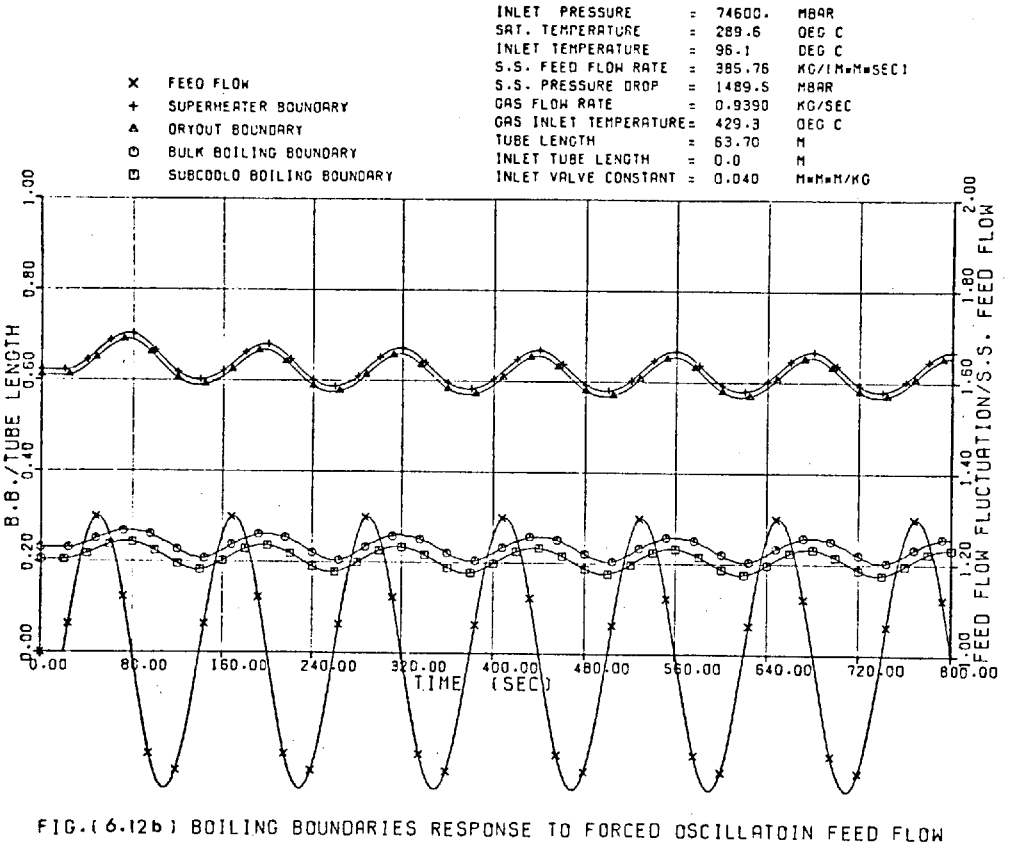


FIG.(6.12b) BOILING BOUNDARIES RESPONSE TO FORCED OSCILLATOIN FEED FLOW

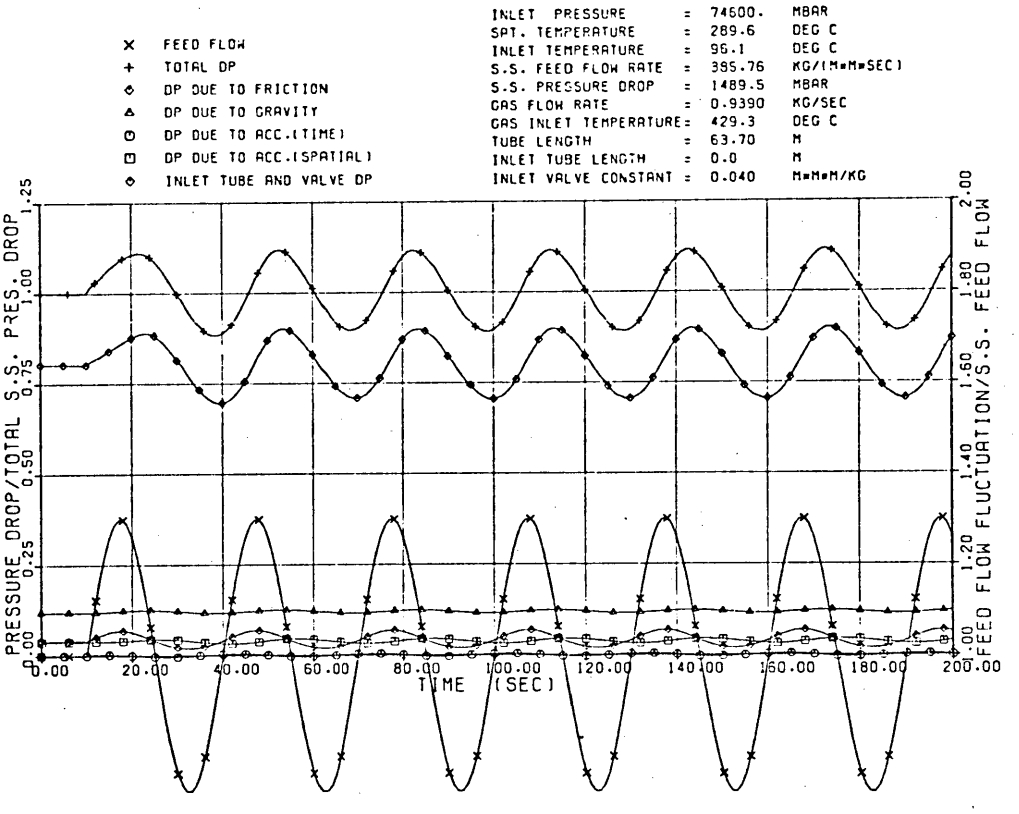


FIG.(6.13 a) DIFFERENT COMPONENTS OF PRESSURE DROP

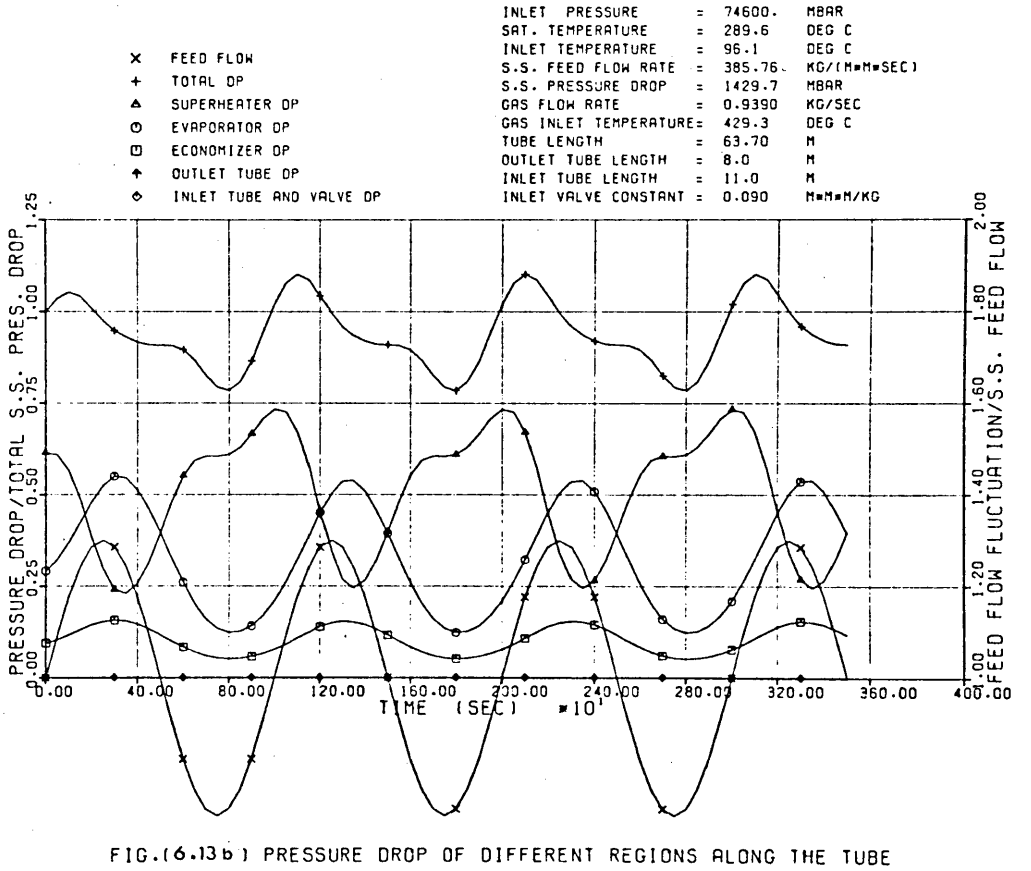


FIG.(6.13 b) PRESSURE DROP OF DIFFERENT REGIONS ALONG THE TUBE

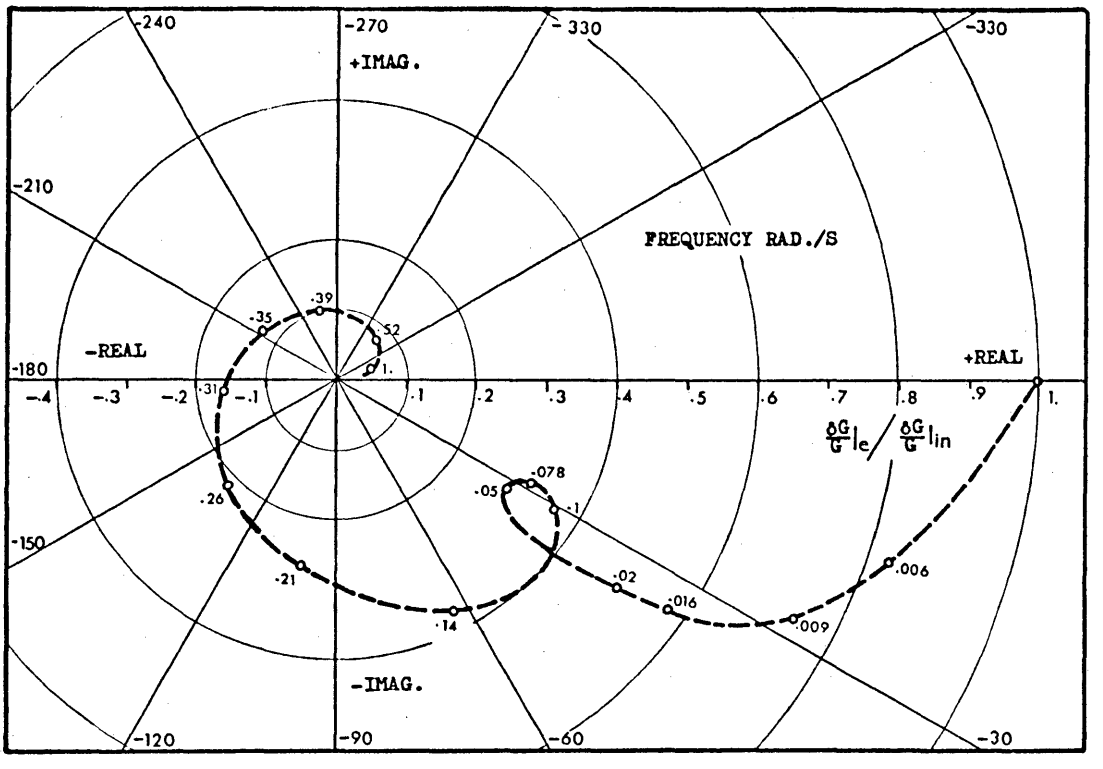


Figure 6.14: Frequency response of steam mass velocity to inlet mass velocity perturbation (Condition No. 1, Table 6.1)

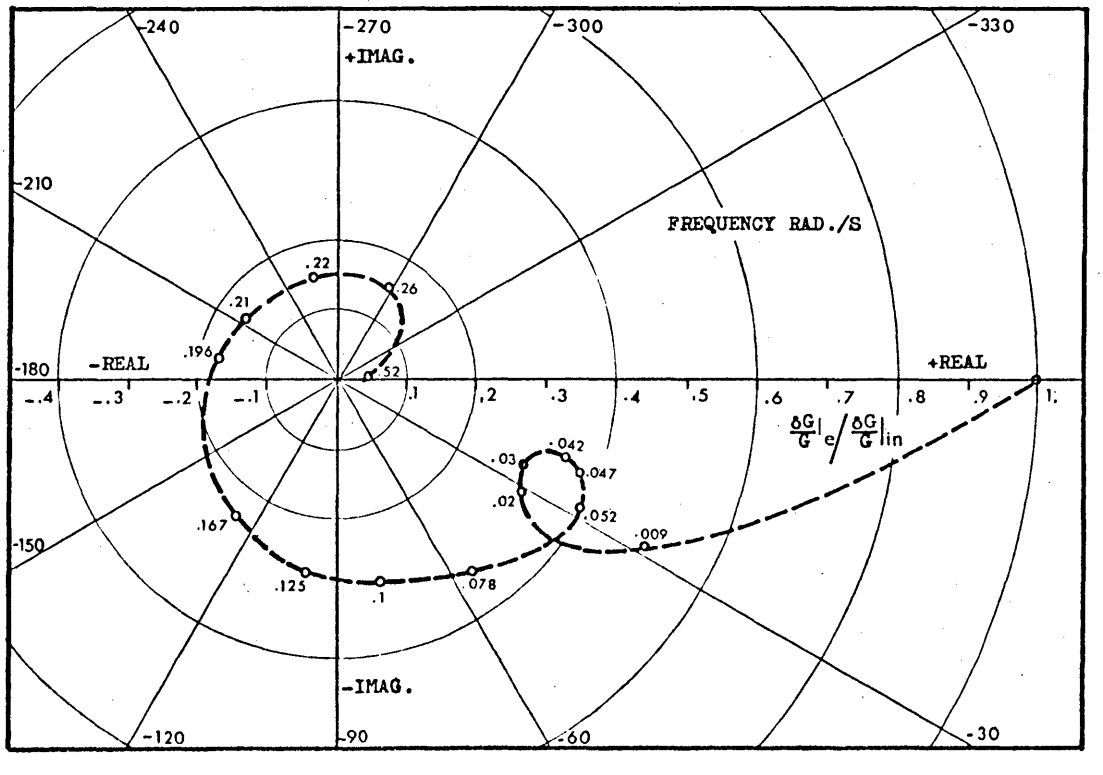
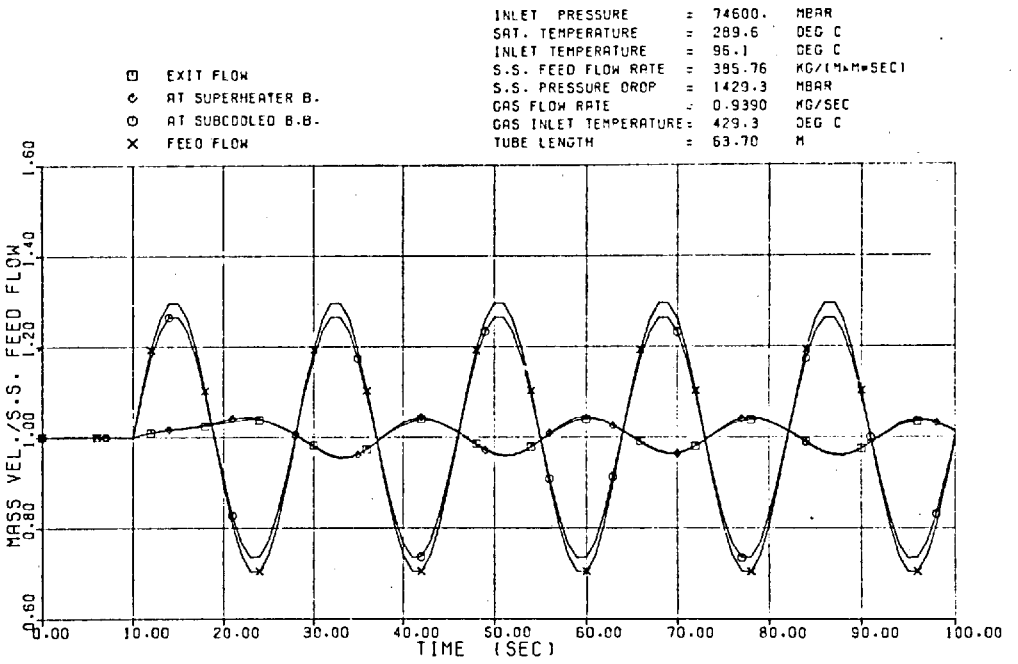
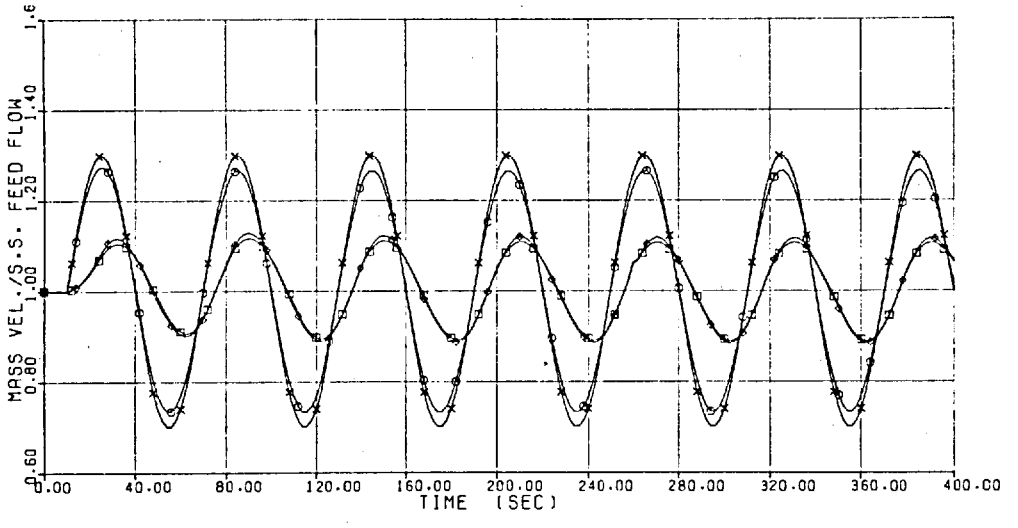


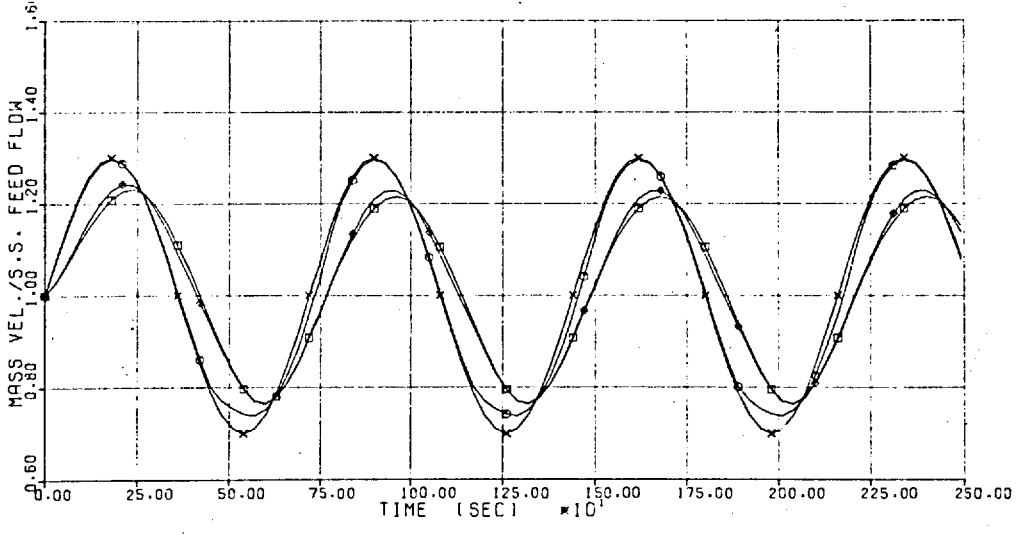
Figure 6.15: Frequency response of steam mass velocity to inlet mass velocity perturbation (Condition No. 2, Table 6.1)



a: ω = ,35 Rad/s



b: ω = ,105 Rad/s



c: ω = ,0087 Rad/s

FIG.(6.16) RESPONSE OF MASS VELOCITIES TO INLET MASS EXCITATION

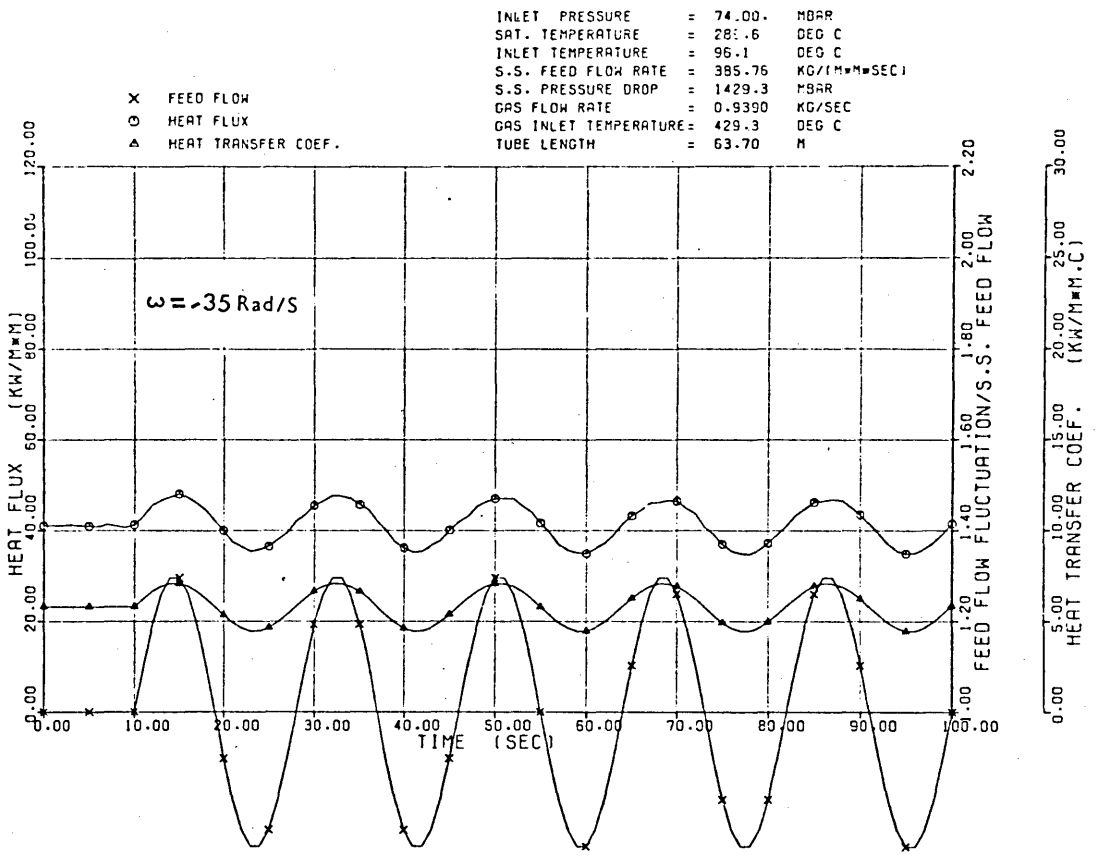


FIG.(6.17a) VARIATION OF HEAT FLUX AND HEAT TRANSFER COEFFICIENT AT SUBCOOLED BOILING BOUNDARY

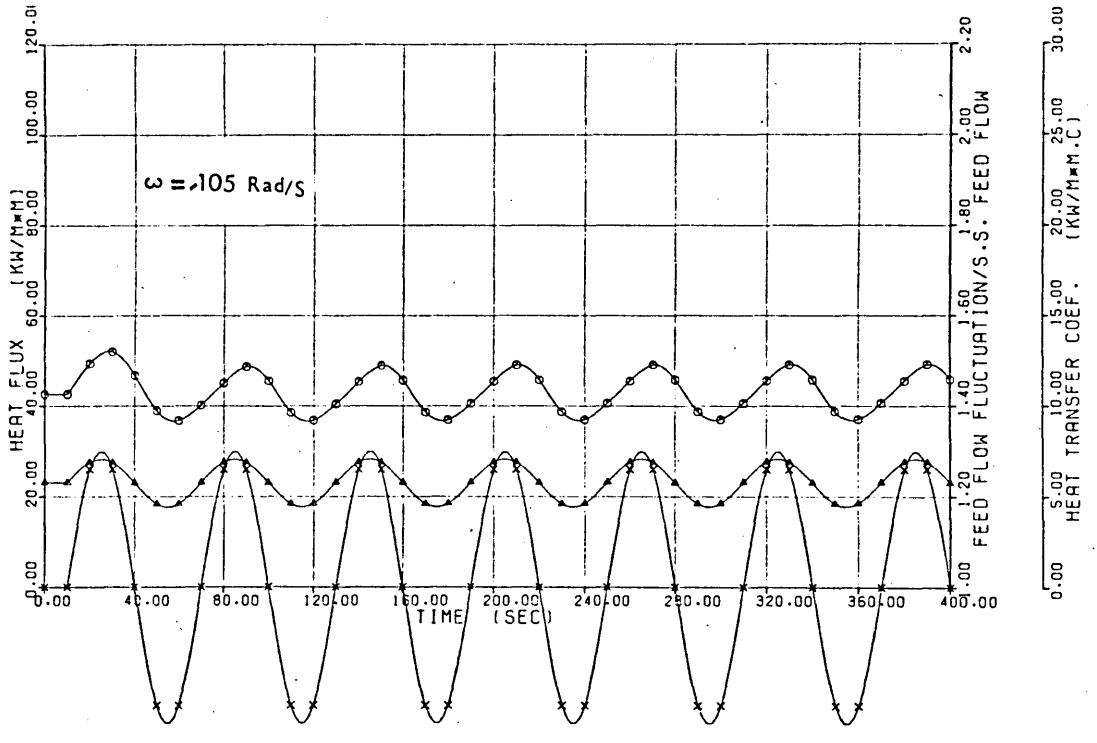


FIG.(6.17b) VARIATION OF HEAT FLUX AND HEAT TRANSFER COEFFICIENT AT SUBCOOLED BOILING BOUNDARY

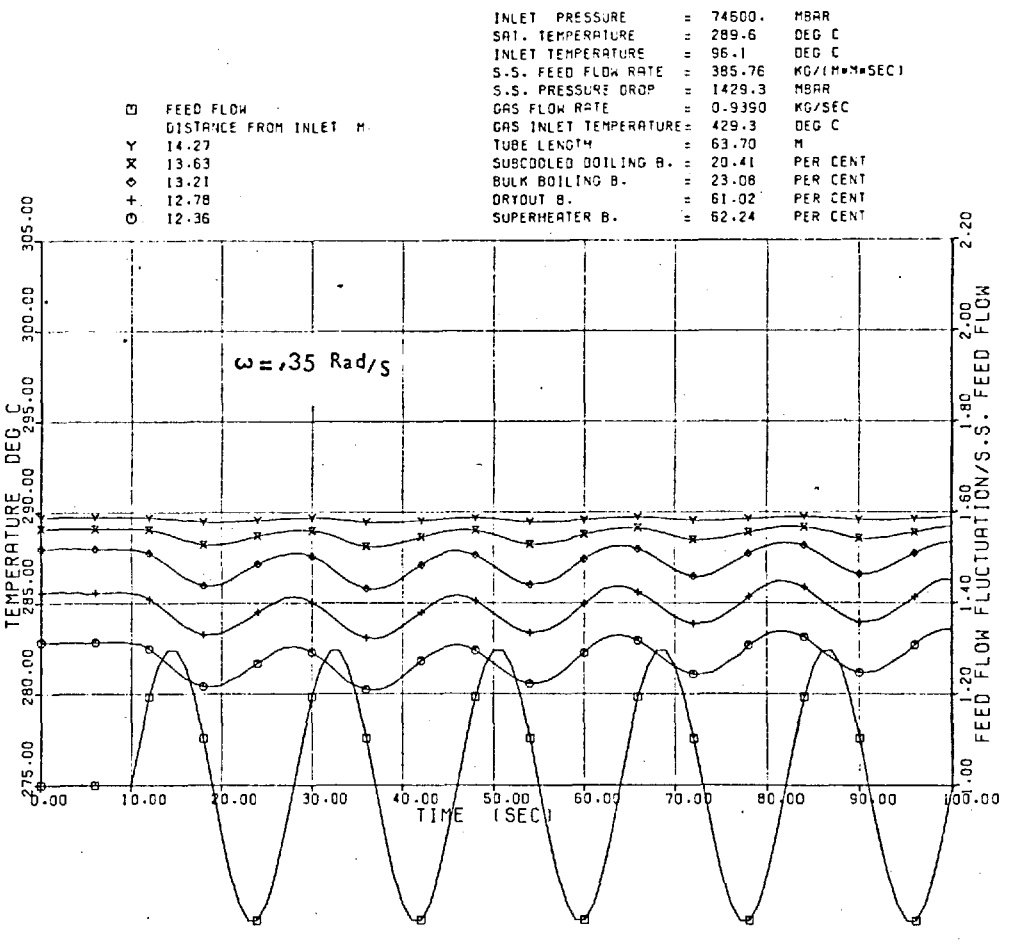


FIG.(6.18a) FLUID TEMPERATURES AT FIXED POSITIONS NEAR SUBCOOLED AND BULK BOILING BOUNDARIES

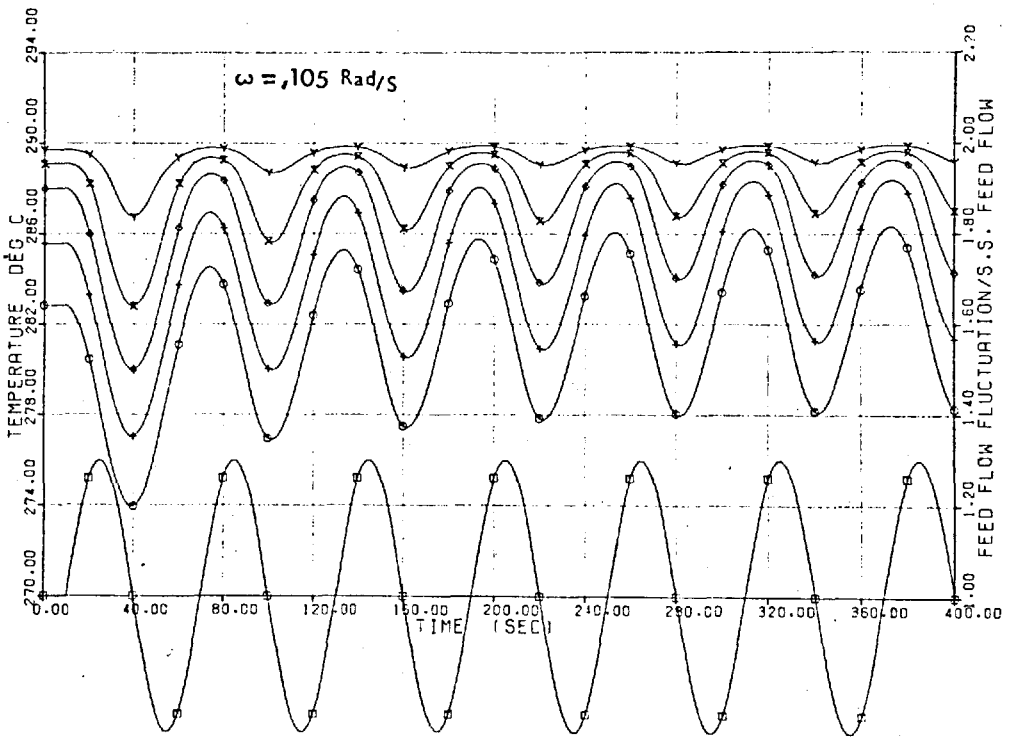


FIG.(6.18b) FLUID TEMPERATURES AT FIXED POSITIONS NEAR SUBCOOLED AND BULK BOILING BOUNDARIES

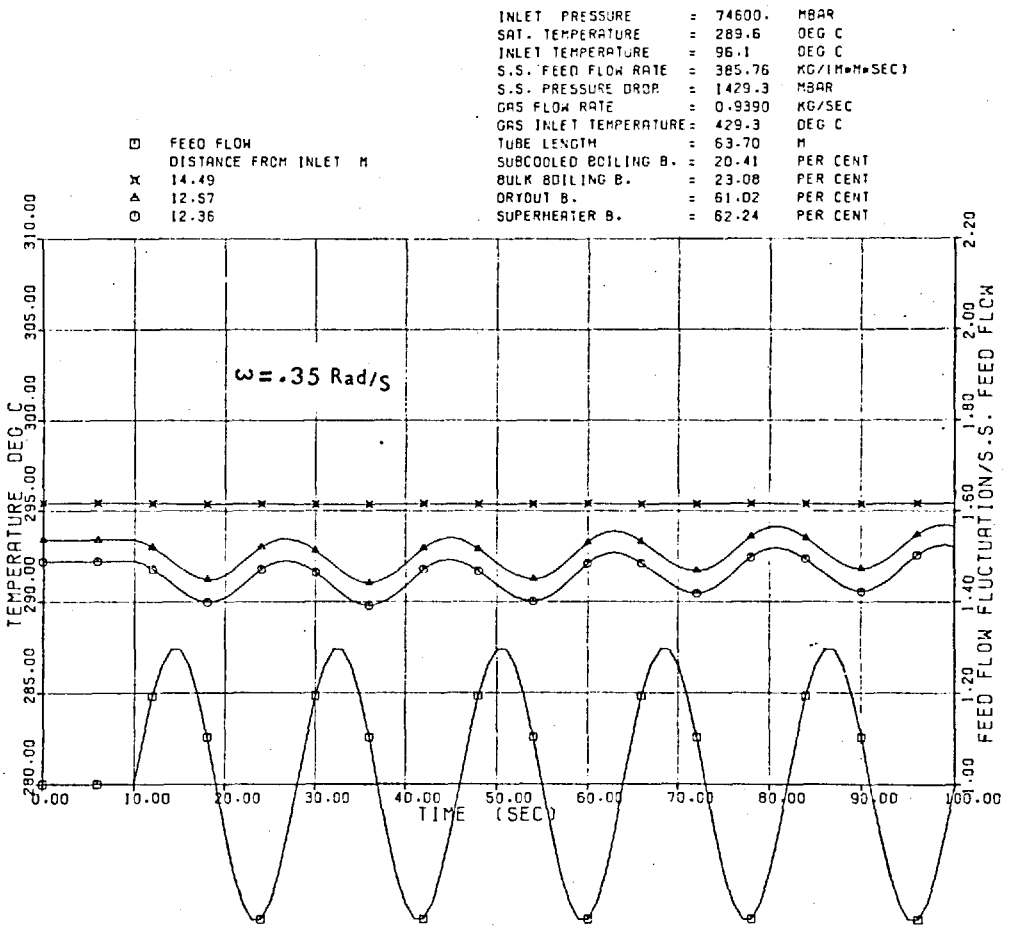


FIG.(6.19a) TUBE WALL TEMPERATURES AT FIXED POSITIONS NEAR SUBCOOLED AND BULK BOILING BOUNDARIES

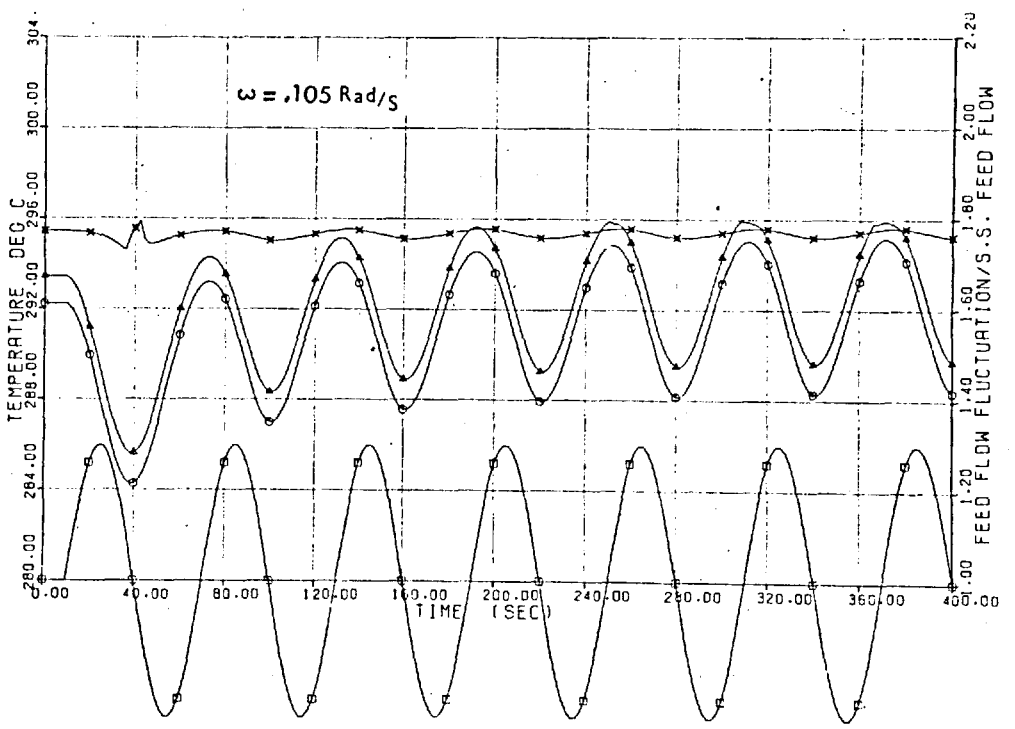


FIG.(6.19b) TUBE WALL TEMPERATURES AT FIXED POSITIONS NEAR SUBCOOLED AND BULK BOILING BOUNDARIES

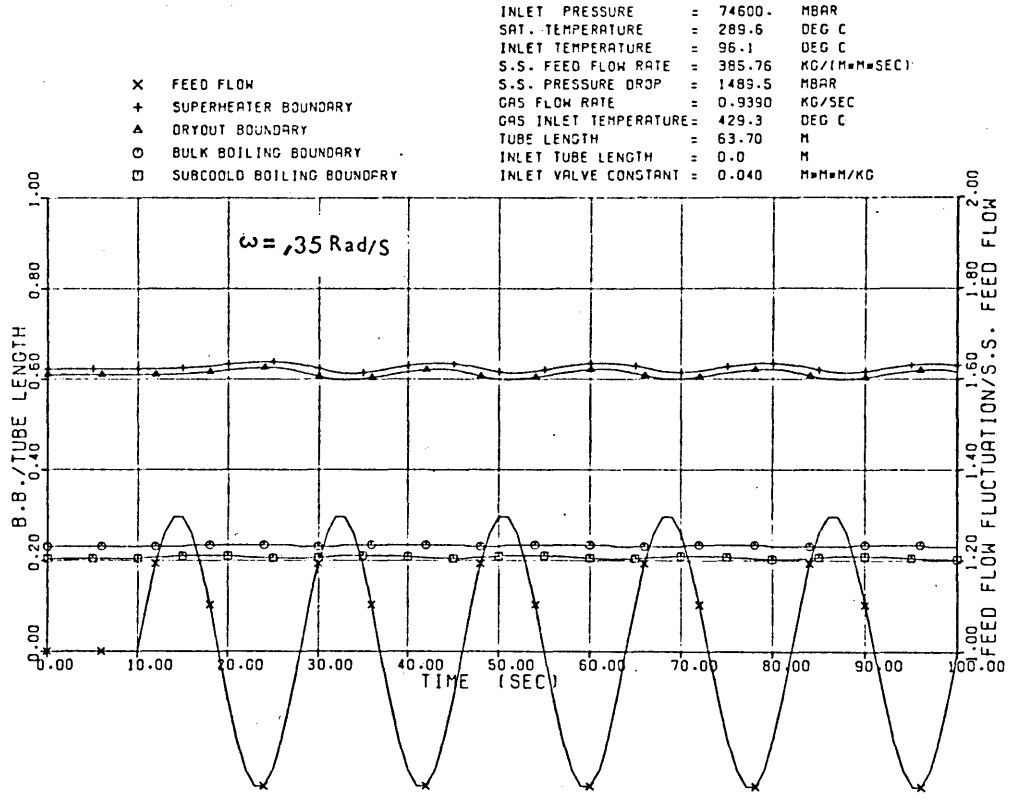


FIG.(6.20a) BOILING BOUNDARIES RESPONSE TO FORCED OSCILLATOIN FEED FLOW

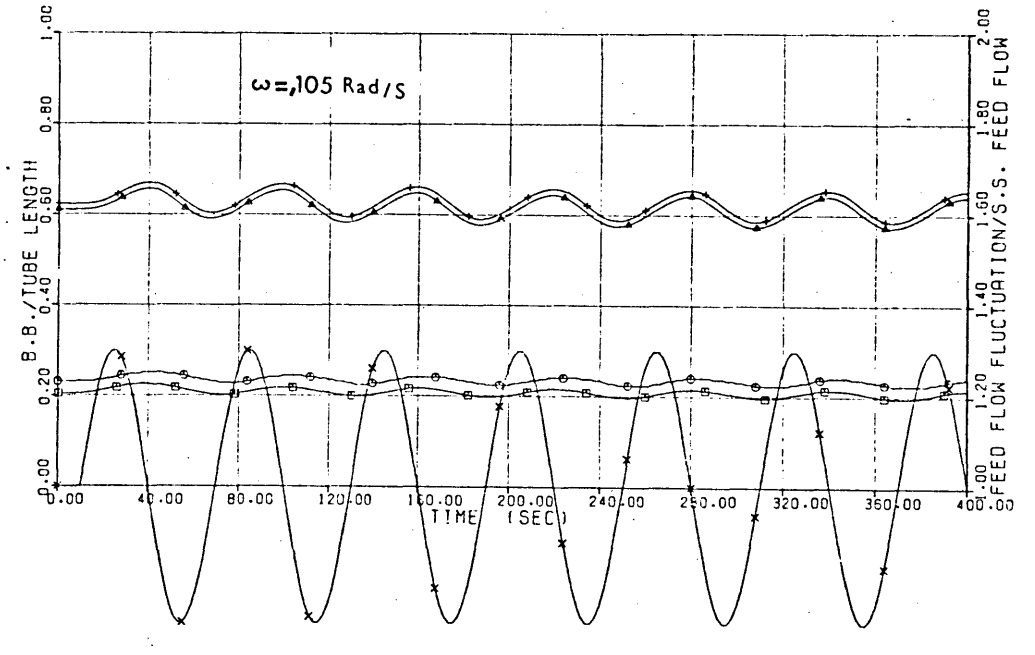
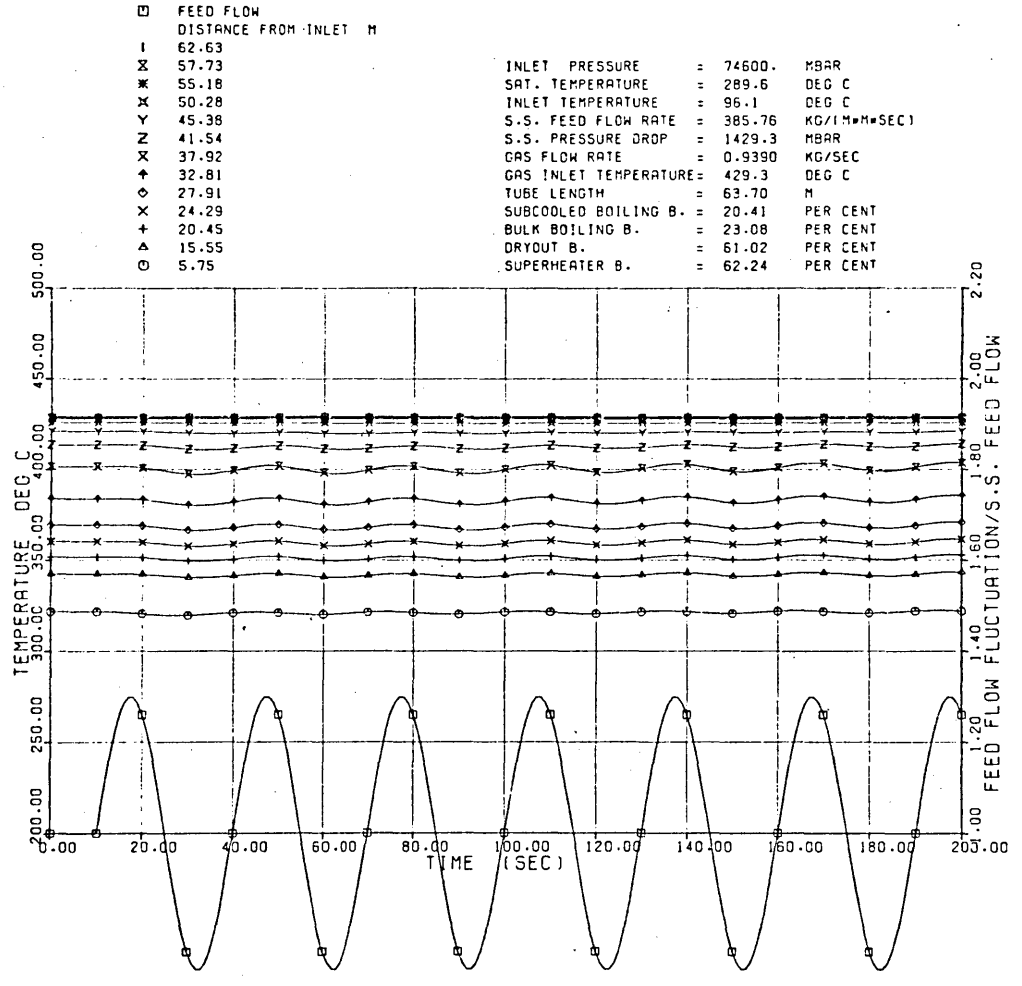
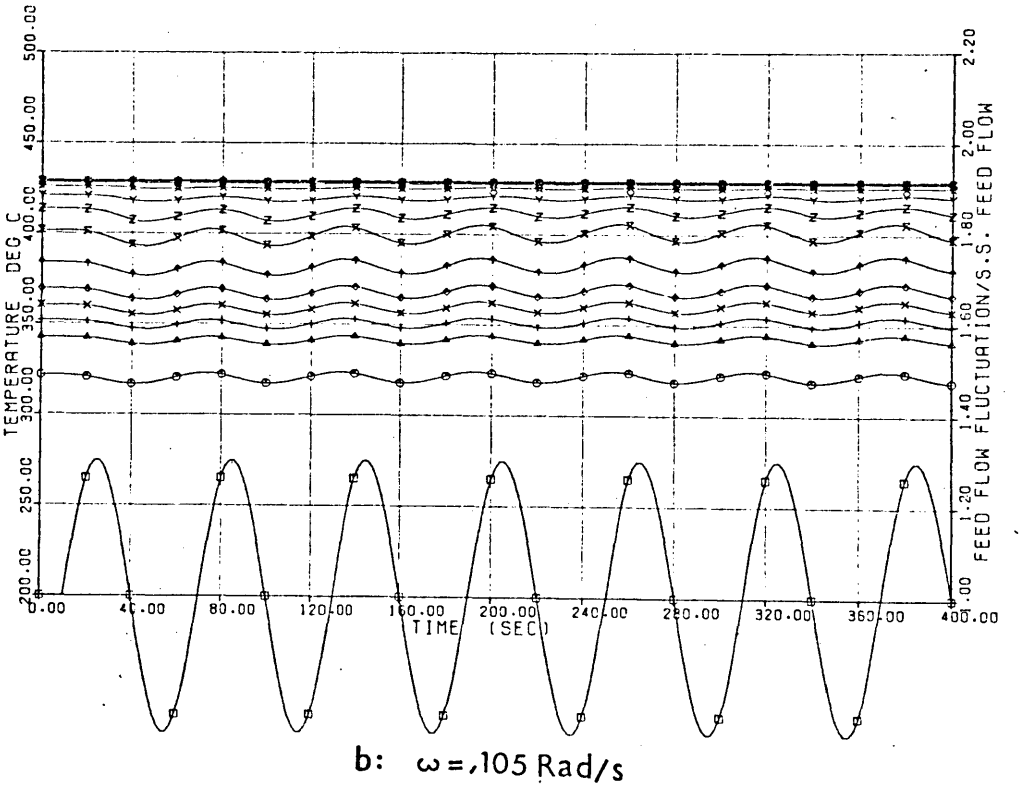


FIG.(6.20b) BOILING BOUNDARIES RESPONSE TO FORCED OSCILLATOIN FEED FLOW

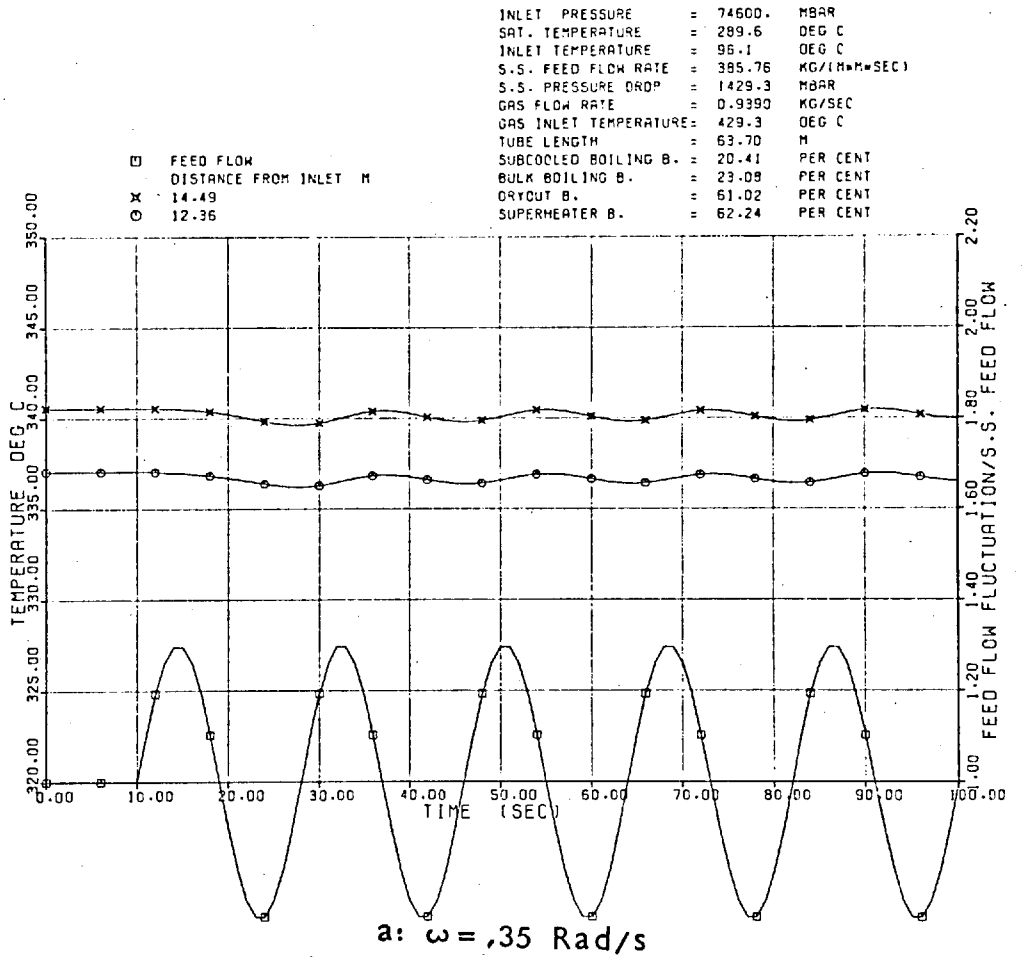


a: $\omega = ,21$ Rad/s

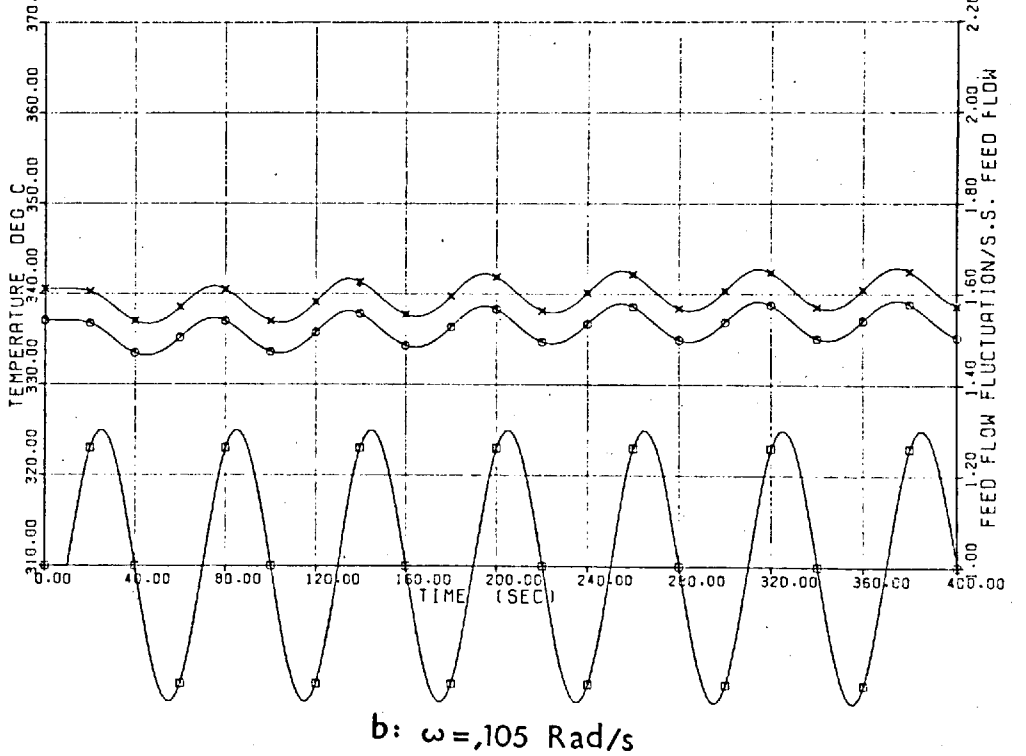


b: $\omega = ,105$ Rad/s

FIG.(6-21) PRIMARY FLUID TEMPERATURES AT FIXED POSITIONS ALONG THE TUBE



a: $\omega = ,35$ Rad/s



b: $\omega = ,105$ Rad/s

FIG.(6.22) PRIMARY FLUID TEMPERATURES AT FIXED POSITIONS NEAR SUBCOOLED AND BULK BOILING BOUNDARIES

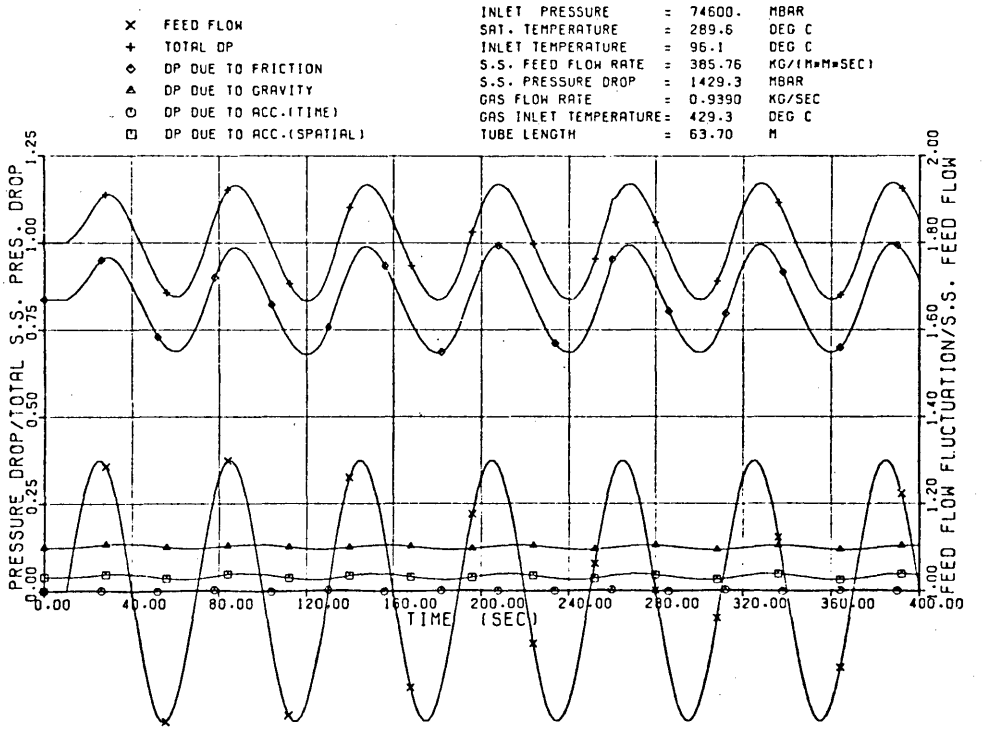


FIG.(6.23a) DIFFERENT COMPONENTS OF PRESSURE DROP

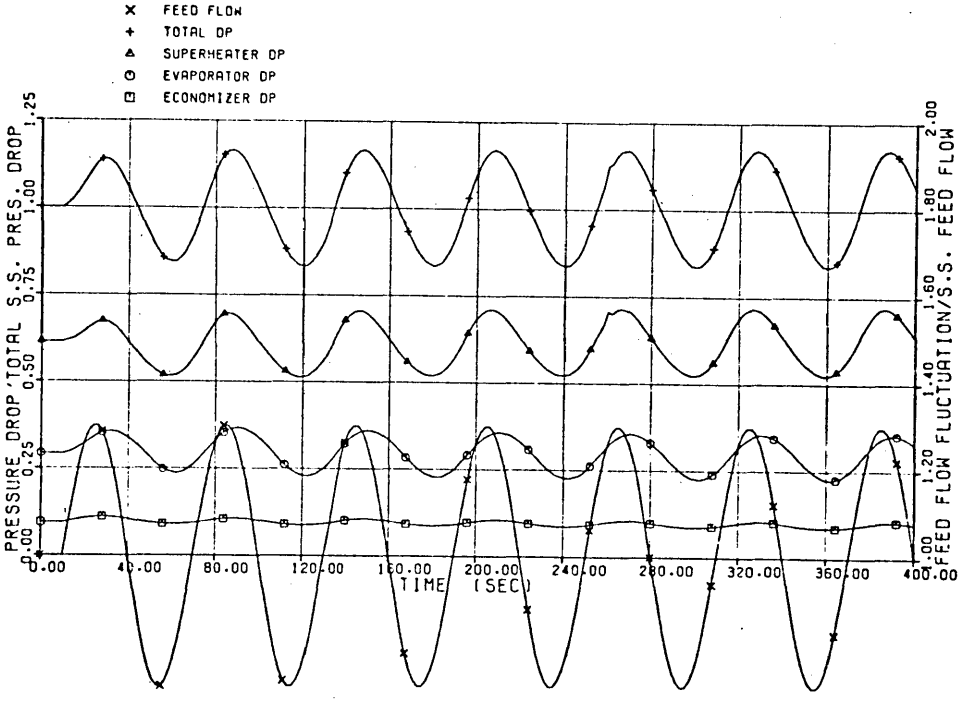


FIG.(6.23b) PRESSURE DROP OF DIFFERENT REGIONS ALONG THE TUBE

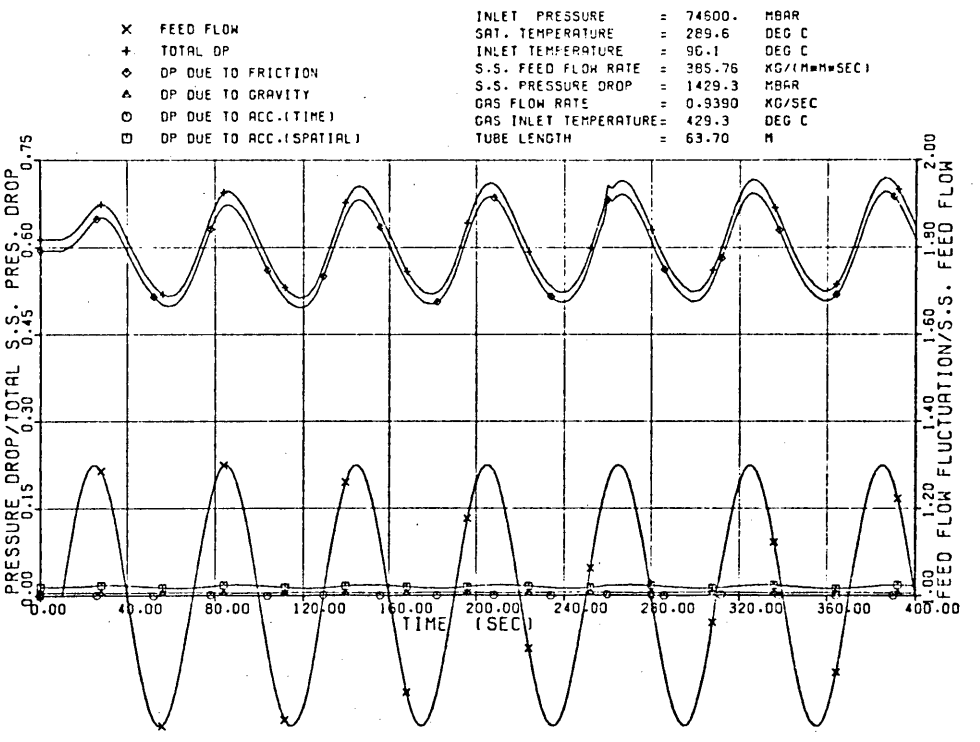


FIG.(6.24a) DIFFERENT COMPONENTS OF SUPERHEATER PRESSURE DROP

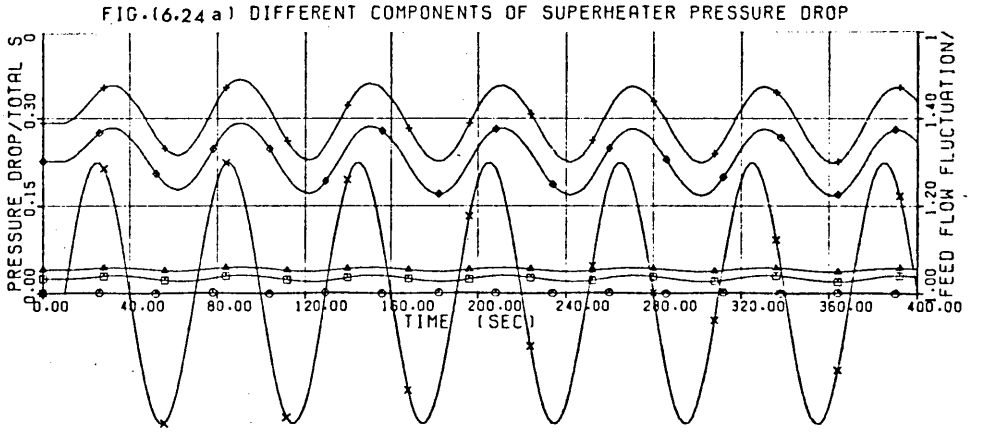


FIG.(6.24b) DIFFERENT COMPONENTS OF EVAPORATOR PRESSURE DROP

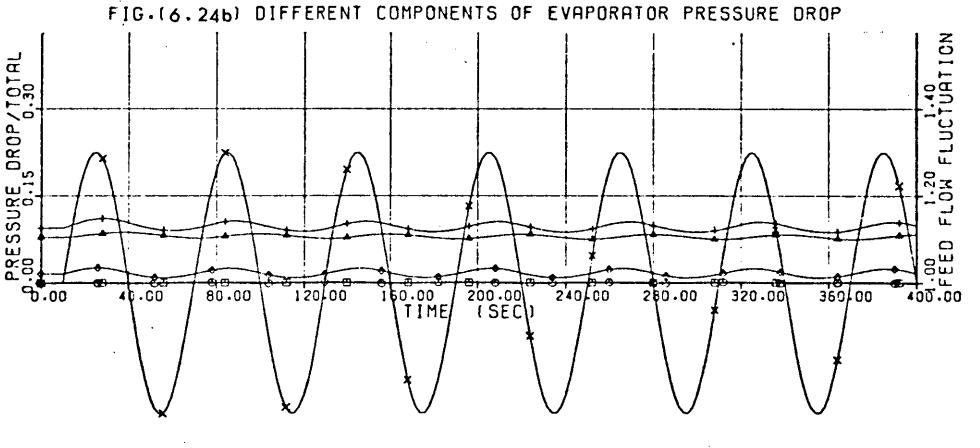


FIG.(6.24c) DIFFERENT COMPONENTS OF ECONOMIZER PRESSURE DROP

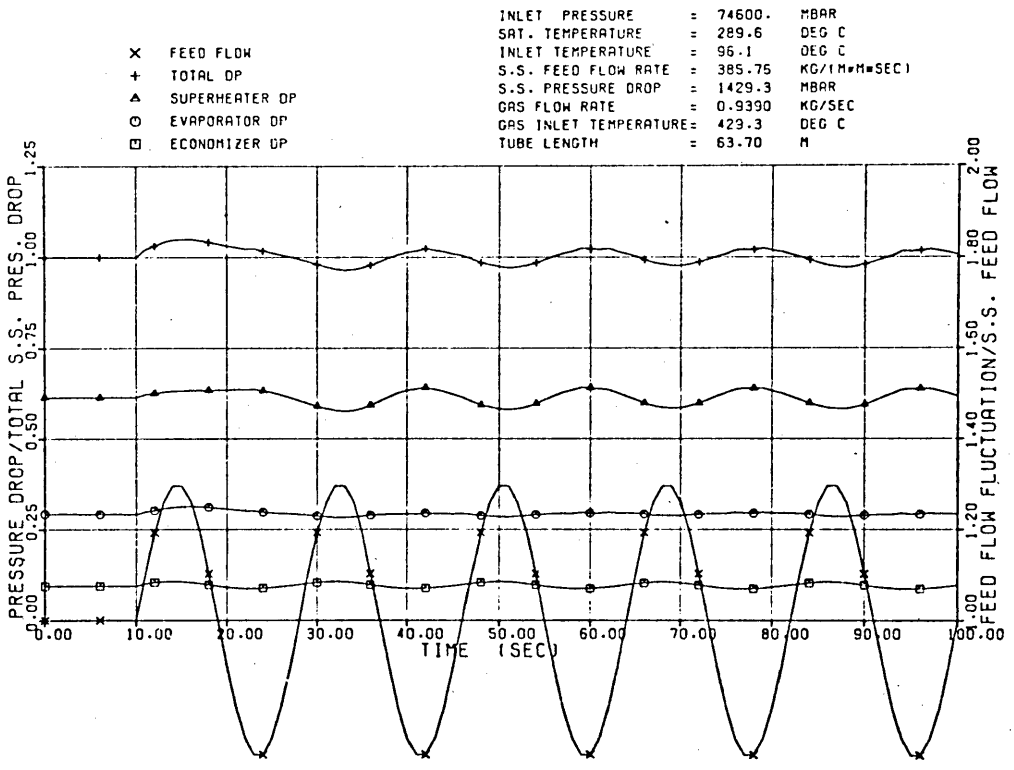


FIG.(6.25a) PRESSURE DROP OF DIFFERENT REGIONS ALONG THE TUBE

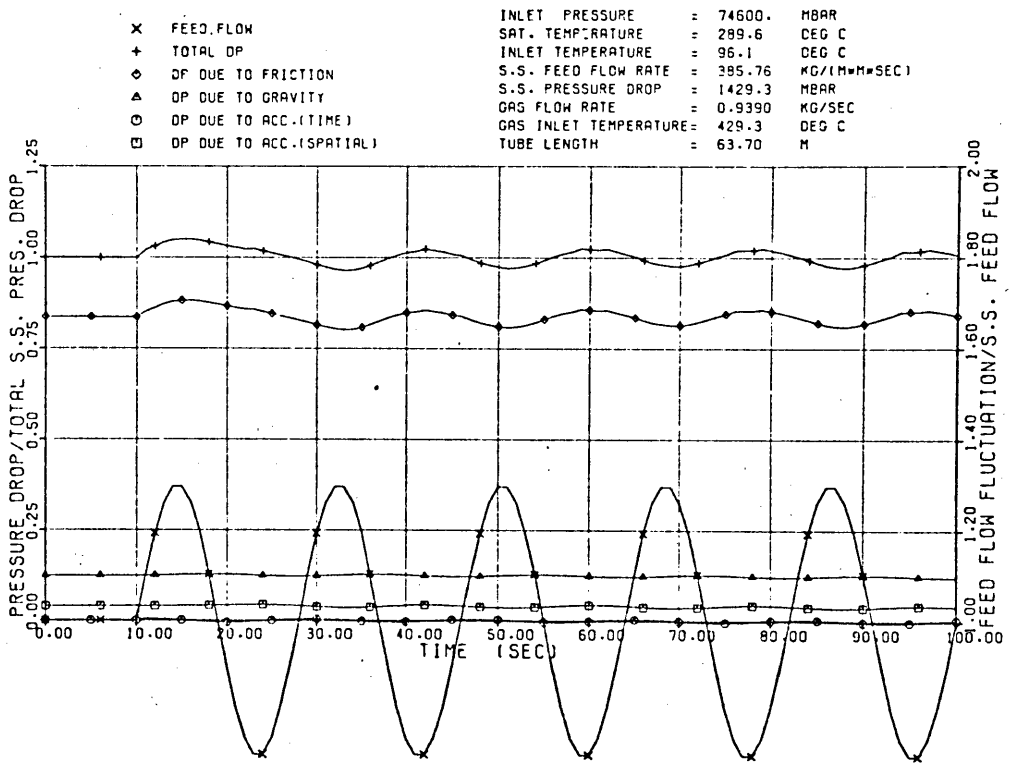


FIG.(6.25b) DIFFERENT COMPONENTS OF PRESSURE DROP

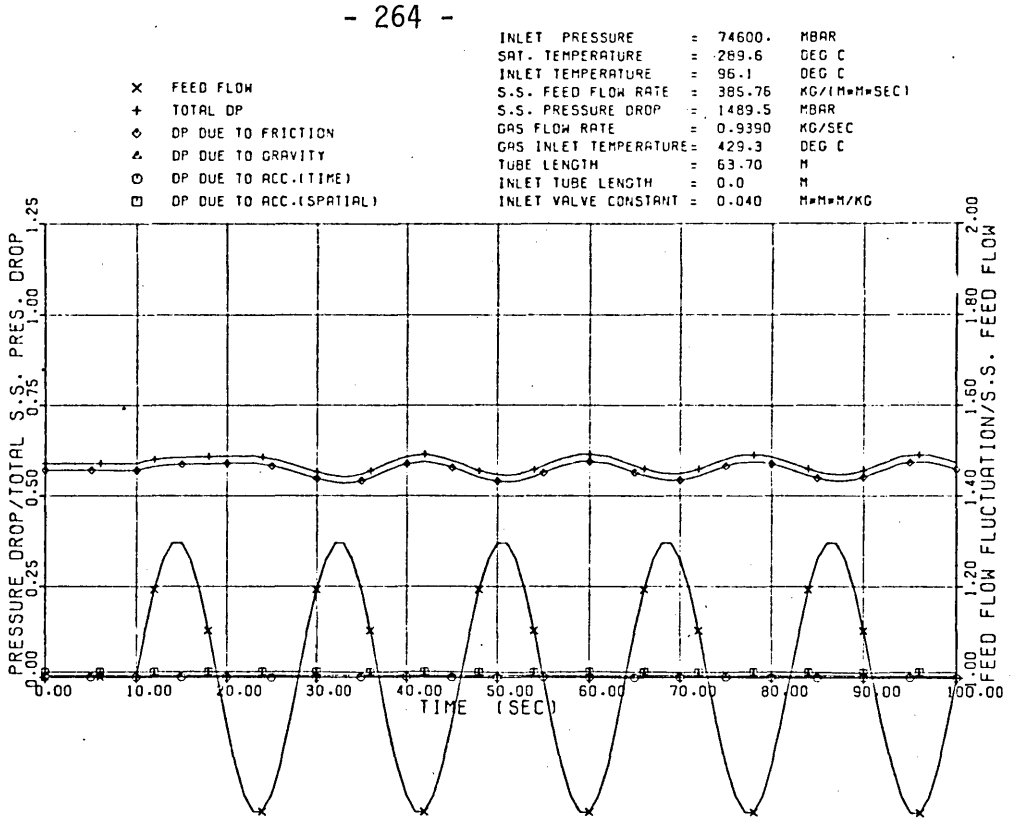


FIG.(6.26a) DIFFERENT COMPONENTS OF SUPERHEATER PRESSURE DROP

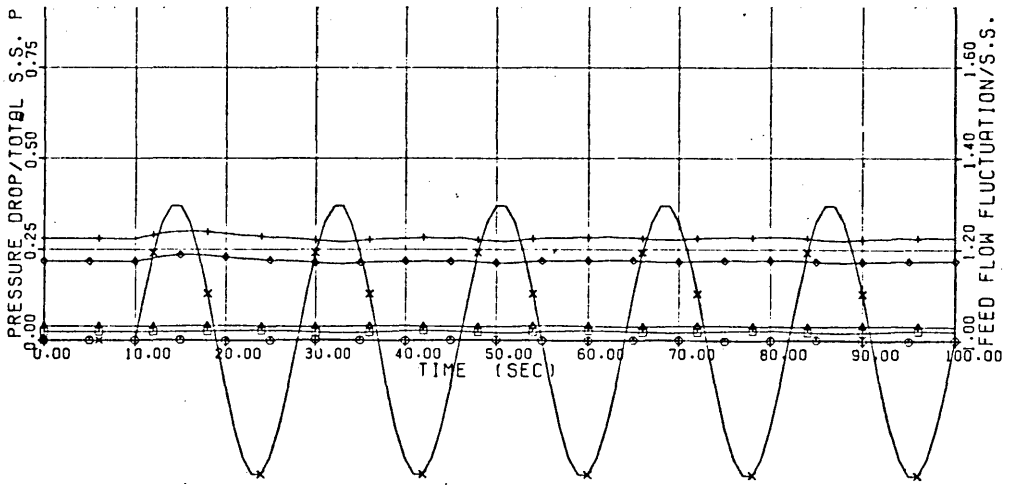


FIG.(6.26b) DIFFERENT COMPONENTS OF EVAPORATOR PRESSURE DROP

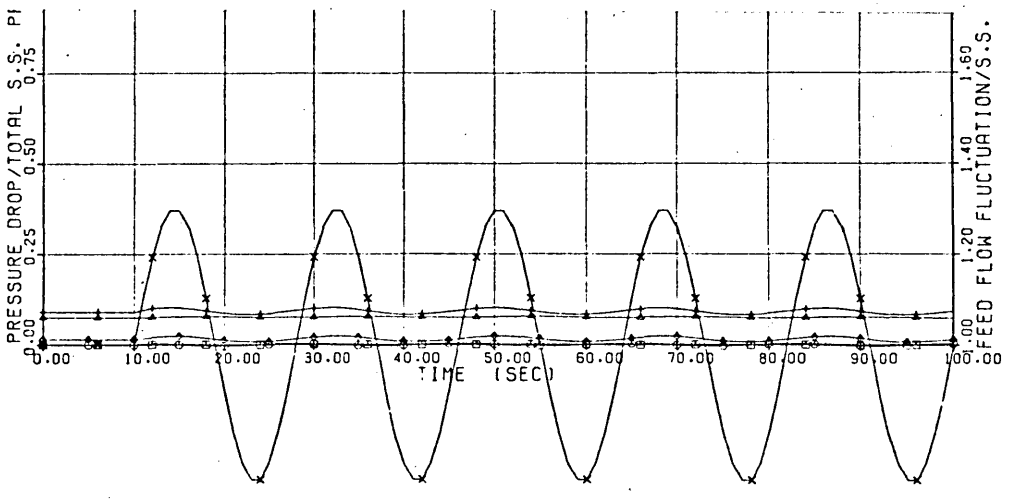


FIG.(6.26c) DIFFERENT COMPONENTS OF ECONOMIZER PRESSURE DROP

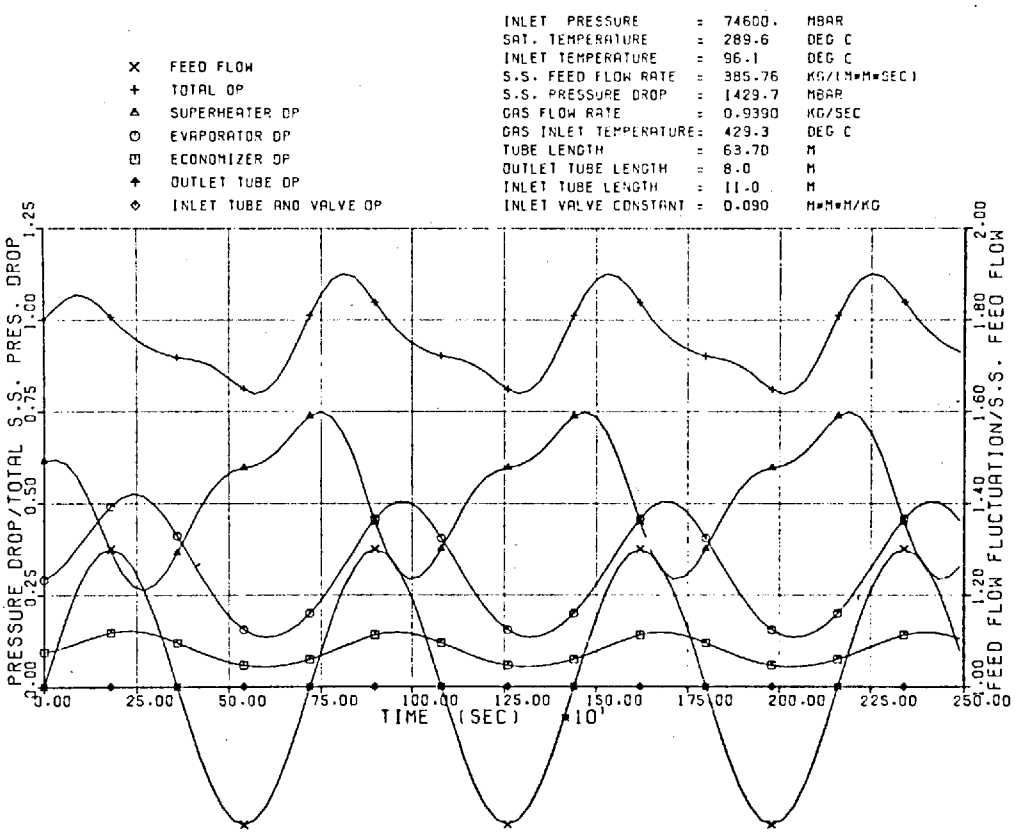


FIG.(6.27a) PRESSURE DROP OF DIFFERENT REGIONS ALONG THE TUBE

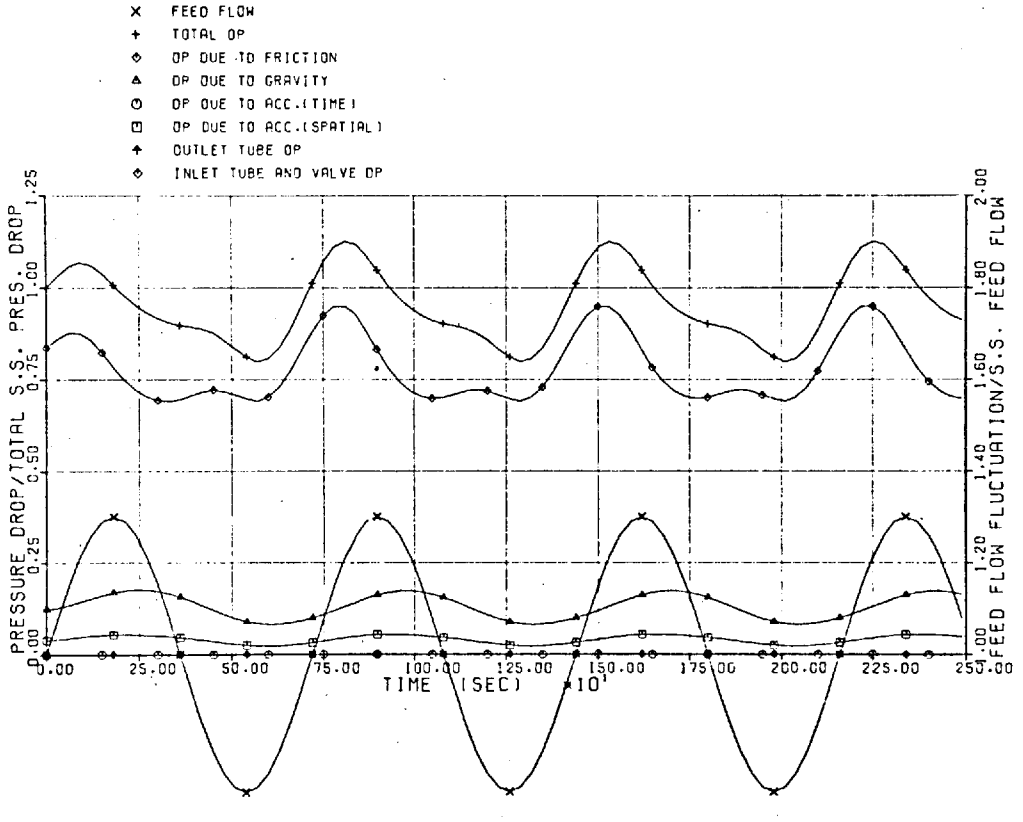


FIG.(6.27b) DIFFERENT COMPONENTS OF PRESSURE DROP

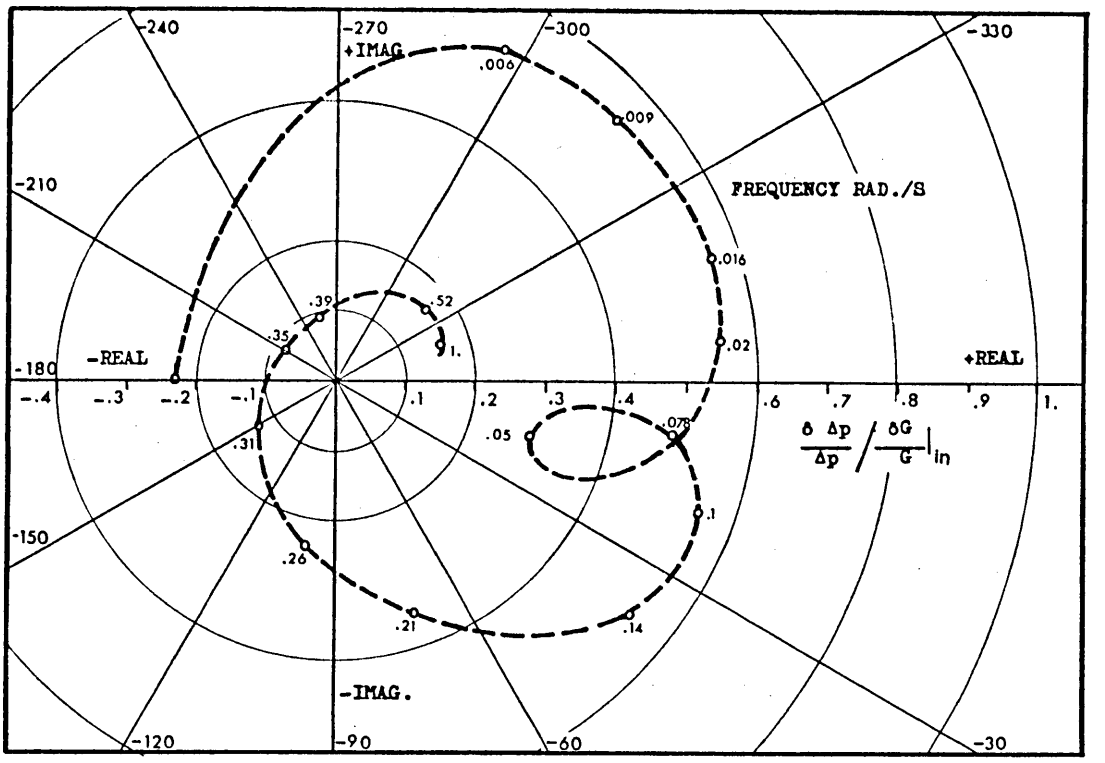


Figure 6.30: Frequency response of the total pressure drop to inlet mass velocity oscillation (Condition No. 1, Table 6.1)

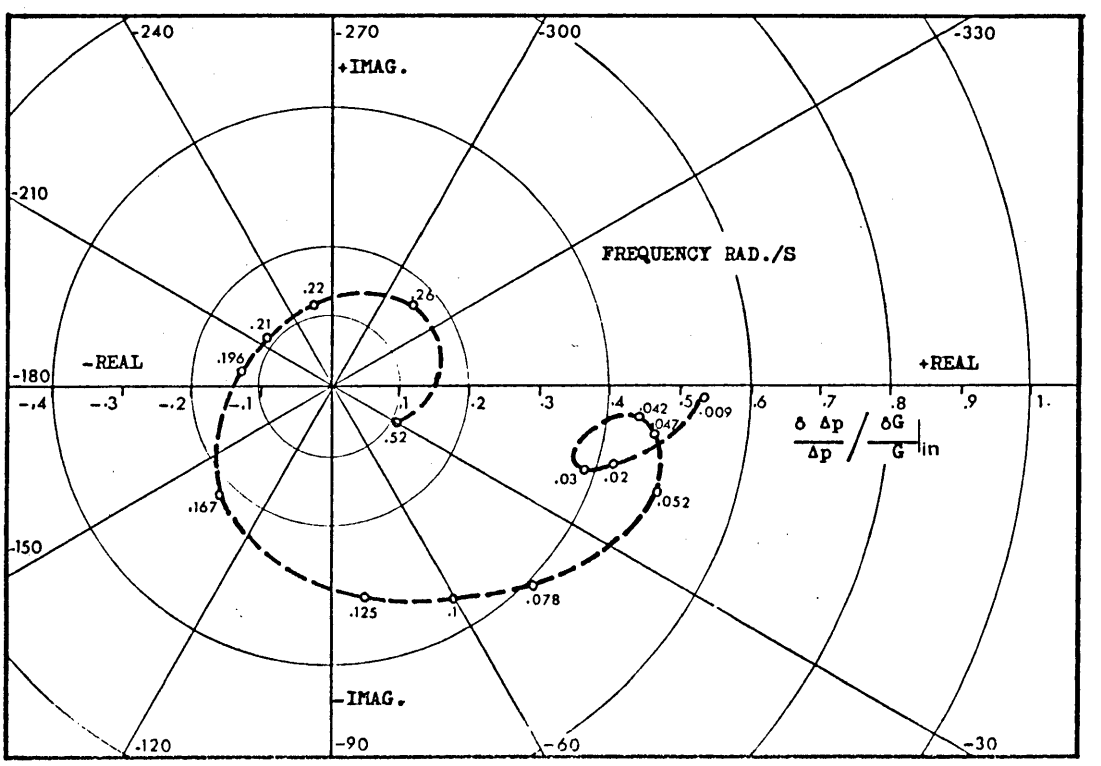
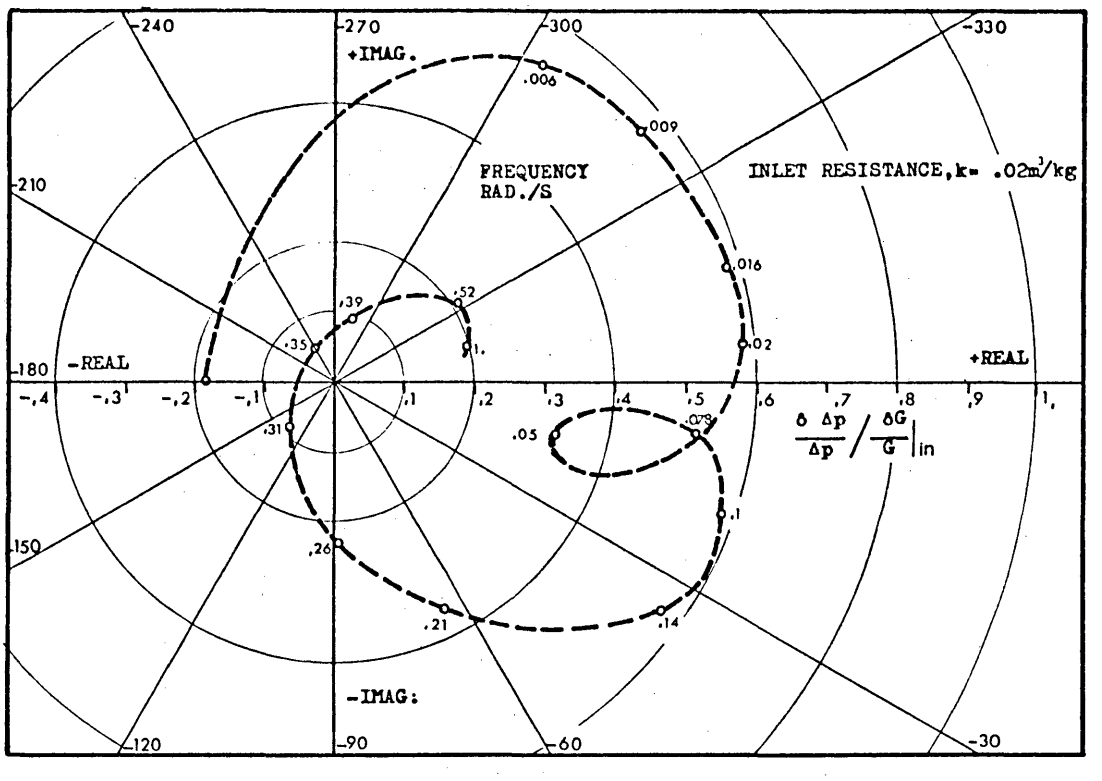
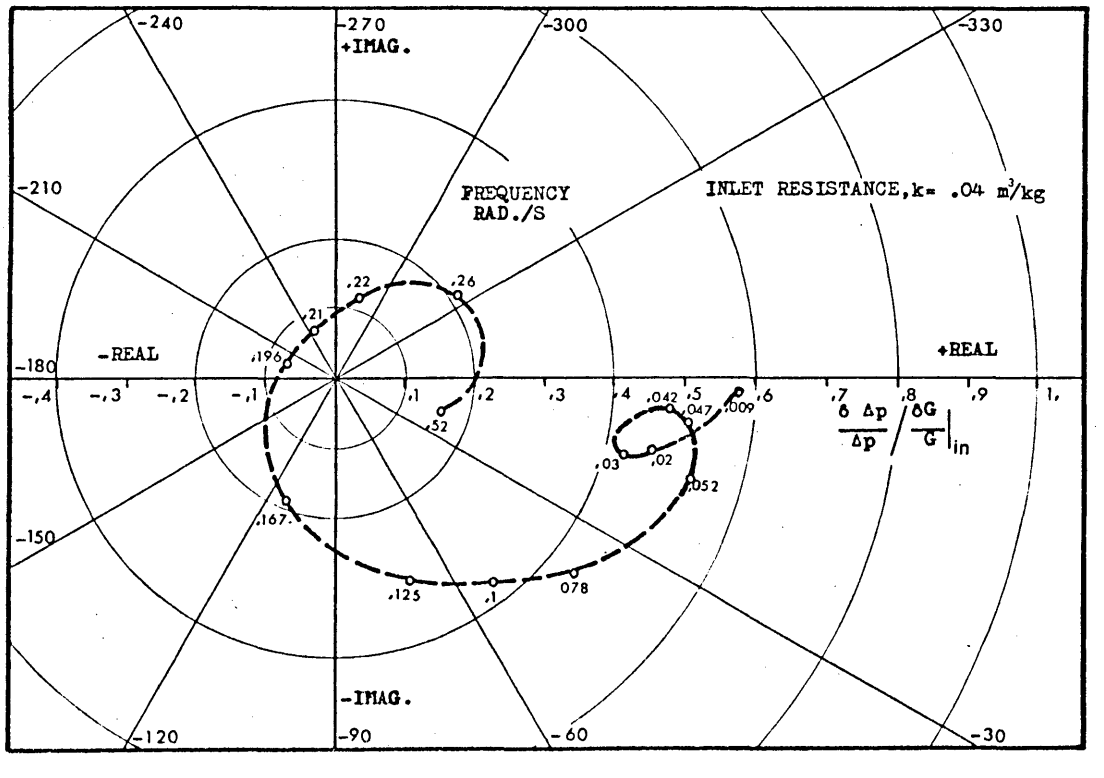


Figure 6.31: Frequency response of the total pressure drop to inlet mass velocity oscillation (Condition No. 2, Table 6.1)



(a) Condition No. 1, Table 6.1



(b) Condition No. 2, Table 6.1

Figure 6.32: Effect of increase of inlet resistance on frequency response curves

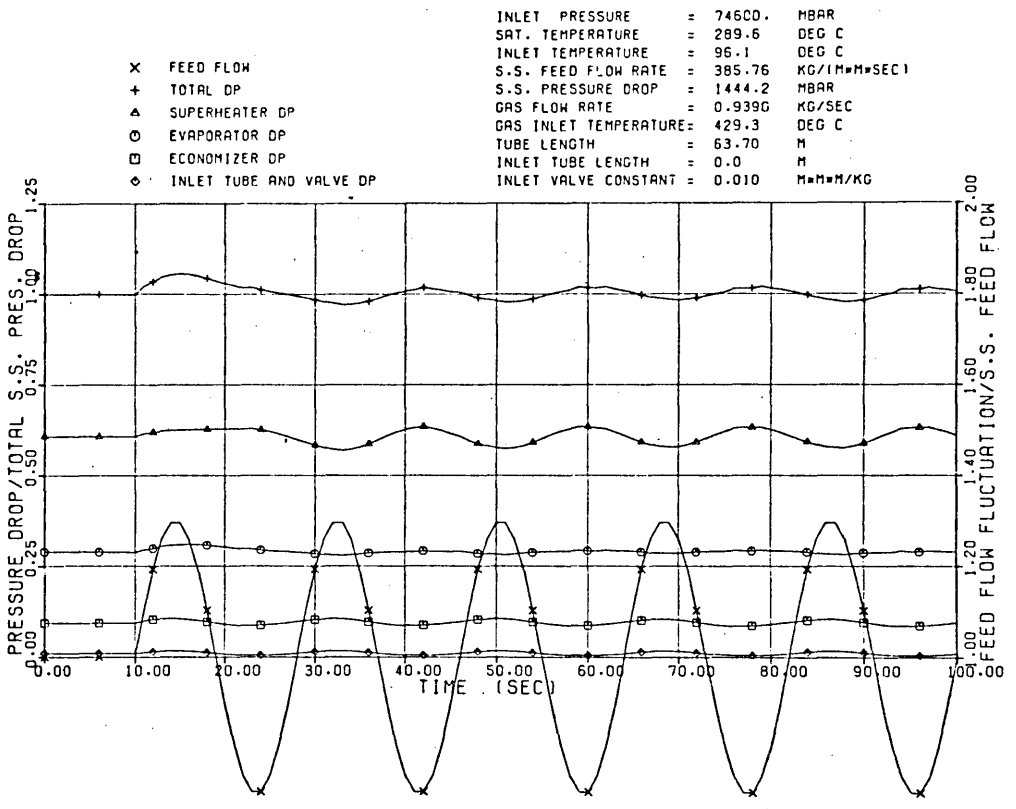


FIG.(6.33a) PRESSURE DROP OF DIFFERENT REGIONS ALONG THE TUBE

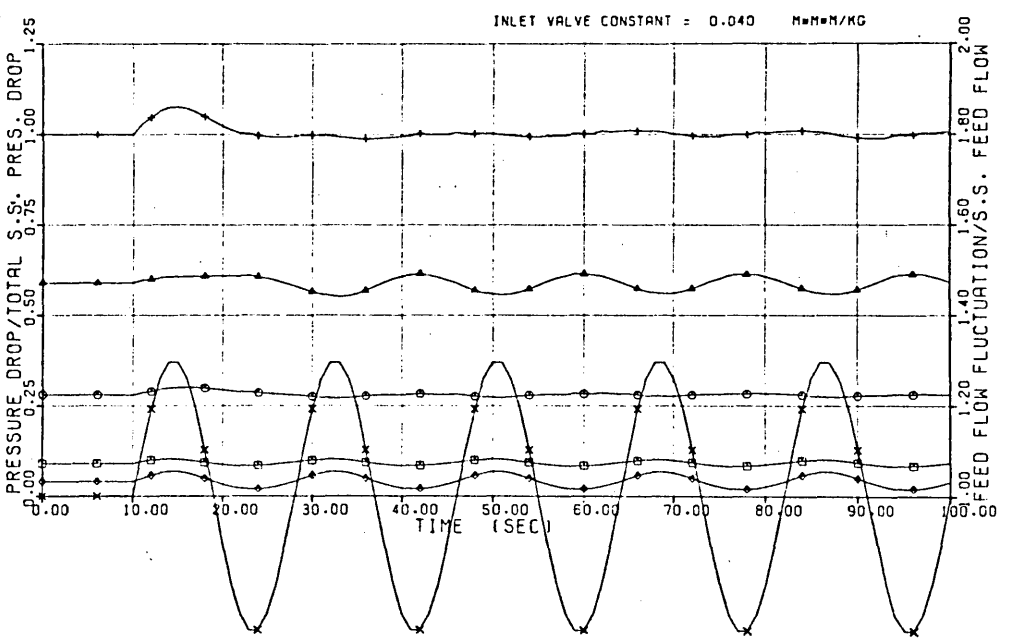


FIG.(6.33b) PRESSURE DROP OF DIFFERENT REGIONS ALONG THE TUBE

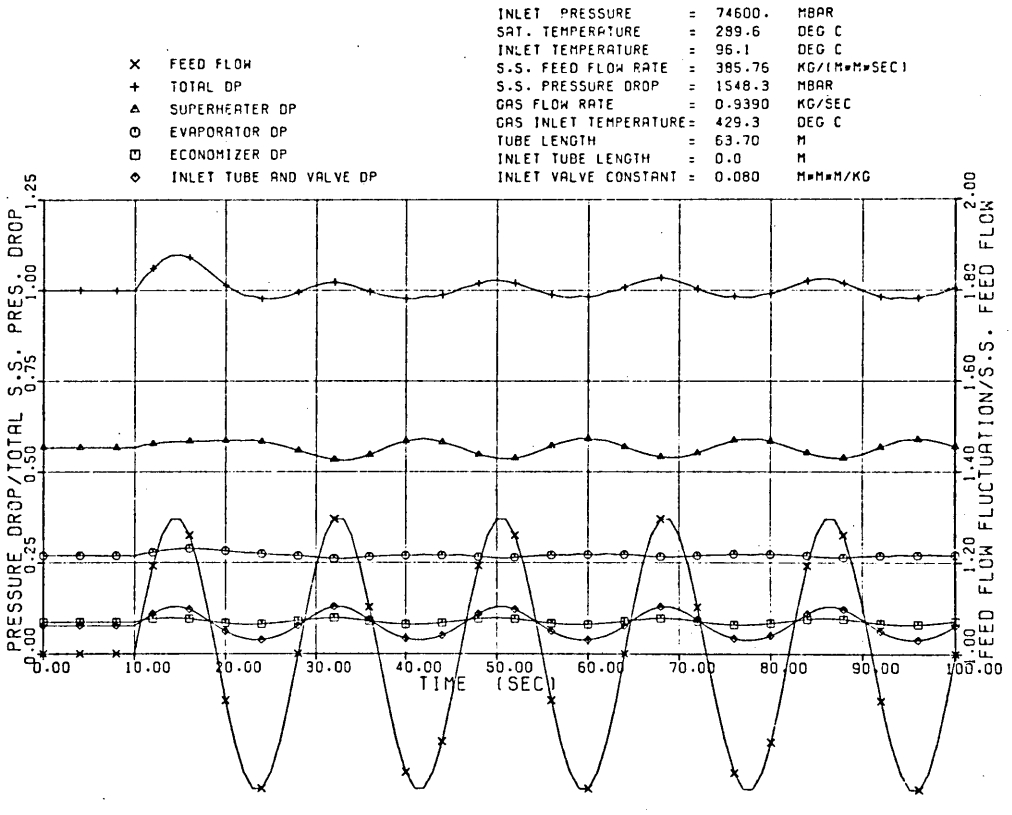


FIG.(6.34a) PRESSURE DROP OF DIFFERENT REGIONS ALONG THE TUBE

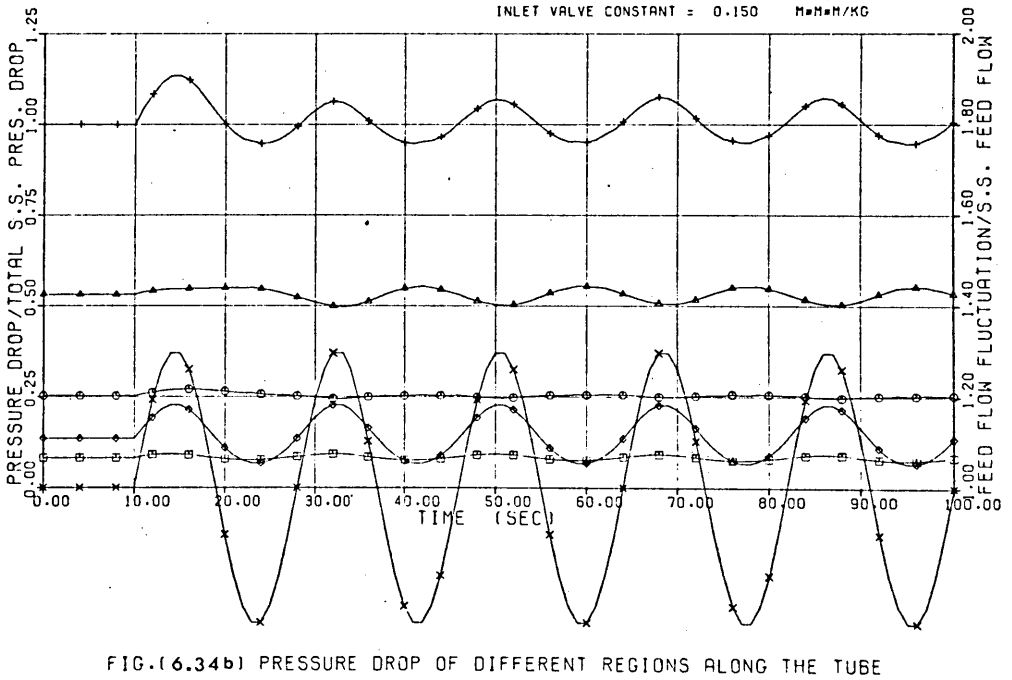
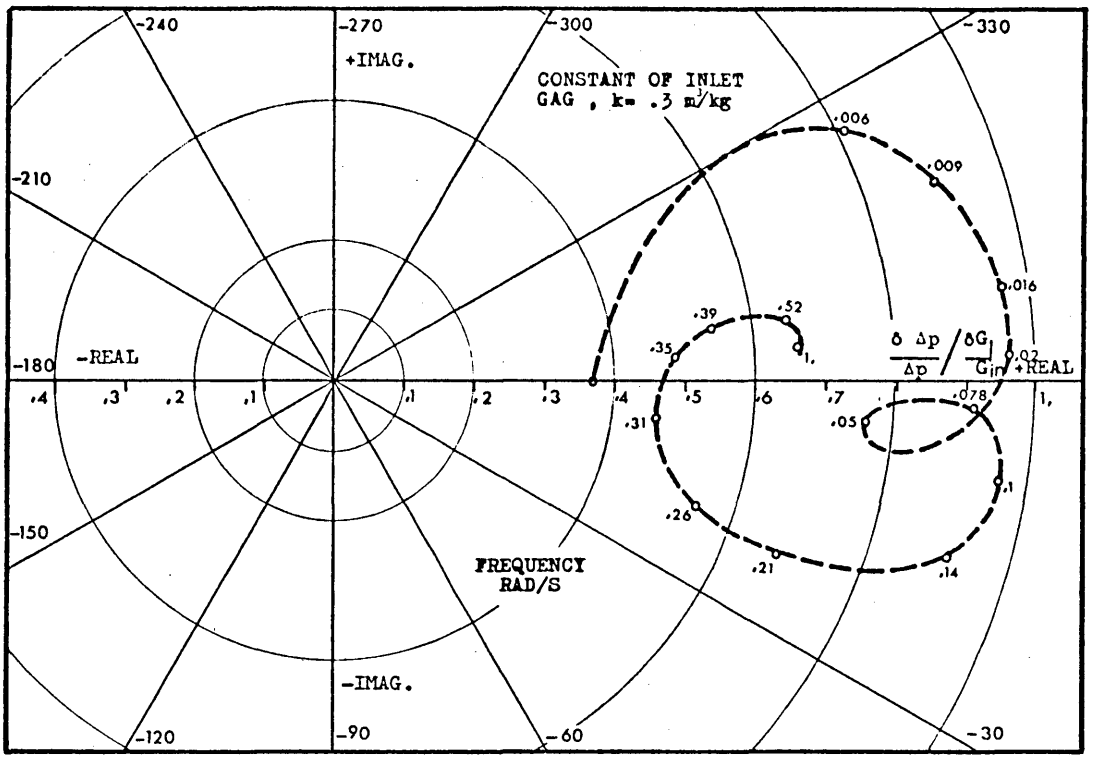
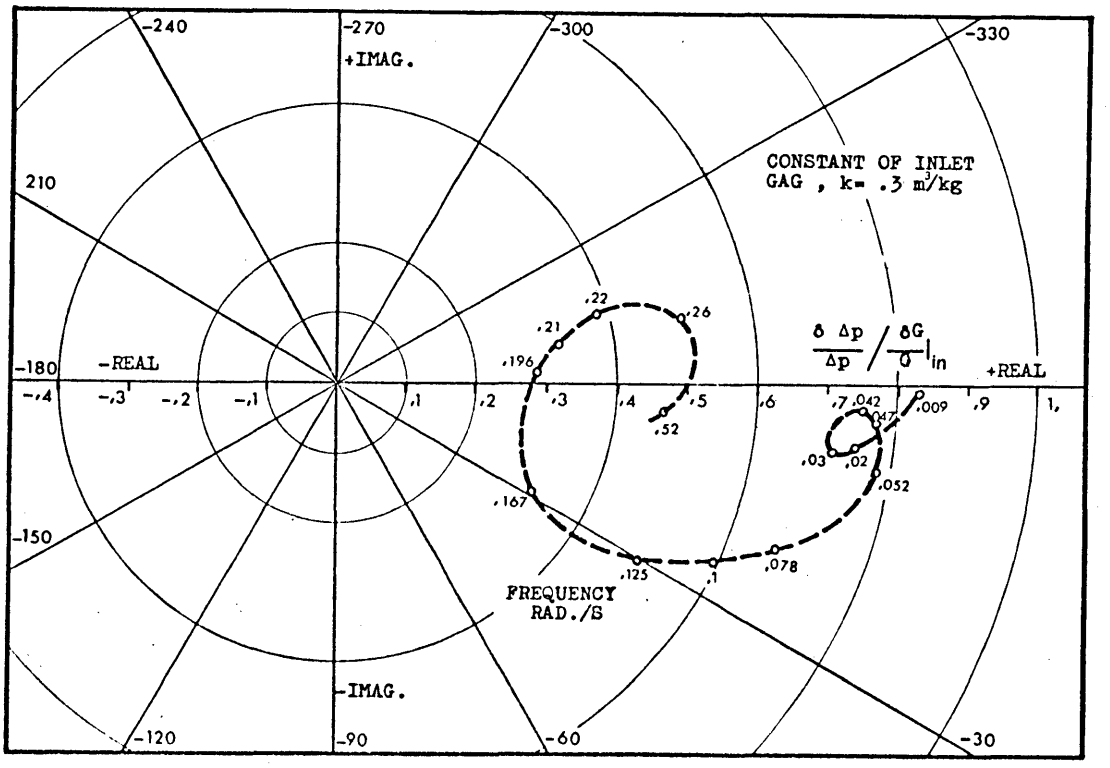


FIG.(6.34b) PRESSURE DROP OF DIFFERENT REGIONS ALONG THE TUBE



(a) Condition No. 1, Table 6.1



(b) Condition No. 2, Table 6.1

Figure 6.35: Effect of the inlet gagging on the open loop frequency response curves

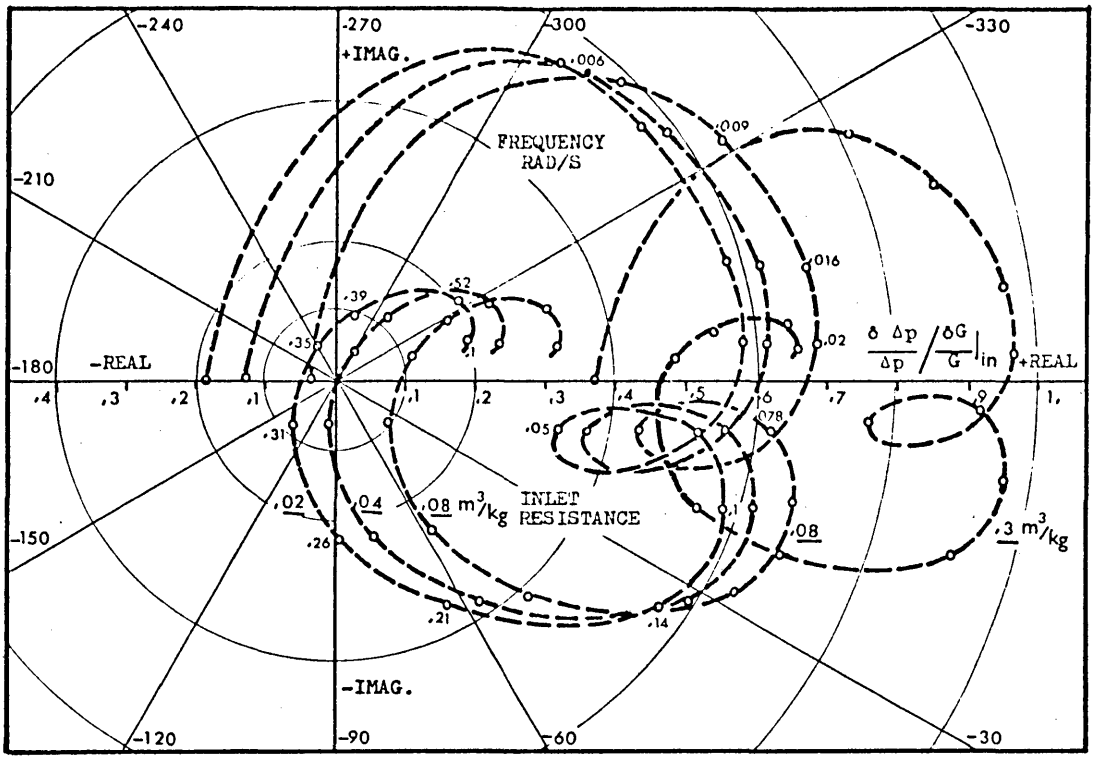


Figure 6.36: Onset of instability and effect of inlet resistance for condition No. 1, Table 6.1

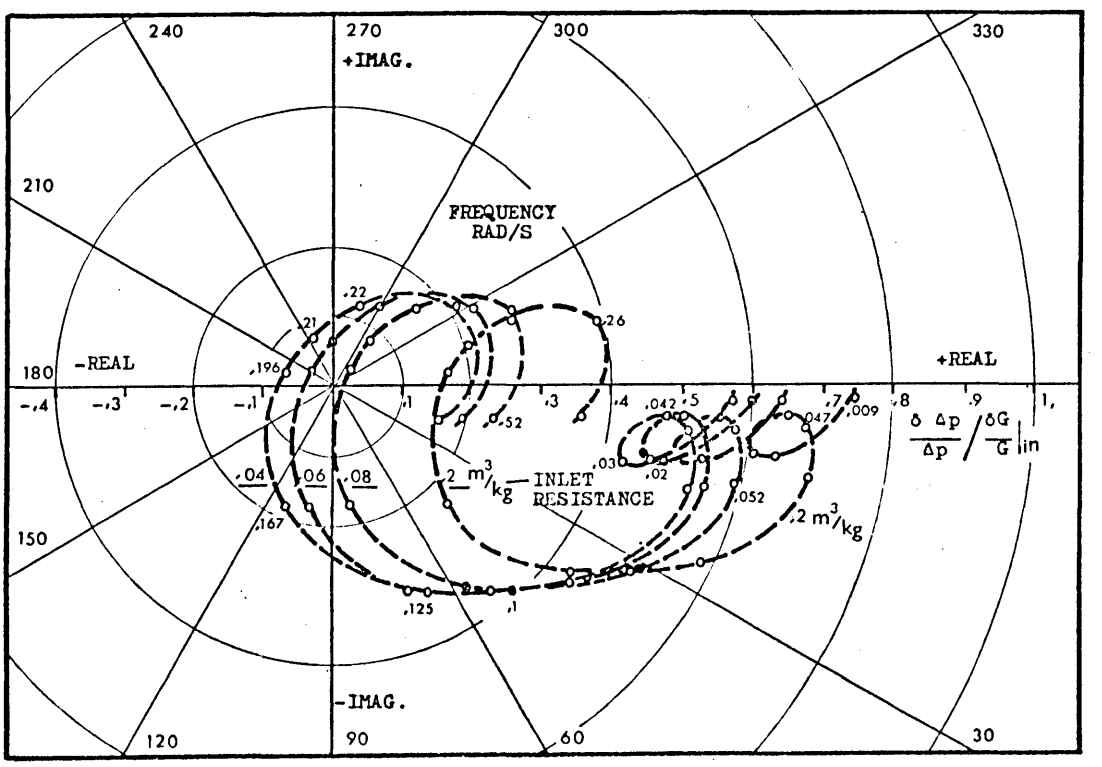


Figure 6.37: Onset of instability and effect of inlet resistance for condition No. 2, Table 6.1

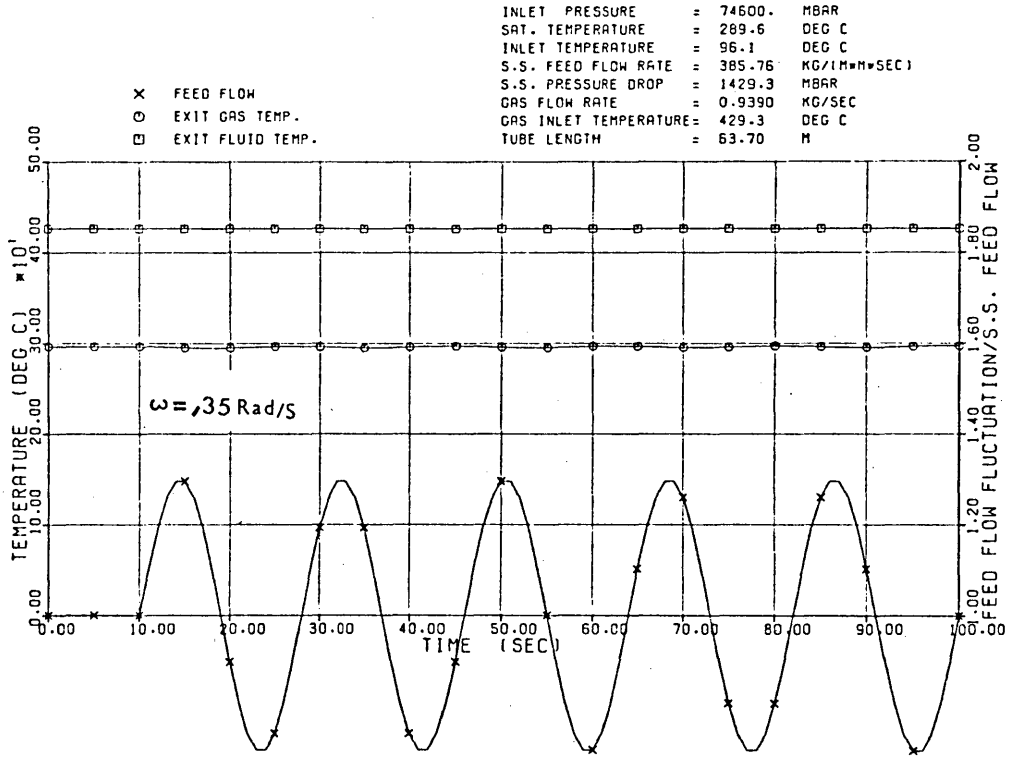


FIG.(6.38a) RESPONSE OF EXIT TEMPERATURES TO INLET MASS EXCITATION

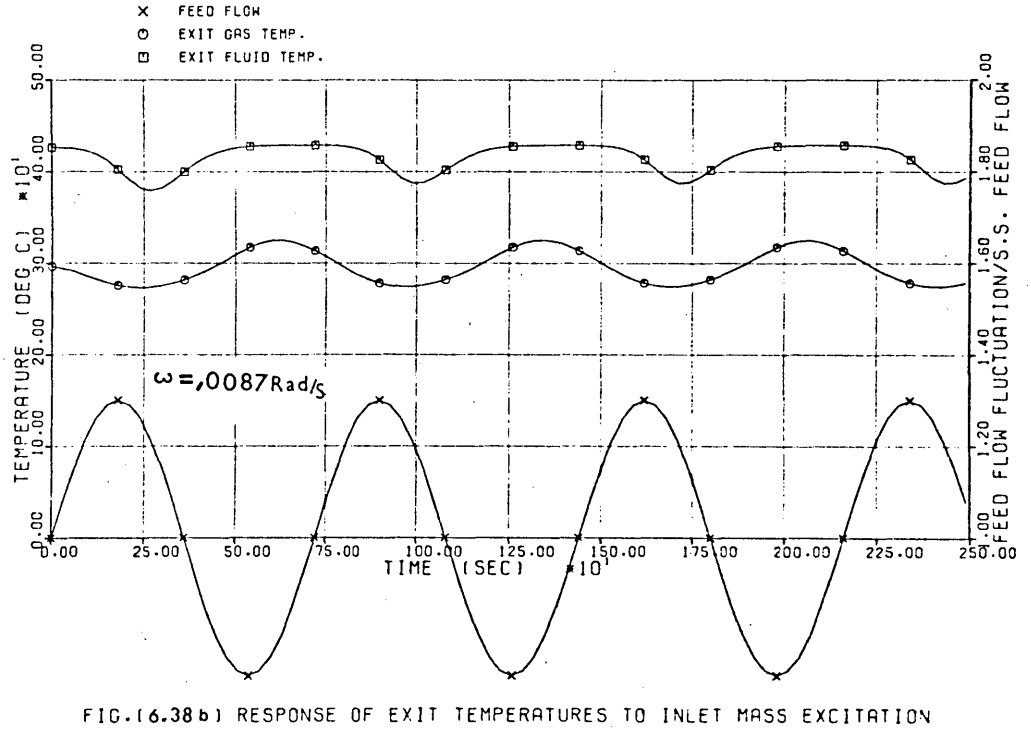
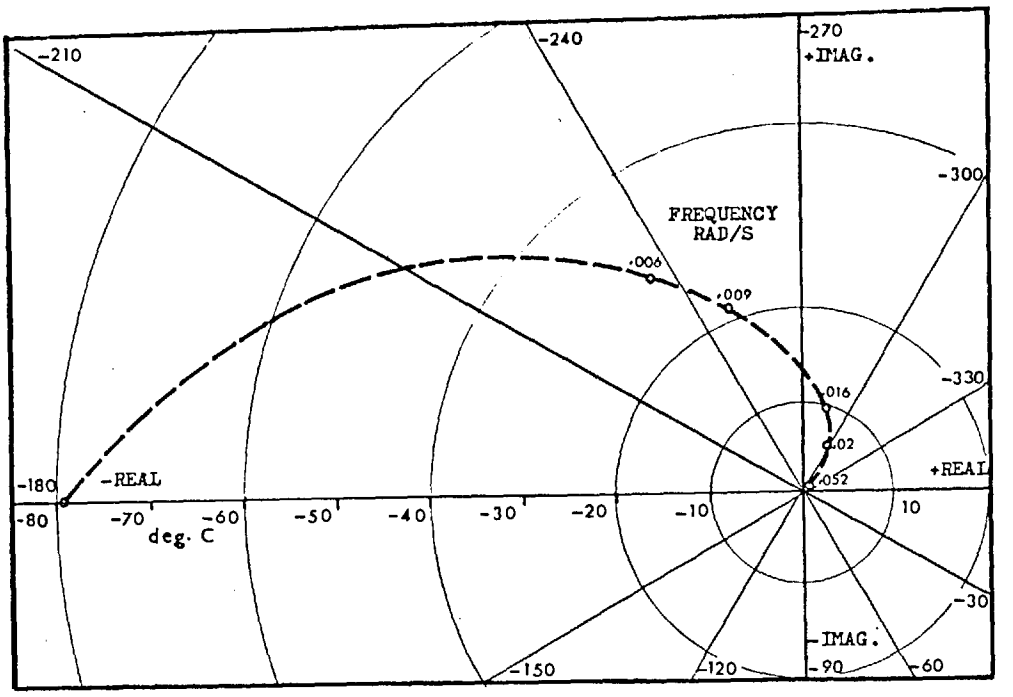
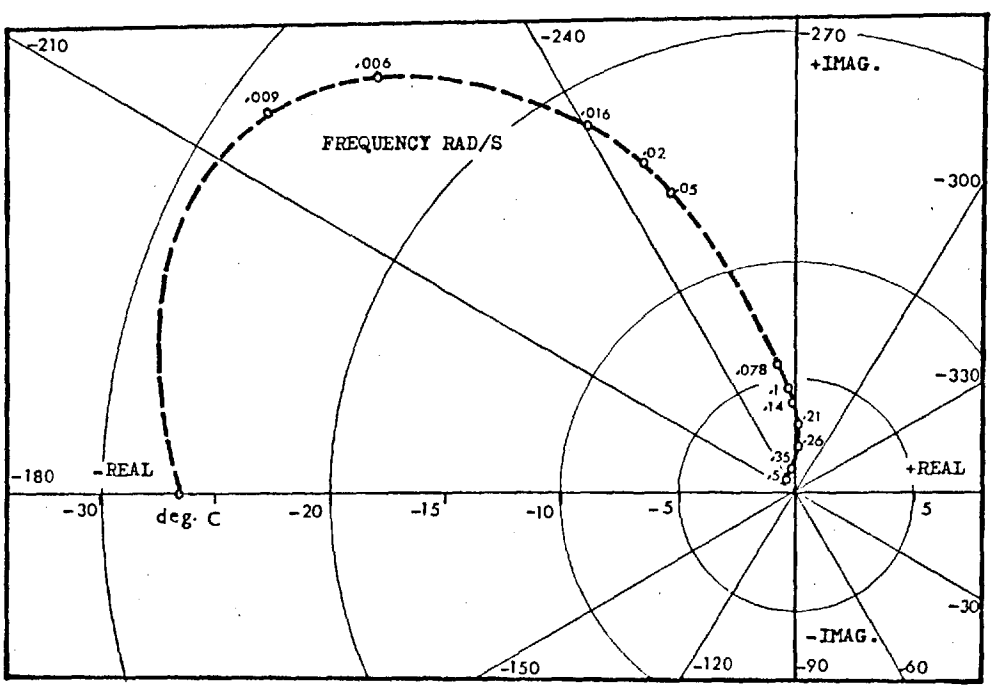


FIG.(6.38b) RESPONSE OF EXIT TEMPERATURES TO INLET MASS EXCITATION



(a) Steam temperature



(b) Gas temperature

Figure 6.39: Frequency response of the outlet temperatures to inlet mass velocity oscillation. Condition No. 1, Table 6.1

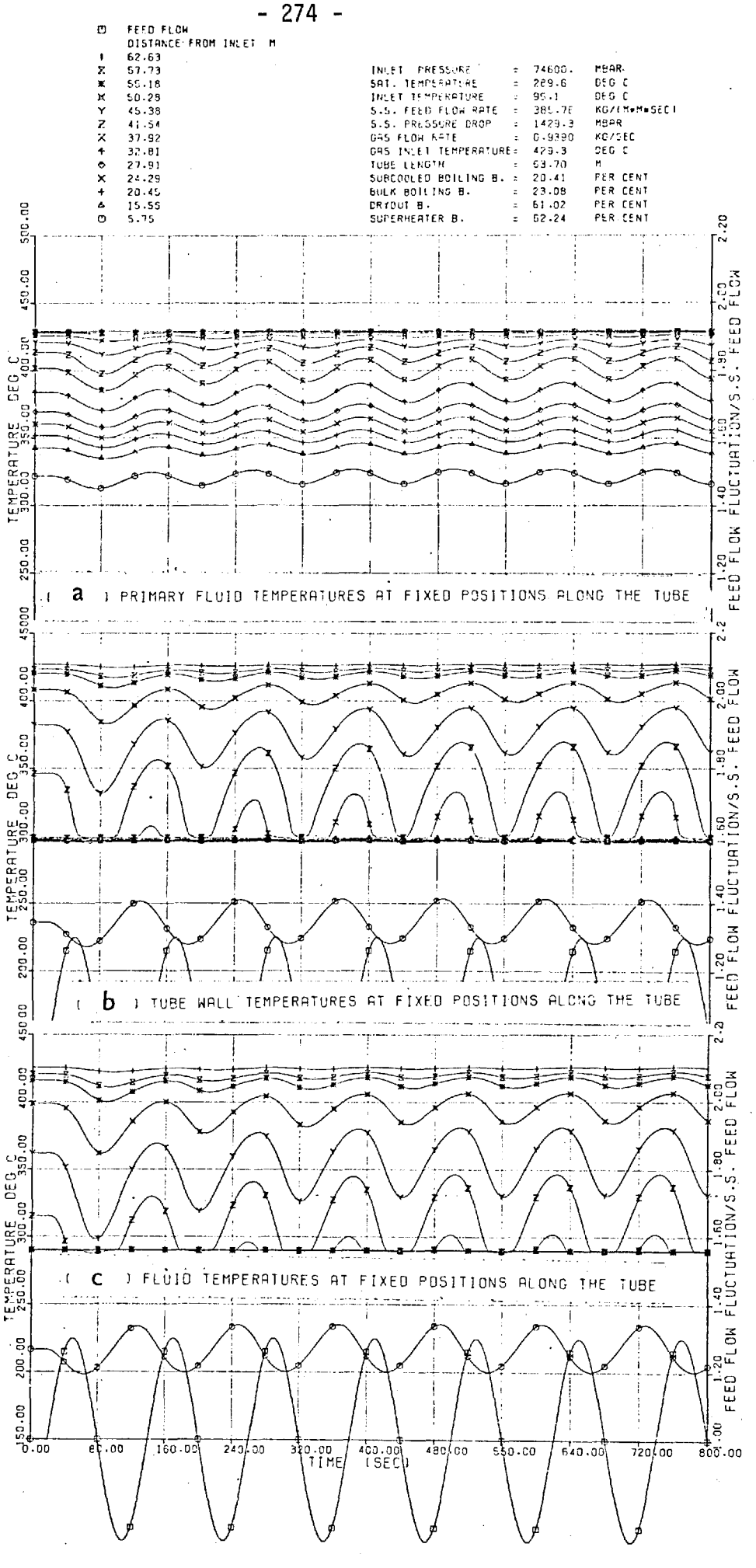


Figure 6.40: Temperature variation at fixed positions along the tube

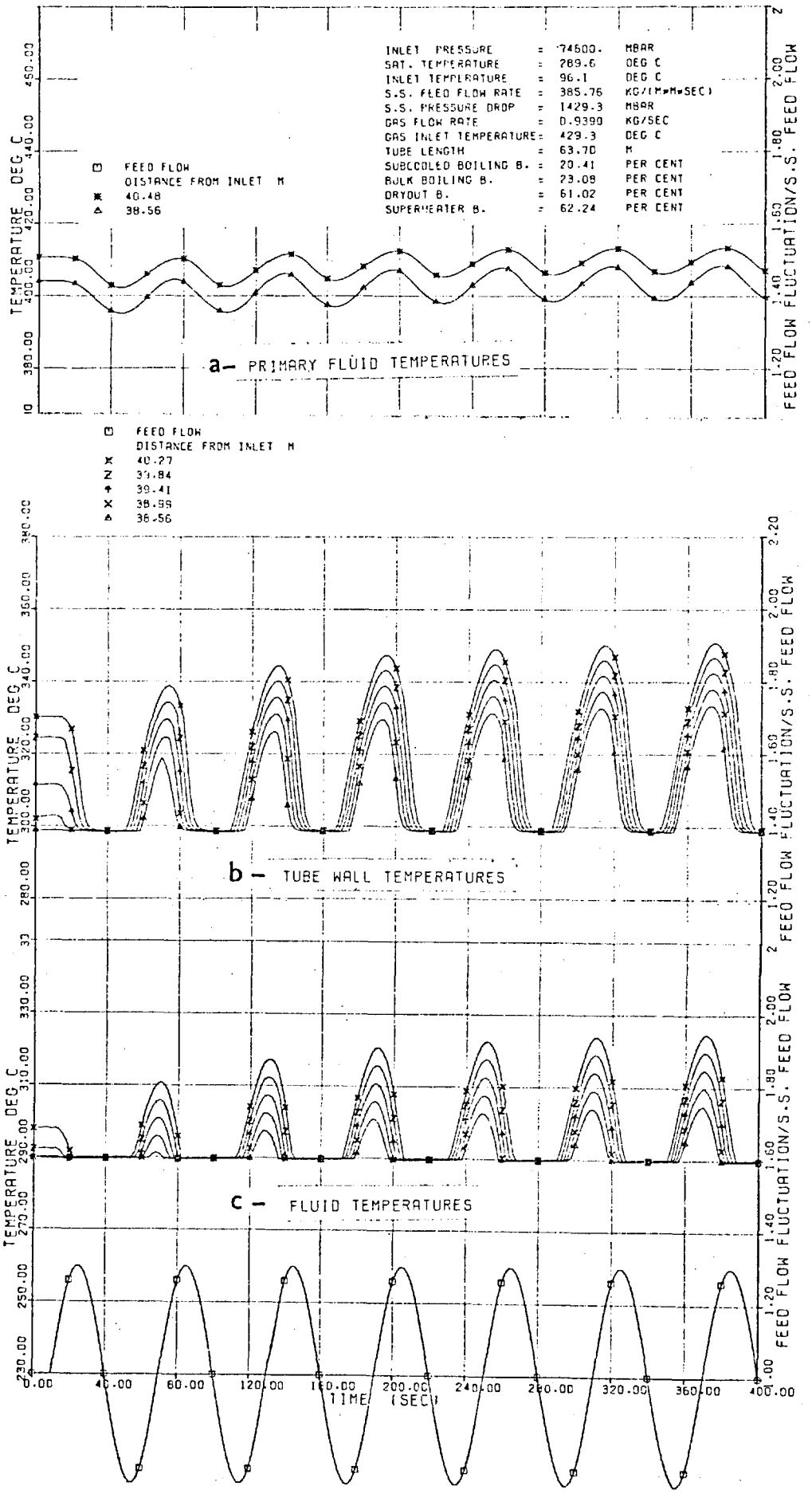


Figure 6.41: Temperature variation at fixed positions near dryout and superheater boundaries

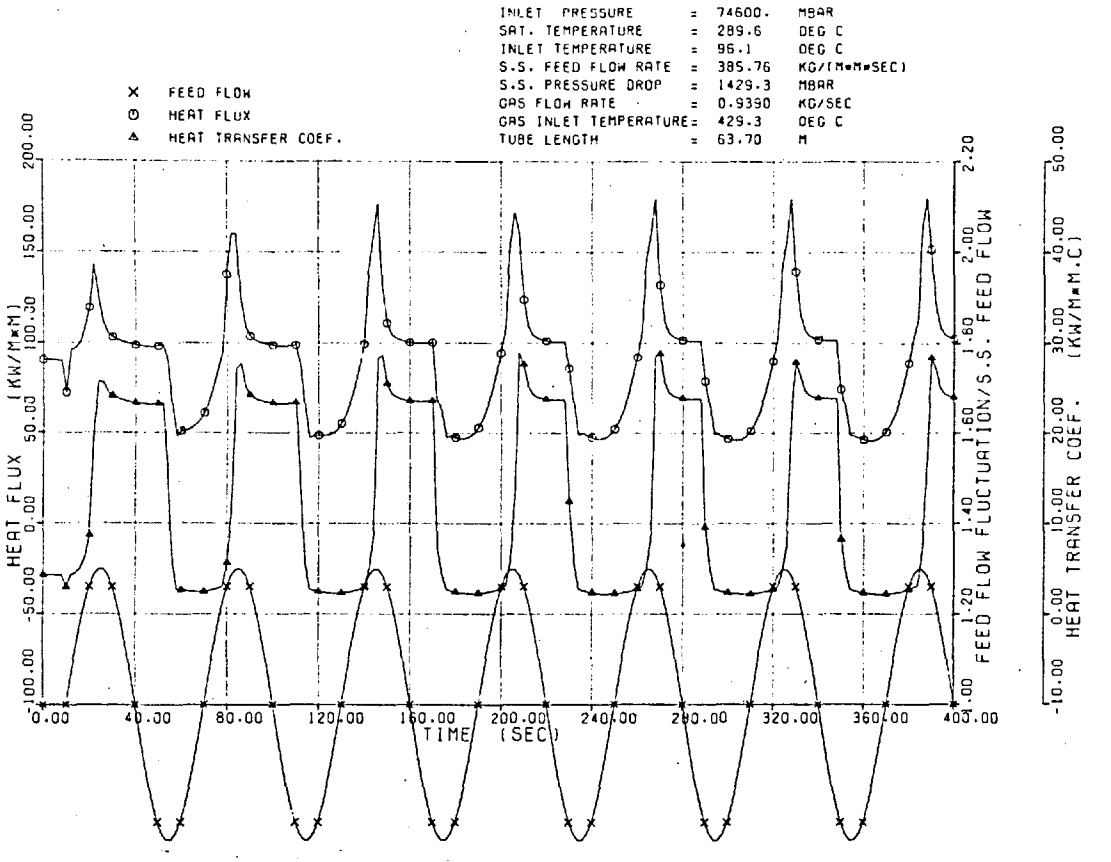


FIG.(6.42) VARIATION OF HEAT FLUX AND HEAT TRANSFER COEFFICIENT AT SUPERHEATER BOUNDARY

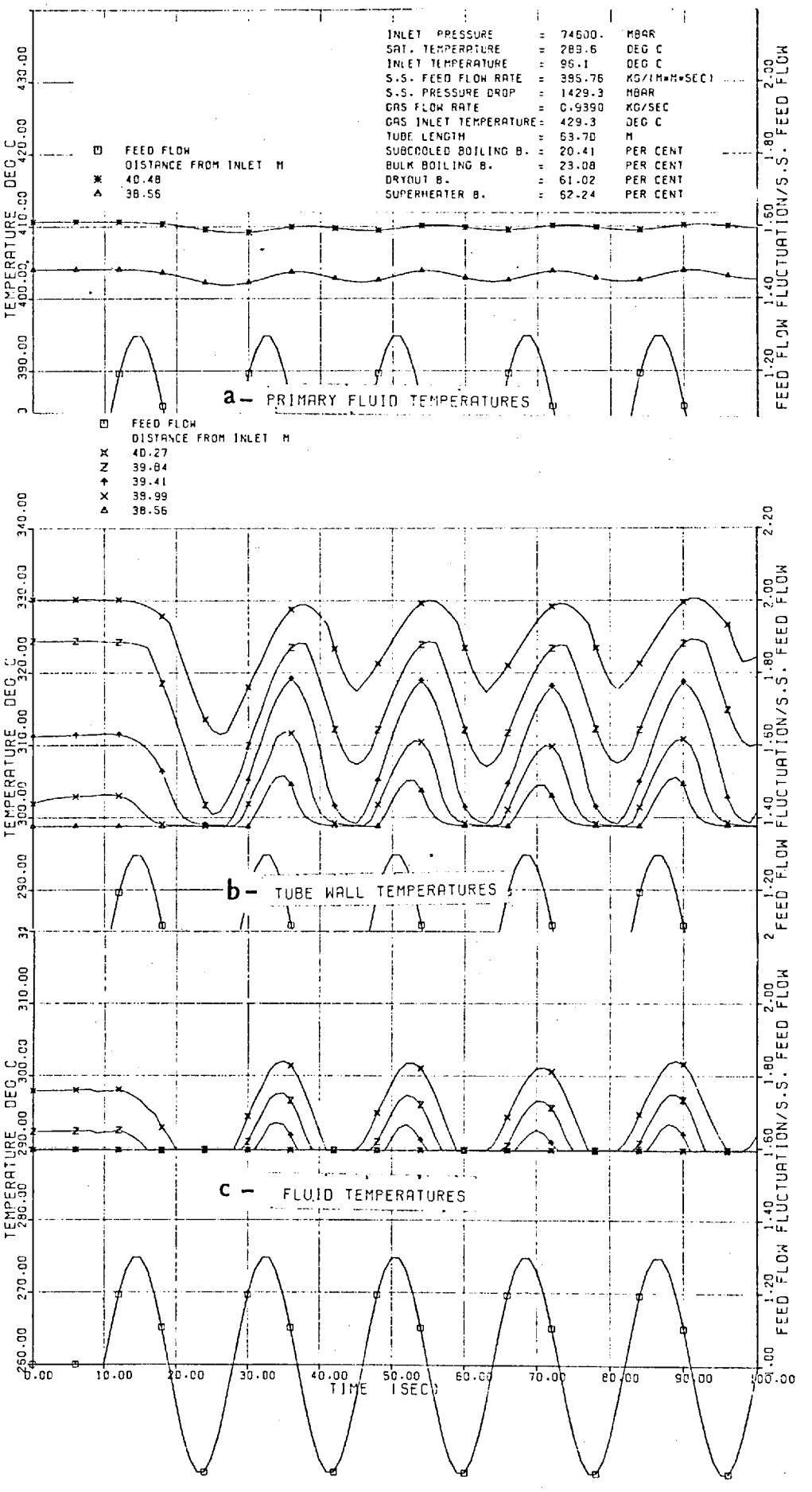


Figure 6.43: Temperature variation at fixed positions along the tube

6.4 FLOW OSCILLATIONS IN FIXED PRESSURE DROP SYSTEMS

In a once-through system with an imposed pressure drop, sustained oscillations can occur under some operating conditions, i.e. at a given heat flux, inlet subcooling and system pressure drop.

In some experimental investigations of once-through systems, as noted in Chapter 2, Figure 2.7, the system was considered stable while having irregular fluctuations with low amplitude. The onset of system instabilty coincided with the appearance of regular and persisting flow oscillations; here, excitation could originate in portions of the system external to the heated tube or could be inherent in the boiling process. At present no information is available with which a suitable forcing function can be defined. In this section, dynamic instability will be, therefore, examined by disturbing one of the steady-state operational conditions.

6.4.1 Character of Prediction

Before presenting the prediction, it is appropriate to examine the character of the model response. For a given geometry and operating condition, the conservation equations are solved for a fixed pressure drop or inlet mass velocity, to determine the corresponding steady-state. Employing the steady-state solution as the initial condition, the flow response to a finite disturbance of inlet velocity or gag pressure drop is examined to assess the system instability.

A disturbance of steady-state condition results in inlet flow oscillations which either increase or decrease in time. A stable steady-state is characterised by flow oscillations which decay in time to a steady flow consistent with the new operating condition. When oscillations of inlet flow increase in time, the system is regarded as

unstable. In this case, the flow oscillations can increase, depending on the input perturbation, to a sustained oscillation of constant amplitude, or it can increase with time.

Typical responses of inlet and outlet mass velocities to a disturbance of feed flow (approximately half a sine) are illustrated in Figure 6.44. The computer program is allowed to run for 20 seconds at the imposed pressure drop without any disturbance. At a certain instant, the inlet flow is varied up to 30% of the steady-state value by half a sine wave. Then the pressure drop is kept constant, equal to the imposed value, and the responses of inlet and exit flow are found. As shown in Figure 6.44, fluctuations of the inlet and outlet mass flow decay rapidly to the initial values. This displays a heavily stable condition.

6.4.2 Self-Sustained Oscillations

Oscillations of the inlet and exit mass velocities in response to a feed flow perturbation are given in Figures 6.45a,b,c and d for the operating conditions shown on the same Figure. The response curves are obtained at different inlet pressure drops by changing the inlet gag constant. Only the inlet flow oscillations on both sides of the instability threshold are plotted. The oscillation of Figure 6.45a is converging slowly at the inlet pressure drop of 63 mbar. As the pressure drop at inlet gagging reduces to 40 mbar, the oscillations become self-sustained (Figure 6.45b). Further reduction of the inlet pressure drop eventually causes the mass flow oscillations to grow (Figures 6.45c and 6.45d). The value of the inlet gagging pressure drop at the threshold of instability is 40 mbar. It can be seen that the transition from the stable to unstable condition is smooth. Comparison of Figures 6.45b and 6.45d shows that as the inlet gagging increases, the frequency of

the oscillation slightly decreases; the period of oscillation reduces from 17 seconds to 16 seconds for Figures 6.45b and 6.45d, respectively. Also, the amplitude of the oscillations is magnified at low inlet gagging as shown in Figure 6.45c and d. These behaviours are in complete agreement with the frequency response analysis of the open loop system as noted in section 6.3.

Examination of Figure 6.45 shows that the oscillation of the exit vapour velocity is approximately out-of-phase with the inlet velocity at the onset of instability. This is in agreement with the frequency response analysis of the previous section.

The pressure drop oscillations of different regions along the boiler and its components are illustrated in Figure 6.46 at the onset of instability. The total pressure drop is constant, equal to the imposed boundary condition. The pressure drop oscillations in the superheater region are out-of-phase with those of the economiser and inlet valve. This is consistent with the mechanism of instability as discussed in section 6.3.8. It also confirms the vectorial explanation of Davies and Potter (1967).

The oscillations of the boiling boundaries are displayed in Figure 6.47. It shows that the oscillations are not significant, particularly in the case of the subcooled boiling boundary. This is caused by the stabilising effect of the heat flux-flow coupling which is shown in Figure 6.48.

For the case of the threshold of instability, the responses of temperatures of the liquid and vapour at various axial positions are shown in Figure 6.49. The largest amplitude appears at the inlet of the economiser and the superheater. These positions correspond to the region of the steepest slope of the axial steady-state temperature

distribution, as noted in Chapter 5, Figure 5.8. The slope is largest immediately at the beginning of the economiser and the superheater. However, the inlet thermal boundary conditions which impose a constant inlet subcooling, impede the maximum amplitude occurring at the entrance of the economiser. This also applies to the onset of the superheater at which the temperature of the vapour is at saturation before being superheated. The amplitude of the oscillations decreases at the positions near to the subcooled boundary and the boiler outlet where the temperatures attain a constant level. The tube wall temperatures at the dryout superheater boundaries are given in Figure 6.50. The maximum oscillations occur at a position between the dryout and the superheater. Comparison of Figures 6.49 and 6.50 shows that at a fixed point in this region, the magnitude of the oscillations of the tube wall temperature is higher than the fluctuation of the fluid temperature. This is consistent with the discussion of section 6.3.9.

The outlet temperatures of the primary gas and vapour (Figure 6.51) show no significant changes at the onset of instability.

Figure 6.52 illustrates the response of the mass velocities on both sides of the instability threshold for operating condition No. 2 in Table 6.1. The period of oscillation at the onset of instability is about 32 seconds, which is in agreement with the frequency response calculation of section 6.3.7 (Figure 6.31). This also closely agrees with the experimental results of Babcock and Wilcox (Appendix A) at similar operating conditions. The discrepancy is due to the effects of the inlet and outlet unheated tubes which are not taken into account in the analysis of Figure 6.52.

As shown in section 6.3.4, the frequency of the oscillation is dependent on the subcooled residence time of the flow. Comparison of

Figures 6.45b and 6.52b supports this behaviour. The subcooled residence times of Figures 6.45b and 6.52b are 22.8 and 56.8 seconds, respectively. This agrees with the findings presented in the frequency response analysis. The self-sustained frequency for a shorter subcooled residence time is higher than that of longer residence time (Figures 6.45b and 6.52b). These results are in agreement with the experimental data as given in Appendix A.

6.4.3 Effect of Operating Parameters on Stability

The influence of changes in the operating condition on the stability of the system is of most interest to designers. In this section, effects of a number of relevant design parameters are investigated by the comparison of flow responses; that is, one of the operating conditions of the system having self-sustained oscillations (nominal condition) is varied, and then the flow response of the new condition is found and compared with the flow oscillations of the nominal condition.

The stability behaviour of a gas fired once-through boiler is a result of many interacting factors, e.g. pressure drop in the economiser, pressure drops in the evaporator and superheater regions, coupling of the primary gas. The effect of certain parameters may be simply judged by comparing the magnitude of the steady-state values with the corresponding factors of the nominal condition. For example, an increase in the economiser pressure drop due to design changes may be regarded as stabilising, as seen in the previous sections. However, this is sometimes misleading, and there can be other consequential counteracting phenomena which may suppress the effect of the economiser pressure drop (Neal (1967), Boure (1967)), e.g. the effect of inlet subcooling (section

2.3.4.3). These remarks are used in the following discussions.

The effect of system pressure on the stability is shown on Figure 6.53. System pressure is increased by 5% from the nominal condition shown on the same Figure. As seen, the oscillations decay and the new condition becomes stable.

When the system pressure increases, with all the other conditions fixed, the temperature level of the evaporator increases; the density ratio of liquid to vapour decreases. Hence, the length of the subcooled region increases, and the effect of change of the average density in the evaporator decreases. Accordingly, this produces a larger pressure drop in the economiser and less pressure drop in the evaporator as compared to the nominal condition.

The responses of the inlet and outlet mass velocities are plotted in Figure 6.54 for a 10% decrease in the inlet temperature of the liquid. Comparison of Figure 6.54b with the nominal condition (Figure 6.54a) reveals that the new operating condition is still liable to self-sustained oscillation.

The amplitude of the oscillations is, however, less than the amplitude of the oscillations of the nominal condition. At large inlet subcooling, the decrease of the inlet temperature would increase the length of the subcooled region, and hence the corresponding pressure drop would increase. Naturally, this has a stabilising effect.

The influence of the angle of the coil is illustrated in Figure 6.55. The angle is increased by three times from that of the nominal value. The gravity effect in the economiser increases with the angle of the coiled tube. Therefore, the economiser pressure drop increases and the system is stabilised.

The effect of the inlet temperature and the mass flow of the

primary side on the stability are shown in Figures 6.56 and 6.57. The inlet temperature and flow are reduced by 2% from that of the nominal values. The stability of the system increases for both changes. As shown in Figure 6.56, when the inlet temperature of the primary side reduces, the new operating condition exhibits a sustained oscillation. However, the amplitude of the oscillations decreases compared to the amplitude of the nominal curve.

When the inlet temperature or inlet mass flow of the primary side decreases, the total heat flux to the secondary side decreases. Accordingly, the length of the economiser increases, while the length of the evaporator and superheater reduces. Consequently, the damping component of the pressure drop increases, and the forcing components decrease. Depending on the balance between the resulting pressure drops at the economiser and evaporator-superheater regions, the inlet mass flow oscillations may decrease (Figure 6.57). On the other hand, it may reach a new self-sustained oscillation (Figure 6.56b), the amplitude of which is less than that of the oscillation of the nominal condition (Figure 6.56a).

The influence of increasing the heat transfer coefficients of the primary and the secondary sides on the boiler stability behaviour is shown in Figures 6.58 to 6.60. The responses of inlet flow are obtained for a 10% increase of the local heat transfer coefficients from the nominal values.

When the heat transfer coefficient of the primary side (Figure 6.58), or the subcooled region of the secondary flow (Figure 6.59), increases, the local heat flux in the economiser increases. It, hence, results in a decrease of the subcooled length which has a destabilising effect. However, the response curves of Figures 6.58 and

6.59 show a stabilising trend due to an increase of the heat transfer coefficients. Two counteracting processes are involved when the heat transfer coefficient increases; one is destabilising as described above, and the other is stabilising. The stabilising process with an increasing heat transfer coefficient is due to the coupling of the primary and secondary sides at the subcooled region. The effect of heat flux-flow coupling increases as the thermal resistance between the primary and the secondary flows decreases. Accordingly, the oscillations of the enthalpy and the subcooled boiling boundary are suppressed and the system stabilises.

The effect of increasing the superheater heat transfer coefficient on the stability of the system (Figure 6.60) appears to be less pronounced in comparison with the economiser (Figure 6.59).

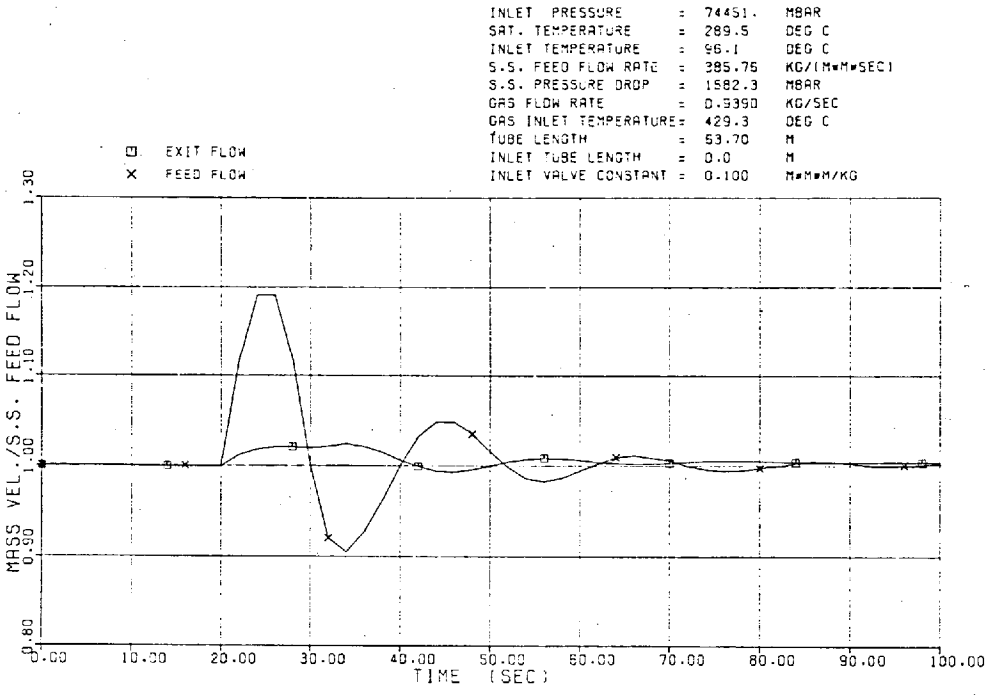


Figure 6.44: Response of mass velocities to a perturbation at inlet flow during parallel channel instability test

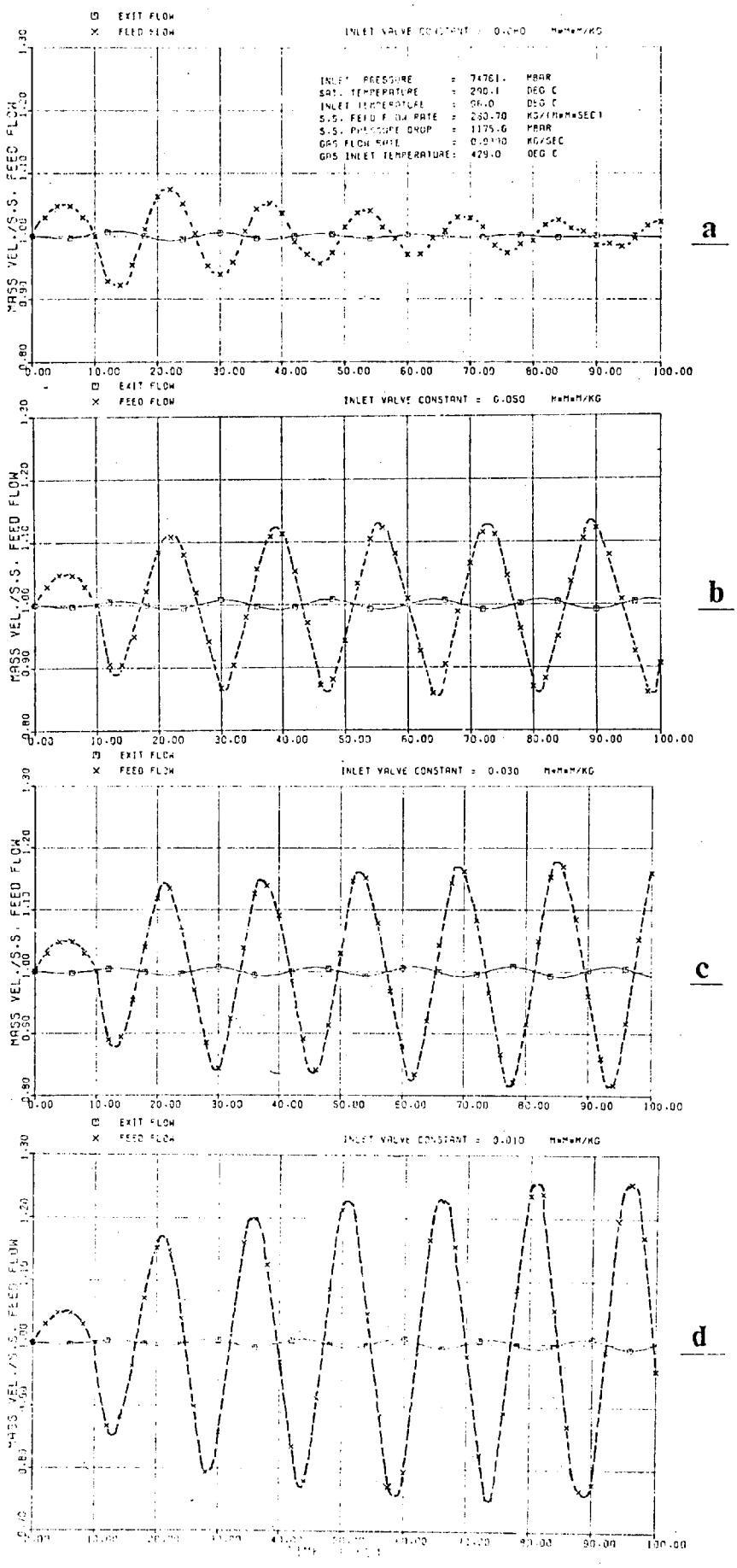


Figure 6.45: Self-sustained oscillation of mass velocities at different inlet gag for an imposed constant pressure drop

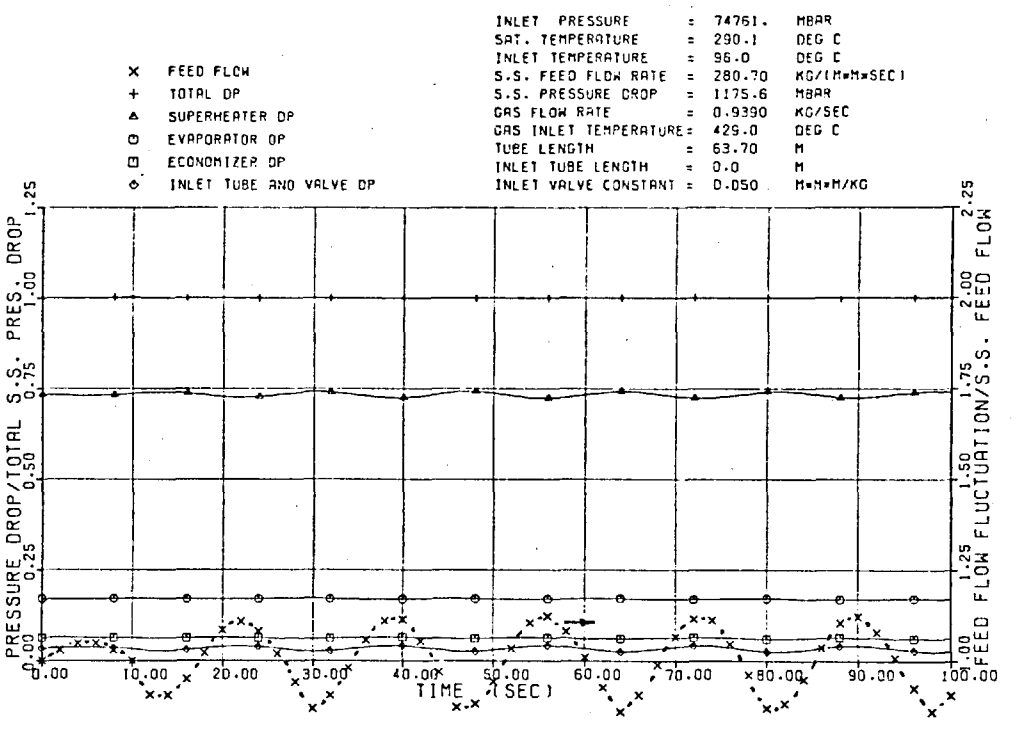


FIG.(6.46a) PRESSURE DROP OF DIFFERENT REGIONS ALONG THE TUBE

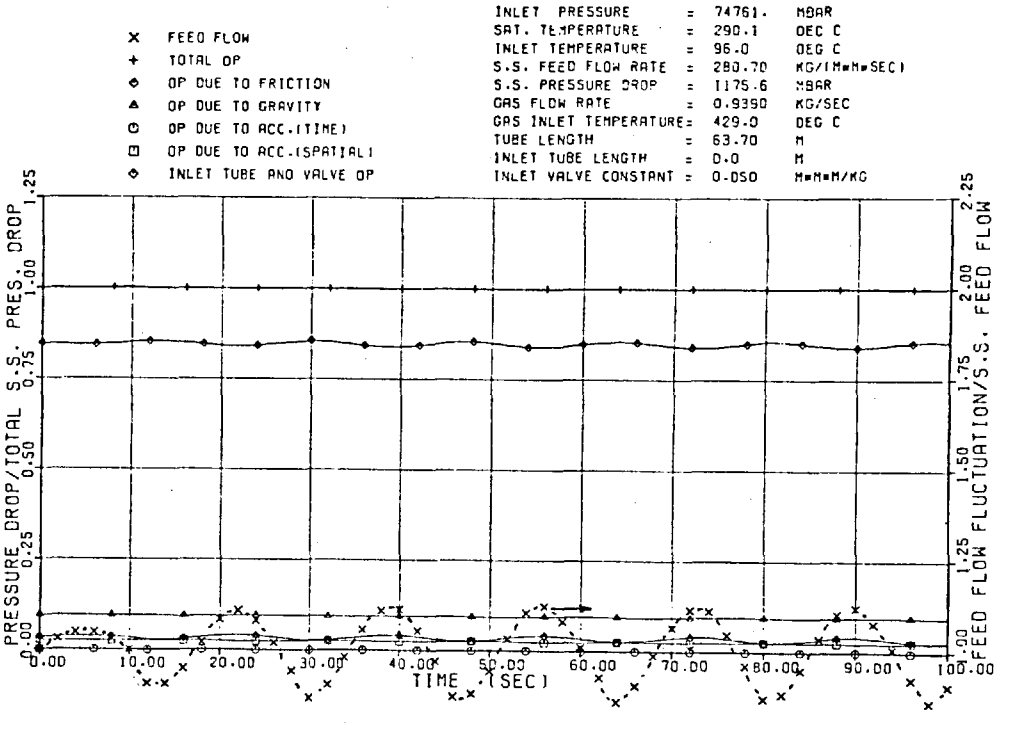


FIG.(6.46b) DIFFERENT COMPONENTS OF PRESSURE DROP

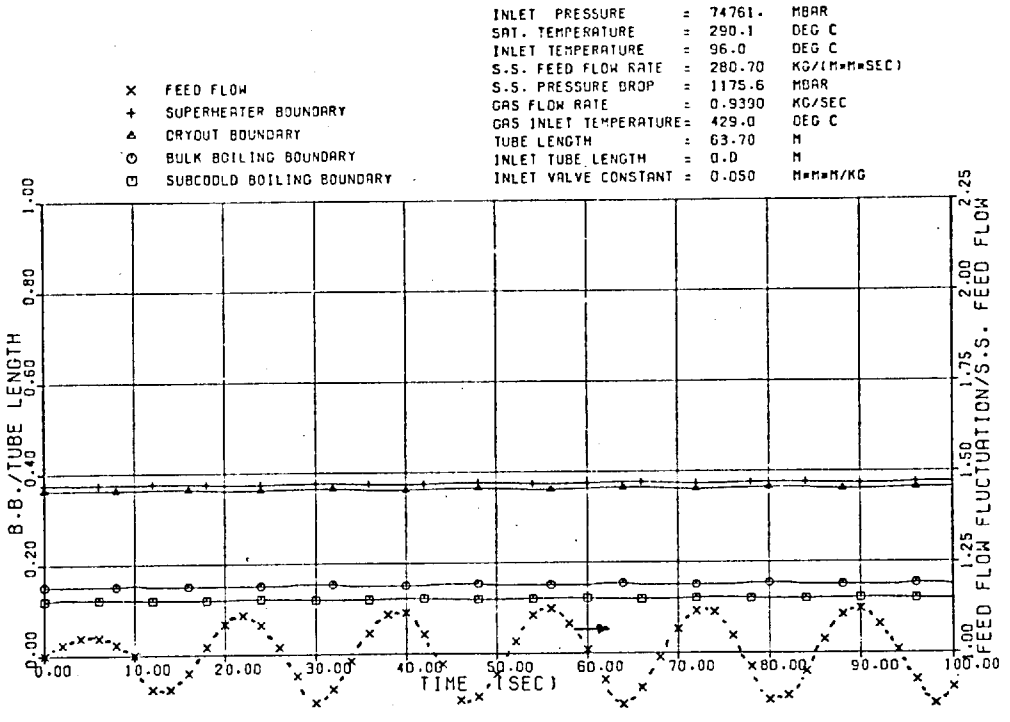


FIG.(6.47) BOILING BOUNDARIES MOVEMENTS DURING PARALLEL CHANNEL INSTABILITY TEST

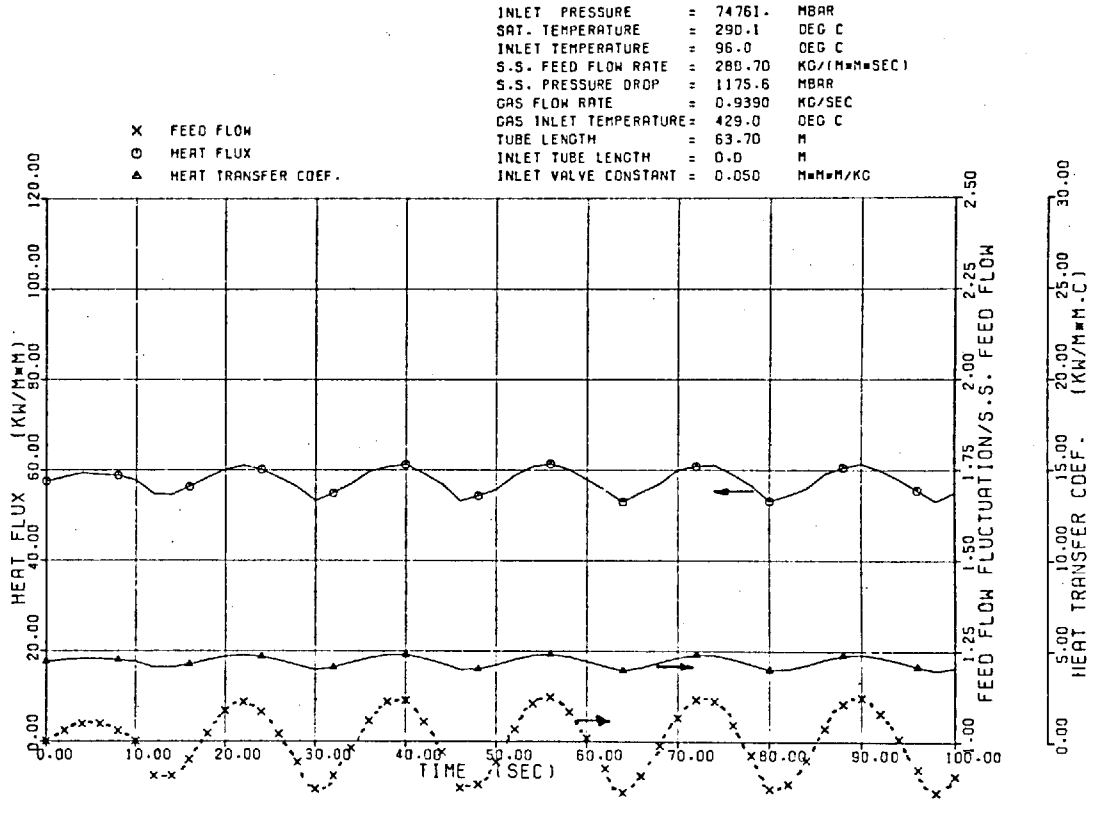


FIG.(6.48) VARIATION OF HEAT FLUX AND HEAT TRANSFER COEFFICIENT AT SUBCOOLED BOILING BOUNDARY

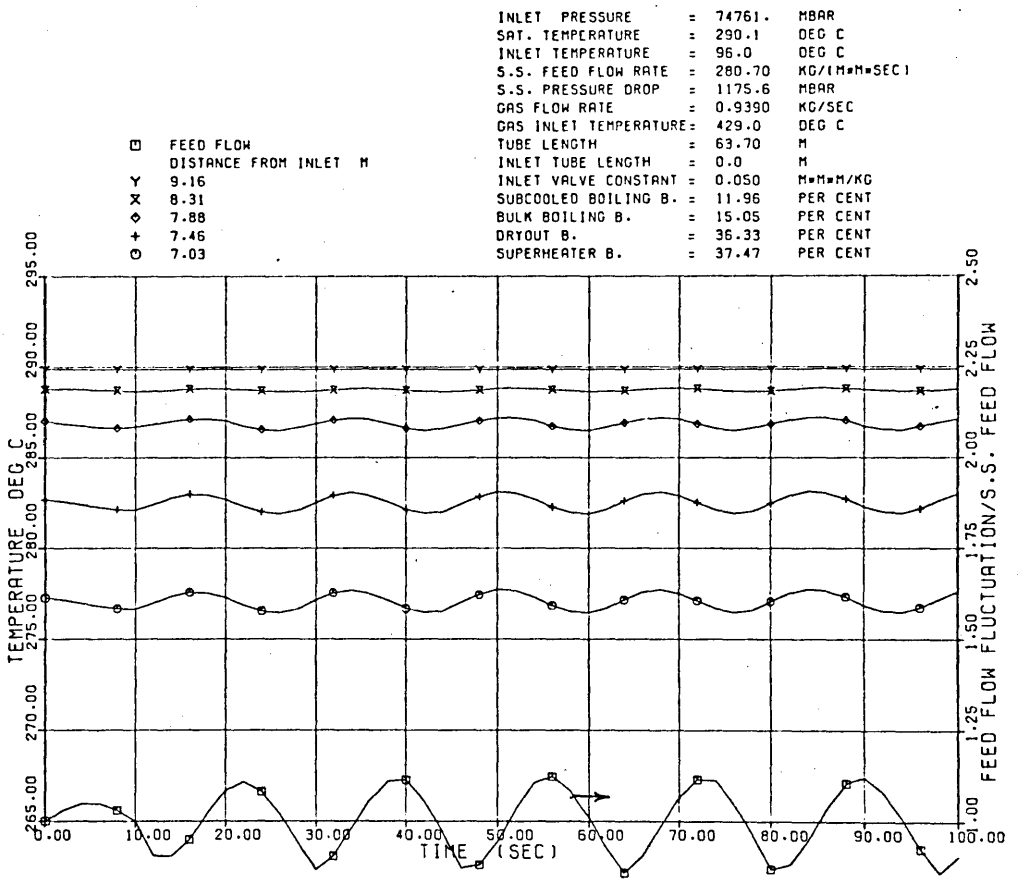


FIG.(6.49a) FLUID TEMPERATURES AT FIXED POSITIONS NEAR SUBCOOLED AND BULK BOILING BOUNDARIES

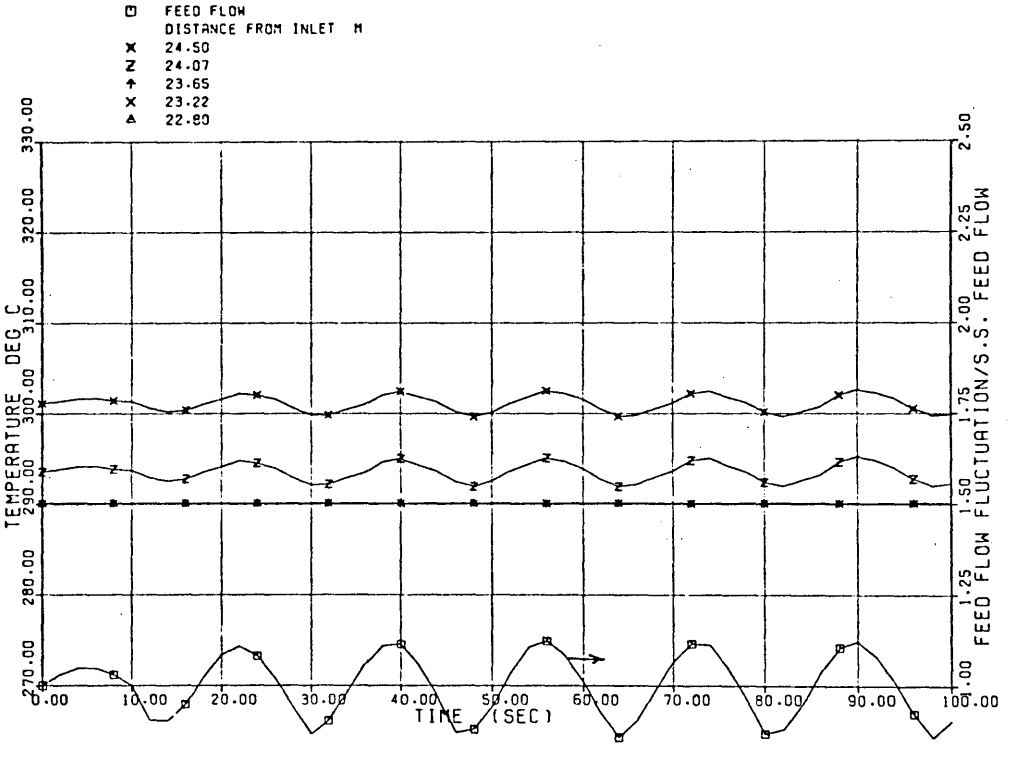


FIG.(6.49b) FLUID TEMPERATURES AT FIXED POSITIONS NEAR DRYOUT AND SUPERHEATER BOUNDARIES

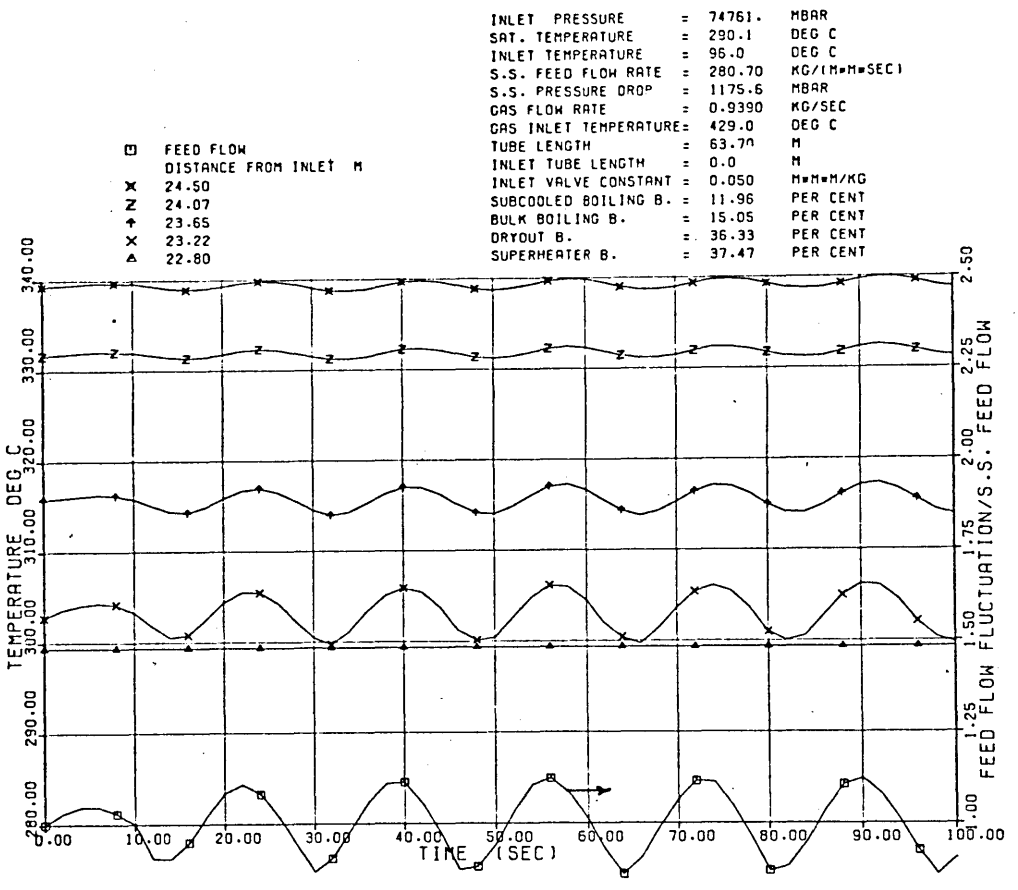


FIG.(6.50) TUBE WALL TEMPERATURES AT FIXED POSITIONS NEAR DRYOUT AND SUPERHEATER BOUNDARIES

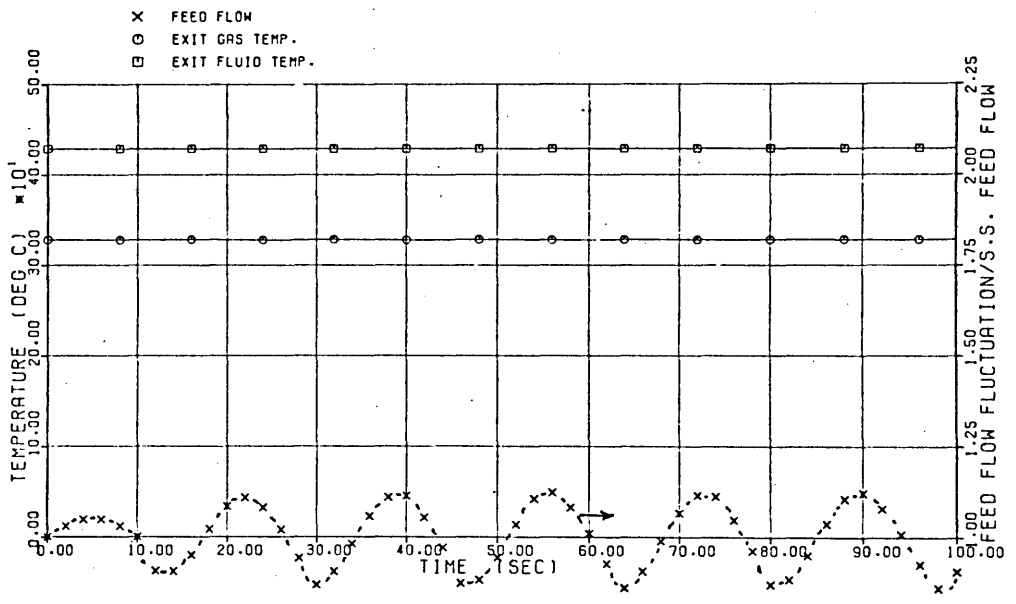


FIG.(6.51) VARIATION OF EXIT TEMPERATURES DURING PARALLEL CHANNEL INSTABILITY TEST

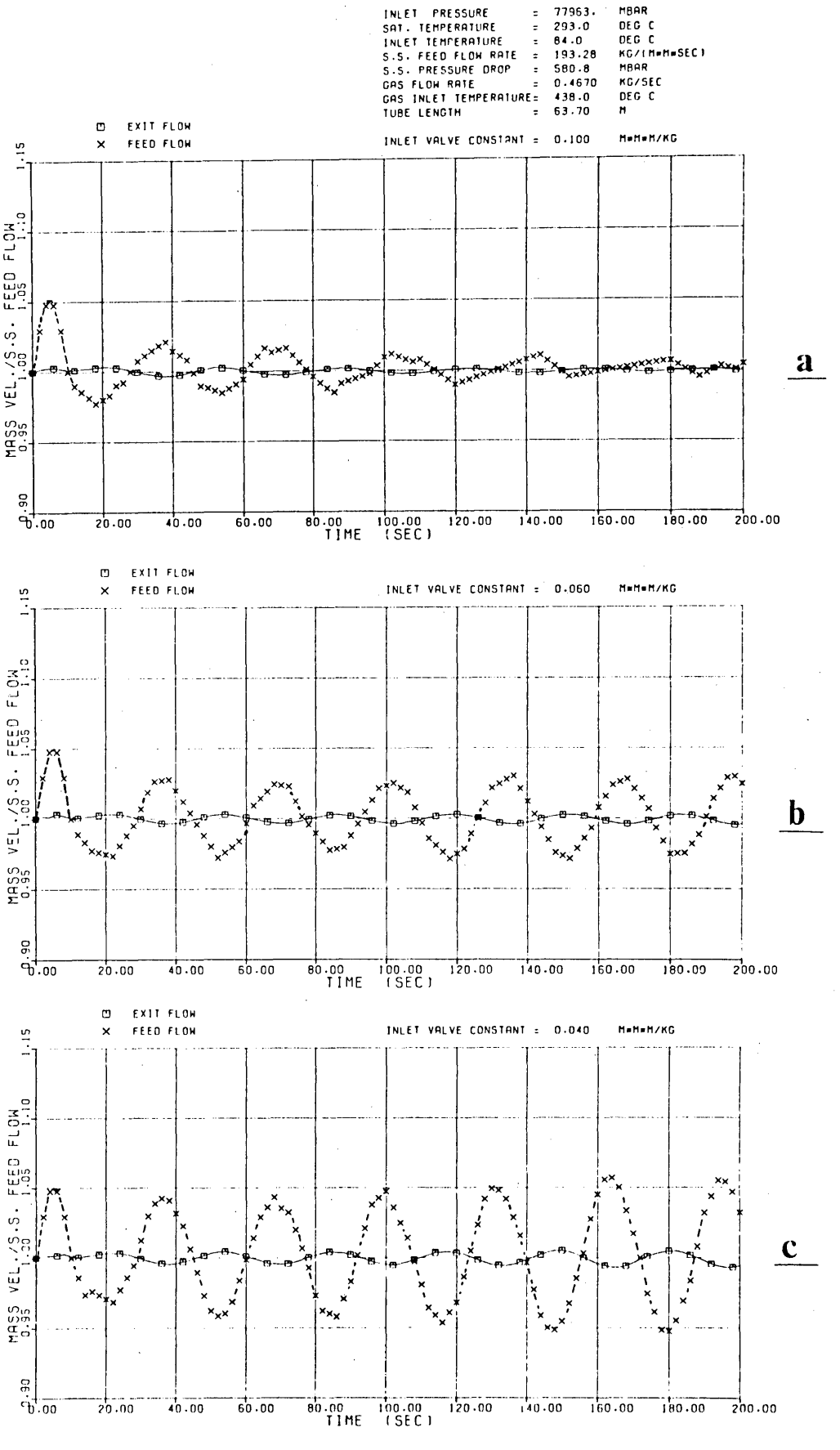


Figure 6.52: Oscillation of mass velocities for an imposed constant pressure drop (parallel channel) at different inlet gags

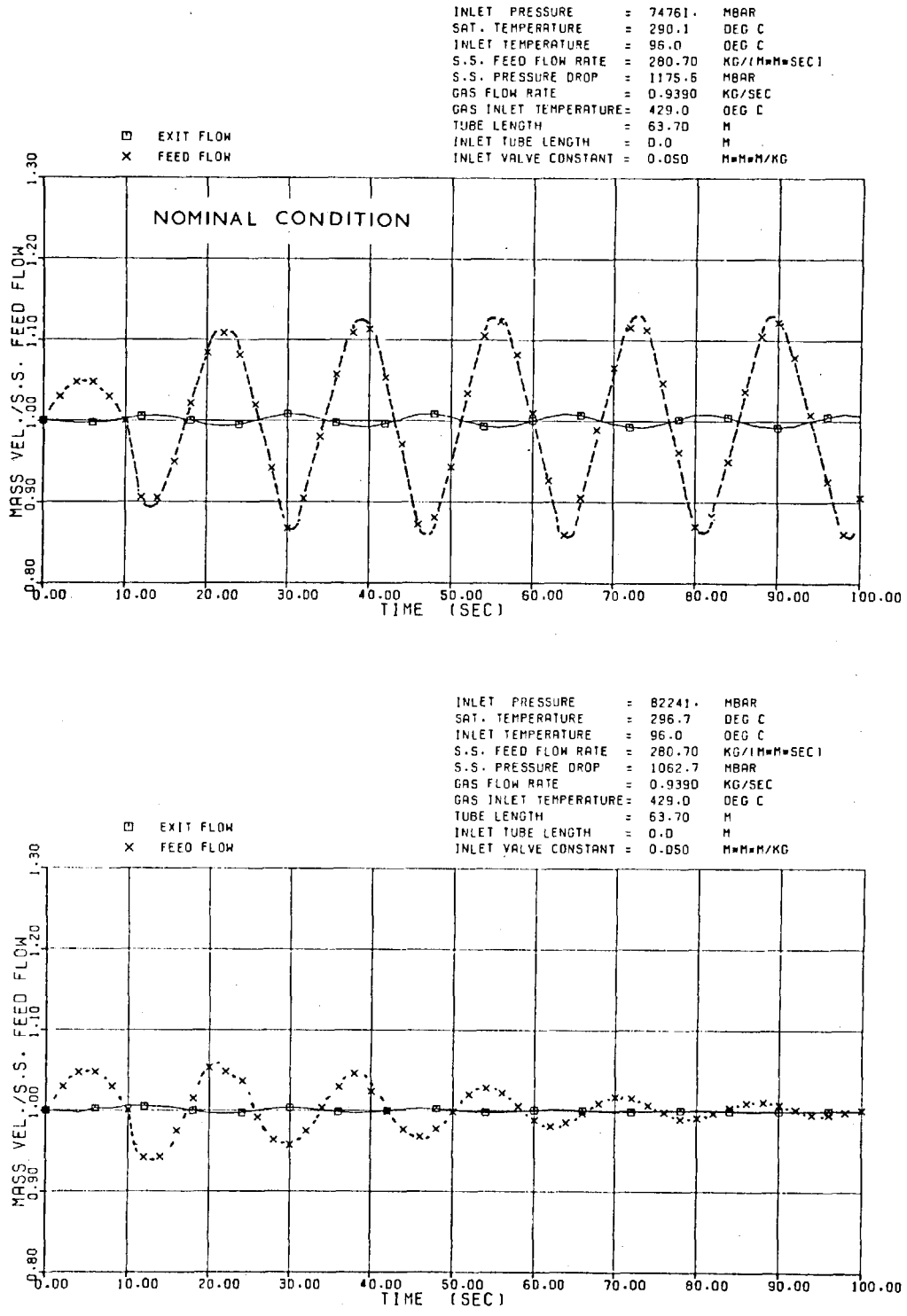
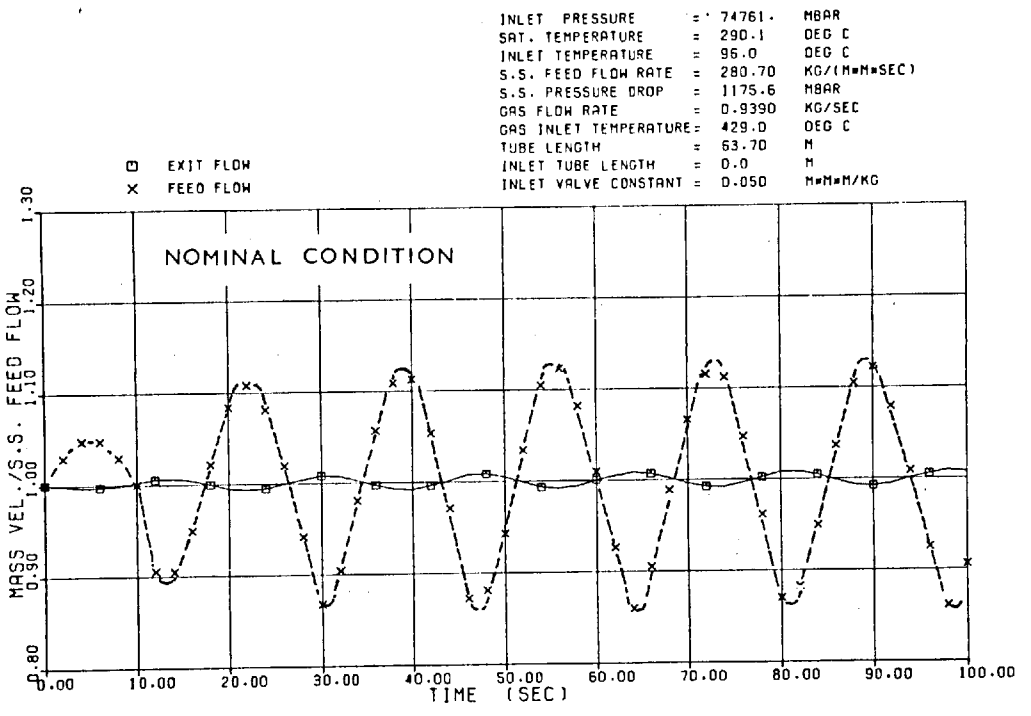
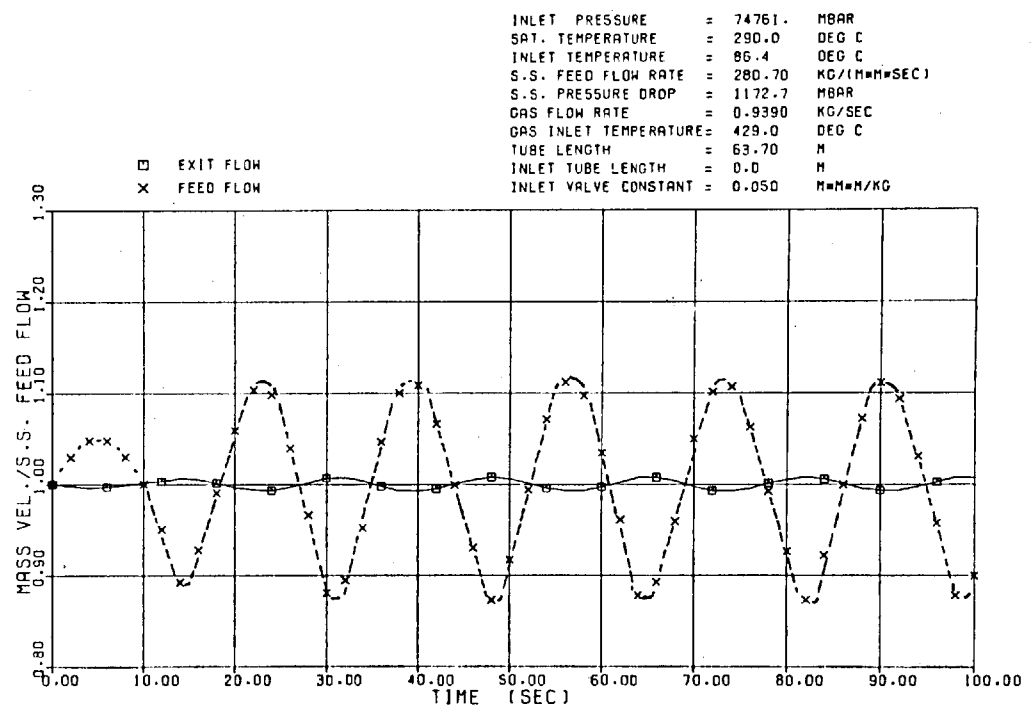


Figure 6.53: Effect of increasing system pressure from nominal condition on the self-sustained oscillation of inlet mass velocity at threshold of instability



a



b

Figure 6.54: Effect of increasing inlet subcooling from nominal condition on the self-sustained oscillation of inlet mass velocity at threshold of instability

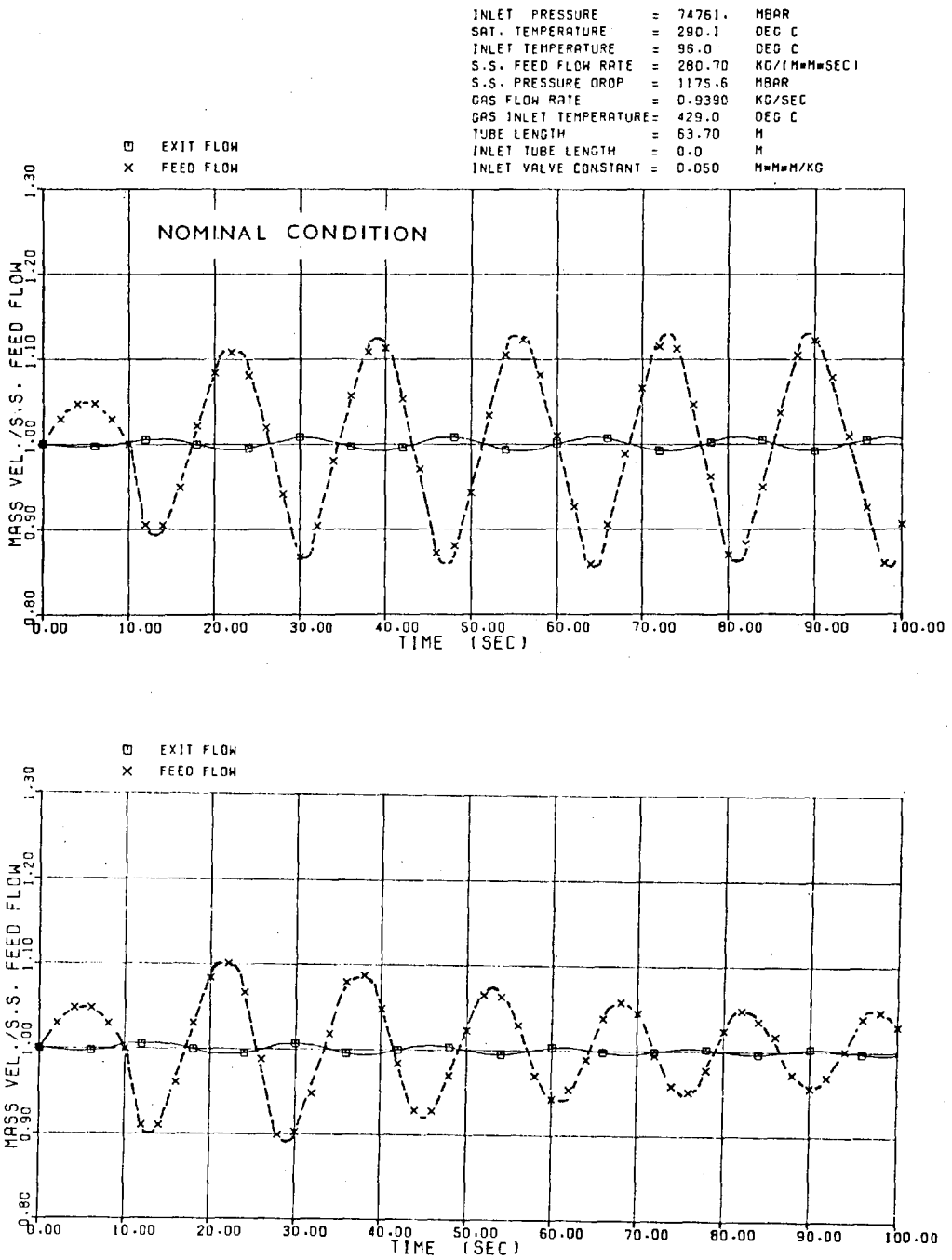
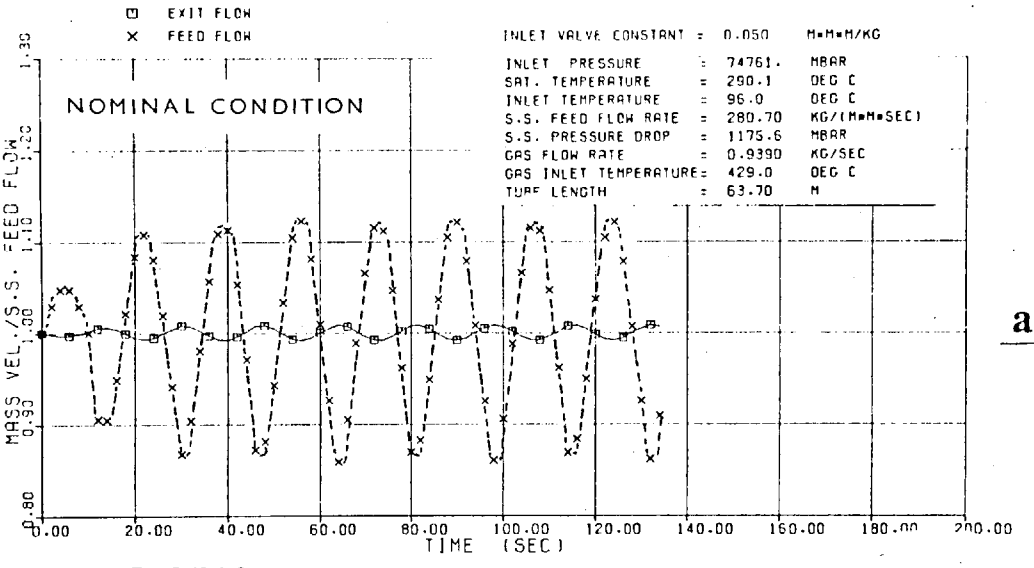


Figure 6.55: Effect of increasing the helix angle from nominal condition on the self-sustained oscillation of inlet mass velocity at threshold of instability



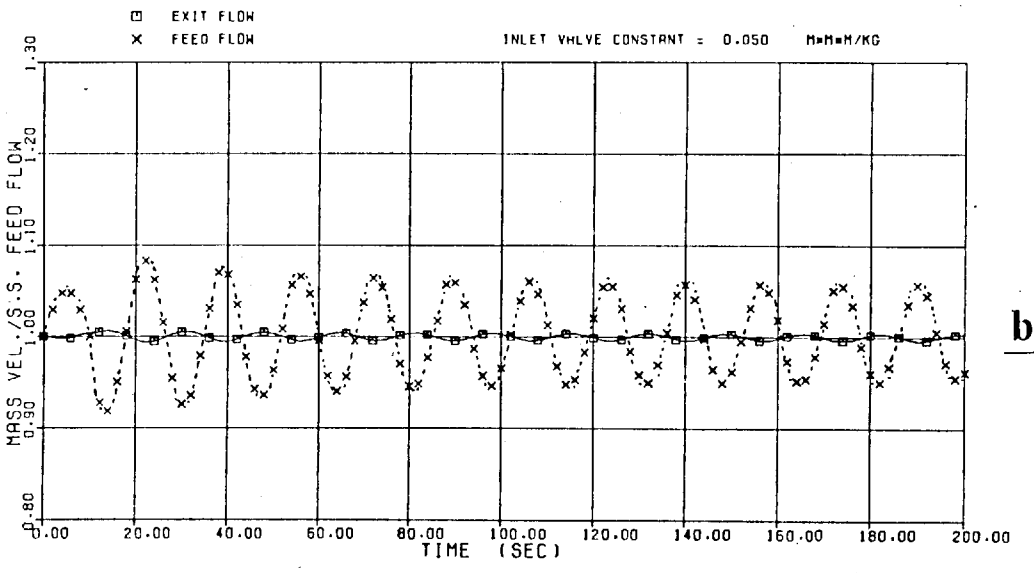


Figure 6.56: Effect of decreasing the inlet temperature of the primary side on the self-sustained oscillation

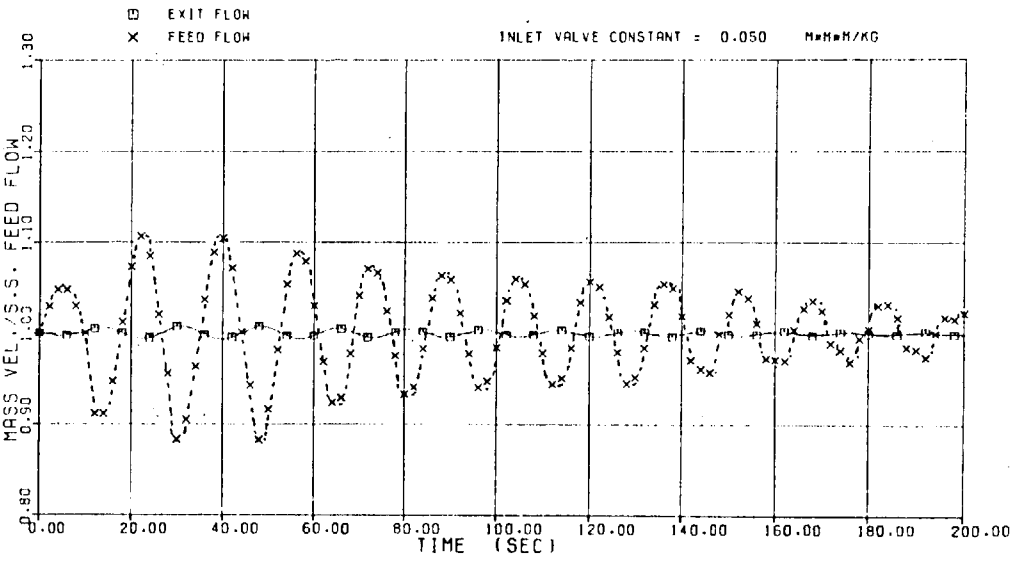


Figure 6.57: Effect of decreasing flow rate of the primary side on the self-sustained oscillation

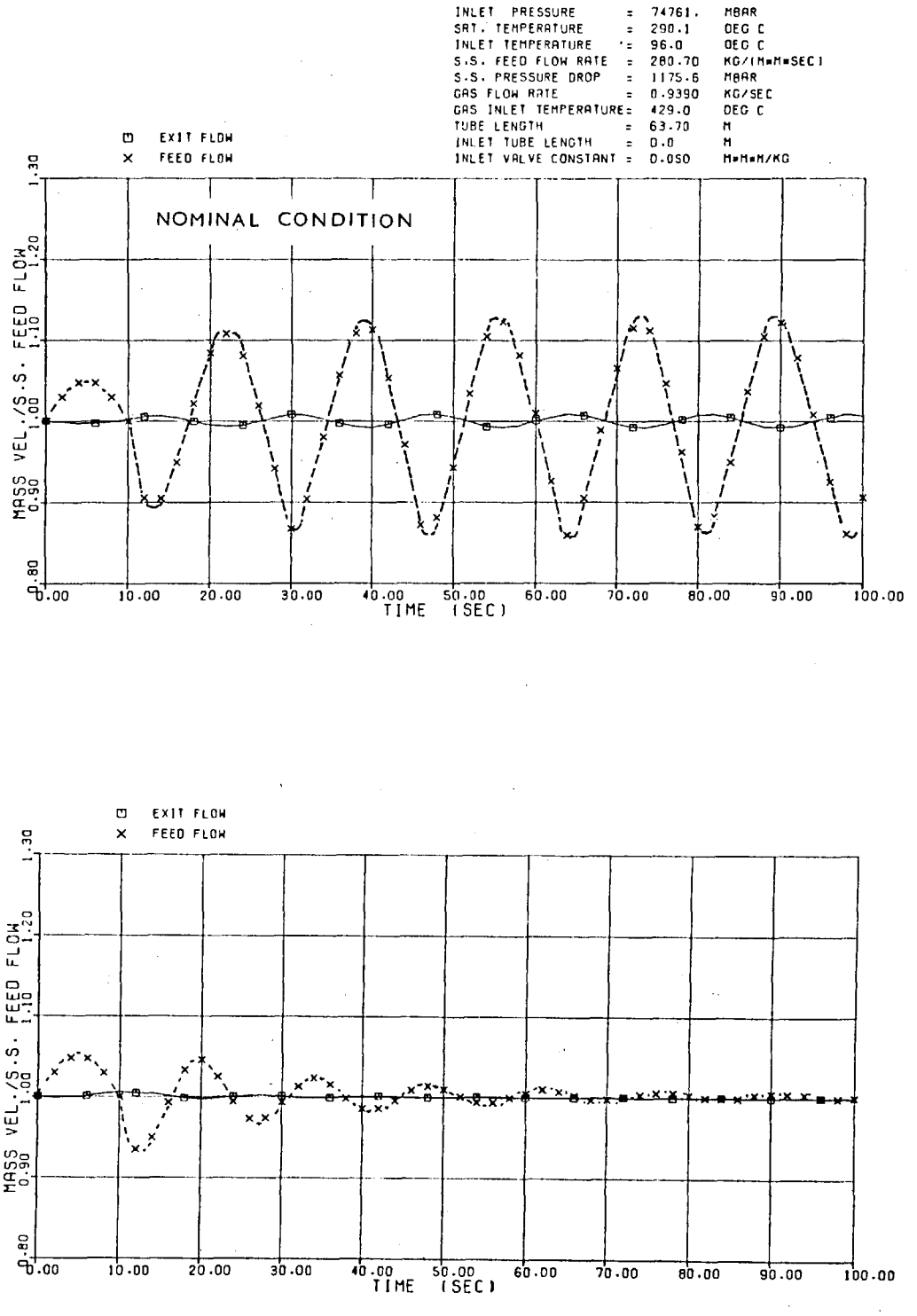


Figure 6.58: Effect of increasing the primary side heat transfer coefficient from the nominal condition on the self-sustained oscillation of inlet mass velocity at threshold of instability

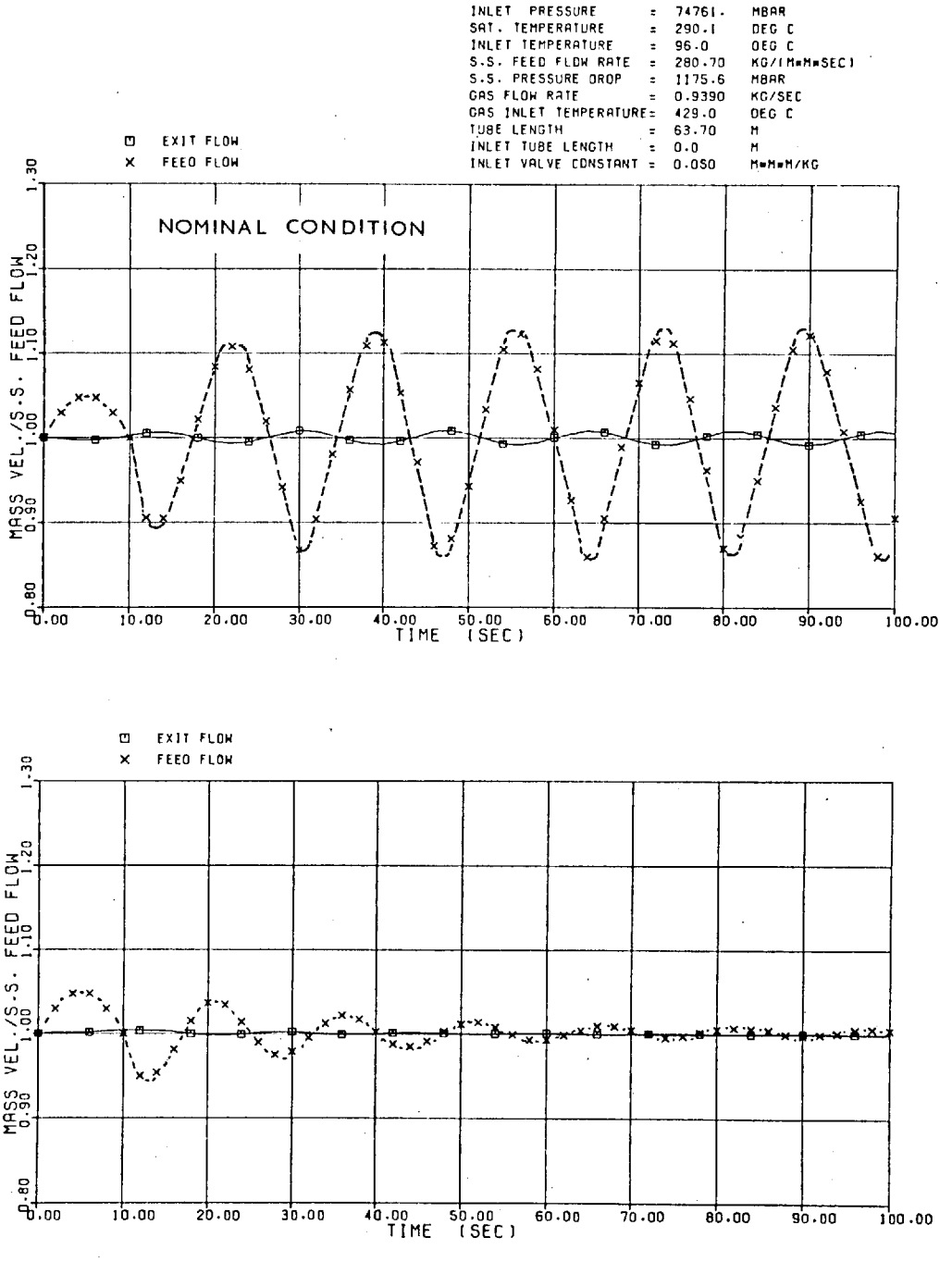


Figure 6.59: Effect of increasing subcooled heat transfer coefficient on the self-sustained oscillation of inlet mass velocity at threshold of instability

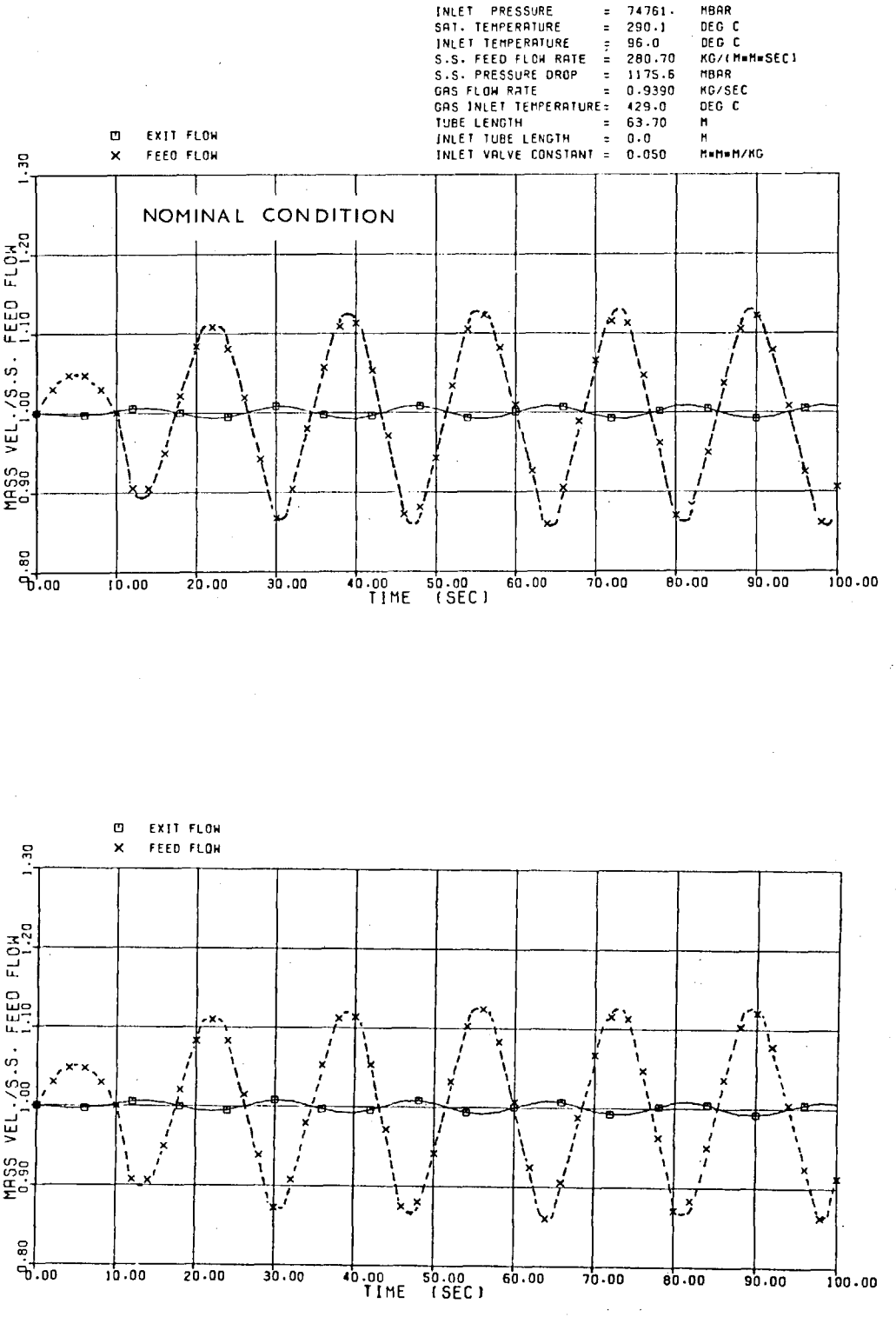


Figure 6.60: Effect of increasing the heat transfer coefficient of superheater from the nominal condition on the self-sustained oscillation of the inlet mass velocity at threshold of instability

6.5 CONCLUDING REMARKS

Dynamic analyses of a helically-coiled tube once-through boiler, heated by a counterflow primary gas, have been carried out by using the simulation program developed in the present work.

The effect of heat flux-flow coupling in the single-phase liquid and two-phase regions has been investigated and discussed. It has been shown that the local heat fluxes at the subcooled boiling and superheater boundaries changed significantly with time when the inlet flow varied. This was caused by changes in the heat transfer mechanism and in the energy stored in the tube wall. The effect was more pronounced at the superheater boundary. Large fluctuations of the tube wall temperatures at the dryout-superheater region resulted.

The transient response of the total pressure drop to step increase in the inlet flow showed that the total pressure drop increased rapidly, and then decreased gradually to a steady value. The new steady value of pressure drop was consistent with the static characteristic (Δp versus G) of the system. Hence, at some particular condition, the eventual pressure drop was lower than the initial one, as inlet mass increased. This agreed qualitatively with the available experimental results.

The frequency response analysis was capable of providing very detailed information. In particular, systematic phase and amplitude calculations of the pressure drop across different regions of the boiler (when the inlet flow was oscillated) gave insight into the mechanism of instability. It was noticed that the out-of-phase component of the pressure drop occurred largely in the superheater region. In this case, the phase lag of the outlet vapour velocity relative to the inlet flow oscillation was approximately -180^{o}.

The frequency response of the outlet vapour mass velocity

perturbation and the system pressure drop oscillation to the inlet flow oscillations showed peculiar behaviour at low frequencies. This was explained by the effect of the heat flux-flow coupling.

A knowledge of the internal dynamic characteristic of a heated tube, defined as the polar plot of the frequency response of the pressure drop oscillations to inlet flow oscillations, enabled prediction of the dynamic stability. The internal dynamic characteristic curve was also used to predict the static stability, this being the limiting case for zero frequency.

It was found that the resonant frequency of the system was strongly affected by the subcooled residence time of the flow; it was lower for a system having a longer residence time. The resonant frequency was slightly affected by the inlet resistance; it decreased as the inlet gagging increased.

The stabilising effect of inlet gagging has been investigated and discussed. A qualitative measure of the amount of inlet gagging required for dynamic and static stability was assessed from the magnitude of the internal characteristic at -180^{o}.

The analysis of self-sustained oscillations at an imposed constant pressure drop was in agreement with the results of the frequency response calculation. This emphasised the correctness of the simulation program. The threshold of instability was obtained by decreasing the magnitude of the inlet gag. It was found that the transition from stable to unstable conditions was gradual with changing inlet gagging. When the inlet gagging value was lower than that necessary for the onset of instability, the amplitude of the self-sustained oscillations was larger than that occurring at the threshold of instability.

The effect of some parametric variations on the threshold of

instability has been shown and discussed. An increase in the heat transfer coefficients of the primary flow and subcooled liquid improved the stability of the system.

CHAPTER 7

CONCLUSIONS AND RECOMMENDATIONS

Theoretical methods of examining stability have been considered and the ability of available methods to predict instability has been discussed.

The importance of instability to the satisfactory performance of helically-coiled tube once-through boilers (heated by counterflow primary gas) was recognised and in view of the limitations imposed by available modelling techniques, it was decided to develop a more basic and generalised theoretical approach. With this in mind, the present study was carried out and the main objectives (section 1.2) have been achieved.

The criteria of the onset of subcooled flow-boiling were hardly applicable for flow inside helically-coiled tubes. A suitable model was therefore developed and a criterion was obtained in terms of dimensionless quantities and the coil geometry. Evaluation of the model was facilitated by available experimental results at high and low pressures and over wide ranges of heat flux and mass velocity. Comparison of the predicted with the experimental values of the onset of subcooled boiling showed close agreement over the entire range of the available data.

Dynamic modelling was based on the solution of the conservation equations of the secondary side, the energy equations of the tube wall and the primary flow, together with suitable expressions for void fraction, the two-phase friction multiplier and the heat transfer coefficients as applicable to helically-coiled tubes. Different regions along the secondary flow were considered and the thermal non-equilibrium of phases in the subcooled region was taken into account. This was essential in the case of non-steady flow conditions; density changes caused high

acceleration in the fluid and this affected the flow oscillations (Boure (1966)). The resulting non-linear partial differential equations of the simulation constituted a boundary value problem which was solved by the method of continuous space and discrete time, using iteration techniques. By executing the numerical integration along the boiler at any time increment, the discontinuous behaviour of the system variables at the boiling boundaries was overcome and an accurate assessment of the movement of the boiling boundaries was achieved. The axial distributions of the primary side temperature, the tube wall temperature, and the temperature, vapour quality (or void fraction), pressure drop, heat transfer coefficient and heat flux of the secondary side were obtained and discussed.

The effect of different correlations of void fraction and two-phase heat transfer coefficients on the steady-state distributions of system variables has been studied. It was shown that the heat flux distribution along the evaporator was strongly controlled by the thermal conditions of the primary flow, and it was less influenced by the different two-phase heat transfer coefficients.

The mechanism of static stability has been investigated and discussed. It was shown that the pressure drop-mass velocity characteristics of a helically-coiled tube once-through boiler in which the heat source was a counterflow primary gas, could possess a negative slope part even at relatively high pressures. This negative slope was due to the decreasing length of the superheater with mass velocity when all other operating conditions were fixed. In this region, the outlet vapour superheating was shown to be sensitive to inlet mass flow changes and stable operation was found to be possible at very low or very high outlet superheating. This was supported qualitatively by the available experimental data.

By applying the transient and frequency response analysis to changes of inlet flow, the damping nature of heat flux-flow coupling was investigated. Emphasis was put on the mechanism of dynamic instabilities, and it was shown that a necessary condition for instability was a negative response of the outlet mass flow, this being heavily damped in relation to inlet flow oscillations. In this case, the oscillations of pressure drops in the evaporator and particularly in the superheater were nearly out-of-phase with those of the economiser region. This supported the vectorial explanation of Davies and Potter (1967). The onset of instability was established by changing the inlet gagging.

Effects of the economiser residence time on the frequency and amplitude of the oscillations were investigated and it was concluded that the frequency increased for systems having shorter subcooled residence times. This was consistent with the experimental results.

The results of this study show that the boiler pressure drop frequency response to forced flow oscillations facilitates stability calculations under specific operating conditions. The primary use of this type of analysis, however, has been to identify the controlling dynamic parameters of the boiler and to evaluate qualitatively the amount of feed resistance needed for stability under specific conditions.

Sustained flow oscillations were predicted for a once-through system under an imposed constant pressure drop. At a particular value of the inlet gagging (all other conditions fixed), no stable steady-state existed. For a fixed perturbation from the steady-state at different inlet gagging, inlet flow oscillations occurred. These either decreased or increased with time to a sustained oscillation of an amplitude which was dependent on the amount of inlet gagging.

The success of the model justified the basic assumptions. The

validity of using steady-state experimental correlations for dynamic calculations was affirmed, together with the correctness of the basic conservation equations. Neal (1967) and Dijkman (1969) maintain that it is not necessary to apply separate momentum and energy equations for the two phases in the case of saturated boiling flow. This concurs with the model predictions.

A major consideration is the range of application of the simulation program, limitations imposed by different designs and varying modes of operation, together with the applicability to the current boiler design and testing. An explicit answer is outside the scope of this work but the conclusions reached so far are given below. A comprehensive knowledge will only be achieved by a great deal more study.

The governing equations of the simluation restrict the use of the program to a counterflow gas fired helically-coiled tube once-through boiler in which the inlet condition is subcooled and the outlet can be either superheated or wet vapour.

The present program can probably be applied to the test rig of Babcock and Wilcox (Appendix A). The dynamics of the by-pass line is not included in the simulation, but can be approximated to a constant pressure drop system due to the large by-pass flow. The computer simulation applies only to a single tube. However, it may be applied to multi-tube systems by assuming a constant pressure drop. Modifications to account for the interaction of the other tubes or a by-pass line should not be difficult.

The mode of heating (by gas or liquid) presents no particular problem. In all cases, however, the appropriate thermal properties of the heating fluid should be used along the primary side. The program is easily modified for cross-flow and parallel flow types of heating and

also when specified heat flux is imposed on the system. These would reduce the computation time.

The original correlations were applied to water-cooled tubes. For any other cooling liquid, therefore, appropriate correlations and fluid thermal properties must be substituted.

The simulation excludes the pressure wave phenomena. The program may be less successful for very high frequency oscillations (comparable with the residence time of an acoustic wave along the tube). In this case, the program should be modified by applying, for example, the method of characteristics. The model neglects radiation of the primary gas but modification to account for this should not prove difficult.

The use of this kind of simulation during the design stages and the application of the program to a new boiler design for which no tests have been made, requires considerable skill and judgement. The program is largely dependent on experimental correlations; these may be examined and modified if some steady-state data are available, the probability of accurate dynamic prediction thereby being increased.

The major use of the program should be to reduce the amount of testing which is necessary, rather than to predict absolute data for particular conditions. For example, the inlet resistive valve may be varied over a wide range to determine the stability threshold for a particular operating condition. Testing would then be centred around the calculated optimum values. Similarly, the program can be applied to study the feasibility of a new design option, the effect of design changes on an existing system, and the effect of different parameters on the dynamic response of the system. The program can also be used to verify other simple models, or to provide some detailed steady-state data for use as initial conditions for linearised models.

APPENDIX A

STABILITY TESTS - TRANSIENT RESULTS AND ANALYSIS

APPENDIX A

STABILITY TESTS - TRANSIENT RESULTS AND ANALYSIS

A preliminary assessment has been made to investigate the periodic oscillations of a helically-coiled tube once-through boiler test rig.

The end conditions of the boiler have been analysed to show that the boiler was subjected to well-defined end constraints by means of the positive displacement feed pump, the single-phase by-pass and the large drum providing downstream pressure communication between the steam and by-pass flows.

A simple mathematical expression giving the condition for parallel circuit instability has been presented in terms of the amplitude of feed and steam flow oscillations and the magnitude of feed and steam flow frictional pressure drops.

CONTENTS

Page

Nomenclature

1. Introduction

2. Data Reduction
   - 2.1 Selection of tests
   - 2.2 Computer processing
   - 2.3 Graphical presentation of results
   - 2.4 Additional data

3. An Analysis of the Main Line Dynamic Characteristics
   - 3.1 Introduction
   - 3.2 Theory
   - 3.3 Sample calculation and comparison with experiment
   - 3.4 Discussion of results

4. An Analysis of the By-Pass Line Dynamic Characteristics
   - 4.1 Introduction
   - 4.2 Theory
   - 4.3 Sample calculation and comparison with experiment
   - 4.4 Discussion of results

5. Investigation of the Basic Criterion Governing Parallel Circuit Instability
   - 5.1 Theory
   - 5.2 Experimental results and discussion

NOMENCLATURE

$a_1, a_2, ..$	:	constants
A	:	cross-section area (m^2) or amplitude
C	:	capacitance (ms^2)
d	:	tube diameter (m)
f	:	friction factor
F	:	flow rate (kg/s)
I	:	inertance (l/m)
k	:	constant
L	:	tube length (m)
p	:	pressure (N/m^2)
R	:	resistance (l/ms)
Re	:	Reynolds number
t	:	time (s)
T	:	period (s)
V	:	volume (m^3)
ρ	:	density (kg/m^3)
μ	:	viscosity (Ns/m^2)
ξ	:	damping factor
φ	:	phase angle (deg)
ω	:	frequency (Rad/s)
ω_n	:	undamped natural frequency (Rad/s)
Δp	:	pressure drop

Subscripts

b	:	by-pass
sub	:	subcooled region

tp	:	two-phase region
sp	:	superheater region
ss	:	steady-state condition

1. INTRODUCTION

An experimental investigation was carried out at Babcock and Wilcox Limited, Renfrew, concerning the stability of once-through steam generators. The rig consisted of a primary hot gas supplying heat to the test section comprising two parallel water-steam circuits of a once-through boiler. For the tests conducted, only one of the two parallel water-steam circuits was used in parallel with a large by-pass and the other was completely isolated at both the water feed and steam manifolds. A diagrammatic arrangement of the rig is shown in Figure 1.

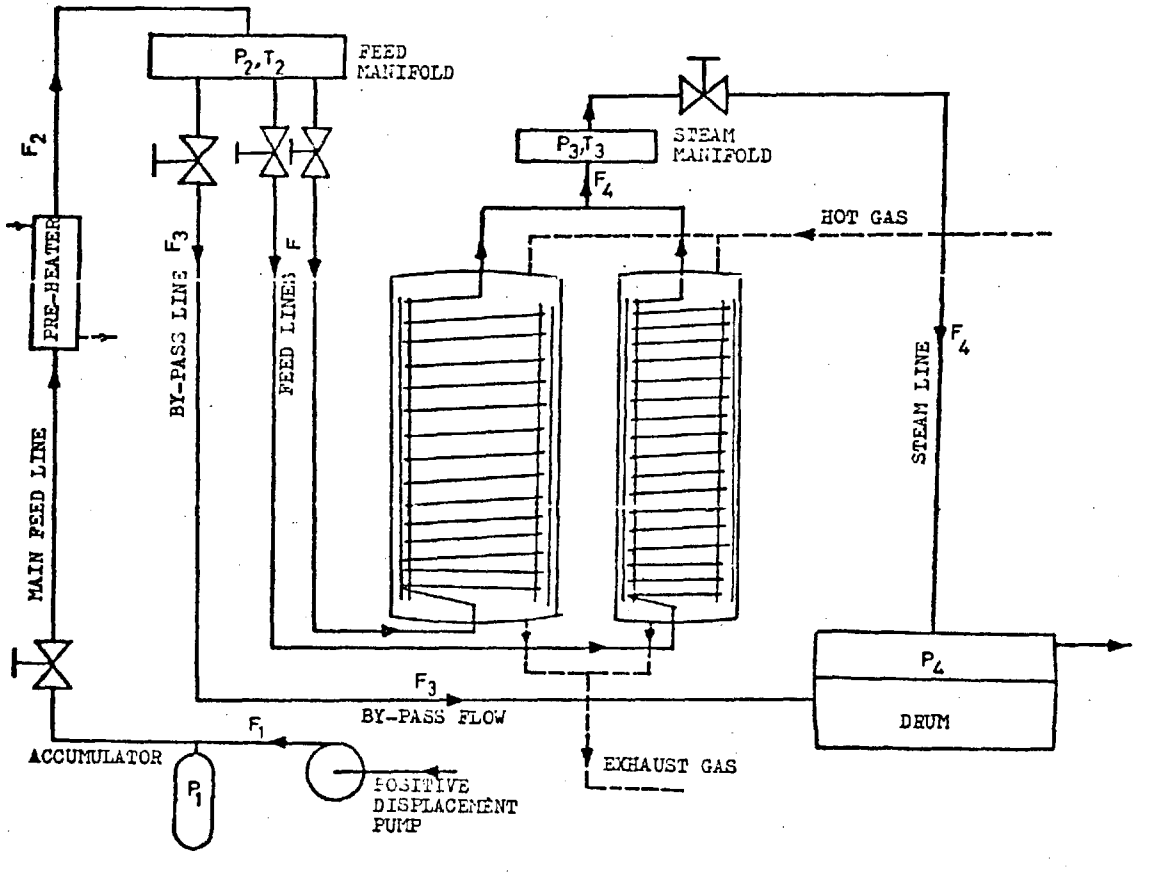


Figure 1: Schematic diagrams of once-through boiler rig

The range of parameters covered in the experiments is shown in Table 1.

Table 1: Range of variables

Parameter	Range
Number of channels	2
Tube length (m)	63.7
Coil diameter (m)	0.58 - 2.36
Channel feed flow (kg/s)	0.0172 - 0.069
Feed subcooling (^{o}C)	170 - 190
System pressure (bar)	50 - 80
Steam exit temperature (^{o}C)	395 - 455
Pressure drop of inlet ferrule valve (m bar)	9.2 - 369
Gas inlet temperature (^{o}C)	400 - 457
Gas flow rate (kg/s)	0.385 - 1.45

The tests were performed in such a way that there was a gradual transition from stable to unstable conditions as any one of the rig parameters controlling stability was changed incrementally. At each set of conditions, a complete data logger scan would normally be taken covering all those parameters appropriate to the test section in operation, and these results have been used to establish the stability threshold conditions. Even though these parameters tend to fluctuate, particularly as unstable conditions are approached, these single full scans are probably adequate for defining the stability threshold. However, in some of the tests, another type of data logger scanning technique was used as well, whereby one or more small groups of channels were selected from the complete scan and each group in turn was scanned continuously over a period of minutes to obtain transient data.

Parameters of particular interest were contained in these groups and efforts were made to include a feed flow measurement (F) in each group so as to give a common time reference between the parameters in each group assuming that the oscillations observed were steady and periodic. A selection of some of the transient results is presented in the following sections.

2. DATA REDUCTION

2.1 Selection of Tests

Sets of transient data, punched on paper tapes, were obtained at many test conditions but only a selected number of these have been processed. The selection was based on the following considerations:

1. Sinusoidal oscillations in feed flow were required and the charts from the continuous pen recorder were inspected to check that this was so.
2. It was desirable to have measurements of all the parameters of interest including feed flow (F), steam flow (F_4), by-pass flow (F_3) and total supply (main) flow (F_2), feed manifold pressure (P_2), and steam manifold pressure (P_4), tube wall temperatures and water/steam temperatures. This required scanning groups of channels in turn and it was therefore necessary to have a feed flow measurement in each group to provide a time reference.
3. Data was required for both the 0.58 m and 2.36 m diameter coil test sections to check that both gave consistent results.
4. Certain additional items of information and test data, e.g. drum level and accumulator volume, were required in order to analyse some of the transients and the availability of this was checked before making a final selection.

2.2 Computer Processing

A computer program, DAB, was written which converted the row data on paper tapes into engineering units and calculated the times for

each parameter. The instrument calibrations and zero readings of the corresponding 'steady-state' stability tests were used and the times were established from the scanning speed of the logger obtained by calibration during stability testing. Table 2 gives the output for test 28-8 when the information on the tapes had been converted.

The pressure drop and static pressure measurements were uncorrected for the buoyancy of the cold water in the pressure tapping lines, although this would not affect the magnitude of their oscillations. In those cases where a parameter was measured by more than one pressure drop transmitter, for example, feed flow F, the high range instrument reading was generally processed by the computer program, because the higher the range of these instruments, the faster their response. Absolute accuracy was sometimes sacrificed in so doing but this was considered to be justified since fluctuations were of prime interest.

2.3 Graphical Presentation of the Results

The transient results are presented graphically in Figures 2 to 4.

Most of these parameters are shown as fluctuations about a mean value, the mean value having been taken as the average of the maximum and minimum values given in each table of computer output. Most of the flow rate fluctuations are also expressed as a percentage of the mean feed flow rate (F), the reason being that non-dimensional parameters referred to the same basis are then produced and are easier to interpret and analyse.

A serious attempt has been made to use the same method of presentation in each test. Thus, the graphs for every test show all the available data on each parameter with the exception of the temperatures

Table 2: Experimental output of processed data

Test 28 Scan 8

Time Lag: 0.0000 0.8451 1.2676 1.4084 1.9718 2.6760 2.8169

Time	F	F_4	P_4	P_2	F_2	F_3	$P_2 - P_3$
0.0000	0.0277	4.1666	78.7700	76.1700	0.4079	0.3934	-2.6000
2.8169	0.0288	4.1309	78.7700	76.1700	0.4079	0.3948	-2.6000
5.6338	0.0286	4.1591	78.7700	76.2200	0.4085	0.3969	-2.5500
8.4507	0.0275	4.2038	78.7200	76.2700	0.4083	0.4032	-2.4500
11.2676	0.0239	4.3333	78.8200	76.2700	0.4077	0.4032	-2.5500
14.0845	0.0218	4.3566	78.8700	76.2700	0.4075	0.4098	-2.6000
16.9014	0.0182	4.4573	78.8700	76.3200	0.4069	0.4098	-2.5500
19.7183	0.0165	4.4764	78.8700	76.3200	0.4067	0.4068	-2.5500
22.5352	0.0171	4.4380	78.9200	76.2700	0.4073	0.4040	-2.6500
25.3521	0.0188	4.4257	78.9200	76.3200	0.4073	0.4021	-2.6000
28.1690	0.0201	4.3940	78.9200	76.3700	0.4073	0.4002	-2.5500
30.9859	0.0219	4.3351	78.9200	76.3200	0.4071	0.3952	-2.6000
33.8028	0.0257	4.2057	78.8700	76.2700	0.4079	0.3930	-2.6000
36.6197	0.0281	4.1554	78.8700	76.2700	0.4079	0.3938	-2.6000
39.4366	0.0286	4.1404	78.8200	76.2700	0.4085	0.3940	-2.5500
42.2535	0.0291	4.1215	78.8200	76.1700	0.4087	0.3952	-2.6500
45.0704	0.0286	4.2149	78.8200	76.2200	0.4077	0.4036	-2.6000
47.8873	0.0242	4.2809	78.8200	76.2700	0.4081	0.4019	-2.5500
50.7042	0.0234	4.3315	78.8700	76.2700	0.4083	0.4045	-2.6000
53.5211	0.0211	4.3833	78.9200	76.3200	0.4071	0.4083	-2.6000
56.3380	0.0183	4.4063	78.8700	76.3200	0.4075	0.4059	-2.5500

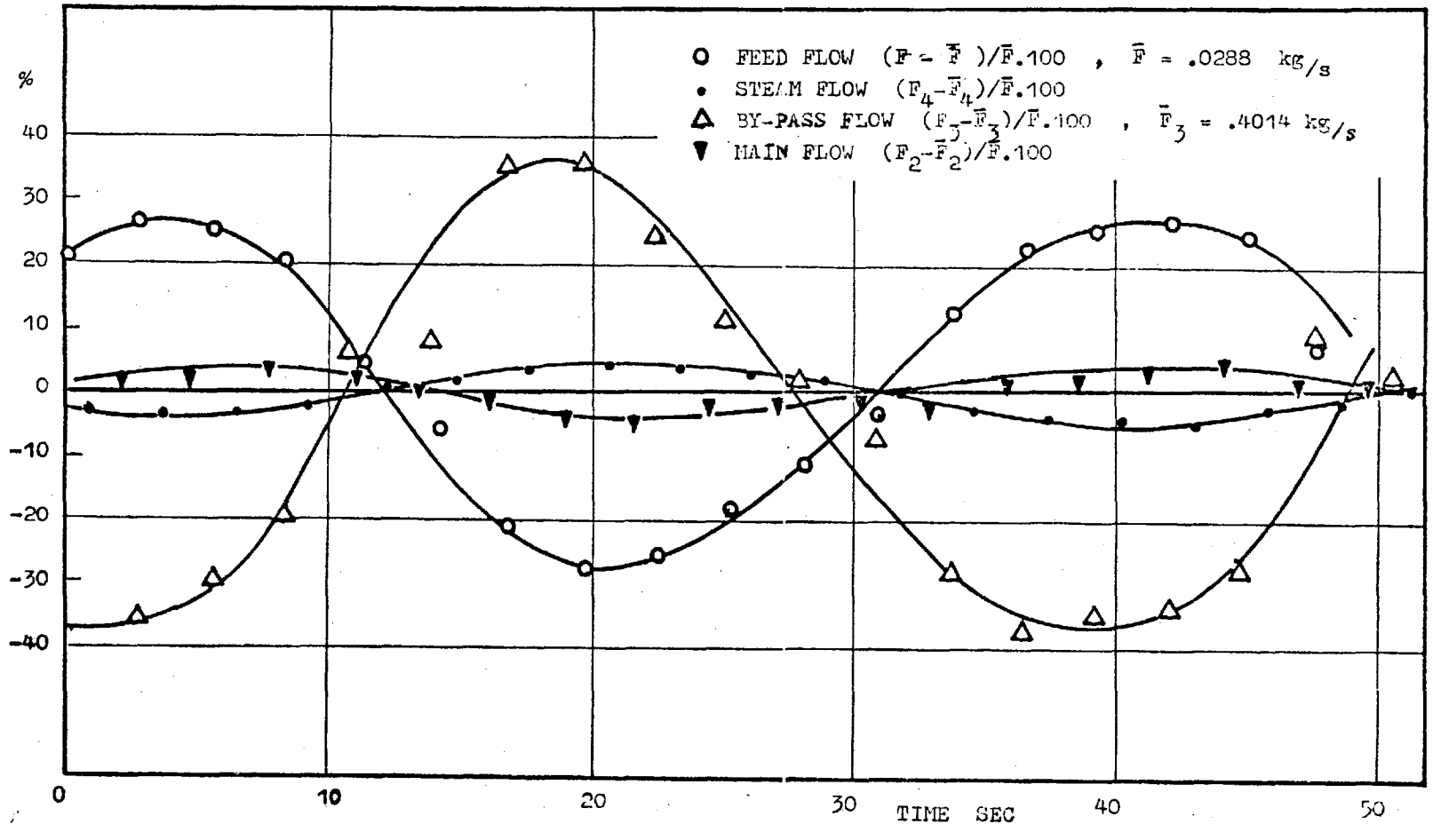


Figure 2: Experimental oscillations of feed flow, steam flow, by-pass flow and main flow for test 28-8

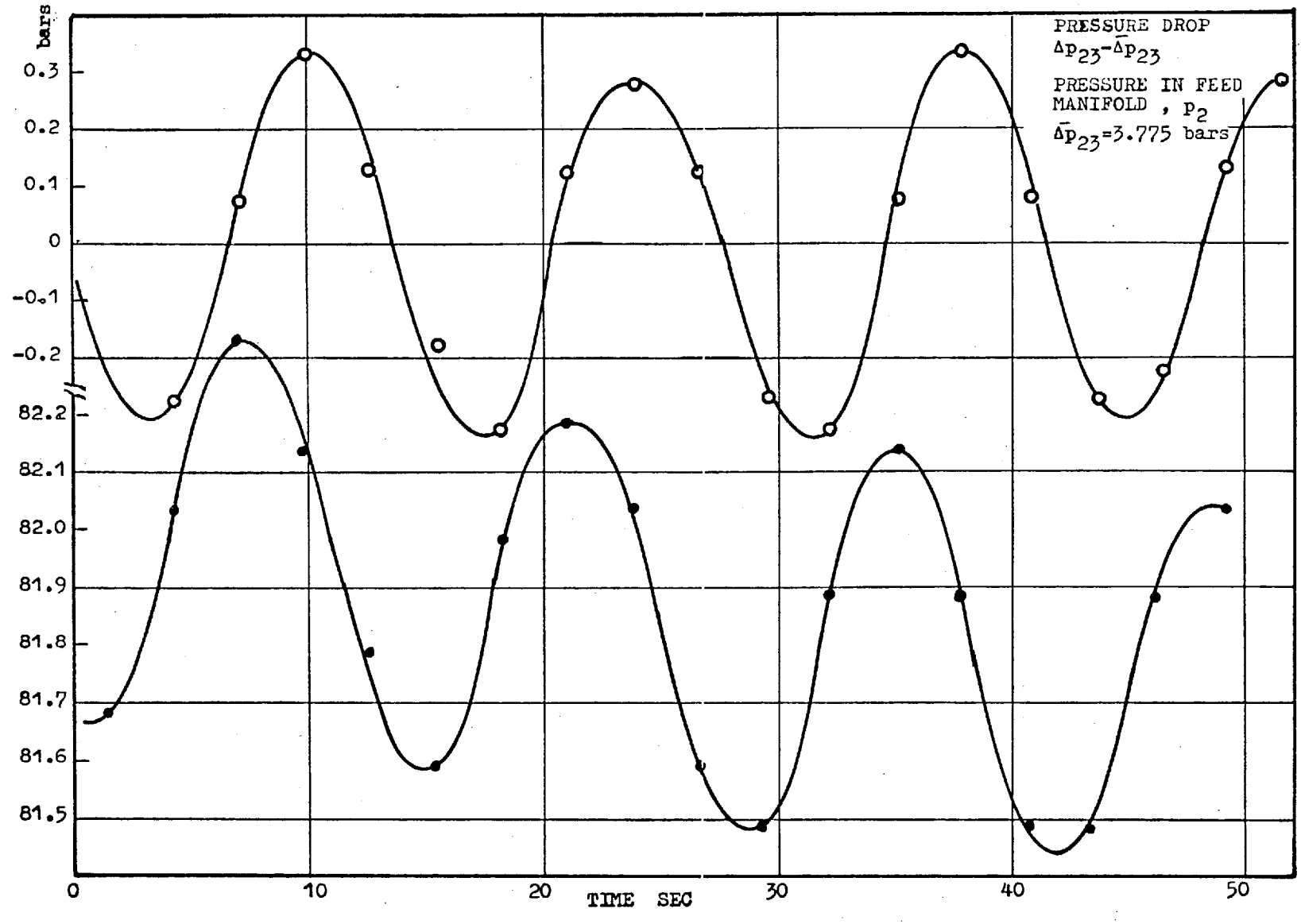


Figure 4: Experimental fluctuations of feed manifold pressure and the pressure drop between manifolds for test 32-9

which have been restricted to a specific time interval. Also, a common time-scale has been used as much as possible.

Also, "like" data has been presented in most cases, the obvious exception being the pressure drop between the manifolds. For the 2.36 m coil this was deduced from the static pressure measurements P_2 and F_4, whereas for the 0.58 m coil it was deduced from the differential pressure measurement, ΔP_{24}.

2.4 Additional Data

During the analysis and interpretation of the transient results, use was made of the following data as well:

1. The charts from the pen-recorders which give an overall description of the oscillatory behaviour at the time these transients were performed.
2. Test observation sheets which contain some recorder and indicator measurements not covered by the data logger instrumentation, for example, the nitrogen pressure in the accumulator.
3. The output from the instrument check computer program which gives the complete data logger scan converted to engineering units for each test.
4. The output from the computer program which gives a detailed breakdown of the pressure drop distributions in the test sections at stable conditions close to the stability threshold in each test.
5. Manufacturing and dimensional survey drawings of the test sections and the rig which give the necessary dimensional data.

3. AN ANALYSIS OF THE MAIN FEED LINE DYNAMIC CHARACTERISTICS

3.1 Introduction

The theory of parallel circuit instability is simplified if it is assumed that the total flow to a boiler remains constant whilst flow fluctuations are occurring in the individual circuits. The system used for stability testing was designed with a view to meeting this condition since the water was supplied to the heated test section and the unheated by-pass by a positive displacement pump, the output of which was insensitive to the discharge pressure.

However, an accumulator and feed valve were installed in the feed line to reduce pump pulsations. This combination can affect flow rate entering the feed manifold. The following analysis compares the flow fluctuations with measured values. Good agreement will show that confidence can be placed in both the measured data and in the methods used to design such feed systems.

3.2 Theory

A schematic diagram of the main feed line is given in Figure 5, together with the equivalent electrical circuit.

The system consists of a pump which raises the pressure of liquid to a value P_1 with constant flow rate F_1; a nitrogen accumulator which is characterised by a capacitance C and a negligible resistance and inertance; and a feed valve and pipe line which are characterised by a resistance R, an inertance I and negligible capacitance. The pipe line between the pump and the accumulator is very short and its resistance and inertance have been neglected.

The object now is to relate oscillations in flow rate F_2 to oscillations in feed manifold pressure P_2.

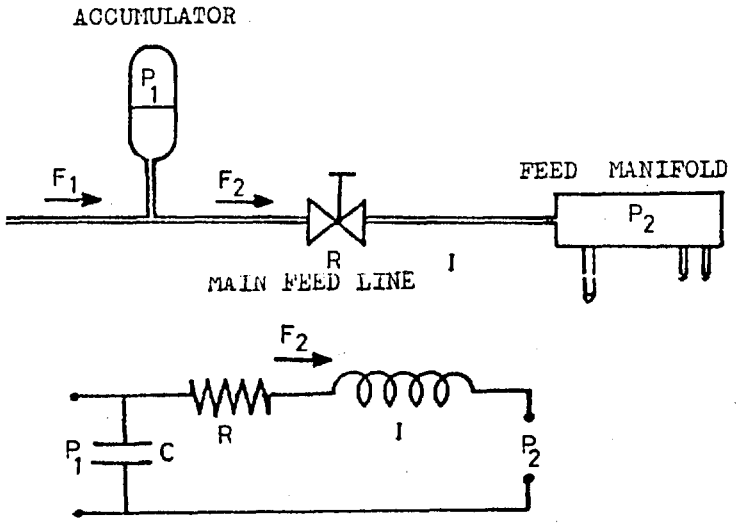


Figure 5: A schematic diagram of main feed line

By the simplified theory of linear hydraulic/pneumatic systems (Shearer et al (1967)), the equation describing the dynamics of the feed line is:

$$\delta p + R\,\delta F + I\,\frac{d\,(\delta F)}{dt} + \frac{1}{C}\int_{o}^{t} (\delta F)\,dt = 0 \qquad \text{(A.3.1)}$$

where δp and δF are perturbations of feed manifold pressure and main flow rate from steady-state values, respectively. I and R in equation (A.3.1) are the fluid inertance and resistance, respectively, and are defined as follows (Shearer et al (1967)) (Figure 5):

$$I = \sum \frac{L}{A} \qquad \text{(A.3.2)}$$

and

$$R = \left(\frac{2\,(P_1 - P_2)}{F_2}\right)_{ss} \qquad \text{(A.3.3)}$$

C in equation (A.3.1) is the accumulator capacitance, which is:

$$C = \left(\frac{\rho V_1}{P_1}\right)_{ss} \tag{A.3.4}$$

where V_1 and P_1 are the volume and pressure of the gas inside the accumulator, respectively.

Taking the Laplace transform of equation (A.3.1), the transfer function between the perturbation of flow and pressure can be written as:

$$Q(s) = \frac{F(s)}{P(s)} = \frac{-s}{I\left(s^2 + \frac{R}{I}s + \frac{1}{C\,I}\right)} \tag{A.3.5}$$

Assume

$$\delta p(t) = p_o \sin \omega t \tag{A.3.6}$$

This reduces the feed manifold pressure transient to a simple sinusoid and ignores the noise and harmonics present. The high frequency component oscillations due to pump pulsation are also ignored throughout the analysis. Employing equation (A.3.6) and equation (A.3.5), the frequency response of the main feed flow may be written as follows:

$$\delta F(t) = A \sin(\omega t - \varphi) \tag{A.3.7}$$

where

$$A = \frac{\frac{\omega}{I} p_o}{\left(\left(\frac{1}{C\,I} - \omega^2\right)^2 + \left(\frac{R}{I}\omega\right)^2\right)^{\frac{1}{2}}} \tag{A.3.8}$$

and

$$\varphi = \frac{\pi}{2} + \tan^{-1} \frac{\frac{R}{I}\omega}{\frac{1}{C\,I} - \omega^2} \tag{A.3.9}$$

3.3 Sample Calculations and Comparison with Experiment

The inertance I is calculated from the geometry of the pipework in the main feed line which is given in Table 3.

Table 3: Sizes of pipework in the main feed line

	O.D. (m)	Thickness (mm)	Length (m)	Area ($m^2 \times 10^4$)
Section 1	0.03287	6.25	13.716	3.366
Section 2	0.05934	3.85	66.843	21.649
Section 3	0.03287	6.25	9.144	3.366

Then, the inertance I (equation (A.3.2)) becomes:

$$I = \sum \frac{L}{A} = \frac{13.716}{3.366 \times 10^{-4}} + \frac{66.843}{21.649 \times 10^{-4}} + \frac{9.144}{3.366 \times 10^{-4}}$$

$$I = 0.9879 \times 10^5 \ m^{-1}$$

The following data is given in the instrument check output and test observation sheets appropriate to test 32-9:

$P_{1ss} = 123.01 \times 10^5 \ N/m^2$ steady-state pressure at feed pump discharge

$P_{2ss} = 84.01 \times 10^5 \ N/m^2$ steady-state feed manifold pressure

$$\rho = 997.2078 \ kg/m^3$$

V_{o1} = 0.05 m^3 total capacity of the accumulator

P_{o1} = 21.01 × 10^5 N/m^2 initial charge pressure on the accumulator

F_{2ss} = 0.6304 kg/s mean feed flow

From equation (A.3.3), the resistance R is as follows:

$$R = \left(\frac{2\ (P_1 - P_2)}{F_2}\right)_{ss} = \frac{2\ (123.01 - 84.01)}{0.6304}$$

$$R = 123.7310 \times 10^5\ m^{-1}s^{-1}$$

The capacitance of the accumulator is calculated from the total accumulator volume V_{o1} and the initial charge on the accumulator P_{o1}, as follows:

$$P_1 V_1 = P_{o1} V_{o1}$$

$$V_1 = \frac{P_{o1} V_{o1}}{P_1} = \frac{21.01 \times 10^5 \times 0.05}{123 \times 10^5}$$

$$V_1 = 0.8541 \times 10^{-2}\ m^3$$

Therefore, the capacitance C (equation (A.3.4)) is:

$$C = \frac{997.2078 \times 0.8541 \times 10^{-2}}{123.01 \times 10^5}$$

$$C = 0.6924 \times 10^{-6}\ ms^2$$

The experimentally obtained fluctuation of feed manifold pressure can be approximated by a sine wave of amplitude 0.38 bar and a period of 14 seconds, and can be expressed as follows:

$$\delta p\ (t) = 0.38 \times 10^5\ sin\ \omega\ t$$

where $$\omega = \frac{2\pi}{T} = 0.4488 \text{ Rad/s}$$

Substituting pressure fluctuation and the calculated values of resistance, capacitance and inertance into equations (A.3.8) and (A.3.9), the amplitude and phase angle of the main feed flow fluctuations can be found as follows:

$$A = 2.97 \times 10^{-3} \text{ kg/s}$$

$$\varphi = 165.6^{\circ} \text{ deg}$$

The flow rate of the test section is 0.06475 kg/s. Therefore, the fluctuation of the main feed flow relative to the flow of the test section becomes:

$$A = 4.3\%$$

A comparison of predicted and experimental results for two tests are given in Table 4.

3.4 Discussion of Results

Table 4 compares the measured and the 'best estimate' of theoretical main flow fluctuations for tests 32-9 and 28-8 on the basis that the observed fluctuations are steady and periodic. The agreement

Table 4: Summary and comparison of main feed line dynamic characteristics

Test Number		32-9	28-8
I (m^{-1})		0.9879×10^5	0.9879×10^5
R $(m^{-1}s^{-1})$		123.731×10^5	118.911×10^5
C $(m\ s^2)$		0.6924×10^{-6}	1.0578×10^{-6}
P_{2ss} (N/m^2)		81.8×10^5	76.28×10^5
P_o (N/m^2)		38000	10000
ω (Rad/s)		0.4488	0.1611
% amplitude of fluctuation	Exp.	4.1	4.0
	Pred.	4.3	3.4
Phase angle (degree)	Exp.	154.3	156.9
	Pred.	165.6	153.4
Damping factor, ξ		16.39	19.46
Undamped natural frequency, ω_n		3.8	3.1

between the theory and experiment is good considering the simplified assumption made in the analysis and interpretation of experimental results.

The value of damping factor (ξ) for the second order system considered in the analysis is given in Table 4. The high value of ξ ($\xi > 1/\sqrt{2}$) is desirable in such a system since it would not result in the build-up of large oscillation.

To find the effect of errors in evaluating the resistance, capacitance and inertance, these values have been varied by ± 50% about the calculated values, and the following results were obtained for

test 32-9:

Parameter Change		New A	New φ	New ξ
Resistance	+ 50%	2.35	172.7	24.6
	- 50%	8.4	152.8	8.2
Capacitance	+ 50%	4.7	172.8	23.1
	- 50%	4.2	152.7	11.59
Inertance	+ 50%	4.6	176.3	11.59
	- 50%	4.56	176.3	23.1

It can be seen that the feed system was indeed very "hard" leading to main flow fluctuations which can probably be neglected in the interpretation of the stability data.

4. ANALYSIS OF THE BY-PASS LINE DYNAMIC CHARACTERISTICS

4.1 Introduction

In order to interpret the stability results, it is necessary to understand the dynamic behaviour of the by-pass line. Bailey et al (1970) and Carver (1970) explain how the theory of parallel channel instability can be applied to the case of a single heated channel in parallel with an unheated by-pass when the dynamics of the by-pass are known. It can be shown in fact that these two systems will have the same stability characteristics in the limit of an infinitely large by-pass ratio (by-pass flow/feed flow), the simple explanation being that a constant pressure difference will be maintained across the heated channel in both cases.

The purpose of the following calculations is to demonstrate how effectively a theoretical analysis of the by-pass line dynamics can be used to predict the fluctuations in pressure drop across the heated test section. Good agreement will show that confidence can be placed in both the measured data and in the theory of the by-pass. A complication in this work arises because the pressure difference was measured between the feed and steam manifolds and not between the feed manifold and the drum where the two flows have pressure communication. This was allowed for, however, but in fact the correction was not great.

4.2 Theory

A schematic diagram of the steam line and the by-pass line communicating at the drum is shown in Figure 6. Assuming that all the pressure drop in the by-pass line occurs across the valve then the equation relating the fluctuations of pressure drop ΔP_{24} and by-pass flow F_3 is:

$$\delta\ (\Delta P_{24}) - R\ \delta F_3 - I\ \frac{d(\delta F_3)}{dt} = 0 \qquad \text{(A.4.1)}$$

where R and I are the resistance and inertance of the by-pass line, respectively. If we assume a sine wave fluctuation for the by-pass flow:

$$\delta F_3 = A\ sin\ \omega\ t \qquad \text{(A.4.2)}$$

Then, from (A.4.1), we have:

$$\delta\ (\Delta P_{24}) = \sqrt{(I^2\ \omega^2 + R^2)}\ A\ sin\ (\omega\ t + \phi) \qquad \text{(A.4.3)}$$

where $$\phi = tan^{-1}\ I\ \omega/R \qquad \text{(A.4.4)}$$

Now, allowance will be made for the effect of the pipe line between the steam manifold and the drum so as to relate the fluctuations in pressure drop measured between the feed manifold and the steam manifold to those required between the feed manifold and the drum.

In order to describe the dynamics of the steam pipe, it has been assumed that the system is at constant temperature. The steam pipe has a capacitance C_1, resistance R and inertance I. The equivalent electrical circuit for the system steam manifold - steam pipe - drum is shown in Figure 7.

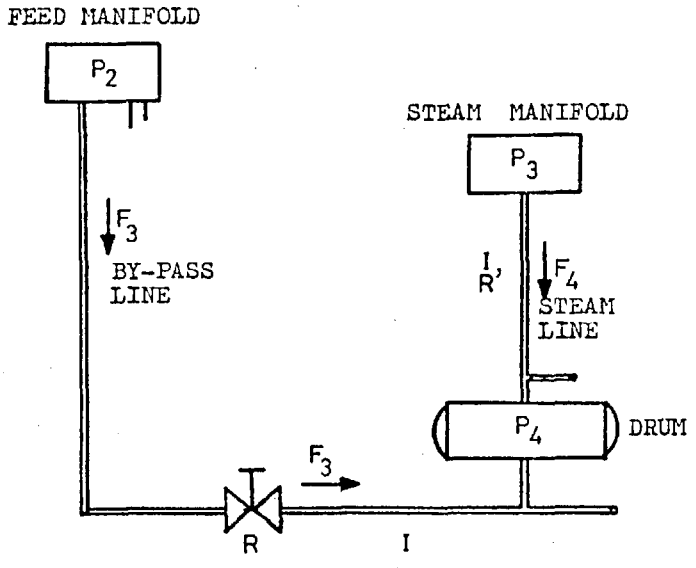


Figure 6: A schematic diagram of the steam and by-pass line

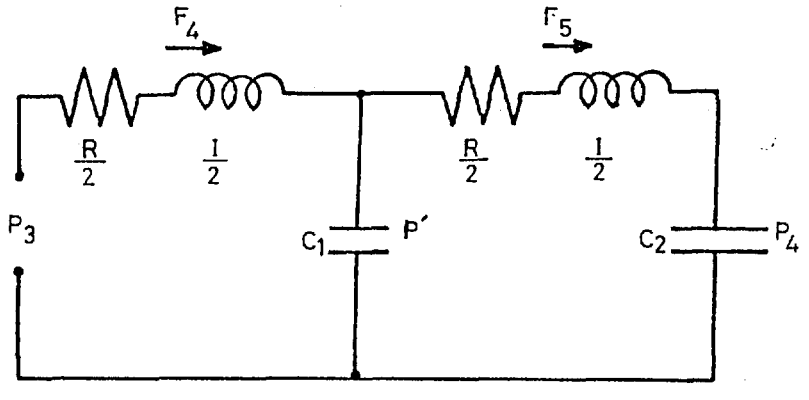


Figure 7: Equivalent electrical circuit of steam line

The following equations describe the dynamics of this system:

$$P_3 = \frac{R}{2} F_4 + \frac{I}{2} \frac{d F_4}{dt} + P' \qquad \text{(A.4.5)}$$

$$P' = \frac{R}{2} F_5 + \frac{I}{2} \frac{d F_5}{dt} + P_4 \qquad \text{(A.4.6)}$$

$$P' = \frac{1}{C_1} \int (F_4 - F_5)\, dt \qquad \text{(A.4.7)}$$

$$P_4 = \frac{1}{C_2} \int F_5\, dt \qquad \text{(A.4.8)}$$

These can be reduced to the following equations:

$$P_3 - \frac{I}{2}\frac{d F_4}{dt} - \frac{R}{2} F_4 - \frac{1}{C_1}\int (F_4 - F_5)\, dt = 0 \qquad \text{(A.4.9)}$$

$$\frac{1}{C_1}\int (F_4 - F_5)\, dt = F_5 \frac{R}{2} + \frac{I}{2}\frac{d F_5}{dt} + \frac{1}{C_2}\int F_5\, dt \qquad \text{(A.4.10)}$$

Consider $p_i = p_i - p_{iss}$ and $F_i = F_i - F_{iss}$

where subscript i denotes an arbitrary location i and ss denotes steady-state conditions. In this case, equations (A.4.5) to (A.4.10) apply to the fluctuations as well.

The Laplace transforms of these equations with zero initial pressure and flow fluctuations are:

$$P_3(s) - F_4(s)\left[\frac{R}{2} + \frac{I}{2}s + \frac{1}{C_1 s}\right] + \frac{F_5(s)}{C_1 s} = 0 \qquad \text{(A.4.11)}$$

$$\frac{F_4(s)}{C_1 s} - F_5(s)\left[\frac{R}{2} + \frac{I}{2}s + \frac{1}{C_1 s} + \frac{1}{C_2 s}\right] = 0 \qquad \text{(A.4.12)}$$

The solution for $F_5(s)$ by equations (A.4.11) and (A.4.12) is:

$$F_5(s) = \frac{4 s P_3(s)}{C_1 I^2 (s^4 + a_1 s^3 + a_2 s^2 + a_3 s + a_4)} \qquad \text{(A.4.13)}$$

From equation (A.4.8), we note that:

$$P_4(s) = \frac{F_5(s)}{C_2 s} \qquad \text{(A.4.14)}$$

From equations (A.4.13) and (A.4.14), we can write:

$$P_4(s) = \frac{a_4 P_3(s)}{s^4 + a_1 s^3 + a_2 s^2 + a_3 s + a_4} \tag{A.4.15}$$

where

$$a_1 = \frac{2R}{I} \tag{A.4.16}$$

$$a_2 = \frac{4}{C_1 I} + \frac{2}{C_2 I} + \frac{R^2}{I^2} \tag{A.4.17}$$

$$a_3 = \frac{4R}{C_1 I^2} + \frac{2R}{C_2 I^2} \tag{A.4.18}$$

$$a_4 = \frac{4}{C_1 C_2 I^2} \tag{A.4.19}$$

Then the transfer function $Q(s)$ will be:

$$Q(s) = \frac{a_4}{s^4 + a_1 s^3 + a_2 s^2 + a_3 s + a_4} \tag{A.4.20}$$

From the diagram of Figure 6, the following relations yield:

$$P_2(s) - P_3(s) = \Delta P_{23}(s) \tag{A.4.21}$$

$$P_2(s) - P_4(s) = \Delta P_{24}(s) \tag{A.4.22}$$

Substituting equations (A.4.15) and (A.4.21) into equation (A.4.22) results in:

$$\Delta P_{24}(s) = P_2(s) - Q(s) P_3(s)$$

$$= P_2(s) - Q(s) \left[P_2(s) - \Delta P_{23}(s)\right]$$

Therefore:

$$\Delta P_{24}(s) = \left(1 - Q(s)\right) P_2(s) + Q(s)\, \Delta P_{23}(s) \qquad \text{(A.4.23)}$$

Having the experimental fluctuations of the feed manifold pressure, P_2, and the pressure drop fluctuations between the manifold, ΔP_{23}, the pressure drop fluctuations between the feed manifold and the drum can be obtained from equation (A.4.23). This represents a measured value of the fluctuations in ΔP_{24} and the results are compared with the theoretical values given by equations (A.4.3) and (A.4.4).

4.3 Sample Calculations and Comparison with Experiment

In the following, a detailed set of calculations for test 32-9 and an abbreviated set of calculations for test 56-8 are carried out.

Firstly, perform the by-pass calculations involving equations (A.4.3) and (A.4.4). According to the transient data:

Mean by-pass flow rate	= 0.5898 kg/s
Mean feed flow rate	= 0.06475 kg/s
Amplitude of by-pass flow fluctuations relative to the mean feed flow rate	= 28%
Period of by-pass flow fluctuations	= 14 seconds
By-pass frictional pressure drop, $P_2 - P_4$	= 4735.3 mbar

The rig drawings give:

Length of by-pass pipe, L	= 22 m
Area of the by-pass pipe, A	= 1.3134×10^{-3} m^2

Then the inertance is:

$$I = \sum \frac{L}{A}$$

$$I = 1.6751 \times 10^4 \text{ m}^{-1}$$

and the resistance is:

$$R = \left(\frac{2\ (P_2 - P_4)}{F_3}\right)_{ss}$$

$$R = \frac{2 \times 4.73533 \times 10^5}{0.5898} = 16.0575 \times 10^5 \text{ m}^{-1}\text{s}^{-1}$$

Experimentally obtained fluctuations in by-pass flow are:

$$F_3 = 0.28 \times 0.06475 \sin \frac{2\pi}{14} t$$

$$= 0.01813 \sin 0.4488\ t \qquad \text{(A.4.24)}$$

By equations (A.4.3) and (A.4.4), we have:

$$\Delta P_{24} = 291.125 \sin (0.4488\ t + \phi) \qquad \text{(mbar)} \qquad \text{(A.4.25)}$$

and

$$\phi = \tan^{-1} \frac{1.6751 \times 10^4 \times 0.4488}{16.0575 \times 10^5} = \tan^{-1} 4.7 \times 10^{-3} = 0.27^{\circ}$$

therefore ϕ is almost = 0 (A.4.26)

The predicted fluctuation of ΔP_{24} is shown in Figure 8.

The second stage is now to find the observed fluctuation of ΔP_{24} from the measured fluctuation in pressure drop between the feed and steam manifold using equation (A.4.23).

The inertance of the steam pipe between the steam manifold and the drum is obtained as follows:

Length of the steam pipe between the steam manifold and the drum	= 23.8 m
Inside diameter of the pipe	= 3.8×10^{-2} m
Cross-sectional area of the pipe	= 1.14×10^{-3} m^2
Volume of the steam pipe, V_1	= 27.133×10^{-3} m^3

Therefore:

$$I = \frac{L}{A} = \frac{23.8}{1.4 \times 10^{3}} = 2.0877 \times 10^{4} \text{ m}^{-1}$$

The measurements of Table 5 have been obtained for different tests. Table 6 gives the calculated value of the resistance and capacitance of the steam pipe between the steam manifold and the drum together with the constants a_1, a_2, etc., required in equation (A.4.20).

Now, from the measured transient data, we have:

$$\delta P_2 = 380 \sin 0.4488\, t \quad \text{(mbar)}$$

$$\delta (\Delta P_{23}) = 330 \sin 0.4488\, t \quad \text{(mbar)}$$

Therefore:

$$P_2(s) = 380 \frac{0.4488}{s^2 + 0.2014} \qquad \text{(A.4.27)}$$

$$\Delta P_{23}(s) = 330 \frac{0.4488}{s^2 + 0.2014} \qquad \text{(A.4.28)}$$

Table 5: Measured parameters

Test	32-9	56-8
Feed manifold pressure, P_2 (bar)	84.46	84.02
Steam manifold pressure, P_3 (bar)	80.66	82.02
Feed manifold temperature (^oC)	106.5	106
Steam manifold temperature (^oC)	410.9	395
ρ_w (kg/m^3)	958.4	958.4
ρ_s (kg/m^3)	28.5	30.352
ρ_c (at 20^oC) (kg/m^3)	1001.97	1001.93
By-pass friction pressure drop due to last stable scan of data (mbar)	4735.3	3462.75
μ (Ns/m^2)	25.9×10^{-6}	25.4×10^{-6}
Re	7.2×10^4	6.4×10^4
Friction factor, f	0.0336	0.0368
Drum level reading	65%	53%
Drum level height from datum (m)	0.543	0.706
Steam volume in drum, V_2 (m^3)	0.7703	0.503
Drum volume (m^3)	1.033	1.033

Table 6: Dynamic characteristics of steam pipe and drum as calculated

Test	32-9	56-8
$R = \frac{f\,LW}{dA^2\rho}$ $m^{-1}s^{-1}$	41.829	32.3878
$C_1 = \frac{V_1\rho}{P}$ $m\,s^2$	9.587×10^{-8}	10.0407×10^{-8}
$C_2 = \frac{V_2\rho}{P}$ $m\,s^2$	2.7217×10^{-6}	1.8614×10^{-6}
a_1	0.401×10^{-2}	0.3103×10^{-2}
a_2	0.2036×10^4	0.1956×10^4
a_3	4.08	3.04
a_4	0.352×10^5	0.491×10^5

Substituting these transforms in equation (A.4.23) gives:

$$\Delta P_{24}(s) = \frac{170.54s^4+0.6822s^3+0.3473\times10^6s^2+0.6958\times10^3s+0.5213\times10^7}{s^6+0.4\times10^{-2}s^5+0.2036\times10^4s^4+4.08s^3+0.3565\times10^5s^2+0.8217s+0.709\times10^4} \qquad \text{(A.4.29)}$$

Equation (A.4.29) is the Laplace transform of ΔP_{24} which was inverted using the Honeywell on-line computer program TRANS. The results of this inversion are shown in Figure 8 from which the steady periodic fluctuations in ΔP_{24} can be found.

Comparison of the experimental values due to equation (A.4.29) with the theoretical values from equation (A.4.25) shows that there is a difference of 30 mbar between them.

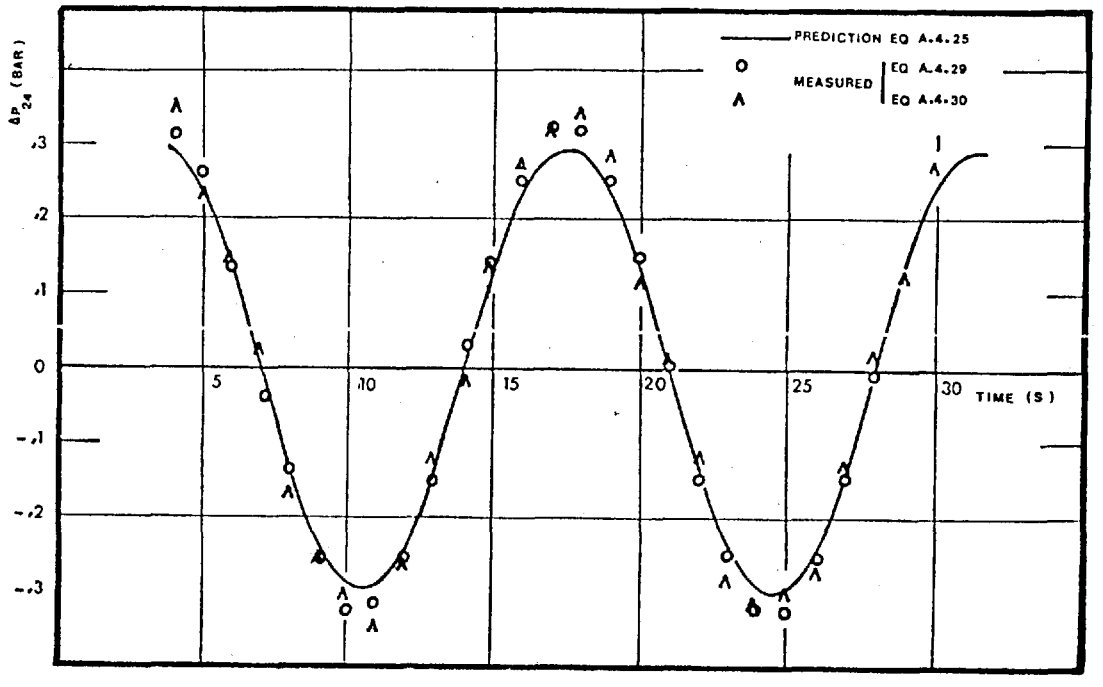


Figure 8: By-pass line pressure drop fluctuation

Figure 8 shows that the experimental and theoretical fluctuations are almost exactly in phase with each other which is very encouraging.

It is also useful to see the effect of feed manifold pressure fluctuations P_2 on the calculation of ΔP_{24} from the measured pressure drop fluctuations between the feed and steam manifolds. Neglecting these static pressure fluctuations means that the terms $P_2(s)$ in equation (A.4.23) must be neglected. Then we have:

$$\Delta P_{24}(s) = Q(s)\,\Delta P_{23}(s) \qquad \text{(A.4.30)}$$

Using this equation for test 32-9 gives the fluctuations shown in Figure 8.

Comparison of the results in Figure 8 and Table 7 shows that the fluctuation of pressure drop calculated by equation (A.4.30) has a greater amplitude than the one calculated by equation (A.4.23) and there is a 0.5 second phase difference.

For test 56-8, no measurements were available for the steam flow and steam manifold pressure fluctuations so that the simplified method represented by equation (A.4.30) was used to relate the measured fluctuations in pressure drop between the manifolds to those between the feed manifold and the drum. Results are given in Table 7.

4.4 Discussion of Results

Table 7 summarises the results obtained for both test 32-9 and test 56-8. The agreement between theory and experiment is good considering that there are many potential sources of error in both experiment and theory, such as:

1. Errors in instrumentation including the effect of response.
2. Smoothing of the transient curves to pure sine waves, so

Table 7: Summary and comparison of calculations of by-pass line dynamics

Test			32-9	56-8
Mean feed flow		kg s^{-1}	0.06475	0.04875
Mean by-pass flow		kg s^{-1}	0.5898	0.71795
Amplitude of by-pass flow fluctuations relative to mean feed flow		%	28%	80%
Amplitude of pressure drop fluctuations between manifolds		mbar	330	350
Period of fluctuations		secs	14	9.2
Theoretical and measured amplitude of fluctuations in pressure drop between feed manifold and drum, ΔP_{24}	by theoretical analysis of equation (A.4.3)	mbar	291	360
	by measurement of equation (A.4.23)	mbar	325	-
	by measurement of equation (A.4.30)	mbar	360	382

ignoring noise and other harmonies.

3. Errors involved in the calculation of capacitance of steam line and drum.

4. Use of linear approximations and lumped parameter methods.

All things, considered, therefore, this work suggests that the prediction methods being used are reasonably adequate and that the measurements obtained are reasonably accurate.

5. INVESTIGATION OF THE BASIC CRITERION GOVERNING PARALLEL CIRCUIT INSTABILITY

5.1 Theory

When there are large numbers of channels in parallel, changes of flow in one channel will have a negligible effect on the bulk flow and hence on the pressure drop between the headers; the condition for instability is therefore that the flow in one of these channels can oscillate at a certain frequency such that there is no change in the pressure drop across the channel (Bailey et al (1970)).

Following Davies and Potter (1967), define the open loop response for this channel as:

$$H = \frac{\delta\ (\Delta P_{tp} + \Delta P_{sp})}{\delta\ (\Delta P)_{sub}} \qquad \text{(A.5.1)}$$

where ΔP is the pressure drop and subscripts sub, sp and tp denote the single-phase liquid, single-phase vapour and two-phase regions, respectively. The stability criterion is that the open loop response (equation (A.5.1)) should not cross the negative real axis outside -1 on a polar diagram (Davies et al (1967)). Thus, it follows that for a large number of parallel channels at the stability threshold:

$$\frac{\delta\ (\Delta P_{tp} + \Delta P_{sp})}{\delta\ (\Delta P)_{sub}} = -1 \qquad \text{(A.5.2)}$$

Now, neglect changes in pressure drop over the two-phase region and consider only fluctuations in frictional pressure drop. As it was noticed in chapter 6, Figures 6.33 and 6.46, these simplifications were justified when frictional pressure drops predominate and when the evaporator is short compared with the superheater and economiser. In

this case, equation (A.5.2) reduces to:

$$\frac{\delta\ (\Delta P)_{sp}}{\delta\ (\Delta P)_{sub}} = -1 \qquad \text{(A.5.3)}$$

where ΔP denotes frictional pressure drop.

Now, suppose that:

$$\Delta P_{sp} = a\ Re^{-n}\ F_{sp}^{2} \simeq k_1\ F_{sp}^{2-n}$$

and

$$\Delta P_{sub} = k_2\ F_{sub}^{2-m}$$

where k_1 and k_2 are constants, n and m range between 0 to 0.25 (Coulson (1970)) and F denotes mass flow rate. Therefore:

$$\delta\ (\Delta P)_{sp} = (2 - n)\ \frac{\Delta P_{sp}}{F}\ \delta F_{sp} \qquad \text{(A.5.4)}$$

$$\delta\ (\Delta P)_{sub} = (2 - m)\ \frac{\Delta P_{sub}}{F}\ \delta F_{sub} \qquad \text{(A.5.5)}$$

Substituting equations (A.5.4) and (A.5.5) into equation (A.5.3) gives:

$$\frac{2 - n}{2 - m}\ \frac{\Delta P_{sp}}{\Delta P_{sub}}\ \frac{\delta F_{sp}}{\delta F_{sub}} = -1 \qquad \text{(A.5.6)}$$

Expressing δF_{sp} and δF_{sub} as sine waves of amplitude $\overline{F}_{sp}$ and $\overline{F}_{sub}$, respectively, and considering that δF_{sp} and δF_{sub} are out of phase by 180^{o} at the onset of instability (Chapter 6, Figure 6.45), it follows:

$$\frac{\Delta P_{sp}}{\Delta P_{sub}}\ \frac{\overline{F}_{sp}}{\overline{F}_{sub}} = \frac{2 - m}{2 - n} \qquad \text{(A.5.7)}$$

Expression (A.5.7) should therefore hold at the stability threshold for a large number of parallel channels. This can be modified for the case of a single heated channel in parallel with an unheated by-pass as follows:

For the heated channel, neglecting the fluctuation of the evaporator pressure drop, and considering just friction, we have:

$$\delta\,(\Delta P) = \delta\,(\Delta P)_{sub} + \delta\,(\Delta P)_{sp}$$

or $$\delta\,(\Delta P) = (2-m)\,\frac{\Delta P_{sub}}{F}\,\delta F_{sub} + (2-n)\,\frac{\Delta P_{sp}}{F}\,\delta F_{sp} \qquad \text{(A.5.8)}$$

If the total flow to the heated channel with an unheated by-pass is kept constant, then a reduction in flow to the heated channel (δF_{sub}) results in a corresponding increase to the by-pass (δF_b) which immediately produces an increase in pressure drop across the by-pass and therefore across the heated channel. Therefore, for the unheated by-pass, we have:

$$\Delta P = k_3\,F_b^{2-p}$$

and $$\delta\,(\Delta P) = (2-p)\,\frac{\Delta P}{F_b}\,\delta F_b$$

or $$\delta\,(\Delta P) = (2-p)\,\frac{\Delta P}{F_b}\,(-\delta F_{sub}) \qquad \text{(A.5.9)}$$

Equating equations (A.5.8) and (A.5.9) yields:

$$\left[1 + \frac{2-p}{2-m}\,\frac{\Delta P}{\Delta P_{sub}}\,\frac{1}{R}\right]\,(2-m)\,\frac{\Delta P_{sub}}{F}\,\delta F_{sub} + (2-n)\,\frac{\Delta P_{sp}}{F}\,\delta F_{sp} = 0 \qquad \text{(A.5.10)}$$

where $R = F_b/F$ is the ratio of by-pass flow to the flow of the heated

channel. Equation (A.5.10) compares with the following relation for a large number of parallel heated channels (without by-pass):

$$(2 - m) \frac{\Delta P_{sub}}{F} \delta F_{sub} + (2 - n) \frac{\Delta P_{sp}}{F} \delta F_{sp} = 0 \qquad \text{(A.5.11)}$$

Comparison of equations (A.5.10) and (A.5.11) shows that the existence of a parallel by-pass line produces additional pressure drop in the heated channel, the magnitude of which is:

$$(\Delta P)_{add} = \frac{2 - p}{2 - m} \frac{\Delta P}{R} \qquad \text{(A.5.12)}$$

Thus, a heated channel in parallel with an unheated by-pass is equivalent to a large number of heated parallel channels having, in the feed line, an additional restriction with a pressure drop given by equation (A.5.12).

Equation (A.5.10) can be rearranged in the following form analogous to equation (A.5.7) at the stability threshold:

$$\frac{1}{\left[1 + \frac{2 - p}{2 - m} \frac{\Delta P}{\Delta P_{sub}} \frac{1}{R}\right]} \frac{\Delta P_{sp}}{\Delta P_{sub}} \frac{\overline{F}_{sp}}{\overline{F}_{sub}} = \frac{2 - m}{2 - n} \qquad \text{(A.5.13)}$$

As the by-pass ratio, $R = F_b/F$, tends to infinity, then equations (A.5.13) and (A.5.7) become identical. This is mainly why tests with a large by-pass are performed.

Equations (A.5.12) and (A.5.13) show that as the by-pass ratio increases, so the system becomes less stable, or alternatively an increase in the by-pass resistance stabilises the system.

Carver (1970) gives a thorough analysis, and deals with the effects of inertance in the by-pass line and other forms of pressure drop

in the heated channel.

5.2 Experimental Results and Discussion

The coefficients m, n and p in equation (A.5.13) depend on the roughness of the pipe and Reynolds number (Coulson (1970)). At high Reynolds number, the coefficients approach zero. Accordingly, in the calculation, the values of m and p for subcooled liquid and by-pass line are taken as 0.25 (1/7 power law for velocity profile), and in the superheater region where the Reynolds number is comparatively high, n is assumed to be 0.01. Therefore, the condition of threshold of the instability (equation (A.5.13)) is reduced to:

$$\frac{1}{1 + \frac{\Delta P}{\Delta P_{sub}} \frac{1}{R}} \frac{\Delta P_{sp}}{\Delta P_{sub}} \frac{\overline{F}_{sp}}{\overline{F}_{sub}} = 0.92 \qquad \text{(A.5.14)}$$

The theoretical condition for instability given by equation (A.5.14) has been compared with two sets of experimental measurements. The results are summarised in Table 8.

Considering the approximate nature of this analysis and the errors involved in the measurement of steam flow and frictional pressure drops, the ratio of 0.88 and 0.92 obtained in these two tests compare favourably with the theoretical value of 0.92.

Table 8: Summary of experimental and theoretical prediction

Test number	28-8	32-9
Phase relation between feed and steam flow fluctuations	180^{o}	180^{o}
Amplitude of feed flow fluctuations (%)	27.6	20.9
Amplitude of steam fluctuations (%)	4.5	4.5
Subcooled liquid frictional ΔP at onset of instability (mbar)	42.68	306.4
Superheater frictional ΔP at onset of instability (mbar)	442.04	3595.88
By-pass frictional ΔP (mbar)	650.12	4735.33
By-pass ratio	16.614	8.84
Left hand side of equation (A.5.14)	0.88	0.92

APPENDIX B

NUMERICAL STABILITY OF CSDT METHOD AS APPLIED TO THE LINEAR HEAT EXCHANGER

In this section, the stability of the numerical approximation of the time derivatives of partial differential equations which describe a simple linear counterflow heat exchanger is discussed. As a first step, a trial solution is attempted which leads us to an eigenvalue problem with the time characterisitcs of the heat exchanger as the eigenvalues. Then the solution of the difference equations is related to the time characteristics, and it is shown that any errors introduced into the computation will decay as time increases.

Consider the equations of a linear counterflow heat exchanger as follows:

$$\frac{\partial T_1}{\partial t} - V_1 \frac{\partial T_1}{\partial z} = k_1 (T_3 - T_1) \tag{B.1}$$

$$\frac{\partial T_2}{\partial t} + V_2 \frac{\partial T_2}{\partial z} = k_2 (T_3 - T_2) \tag{B.2}$$

$$\frac{\partial T_3}{\partial t} = \mu_1 (T_1 - T_3) + \mu_2 (T_2 - T_3) \tag{B.3}$$

where indices *1*, *2* and *3* refer to the primary flow, secondary flow and tube wall, respectively.

Before proceeding to the finite difference approximation, let us examine the solution by the separation of variables method as:

$$T_i - T_{ss,i} = f(t) \cdot g_i(z) \quad , \quad i = 1, 2 \text{ or } 3 \tag{B.4}$$

where T_{ss} is the steady-state solution and $f(t)$ and $g(z)$ are only

functions of time and length, respectively. Substituting equation (B.4) into equation (B.1), we obtain:

$$g \cdot \frac{\partial f}{\partial t} - V_1 \cdot f \cdot \frac{\partial g}{\partial z} = k_1 (g_3 - g_1) \cdot f \qquad (B.5)$$

Dividing both sides of equation (B.5) by $f.g$ and rearranging gives:

$$\frac{1}{f}\frac{\partial f}{\partial t} = V_1 \frac{1}{g_1}\frac{\partial g_1}{\partial z} + k_1 \left(\frac{g_3 - g_1}{g_1}\right) \qquad (B.6)$$

Now, the left hand side of equation (B.6) is clearly independent of z. Hence, the right hand side of equation (B.6) must also be independent of z. Similarly, each member of equation (B.6) must be independent of t. Therefore, each side of the equation must be a constant, say $-\lambda$, and we can write:

$$\frac{1}{f}\frac{\partial f}{\partial t} = -\lambda \qquad (B.7)$$

$$V_1 \frac{1}{g_1}\frac{\partial g_1}{\partial z} + k_1 \cdot \frac{g_3 - g_1}{g_1} = -\lambda \qquad (B.8)$$

Thus, the solution of the original partial differential equations has been reduced to the determination of the solutions of the ordinary differential equations (B.7) and (B.8).

If the value of λ is negative, therefore $-\lambda$ becomes positive, say $-\lambda = p^2$, and from equation (B.7) we have:

$$f = C \cdot e^{p^2.t} \qquad (B.9)$$

Since equation (B.9) indicates that the temperature $T - T_{ss} = f \cdot g$ increases beyond all bounds as time t increases, we reject the

possibility that $\lambda > 0$. It can be shown that $\lambda = 0$ leads to a trivial solution $T - T_{ss} = 0$, and therefore it must also be rejected. Then, λ must be a positive value which results in:

$$f = C \cdot e^{-\lambda . t} \tag{B.10}$$

Therefore, as t increases, the value of f will decay and hence T will approach the steady-state solution for a certain boundary. The value of λ defines the time characteristics of the heat exchanger, and it is the eigenvalues of the following boundary value problem which are produced by applying a similar procedure to equations (B.2) and (B.3):

$$V_1 \frac{\partial g_1}{\partial z} - (k_1 - \lambda) \cdot g_1 = - k_1 \cdot g_3 \tag{B.11}$$

$$V_2 \frac{\partial g_2}{\partial z} + (k_2 - \lambda) \cdot g_2 = k_2 \cdot g_3 \tag{B.12}$$

$$g_3 = \frac{\mu_1 g_1 + \mu_2 g_2}{\mu_1 + \mu_2 - \lambda} \tag{B.13}$$

$$\begin{matrix} g_1(L) = 0 \\ g_2(0) = 0 \end{matrix} \quad , \quad 0 < z < L \tag{B.14}$$

Returning now to the finite difference approximation of the time derivatives, rewriting equations (B.1) to (B.3) at the time step n as follows gives:

$$\frac{T_1^n - T_1^{n-1}}{\Delta t} - V_1 \frac{\partial T_1^n}{\partial z} = k_1 (T_3^n - T_1^n) \tag{B.15}$$

$$\frac{T_2^n - T_2^{n-1}}{\Delta t} + V_2 \frac{\partial T_2^n}{\partial z} = k_2 (T_3^n - T_2^n) \tag{B.16}$$

$$\frac{T_3^n - T_3^{n-1}}{\Delta t} = \mu_1 (T_1^n - T_3^n) + \mu_2 (T_2^n - T_3^n) \qquad \text{(B.17)}$$

As with differential equations, in the case of the differential difference equations we seek solutions at each time step in the following forms:

$$T_i - T_{ss,i} = \beta^n \cdot G_i(z) \quad , \quad i = 1, 2 \text{ or } 3 \qquad \text{(B.18)}$$

where the value of β is some constant to be determined. Substituting equation (B.18) into equations (B.15) to (B.17), and rearranging them, we obtain:

$$V_1 \frac{\partial G_1}{\partial z} - (k_1 - \frac{1 - \beta}{\beta \Delta t}) \cdot G_1 = - k_1 \cdot G_3 \qquad \text{(B.19)}$$

$$V_2 \frac{\partial G_2}{\partial z} + (k_2 - \frac{1 - \beta}{\beta \Delta t}) \cdot G_2 = k_2 \cdot G_3 \qquad \text{(B.20)}$$

$$G_3 = \frac{\mu_1 G_1 + \mu_2 G_2}{\mu_1 + \mu_2 - \frac{1 - \beta}{\beta \Delta t}} \qquad \text{(B.21)}$$

and boundary conditions can be transformed to the following form by employing equation (B.18):

$$\begin{aligned} G_1(L) &= 0 \\ G_2(0) &= 0 \end{aligned} \qquad \text{(B.22)}$$

It appears that the distribution of $G_i(z)$ is identical to $g_i(z)$ from equations (B.11) to (B.14) where λ has been replaced by the form:

$$\lambda = \frac{1 - \beta}{\beta \Delta t} \qquad \text{(B.23)}$$

Therefore, the characteristic values of the differential difference equations, β, may be found from the eigenvalue problem (equations (B.11) to (B.14)). However, for the purpose of stability of the numerical solution, the value of β can be related to the time characteristics of the heat exchanger λ by rearranging equation (B.23) as follows:

$$\beta = \frac{1}{1 + \lambda \cdot \Delta t} \tag{B.24}$$

It was argued that λ is a positive constant and hence the value of β from equation (B.24) is always less than unity:

$$\beta < 1 \tag{B.25}$$

and as n increases, β^n decreases. Therefore, as the number of time step n becomes large, solutions approach the steady-state for any size of the time step Δt.

REFERENCES

AKAGAWA, K., and SAKAGUCHI, T. (1972)

"Frictional pressure drop in steam generating tubes",

Bulletin of JSME, Vol. 15, No. 80, p. 264.

AKAGAWA, K., SAKAGUCHI, T., and UEDA, M. (1971)

"Study on gas-liquid two-phase flow in helically coiled tubes",

Bulletin of JSME, Vol. 14, No. 72, pp. 564-571.

ANGLESEA, W.T., CHAMBERS, D.J.B., and JEFFREY, R.C. (1974)

"Measurement of water/steam pressure drop in helical coils at 179 bars",

Paper presented at the Symposium on Multi-Phase Flow Systems, Inst. Chem. Mech. Engrs., Strathclyde University, April 1974.

ANGLESEA, W.T.

Private communication, Babcock and Wilcox (Operations) Limited, Renfrew.

BAILEY, N.A., DAVIES, A.L., et al. (1971) and (1972)

"Instabilities in two-phase flow systems",

HTFS-DR-17, AERE-R6456 (1971). Also, HTFS-DR-29, AERE-R7210 (1972). Commercial reports.

BAILEY, N.A., COLLIER, J.G., and RALPH, J.C. (1973)

"Post dryout heat transfer in nuclear and cryogenic equipments",

ASME, Paper 73-HT-16.

BAILEY, N.A. (1970)

"A review of data on heat transfer to superheated steam at high subcritical pressure",

AEEW-R678.

BANARJEE, S., RHODES, E., and SCOTT, D.S. (1967)
"Film inversion of co-current two-phase flow in helical coils",
A.I.Ch.E. Jnl., Vol. 13, pp. 189-191.

BANARJEE, S., RHODES, E., and SCOTT, D.S. (1969)
"Studies on co-current gas-liquid flow in helically coiled tubes",
Can. J. Chem. Eng., Vol. 47, pp. 445-453.

BANARJEE, S., SCOTT, D.S., and RHODES, E. (1970)
"Studies on co-current gas-liquid flow in helically coiled tubes:
II - Theory and experiments on turbulent mass transfer with and
without chemical reaction",
Can. J. Chem. Eng., Vol. 48, p. 542.

BANKOFF, S.G. (1960)
"A variable density single-fluid model of two-phase flow with
particular reference to steam-water flow",
Trans. ASME J. Heat Transfer, Series C, Vol. 82, No. 4, p. 265.

BARUA, S.N. (1963)
"On secondary flow in stationary curved pipes",
Quart. J. Mech. and Appl. Maths., Vol. 16, Pt. 1, p. 61.

BECKER, K.M., JAHNBERG, S., HAGA, I., HANSSON, P.T., and MATHISEN, R.P.
(1964)
"Hydrodynamic instability and dynamic burnout in natural circulation
two-phase flow. An experimental and theoretical study",
Third United Nations Int. Conf. on the Peaceful Uses of Atomic
Energy, A/Conf. 28/P/607, May 1964.

BECKMANN, G., FRITZ, K., LENDL, H., and GILLI, P.V. (1973)
"Flow stability and dynamic behaviour of nuclear boilers",
Paper 15 and also discussion PF4, Proc. Int. Conf. on the Boiler
Dynamics and Control in Nuclear Power Stations, B.N.E.S., March 1973.

BELL, K.J., and OWHADI, A. (1969)

"Local heat transfer measurements during forced convection boiling in a helically coiled tube",

Symp. on Fluid Mechanics and Measurements in Two-Phase Flow Systems, University of Leeds, Paper No. 7, September 1969.

BELL, K.J. (1976)

"Single-phase heat transfer and convective boiling phenomena in helically coiled tubes",

Seminar held at Imperial College on 24 June 1976.

BENNETT, A.W., HEWITT, G.F., KEARSEY, H.A., and Keeys, R.K.F. (1968)

"Heat transfer to steam-water mixture flowing in uniformly heated tubes in which the critical heat flux has been exceeded",

Paper presented at Thermodynamics and Fluid Mechanics Convention, I. Mech. E., Bristol, March 1968. Also AERE-R5373.

BERGLES, A.E., LOPINA, R.F., and FIORI, M.P. (1967)

"Critical heat flux and flow pattern observations for low pressure water flowing in tubes",

J. Heat Transfer, Vol. 70, pp. 69-75.

BERGLES, A.E., and DORMER, Jr., T. (1969)

"Subcooled boiling pressure drop with water at low pressure",

Int. J. Heat Mass Transfer, Vol. 12, pp. 459-470.

BICKERS, B.H., and CARSTAIRS, R.L. (1973)

"Operational and fault transient studies of a once-through AGR boiler using the OSCA digital computer program",

Paper 11, Proc. Int. Conf. on the Boiler Dynamics and Control in Nuclear Power Stations, B.N.E.S., March 1973.

BISHOP, A.A., et al. (1964)

"Forced convection heat transfer to superheated steam at high pressure and high Prandtl numbers",

WCAP-2056, Pt. III.

BISHOP, A.A. (1965)

"Forced convective heat transfer at high pressure after the critical heat flux",

ASME, Paper 65-HT-31.

BOSGRA, G.H., and BAIS, J.P. (1970)

"Hybrid computer solution of the hyperbolic equations describing forced flow steam generator dynamics",

Proc. 6th AICA Conf. on Hybrid Computations, Munich, pp. 399-407.

BOURÉ, J.A. (1966)

"The oscillatory behaviour of heated channels: An analysis of density effect. Parts I and II",

CEA-R-3049.

BOURÉ, J.A., and MIHAILA, A. (1967)

"The oscillatory behaviour of heated channels",

Symp. on Two-Phase Flow Dynamics, Eindhoven, EUR-4288e, pp. 695-720.

Discussion on p. 1113.

BOURÉ, J.A., and REOCREUX, M. (1972)

"General equations of two-phase flow: Applications to critical flows and to non-steady flows",

4th All-Union Heat Transfer Conf., Minsk.

BOURÉ, J.A., BERGLES, A.E., and TONG, L.S. (1973)

"Review of two-phase flow instability",

Nuclear Engineering and Design, Vol. 25, pp. 165-192.

BOURÉ, J.A. (1975)

"Constitutive equations for two-phase flows",
Lecture on Two-Phase Flow with Application to Nuclear Reactor Design Problems, VKI-LS-71, University of Cambridge, December 1975.

BOWRING, R.W. (1962)

"Physical model, based on bubble detachment, and calculation of steam voidage in the subcooled region of a heated channel",
Halden, HPR-10, December 1962.

BOYCE, B.E., COLLIER, J.G., and LEVY, J. (1968)

"Hold-up and pressure drop measurements in the two-phase flow of air-water mixtures in helical coils",
Proc. Int. Symp. on Research in Co-Current Gas-Liquid Flow, University of Waterloo, Ontario, Canada, pp. 203-231, September 1968.

BRERETON, D.H., and CARLING, L.N. (1967)

"Steam generator, stage 4",
CEGB, RD/C/R 59.

BRIGGS, D.E., and YOUNG, E.H. (1965)

"Convection heat transfer and pressure drop of air flow across triangular pith banks of finned tubes",
A.I.Ch.E. Chem. Eng. Prog. Symp., Series No. 41.

CARLING, L.N. (1965)

"Solution of counterflow heat exchanger equations on a hybrid computer",
CEGB, RD/C/R 38.

CARVER, J.R., KAKALARA, C.R., and SLOTNIK, J.S. (1964)

"Heat transfer in coiled tubes with two-phase flow",
Atomic Energy Commission Document, TID 20983.

CARVER, M.B. (1967)

"An analytical model for the prediction of hydrodynamic instability in parallel heated channels",

AECL-2681.

CARVER, M.B. (1970)

"Effect of by-pass characteristics on parallel channel flow instabilities",

Proc. Inst. Mech. Engrs., Vol. 184, Pt. 3C, pp. 84-92.

CENTRAL ELECTRICITY GENERATING BOARD (CEGB) (1971)

"Nuclear power generation",

Modern Power Station Practice, Vol. 8, Pergamon Press.

CHEN, J.C. (1963)

"A correlation for boiling heat transfer to saturated fluids in convective flow",

ASME, Paper 63-HT-34.

CHEXAL, V.K., and BERGLES, A.E. (1973)

"Two-phase instabilities in a low pressure natural circulation loop",

A.I.Ch.E. Symp., Series No. 131, Vol. 69, pp. 37-45.

COLLIER, J.G. (1972)

Convective Boiling and Condensation,

McGraw Hill.

COLLIER, J.G., and PULLING, D.J. (1962)

"Heat transfer to two-phase gas-liquid systems. Part II: Further data on steam/water mixtures in the liquid dispersed region in an annulus",

AERE-R3809.

COLLINS, D.B., and GASCESA, M. (1970)

"Hydrodynamic instability in a full-scale simulated reactor channel", Proc. Inst. Mech. Engrs., Vol. 184, Pt. 3C, pp. 115-126.

COLLINS, D.B., GASCESA, M., and PARSONS, C.B. (1971)

"Study of the onset of premature heat transfer crisis during hydrodynamic instabilities in a full-scale reactor channel", ASME, Paper 71-HT-11.

CONTE, S.D. (1965)

Elementary Numerical Analysis, McGraw Hill.

COULSON, J.M., and RICHARDSON, J.F. (1970)

"Fluid flow, heat transfer and mass transfer", Chemical Engineering, Vol. 1, Pergamon Press.

CRAIN, Jr., B., and BELL, K.J. (1973)

"Forced convection heat transfer to an two-phase mixture of water and steam in a helical coil", A.I.Ch.E. Symp., Heat Transfer, Series No. 131, Vol. 69, pp. 30-36.

CROWLEY, J.D., DEANE, C., and GOUSE, S.W. (1967)

"Two-phase flow oscillations in vertical parallel heated channels", Symp. on Two-Phase Flow Dynamics, Eindhoven, EUR-4288e, pp. 1131-1171.

CUMMINGS, H.G. (1955)

"The secondary flow in curved pipes", ARC R & M 2880.

CUMO, M., FARELLO, C.E., and FERRARE, G. (1971)

"The influence of curvature in post-dryout heat transfer", Paper presented at European Two-Phase Flow Group Meeting, Risø, Denmark, June 1971.

CURRIN, H.B., HUNIN, C.M., RIVLIN, L., and TONG, L.S. (1961)
"HYDNA - Digital computer program for hydrodynamic transients in a pressure tube reactor or a closed channel core",
US Atomic Energy Commission Report, CVNA-77.

DALEAS, R.S., and BERGLES, A.E. (1965)
"Effect of upstream compressibility on subcooled critical heat flux",
ASME, Paper 65-HT-67.

DAVIES, A.L., and POTTER, R. (1967)
"Hydraulic stability: An analysis of the causes of unstable flow in parallel channels",
Symp. on Two-Phase Flow Dynamics, Eindhoven, EUR-4288e, pp. 1225-1266.

DIJKMAN, F.J.M. (1969)
"Some hydrodynamic aspects of a boiling water channel",
Doctorate Thesis, Eindhoven University of Technology, The Netherlands, WW-R144.

DUCHATELLE, L., DE NUCHEZE, L., and ROBIN, M.G. (1973)
"Departure from nucleate boiling in helical tubes of liquid metal heated steam generators",
ASME, Paper 73-HT-57.

EFFERDING, L.E. (1968)
"DYNAM - A digital computer program for the study of the dynamic stability of once-through boiling flow with steam superheat",
US Atomic Energy Commission Report, GAMD-8656.

FALLOWS, T., HITCHCOCK, J.A., JONES, R.C., LIS, J., and NORTHOVER, E.W. (1973)
"A study of oscillatory instabilities in the parallel channels of a high pressure once-through boiler rig",
Paper 14 and discussion p. F5, Proc. Int. Conf. on Boiler Dynamics and Control in Nuclear Power Stations, B.N.E.S., March 1973.

FRAAS, A.P., and OZISIK, M.N. (1965)

Heat Exchangers Design,

John Wiley and Sons.

GILLI, P.V. (1964)

"Heat transfer characteristics of helical tube bundles as used in steam generators of gas-cooled reactors",

3rd Int. Conf. on Peaceful Uses of Atomic Energy, Geneva,

Paper A/CONF28/P/519.

GROSS, R.J., and SEE, F.T. (1973)

"A contribution to thermal-hydraulic stability analysis",

ASME, Paper 73-WA/HT-23.

HANCOX, W.T., and NICHOLL, W.B. (1971a)

"A general technique for the prediction of void distributors in non-steady two-phase forced convection",

Int. J. Heat Mass Transfer., Vol. 14, pp. 1377-1394.

HANCOX, W.T., and NICHOLL, W.B. (1971b)

"Prediction of time-dependent diabatic two-phase water flows",

Paper 1-6, Int. Symp. on Two-Phase Systems, Haifa, August 1971.

HANNSON, P.T., and AXELSSON, E. (1965)

"HYDRO - A digital model for one-dimensional time-dependent two-phase hydrodynamics",

AE-RFR-492, RFN-210.

HEINEMAN, J.B. (1960)

"An experimental investigation of heat transfer to superheated steam in round and rectangular channels",

ANL-6213.

HOPE, J.H. (1973)

"Design sensitivity for AGR once-through boilers",
Paper 9, Proc. Int. Conf. on Boiler Dynamics and Control in Nuclear Power Stations, B.N.E.S., March 1973.

ISHII, M., and ZUBER, N. (1970)

"Thermally induced flow instabilities in two-phase mixtures",
4th Int. Heat Transfer Conf., Paris, pp. B5.11-12.

ITO, H. (1959)

"Friction factors for turbulent flow in curved pipes",
J. Basic Engng., Trans. ASME, D81, pp. 123-134.

JEGLIC, F.A., and GRACE, T.M. (1965)

"Onset of flow oscillations in forced flow subcooled boiling",
NASA-TN-D-2821.

JENS, W.H., and LOTTES, P.A. (1951)

"Analysis of heat transfer burnout, pressure drop and density data for high pressure water",
ANL-4627.

JIJI, L.M., and CLARK, J.A. (1962)

"Bubble boundary-layer and temperature profiles for forced convection boiling in channel flow",
ASME, Paper 62-WA-141.

JONES, A.B., and DIGHT, A.G. (1961-1964)

"Hydrodynamic stability of a boiling channel",
US Atomic Energy Commission Report, Part 1, KAPL-2170 (1961); Part 2, KAPL-2208 (1962); Part 3, KAPL-2290 (1963); Part 4, KAPL-3070 (1964).

KAKAC, S., VEZCROGLU, T.N., AKSU, H.B., and ALP, Y. (1973)
"Boiling flow instabilities in a four parallel channel upflow system",
Proc. Int. Meeting on Reactor Heat Transfer, Kernforschungszentrum Karlsruhe, pp. 404-420, October 1973.

KASTURI, G., and STEPANEK, J.B. (1972)
"Two-phase flow. I - Pressure drop and void measurements in co-current gas-liquid flow in coils",
Chem. Engng. Sci., Vol. 27, pp. 1871-1880.

KNOWLES, J.B., and ROBINS, A.J. (1973)
"Heat transfer regimes and transitions in boiler dynamic models",
Paper 12, Proc. Int. Conf. on Boiler Dynamics and Control in Nuclear Power Stations, B.N.E.S., March 1973.

KOSHELER, J.I., SURNOV, A.V., and NIKITINO, L.V. (1970)
"Inception of pulsations using a model of vertical water wall tubes",
Heat Transfer, Soviet Research, Vol. 2, p. 3.

KOZEKI, M., NARIAI, H., FURUKAWA, T., and KUROSU, K. (1970)
"A study of helically coiled tube once-through steam generators",
Bulletin of JSME, Vol. 13, No. 66, pp. 1485-1494.

KOZEKI, M. (1973)
"Film thickness and flow boiling for two-phase annular flow in helically coiled tubes",
Proc. Int. Meeting on Reactor Heat Transfer, Kernforschungzentrum Karlsruhe, pp. 351-372, October 1973.

KUBAIR, Y., and KULOOR, N.R. (1966)
"Heat transfer to Newtonian fluids in coiled pipes in laminar flow",
Int. J. Heat Mass Transfer, Vol. 9, pp. 63-75.

LACEY, P.M.C. (1970)

"Two-phase flow in curved ducts",

Paper presented at Annual Meeting of DECHEMA, Frankfurt/Main, June 1970.

LACEY, P.M.C. (1967)

Discussion on "Regimes of deteriorated heat transfer at forced flow of fluids in curvilinear channels" by Miropolski et al, Proc. 3rd Int. Heat Transfer Conf., Vol. 6, pp. 137-139, A.I.Ch.E., New York.

LARSEN, P.S., and TONG, L.S. (1969)

"Void fractions in subcooled flow boiling",

J. Heat Transfer, Trans. ASME, pp. 471-476.

LEDINEGG, M. (1954)

"Instability of flow during natural and forced circulation",

Die Wärme, Vol. 61 (1938), and AEC-tr-1861 (1954).

LOCKHART, R.W., and MARTINELLI, R.C. (1949)

"Proposed correlation of data for isothermal two-phase, two component flow in pipes",

Chem. Engng. Progress, Vol. 45, No. 1. p. 39.

MADDOCK, C., LACEY, P.M.C., and PATRICK, M.A. (1974)

"The structure of two-phase flow in a curved pipe",

Paper presented at Symp. on Multi-Phase Flow Systems, Inst. Chem. Mech. Engrs., Strathclyde University, April 1974.

MARGETTS, R.J. (1972)

"Excursive instability in feed water coils",

Paper 16, 13th National Heat Transfer Conf. A.I.Ch.E. - ASME, Denver, Colorado, USA.

MARTINELLI, R.C., and NELSON, D.B. (1948)

"Prediction of pressure drop during forced circulation boiling of water",

Trans. ASME, Vol. 70, p. 695.

MASSENA, W.A. (1960)

"Steam-water pressure drop",

Hanford Report, HW-65706.

MATHISEN, R.P. (1967)

"Out of pile channel instability in the loop Skalve",

Symp. on Two-Phase Flow Dynamics, Eindhoven, EUR-4288e, pp. 19-63.

MAULBETSCH, J.S., and GRIFFITH, P. (1966)

"System-induced instabilities in forced convection flows with subcooled boiling",

Proc. 3rd Int. Heat Transfer Conf., Vol. 4, pp. 247-257, Chicago, Illinois, USA.

MAULBETSCH, J.S., and GRIFFITH, P. (1967)

"Prediction of the onset of system-induced instabilities in subcooled boiling",

Symp. on Two-Phase Flow Dynamics, Eindhoven, EUR-4288e, pp. 799-826.

MEYER, J.E., and ROSE, R.P. (1963)

"Application of a momentum integral model to the study of parallel channel boiling flow oscillations",

J. Heat Transfer, pp. 1-9.

McADAMS, W.H. (1950)

Heat Transmission,

McGraw Hill.

McCRACKEN, D.D., and DORN, W.S. (1965)

Numerical Methods and Fortran Programming,

John Wiley and Sons.

M.E. BOILERS LIMITED

"Coil boilers for heavy oil recovery",

23 Bedford Row, London W.C.1.

MIROPOLSKIY, Z.L., PIKUS, V.J., and SHITSMAN, M.E. (1966)

"Regimes of deteriorated heat transfer at forced flow of fluids in curvilinear channels",

Proc. 3rd Int. Heat Transfer Conf., Paper 50, pp. 95-101, Chicago, Illinois, USA, August 1966.

MIROPOLSKIY, Z.L., and PIKUS, V.J. (1969)

"Critical boiling heat fluxes in curved channels",

Heat Transfer, Soviet Research, Vol. 1, No. 1, pp. 74-79.

MIROPOLSKIY, Z.L., ANNADURDYEV, K.H., and KAKABAEV, A. (1969)

"Heat transfer and pressure drop in the heating and cooling of liquids in curvilinear channels",

Int. Chem. Engng., Vol. 9, No. 3, pp. 410-414.

MORI, Y., and NAKAYAMA, W. (1967)

"Study of forced convective heat transfer in curved pipes",

Int. J. Heat Mass Transfer, Vol. 10, pp. 37-59, and Vol. 10, pp. 681-695.

MOXON, D. (1968)

"SLIP - A dynamic program for the thermal-hydraulic behaviour of boiling loops",

AEEW-R448.

MOXON, D. (1973)

"Stability of once-through steam generators",

ASME, Paper 73-WA/HT-24.

NAITOH, N., NAKMURA, A., and OGASAWARA, H. (1974)

"Dryout in helically coiled tubes of sodium heated steam generators",

ASME, Paper 74-WA/HT-48.

NEAL, L.G., ZINI, S.M., and WRIGHT, R.W. (1967)

"The mechanism of hydrodynamic instabilities in boiling systems",

Symp. on Two-Phase Flow Dynamics, Eindhoven, EUR-4288e, pp. 957-980,

and Chairman's remarks.

NORONHA, L.G., PO, C.Y., and WOMACK, J.W. (1968)

"Hybrid computation of the dynamics of a distributed system",

The Computer Journal. Vol. II, No. 2, pp.

OGATA, K. (1970)

Modern Control Engineering,

Prentice-Hall.

OWHADI, A. (1966)

"Boiling in self-induced radial acceleration fields",

Ph.D. Thesis, Oklahoma State University.

OWHADI, A., and BELL, K.J. (1967)

"Forced convection boiling inside helically coiled tubes",

Int. J. Heat Mass Transfer, Vol. 10, No. 3, p. 397.

OWHADI, A., BELL, K.J., and CRAIN, Jr., B. (1968)

"Forced convection boiling inside helically coiled tubes",

Int. J. Heat Mass Transfer, Vol. 11, pp. 1779-1793.

PATANKAR, S.V., PRATAP, V.S., and SPALDING, D.B. (1974)

"Prediction of laminar flow and heat transfer in helically coiled pipes",

J. Fluid Mech., Vol. 62, Pt. 3, pp. 539-551; also

"Prediction of turbulent flow in curved pipes",

Imperial College Internal Report, HTS/74/1.

POTTER, R. (1973)

"A review of two-phase flow instability aspects of boiler dynamics",

Paper 13, Proc. Int. Conf. on Boiler Dynamics and Control in Nuclear Power Stations, B.N.E.S., March 1973.

PRESTON, R.W., LIS, J., and HITCHCOCK, J.A. (1973)

"Comparison of the boiler model NUBOIL with transient measurements on a once-through boiler rig",

Paper 17, Proc. Int. Conf. on Boiler Dynamics and Control in Nuclear Power Stations, B.N.E.S., March 1973.

QUANDT, E.R. (1961)

"Analysis and measurement of flow oscillations",

Chem. Engng. Prog. Symp. Series No. 32, Vol. 5, pp. 111-126.

RAKOPOULOS, C. (1976)

Private communication, Imperial College, London.

RIPPEL, G.R., EIDT, C.M., and JORDAN, H.B. (1966)

"Two-phase flow in a coiled tube",

Ind. Engng. Chem. Process Design Dev., Vol. 5, No. 1, pp. 32-39.

ROGERS, G.F.C., and MAYHEW, Y.R. (1964)

"Heat transfer and pressure loss in helically coiled tubes with turbulent flow",

Int. J. Heat Mass Transfer, Vol. 7, pp. 1207-1216.

RUFFEL, A.E. (1970)

"Communications",

Proc. Inst. Mech. Engrs., Vol. 184, Pt. 1, No. 36, p. 658.

RUFFEL, A.E. (1974)

"The application of heat transfer and pressure drop data to the design of helical coil once-through boilers",

Paper presented at Symp. on Multi-Phase Flow Systems, Inst. Chem. Mech. Engrs., Strathclyde University, April 1974.

SCHROCK, V.E., and GROSSMAN, L.M. (1959)

"Forced convection boiling studies",

US Atomic Energy Commission Report, TID-14632.

SEBAN, R.A., and McLAUGHLIN, E.F. (1963)

"Heat transfer in tube coils with laminar and turbulent flow",

Int. J. Heat Mass Transfer, Vol. 6, No. 5, pp. 387-395.

SHEARER, J.L., MURPHY, A.T., and RICHARDSON, H.H. (1967)

Introduction to System Dynamics,

Addison-Wesley Publishing Company.

SHERWIN, K. (1972)

"Development of finned tubes for forced draught air-cooled heat exchangers",

Conf. on Recent Developments in Compact High Duty Heat Exchangers, Inst. Mech. Engrs., October 1972.

SHIRES, G.L., and KHANNA, R.D. (1971)

"Two-phase flow and heat transfer in helical coils",

Heat Transfer and Fluid Flow Research Symp., AEEW-M1023.

SMITH, S.L. (1970)

"Void fraction in two-phase flow: A correlation based on an equal velocity head model",

Proc. Inst. Mech. Engrs., Vol. 184, Pt. 1, No. 36, pp.

SOLBERG, K.O., and BAKSTAD, P. (1967)

"A model for the dynamics of nuclear reactors with boiling coolant with a new approach to the vapour generation process",

Symp. on Two-Phase Flow Dynamics, Eindhoven, EUR-4288e, pp. 871-934.

SOLBERG, K.O. (1966)

"Resultates des essais d'instabilites sur la boucle 'Caline' et comparaisons avec un code de calcul",

GENG Note 225.

SPIGHT, C.L. (1966)

"On the hydraulic characteristics of a boiling water channel with natural circulation",

WW-016-R92.

SRINIVASAN, P.S., NANDAPURKAR, S.S., and HOLLAND, F.A. (1968)

"Pressure drop and heat transfer in coils",

The Chem. Engr., pp. CE113-CE119.

SRINIVASAN, P.S., NANDAPURKAR, S.S., and HOLLAND, F.A. (1970)

"Friction factors for coils",

Trans. Inst. Chem. Engrs., Vol. 48, pp. T156-T161.

STENNING, A.H., and VEZIROGLU, T.N. (1964)

"Instabilities in the flow of boiling liquid",

NASA-CR-164.

STENNING, A.H., and VEZIROGLU, T.N. (1965)

"Flow oscillation modes in forced convection boiling",

Proc. 1965 Heat Transfer and Fluid Mech. Inst., Stanford University Press, pp. 301-316.

STENNING, A.H., VEZIROGLU, T.N., and CALLAGHAN, G.M. (1967)

"Pressure drop oscillations in forced convection flow boiling",

Symp. on Two-Phase Flow Dynamics, Eindhoven, EUR-4288e, pp. 405-428.

TAYLOR, P.A., URQUHART, W.M., and JEFFREY, R.C. (1973)

"The development of once-through boilers for gas-cooled reactors", Convention on Steam Plant Operation, Inst. Mech. Engrs., May 1973.

TAYLOR, E. (1973)

"Modelling of once-through boiler dynamics", Paper 10, Proc. Int. Conf. on Boiler Dynamics and Control in Nuclear Power Stations, B.N.E.S., March 1973.

THOM, J.R.S. (1964)

"Prediction of pressure drop during forced circulation boiling of water", Int. J. Heat Mass Transfer, Vol. 7, No. 7, p. 709.

THOM, J.R.S., WALKER, W.M., FALLON, T.A., and REISING, G.F.S. (1965)

"Boiling in subcooled water during flow up heated tubes of annuli", Paper 6, presented at Symp. on Boiling Heat Transfer in Steam Generating Units and Heat Exchangers, Inst. Mech. Engrs., Manchester, September 1965.

THOMPSON, T.S. (1970)

"Liquid film breakdown and dry-patch stability of steam-water flows with heat transfer", Ph.D. Thesis, University of London.

TONG, L.S. (1965)

Boiling Heat Transfer and Two-Phase Flow, Chapter 3, John Wiley and Sons.

TONG, L.S. (1972)

"Boiling crisis and critical heat flux", US Atomic Energy Commission Report, TID-25887.

VEZIROGLU, T.N., and LEE, S.S. (1970)
"Boiling flow instabilities in parallel channels",
Proc. Inst. Mech. Engrs., Vol. 184, Pt. 3C, pp. 7-17.

VERHEUGEN, A.N.J., DIJKMAN, F.J.M., LAMEIN, H.J., and TONG, L.S. (1967)
"The influence of the response characteristics of the heated rod on the stability and burnout characteristics of a boiling channel",
Symp. on Two-Phase Flow Dynamics, Eindhoven, EUR-4288e, pp. 841-869.

WALLIS, G.B., and HEASLEY, J.H. (1961)
"Oscillations in two-phase flow systems",
J. Heat Transfer, Vol. 83, pp. 363-369.

WASZINK, R.P., and EFFERDING, L.E. (1974)
"Hydrodynamic instability and thermal performance tests of 1 MWt sodium heated once-through steam generator models",
ASME, Paper 73-PWR-16.

ZUBER, N. (1967)
"Flow excursions and oscillations in boiling two-phase flow systems with heat addition",
Symp. on Two-Phase Flow Dynamics, Eindhoven, EUR-4288e, pp. 1071-1089.

ZUBER, N., and DOUGHERTY, D.E. (1967)
"Liquid metals challenge to the traditional methods of two-phase flow investigations",
Symp. on Two-Phase Flow Dynamics, Eindhoven, EUR-4288e, pp. 1091-1109.